Role of lysosome positioning in bladder cancer progression

Pallavi Mathur

PSL UNIVERSITÉ PARIS

THÈSE DE DOCTORAT
DE L'UNIVERSITÉ PSL

Préparée à Institut Curie

Role of lysosome positioning in bladder cancer progression

(Positionnement du lysosome dans la progression du cancer de la vessie)

Soutenue par
Pallavi MATHUR

Ecole doctorale n° 515
ED 515 - Complexité du vivant

Spécialité
Biologie cellulaire et développement

Composition du jury :

Ana-Maria, LENNON Directeur de recherche, Institut Curie	*Président*
Mojgan, DJAVAHERI-MERGNY Chargé de recherche, Centre de Recherche des Cordeliers	*Rapporteur*
Guillaume, VAN NIEL Directeur de recherche, Institute of Psychiatry and Neuroscience of Paris	*Rapporteur*
Harald, STENMARK Professor / Researcher /Group leader, Department of Molecular Cell Biology, Institute for Cancer Research, Oslo University Hospital	*Examinateur*
Ana-Maria, LENNON Directeur de recherche, Institut Curie	*Examinateur*
Kristine, SCHAUER Chargé de recherche, Gustave Roussy	*Directeur de thèse*

institut Curie

ACKNOWLEDGMENTS

I would like to start by thanking the members of my PhD jury for kindly agreeing to evaluate my work. Guillaume van Niel and Mojgan Mergny for agreeing to take the lengthy task of being the reporters for my thesis; Harald Stenmark for agreeing to be an examiner and Ana-Maria Lennon for agreeing to be an examiner and the president of the jury for my defense.

This project would not have been possible without the support and guidance of many people. I take this opportunity to thank them all for being there during these years of the PhD. First and foremost, I would like to start by thanking Kristine Schauer for her excellent guidance over the last four years. I am very grateful to Kristine for giving me an opportunity to work on this very interesting project. She has been enthusiastically involved in the progress of this work, throughout. Her suggestions have been very insightful in driving the project forward which has helped me sharpen my skills and grow as a researcher. I am very thankful for her constant support of my ideas and for being equally invested in my professional growth. She is an excellent mentor and I greatly appreciate all the efforts she had made for me. I would also like to thank Bruno Goud for accepting me in his team and giving me an opportunity to join Institut Curie to pursue my PhD studies. I greatly appreciate the continual support that I have received from Bruno for progress of my research. His scientific inputs and advices have been especially valuable not only in the advancement of this project but also in directing my scientific career.

Next, I would like to thank the members of my thesis advisory committee, Danijela Vignjevic, Maria Carla Parrini and Michel Cohen for monitoring the growth of this project. They have helped me advance in this work through their valuable discussions and suggestions, for which I am very thankful. I would also like to thank our collaborators; Cedric Allier (CEA LETI, Grenoble) for the time he invested in analysis of the data we obtained from the lens-free microscopy and also for his kind explanations of the analysis; Gilles Gasser (Chimie ParisTech) for allowing us to use the Seahorse setup in his lab and also many thanks to Marta Jakubaszek for helping me perform the Seahorse assays.

I am also thankful to the team of Institut Curie training unit who helped me settle in Paris and the PhD program, IC3i ‘European Union’s Horizon 2020 research and

innovation programme under the Marie Skłodowska-Curie grant' for funding this project.

I would like to thank all the members of the our lab who have helped me integrate in the team, facilitated excellent scientific discussion which has enriched the PhD experience for me. I would like to thank Sabine, Hugo , Stephanie, Pierre and Chandini for creating a friendly and comfortable working environment. Sabine for always helping me out whenever I was in need. Stephanie for encouraging me to participate in various scientific events. Pierre and Hugo for being great friends and for always being ready to talk and help out. I am also very thankful to all the past members of the lab, Surya, Gehenna, Nathan, David, Samuel, Yamini, Anna and Katerina for making me feel welcomed to the team. Surya and Gehenna especially, for always being there to provide support and advices. I would also like to thank all my friends whom I met in Paris and with whom I have made connections for a lifetime. Most importantly, I want to thank my friend Vibha for being my family away from home. I am immensely grateful for all her moral support and kindness, throughout all these years of PhD, which has made this journey so much easier.

Finally, I would like to end by thanking my family, and the loved ones who have encouraged me to take up this difficult study. I am immensely grateful for their understanding, care and consistent support through and through.

CONTENTS

List of Contents

List of Figures

List of Tables

Chapter 1

Introduction

1.1. Bladder Cancer: Classification and Molecular Subtypes

Bladder cancer is among the most prevalent cancers. In 2022, an estimate of about 573,278 cases of bladder cancers were detected worldwide (Source: Cancer.net; bladder cancer statistics). It has been observed as the 9th most common cancer worldwide, and 4th most common cancer in men, with the high prevalence in older people above the age of 55, and a median age of diagnosis of 65 years. Medical comorbidities are thus a crucial consideration in patient management in this cancer (Clark et al., 2013). Bladder cancers can be classified based on their invasiveness, non-muscle-invasive bladder cancers (NMIBC) or muscle-invasive bladder cancers (MIBC).

Tran et al.,2021

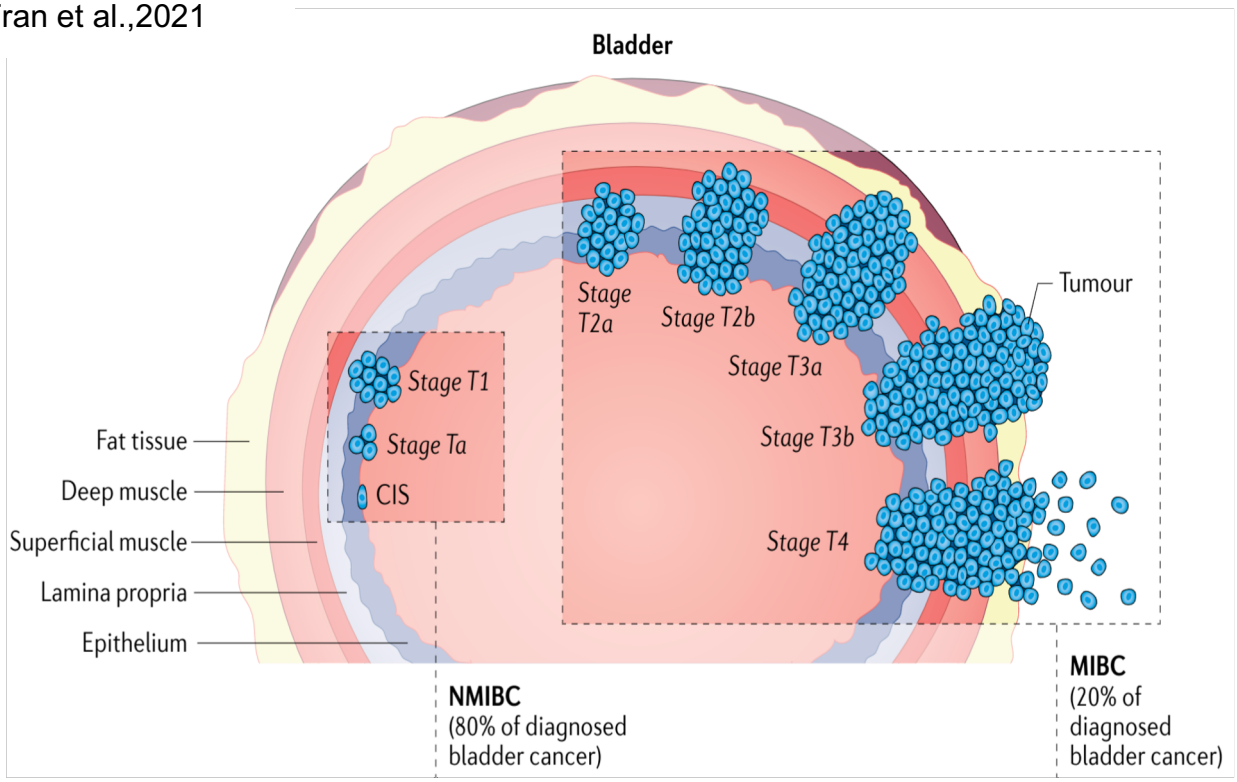

Fig 1: Classifications of Bladder Cancer

NMIBC could be of Stage T1, Ta and CIS (Carcinoma In Situ). CIS cancers are usually aggressive but are still limited to the inner bladder cancer linings; Ta and T1 NMIBC are both superficial cancers found at the inner most lining/wall of the bladder, with T1 being the stage that starts growing into the connective tissue of the bladder (**Fig 1**) (Source: cancerresearchuk.org; bladder cancer stages and grades).

MIBC are categorized in Stage T2, T3 and T4. At T2, the cancer has progressed to invade the muscles around the bladder, T2a invading the superficial muscles and T2b invading the deeper muscles. T3 cancers progress to the adipose tissue around the bladder and T4 are the most aggressive, metastatic cancers that can spread to other neighboring organs. (Source: cancerresearchuk.org; bladder cancer stages and grades).

Both, NMIBC and MIBC have widely varied molecular alterations driving the cancer and can thus be further classified into different subtypes. Chief among the various molecular changes present in bladder cancers is the activating mutation in the Telomerase Reverse Transcriptase (TERT), which is found to be present in about 80% of the bladder cancer cases (Leão et al., 2019)

Molecular features of the non-muscle invasive bladder cancers (NMIBC): NMIBC are the most frequently detected bladder cancers with a high rate of recurrence within 5 years post treatments (Hidas et al., 2013). In clinical practice, NMIBC are diagnosed in about 80% of the patients with a good survival rate (5-year survival rates greater than 85%). The chances of this kind of bladder cancers to progress to invasive diseases remain low about 7% (Berdik, 2017). As per the TNM system (Tumor, lymph node, metastasis), these NMIBC can further be classified into 3 subtypes (Hedegaard et al., 2016): Class 1, Class 2 and Class 3. Class 1 NMIBC show an upregulation or activation of Fibroblast Growth Factor Receptor 3 (FGFR3) and also depict elevated levels of early cell cycle regulators (such as, CCDN1). These class 1 NMIBC are mostly low grade, are well differentiated with luminal-like features and have a good prognosis. Class 2 NMIBC show upregulation of late cell cycle regulators, and they also have elevated levels of transcription factors responsible for epithelial to mesenchymal transition (EMT). These cancers also present luminal-like features. Class 2 NMIBCs are described to be associated with very poor prognosis and low survival rates. Both class 1 and class 2 NMIBC have a high expression of Uroplakins (UPK) which is a marker of luminal cells and which is responsible for their luminal like features (Hedegaard et al., 2016). Class 3 NMIBC have more basal like features due the overexpression of KRT5 and KRT15, markers of undifferentiated or basal cells. Class 3 NMIBC can also possess mutations in the FGFR3 gene (The Cancer Genome Atlas Research Network, 2014). (**Fig2**)

Tran et al., 2021

NMIBC

MIBC

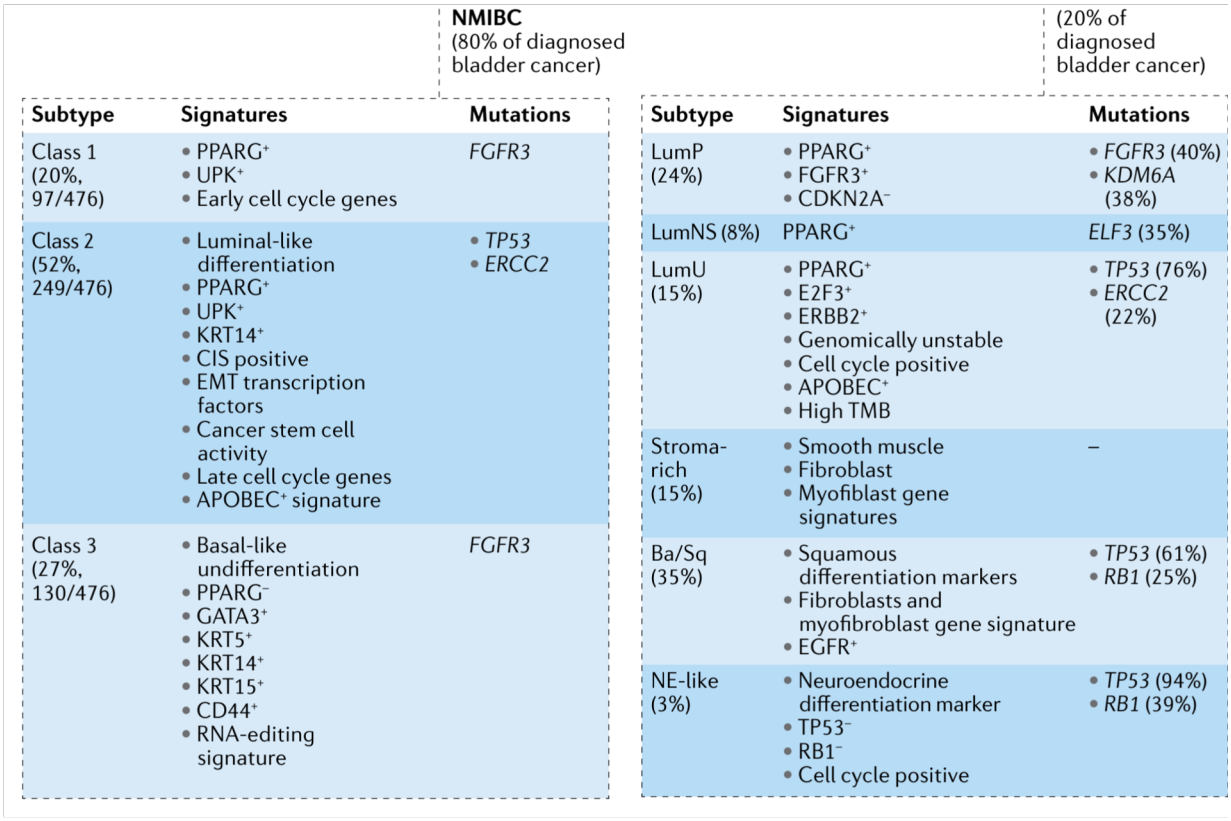

NMIBC (80% of diagnosed bladder cancer)

Subtype	Signatures	Mutations
Class 1 (20%, 97/476)	• PPARG$^+$ • UPK$^+$ • Early cell cycle genes	*FGFR3*
Class 2 (52%, 249/476)	• Luminal-like differentiation • PPARG$^+$ • UPK$^+$ • KRT14$^+$ • CIS positive • EMT transcription factors • Cancer stem cell activity • Late cell cycle genes • APOBEC$^+$ signature	• *TP53* • *ERCC2*
Class 3 (27%, 130/476)	• Basal-like undifferentiation • PPARG$^-$ • GATA3$^+$ • KRT5$^+$ • KRT14$^+$ • KRT15$^+$ • CD44$^+$ • RNA-editing signature	*FGFR3*

(20% of diagnosed bladder cancer)

Subtype	Signatures	Mutations
LumP (24%)	• PPARG$^+$ • FGFR3$^+$ • CDKN2A$^-$	• *FGFR3* (40%) • *KDM6A* (38%)
LumNS (8%)	PPARG$^+$	*ELF3* (35%)
LumU (15%)	• PPARG$^+$ • E2F3$^+$ • ERBB2$^+$ • Genomically unstable • Cell cycle positive • APOBEC$^+$ • High TMB	• *TP53* (76%) • *ERCC2* (22%)
Stroma-rich (15%)	• Smooth muscle • Fibroblast • Myofiblast gene signatures	–
Ba/Sq (35%)	• Squamous differentiation markers • Fibroblasts and myofibroblast gene signature • EGFR$^+$	• *TP53* (61%) • *RB1* (25%)
NE-like (3%)	• Neuroendocrine differentiation marker • TP53$^-$ • RB1$^-$ • Cell cycle positive	• *TP53* (94%) • *RB1* (39%)

Fig 2 : Molecular features of bladder cancers

Molecular subtypes of the muscle invasive bladder cancers (MIBC): Several studies have worked towards dissecting clear molecular subtypes of MIBC. Large number of criteria were taken in account to reach a consensus of non-overlapping and distinct molecular subtypes of this strongly mutated type of cancer (Tran et al., 2021). Classifications of MIBC have been considered on the bases of effectiveness of therapy, biological features and clinical outcomes (Damrauer et al., 2014; Robertson et al., 2017; Seiler et al., 2017). The MIBC are thus classified in 6 molecular subtypes: Luminal unstable (LumU), Luminal non-specified (LumNS), Luminal papillary (LumP), Stromal rich, Basal / Squamous (Ba/SQ) and neuroendocrine like (NE-like) (Tran et al., 2021) (**Fig 2**). As per the common consensus, the luminal types i.e. the LumP, LumNS and LumU MIBC showed PPARG (Peroxisome proliferator- activated receptor gamma) mutations as well as gene mutation or genomic replication of FGFR3. Among the Luminal types MIBC, LumP were observed to be less aggressive and also a good target of FGFR3-based therapies due to multiple FGFR3 mutations observed in this subtype of MIBC. The luminal subtypes of MIBCs also showed an enriched urothelial

differentiation. Contrary, the Stromal rich MIBC showed lesser urothelial differentiation. This cancer subtype had a more endothelial, smooth muscle, myofibroblast like genetic signature. The Ba/Sq type MIBC were the most aggressive, showed most frequent mutations of tumor protein P53 (TP53) and retinoblastoma protein (RB1) genes. These cancers also depicted an upregulation of the Epidermal Growth Factor Receptor (EGFR) and hypoxia inducible factor 1A (HIF1A) activity. Moreover, they had a characteristic loss of luminal markers such as GATA3 and FOXA1. Finally, the NE-like MIBC, were the most homogenous, and about 80% of the NE-like cancers showed neuro-endocrine like histology. These were also characterized by ubiquitous TP53 mutations along with RB1 mutations. NE-like cancers were also among the most aggressive MIBCs with a mean survival of the patient after diagnosis to be about 1 year.

1.2. Signaling pathways implicated in bladder cancer

Bladder cancers have been shown to progress through multiple signaling pathways. Thus, exploring the molecular targets implicated in bladder cancers is an important step for the development of novel cancer therapies. Below I discuss, briefly, some of the crucial signaling pathways described in NMIBCs and MIBCs.

Ras/Raf/MAPK pathway:

Ras proteins are a part of a super family of small GTPases (GTP binding proteins) that control temporal signal transduction in mammalian cells. Ras super family includes proteins from 6 different families namely, Ras, Rab, Rho, Arf, Ran and Rad. The members of the Ras protein family are H-Ras, K-Ras, N-Ras and R-Ras. Mutations in one or more of these Ras proteins have been found in several different cancers, and they support cell proliferation and cancer growth. H-Ras mutations are very frequently found in NMIBC. In-fact, overexpression of this oncogene (since Ras mutations have potential to cause cancer) in animal models has been demonstrated to induce low-grade non-invasive papillary tumors which indicates that H-Ras mutations could be an inductor of bladder cancers (Zhang et al., 2001). Mutated Ras leads to extensive cell proliferation and survival by activation of mitogen-activated protein kinase (MAPK) pathway.

Additionally, the majority of the NMIBC were also shown to have activating mutations in FGFR3 as discussed above. FGFR3 activating mutations also contribute to activation of the MAPK pathway in addition to the Ras family proteins (Mitra et al., 2006). In fact, activating mutations in both Ras proteins and FGFR3 have been shown to activate MAPK pathway in a mutually exclusive manner. This suggested that both pathways could activate the MAPK pathway independently and could be a precursor in the induction of NMIBC. Indeed, this has been shown to be the case in about 85% of cases of these low grade cancers (Hernández et al., 2006).

P53 pathway:

While the FGFR3 activating mutations appear as a precursor for less aggressive bladder cancers, mutations in P53 are a characteristic of a majority of high grade MIBC (>50%) (Esrig et al., 1994). P53 is a nuclear phosphoprotein coded by the gene TP53 which is a tumor suppressor protein as it acts as a gatekeeper of G1-S checkpoint of the cell cycle (Levine, 1997). P53 binds to damaged DNA to prevent cell division and signals cells to undergo apoptosis thus acting as a tumor suppressor. Deletions and inactivating mutations in TP53 lead to reduced activity of this tumor suppressor in bladder cancers, and thus uninhibited cell cycle progression. P53 accumulation in the nucleus is associated with poor prognosis in patients suffering from bladder cancer (Esrig et al., 1994). However, it has been shown that inducing P53 mutations in mouse urothelium induces tumor formation, which does not progress to advanced invasive stages (Gao et al., 2004). This pointed towards the hypothesis that single mutations in certain genes were not sufficient to drive development of muscle invasive bladder cancers. In another study, it has been shown that simultaneous mutations/ deletions in TP53 and PTEN (Phosphatase and tensin homology) genes resulted in highly aggressive bladder cancers, with metastasis to lymph nodes and other distant organs such as liver, spleen etc. (Puzio-Kuter et al., 2009).

Wnt signalling pathway:

The Wnt pathway regulates several crucial cellular processes such as cell fate determination, cell polarity, motility etc. Wnt signaling is initiated by binding of Wnt to the cell surface receptors called Frizzled (FZD) leading to phosphorylation and activation of effector protein called lipoprotein receptor related protein (LRP). The Wnt – FZD-LRP complex then recruits proteins dishevelled (DVL) and Axin and inhibits β-

catenin phosphorylation. When inhibited β-catenin is targeted to the scaffold protein Adenomatous polyposis coli (APC) (He et al., 2004; MacDonald and He, 2012). Wnt signalling pathway has been shown to be implicated in cases of several cancers mostly through mutations in the protein Adenomatous polyposis coli (APC). APC acts as a scaffold for β-catenin, which is the key downstream responder of Wnt signaling. Somatic and germline mutations in APC have been reported in a large percentage of colorectal cancers (Kinzler et al., 1991; Rubinfeld et al., 1993). The role of Wnt signalling pathway in bladder cancers remains unclear and somewhat controversial. Some studies have reported somatic LOH (loss of heterozygosity) mutations in APC in only about 6% of analysed bladder cancers (Miyamoto et al., 1996), whereas, another study reported mutation in APC in about 50% of analysed tumor samples (Böhm et al., 1997). Contradicting both of these findings, another larger study reported no mutations in APC in the 22 bladder cancer tumor samples and 4 cell lines studied (Stoehr et al., 2002). All these studies however do not differentiate between NMIBC and MBIC. Immunohistochemistry analyses of several bladder cancer samples have shown an upregulation of β-catenin indicating that Wnt signalling (Kashibuchi et al., 2006; Shimazui et al., 1996) and mutations in APC or other proteins of this signalling pathway could be present in bladder cancers. Inhibition of Wif1 (Wnt inhibitory factor 1), an inhibitor of Wnt signalling, was reported through CpG island hypermethylation of Wif1 promotor, supporting the hypothesis of upregulation of Wnt signalling in bladder cancers (Urakami et al., 2006). Epigenetic inhibition of another antagonist of Wnt signalling, secreted frizzled receptor proteins (SFRP), was found to be associated with MIBC. Positive linear correlation was found between MIBC, frequency of methylation (thus inactivation) of Wnt antagonist SFRPs and overall patient survival in a study of a cohort of 355 patients, suggesting involvement of this signalling pathways in MIBC (Marsit et al., 2005). Overall, Wnt signalling appears to be important in invasive bladder cancers. A strong anti-correlation between Wnt signalling activation and activation of either the MAPK pathway or PI3K pathway has also been implicated in bladder cancers (Ahmad et al., 2012).

In summary, several crucial cell proliferation, motility and cell fate pathways are implicated in bladder cancers (**Fig 3**). Some are specific and more prominent in NMIBC, as for instance the RAS/MAPK pathway, and others are found in MIBC, including the PTEN/PI3K pathway. However, most of these findings come from genetic and epigenetic studies.

PI3K-Akt-mTOR pathway:

PTEN (Phosphatase and tensin homology) is a lipid phosphatase, which functions in the dephosphorylation of phosphatidyl-3,4,5-triphosphate. PTEN-dependent dephosphorylation of this lipid is antagonistic to the function of class I phosphoinositide-3-kinase (PI3K). PTEN activity leads to decrease in cell proliferation and survival signals. Indeed, PI3K activity is important for the phosphorylation of AKT (or protein kinase B), the serine/ threonine kinase that regulates multiple cellular processes such as cell proliferation, glucose metabolism etc. PI3K dependent phosphorylation and activation of the AKT signaling pathway. This pathway is crucial for cell proliferation through downstream activation of mammalian target of rapamycin complex 1 (mTORC1). Thus, PTEN activity collectively leads to inhibition of cell growth and survival (Dahia, 2000). Inhibitory PTEN mutations or loss of PTEN heterozygosity have been reported mostly in MIBC, and have been found in about 94% of advanced bladder cancer cases (Tsuruta et al., 2006). In the case of NMIBC, PTEN mutations are found to be very rare. In fact, the degree of the decrease in PTEN expression has been positively correlated to bladder cancer aggressiveness (Tsuruta et al., 2006). Because PTEN inhibition leads to aberrant cell proliferation, as a result of uninhibited AKT signaling and downstream mTORC1 activation, studies have focused on the effect of mTORC1 inhibitors in MIBC (Ching and Hansel, 2010). A whole genome sequencing approach was performed to identify the genetic basis of durable remission of MIBC patients that were treated with the mTORC1 inhibitor everolimus (Iyer et al., 2012). They found that loss of function mutations in tuberous sclerosis complex 1 (TSC1), which is a negative regulator of mTORC1 pathway (discussed in more details in later sections), correlated with the response to everolimus therapy in muscle invasive bladder cancers (Iyer et al., 2012). Identifying TSC1 mutations as a possible biomarker for using mTORC1 inhibitor during therapy. Additionally, mammalian target of rapamycin complex 2 (mTORC2) activation levels have also been found to be significantly increased in MIBC (Gupta et al., 2013). Interestingly, histology of tumors from mice with simultaneous deletions of P53 and PTEN showed elevated levels of phosphorylated mTORC1, and rapamycin treatment of these mice (that inhibits mTORC1) led to regression of tumors (Puzio-Kuter et al., 2009).

Ahmad et al., 2012

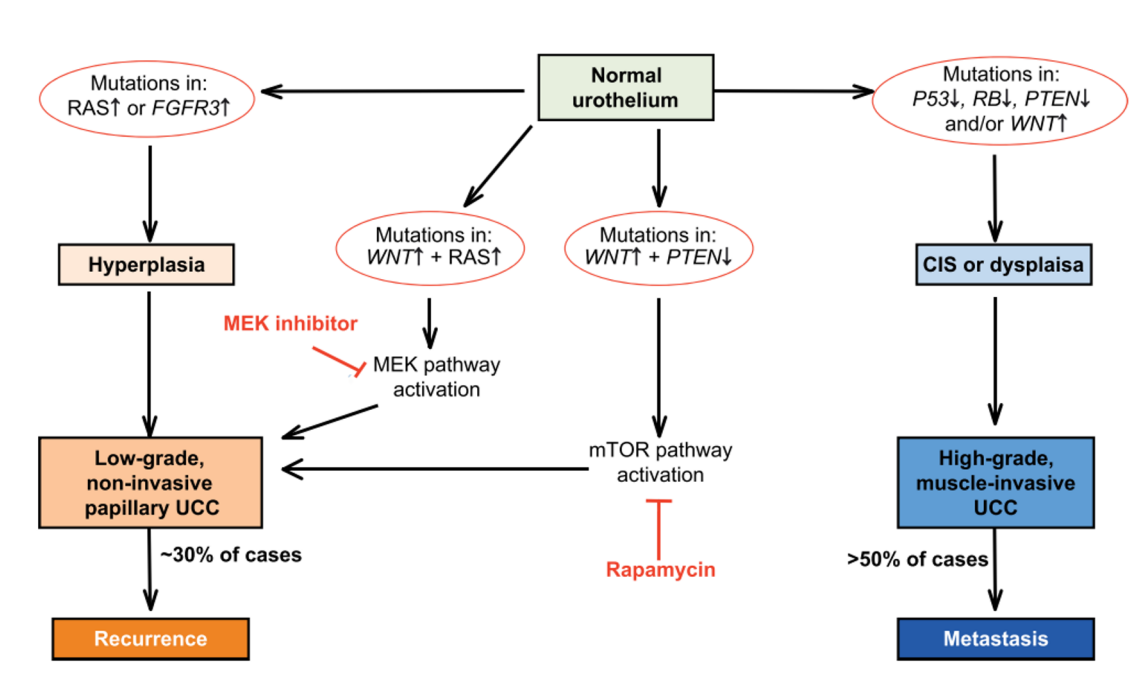

Fig 3 : Signaling pathways implicated in Bladder cancers

1.3. Bladder cancer therapies

NMIBC therapeutic strategies:

Targeting NMIBC is relatively mild to the patients, as the therapy can be applied directly to the intraluminal regions of the bladder. This is termed as intravesical chemotherapy, avoiding the exposure of the rest of the body to toxic chemicals. Given the high chances of reoccurrence of NMIBC, relapses of cancer therapy are very frequent and add complexity to their treatment. Intravesical therapeutic drugs, such as mitomycin C, doxorubicin, gemcitabine etc., all targeting the process of DNA synthesis in mammalian cells, are currently in use for treatments of bladder cancers. Focus of several studies is the better delivery of cancer therapeutics to the bladder in order to increase the intravesical dwell time of these drugs and enhance their effectiveness on the tumor cells lining the bladder (Tran et al., 2021). This is being achieved by implantation of carriers of therapeutics into bladder, thus, facilitating slow diffusion of the drug into tumor cells. One such carrier system is the gemcitabine-releasing intravesical system (TAR-200) that is being used in NMIBC (Tran et al., 2021). Mixing the chemotherapeutic drugs with hydrogels has also shown to improve dwell time and

efficiency of the drug in NMIBC. Clinical trials using Mitomycin C with hydrogels for NMIBC has been successful in reducing the reoccurrence rate of the disease and has recently been approved by the FDA.

Immunotherapies are also being employed for the treatments of NMIBC. Bacillus Calmette-Guerin (BCG) immunotherapy has been used as a standard treatment for NMIBC. Especially for the cases with a high risk of reoccurrence, this therapy has been very effective at preventing relapse and results in better patient survival (Lamm et al., 2000). However, BCG refractory cases, in which the cancer reappears after 6 months of BCG treatment, also exists, and in these cases combining BCG therapy with other therapies is being evaluated. Other immunotherapies include the ICIs (Immune Checkpoint Inhibitors) therapy (Bellmunt et al., 2017). Recently, pembrolizumab, which is a blocking antibody against Programmed Death 1 (PD-1), was approved by FDA as an ICI therapy drug that could be used in combination with the BCG therapy for 'BCG refractory' patients. PD-1 receptor protein is expressed on the surface of T cells and has an inhibitory activity on them. Blocking of PD-1 helps to activate T cells, and thus, facilitates the targeting of tumor cells by patient immune system (**Fig 4**). Several other immunotherapies are currently being used to treat patients of NMIBC such as IFNα, IL15, IL2 etc. to mention a few.

MIBC therapeutic strategies:

The focus of the treatments of MIBC aims at slowing down the metastatic disease and preventing reoccurrence of tumors at the metastatic sites post treatment. One important consideration of MIBC treatments is predicting chemotherapy sensitivity of patients in order to prevent exposure to unnecessary toxicity to the ones resistant to chemotherapy. Expression of certain genes is monitored to predict sensitivity of patients to chemotherapies. For instance, high expression of copper transporter 1 (CTR1), which delivers cisplatin to bladder cancer cells, is associated with better sensitivity to chemotherapy. Additionally, patients with loss of function mutations in the DNA damage response genes, such as BRCA1, ERCC1 and ERCC2, have also been reported to have better cisplatin sensitivity and better survival post chemotherapies (Teo et al., 2017).

Another approach of treatment of MIBC is monitoring the expression of different cell surface markers on the bladder cancer cells. Targeting abundantly expressed cell surface markers with a specific antibody that is tagged with a toxin or drug has given

rise to specific chemotherapeutics termed ‘antibody-drug conjugates’ (ADC). FDA has recently approved one such ADC called enfortumab vedotin that has given positive outcomes in phase II clinical trials and is now being used for patients suffering from metastatic bladder cancers (Tran et al., 2021).

ICIs (Immune Checkpoint Inhibitors) therapy is also used in MIBC. ICIs have proven to be very successful against cancers, which have a very high frequency of mutations including melanomas and non-small-cell lung carcinomas. In MIBC, instead of targeting the PD-1 receptor described previously for NMIBC, Programmed Death Ligand 1 (PDL1) targeted therapies are approved by the FDA and are used. PDL1 is present on tumor cells, binds to PD1 on activated T cells and exerts inhibitory signals to T cells to escape their antitumor signals (**Fig 4**) (Lei et al., 2020).

Lei et al., 2020

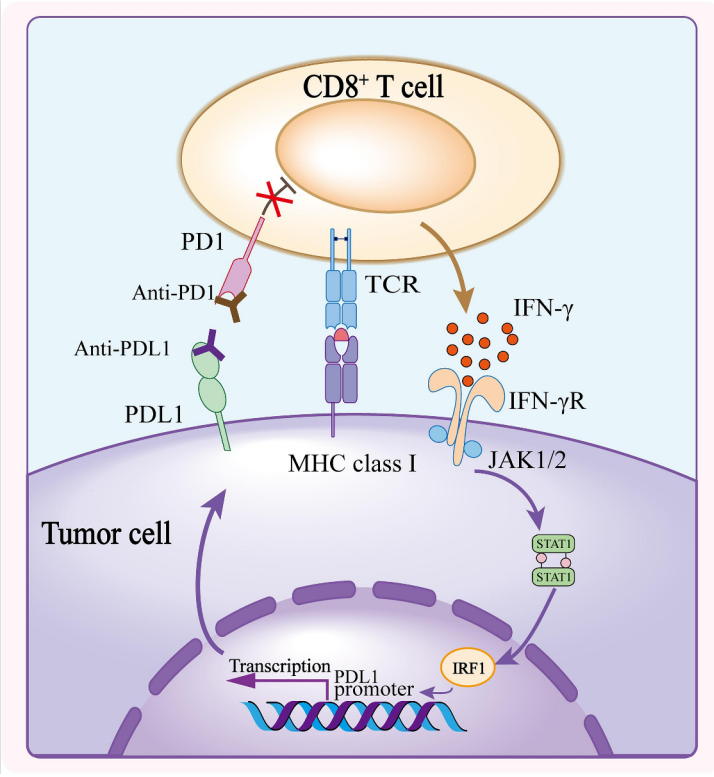

Fig 4 : PD1-PDL1 therapy axis

Avelumab is one such anti-PDL1 therapy drug that is used as the first line treatment for the patients suffering from MIBC.

Described above are some basic and general therapies for patients suffering from NMIBC or MIBC, focusing on blocking DNA synthesis in tumor cells or targeting them through the patient immune system. Additionally, building on the knowledge of various 'omics' studies, describing the pathways and molecular players involved in bladder cancers, several pathway specific drugs are also in clinical trials for treatments of bladder cancers, as discussed next.

Pathway specific bladder cancer therapeutics:

As mentioned earlier, reoccurrence and relapses are one of the pressing concerns of NMIBC. This makes it important to build on the current therapies, but also develop novel targeted therapies based on our current understanding of the molecular players driving bladder cancers. Because the most frequent mutations observed in NMIBC are whose in FGFR3 and Ras (discussed above), and both of these pathways lead to the activation of MAPK signaling, most of the targeted therapeutics for NMIBC have focused on inhibiting these targets. One tested way of inhibiting Ras proteins is targeting their lipidation, or more precisely their farnesylation. Farnesylation is facilitated by the farnesyltransferase, and farnesyltransferases inhibitors (FTIs) have shown positive results in the inhibition of tumor growth when tested on bladder cancer cell lines (Wu, 2005). In clinical trials however, FTIs have not been very successful, which has been attributed to the capability of tumor cells to compensate farnesyltransferase inhibition with geranylgeranyl transferase. Several other Ras inhibitors, for instance the dominant negative Ras mutant N116Y, have been shown to have significant tumor reduction in aggressive bladder cancer cell lines (Wallerand et al., 2011). Several other Ras pathway inhibitors have been tried and shown positive results in bladder cancer cell lines, but unfortunately they have not been successful in clinical trials (Wallerand et al., 2011) (**Fig5**) .

Anti-FGFR therapies are also developed for the use in NMIBC. Monoclonal antibodies targeting FGFR3 extracellular domain have shown anti-tumor effects in preclinical studies (for instance the bladder cancer cell lines RT112 used in the course of this project, table 1). Moreover, specific small molecule inhibitors against FGFR3 that target the cytoplasmic, catalytic domain have shown cytotoxic effects in tumor cells

with FGFR3 mutations (Zhu et al., 2005). **Fig 5** below highlights the various targeted therapies (mentioned in brief above) being tested for the treatments of NMIBC.

Wallerand et al., 2011

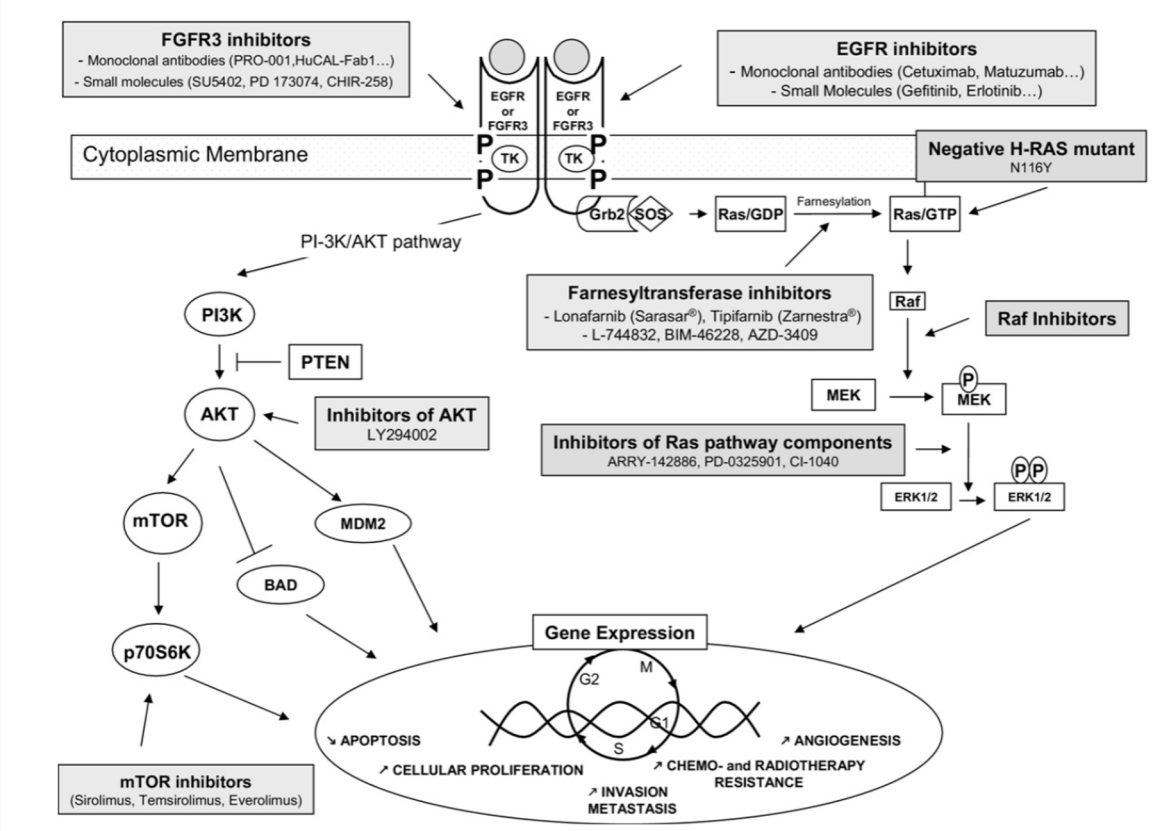

Fig 5. Targeted therapies against the potential molecular players and pathways implicated in NMIBCs.

Anti-FGFR therapeutics are currently in several clinical trials for the treatment of MIBC. In addition to the FGFR targeted therapeutics, the PI3K/AKT/mTOR pathway is targeted, which has also been reported to be important in advanced bladder cancers with PTEN mutations (discussed above). Because PTEN mutations are most prevalent in advanced bladder cancers, and mutant PTEN leads to downstream activation of PI3K, several components of this pathway have been studied as molecular targets of possible importance in MIBC. Drugs targeting PI3K, AKT or mTOR are currently in clinical trials, however, have not given promising results in slowing cancer progression in advanced MIBC. Rapamycin or sirolimus is one such mTOR inhibitor that is used in treatments of pancreatic and kidney cancers. Although these drugs have shown to slow down the proliferation in bladder cancer cell lines (Mansure et al., 2009), they

unfortunately did not show a promising result in clinical trials (Thomas and Sonpavde, 2022). Additionally, Everolimus, another mTOR inhibitor used in phase II clinical trials with patients suffering from advanced bladder cancers with mTOR or TSC1/2 mutations (tuberous sclerosis complex 1 / 2, upstream regulator of mTORC1), has also not shown positive results (Adib et al., 2021).
Failure of PI3K / AKT/ mTOR pathway inhibitors in advanced bladder cancers has been attributed to crosstalk with the Ras-MAPK pathway as well as to redundancy in the downstream effectors between these two signaling axes. This inter-pathway crosstalk helps cancer cells to escape the inhibition of one signaling pathway by upregulation of the other one, and hence makes therapy less effective or failing. This kind of interdependency has also been observed in cases of melanomas (Nazarian et al., 2010).

In addition to the inhibition of these classical signaling pathways, novel therapies specific to lysosome functions and autophagy are emerging in the treatment of bladder cancers (Lin and Hwang, 2017). Autophagy inhibitors such as Chloroquine (CQ) and Hydroxychloroquine (HCQ) are used as adjuncts along with routine chemotherapeutics, such as cisplatin and mitomycin C (discussed above), and have proved to be quite effective against bladder cancer (Ojha et al., 2016). Additionally, increased autophagy and lysosome acidity have been highlighted in bladder cancers without a clear explanation on the driver of these phenotypes or its importance in cancer development. Inhibition of basal autophagy has been shown to induce apoptosis in bladder cancer cells (Lin et al., 2016).

These observations point towards the importance of autophagy and lysosomal pathways in bladder cancers. Lack of effective treatments also makes it crucial to understand better the supporting features of lysosomal pathways in bladder cancers. Additionally, as cancer cells are adapted to escape most of the molecular targeted therapies by compensation mechanism, targeting cancer cells at a higher cellular scale, such as at organelle levels, could provide alternative and more effective strategies. During my PhD, I have focused on studying the lysosome-dependent dysregulation in the bladder cancer model employing several cell lines representing different molecular features and grades.

1.4. Lysosomal functions: General overview and lysosomal signaling pathways

Lysosomes are organelles discovered in 1955 by Christian de Duve (de Duve et al., 1955). They perform diverse functions, starting from their classical role in degradation, which was considered their primary function for a long time, to a wide range of other crucial functions often implicated in cancers. There are multiple models in literature explaining the formation of lysosomes. First model describes the 'maturation' pathway, where endocytic vesicles (EV) with the endocytosed cargo mature into early endosomes (EE) and then late endosomes (LE) and subsequently to lysosomes. Cargo could be recycled through recycling vesicles (RV) or degraded in lysosomes. In this model, lysosomes are formed during vesicular transport that involves formation of multi vesicular bodies (MVB) with intraluminal vesicles (ILVs) from the endocytic vesicles, transport of cargo from early to late endosomes (LE) and finally fusion with lysosomes. Another model of lysosome formation is the 'kiss and run' mechanism where LE derived from the endocytic vesicles, establish contacts with lysosomes to deliver the cargo and then dissociate again back to LE and Lysosomes. Lastly, another model describes a fusion and fission event involving fusion of LE and lysosomes to give a hybrid organelle and lysosomal reformation (Trivedi et al., 2020) (**Fig 6**). Lysosomes have gained attention over the last decade and emerge a crucial organelle not only for lysosome-specific functions but also for the integration of different metabolic pathways.

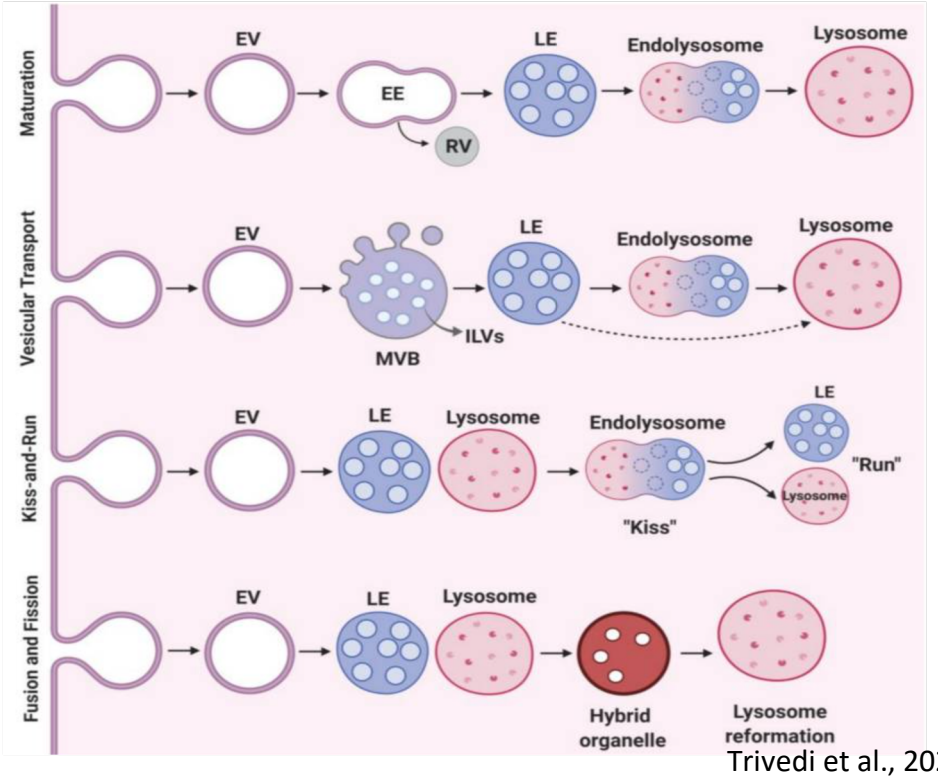

Trivedi et al., 2020

Fig 6. Pathways of lysosome formation

Multiple Functions of Lysosomes - an overview:

The primary role of lysosomes as 'the garbage disposal system' or 'digestive bodies' of the cell is based on findings that lysosomes contain a plethora of hydrolases that can break down / digest proteins, carbohydrates, lipids and nucleic acids that are delivered to lysosomes (Gordis, 1966; Schröder et al., 2010). The intracellular pH of lysosomes is maintained at an acidic range of 4.5-5.0. This acidic pH is achieved through the vacuolar ATPase (v-ATPase) H^+ pump, present as an integral membrane protein at the lysosomes (Ohkuma et al., 1982). In addition to v-ATPases, lysosomes contain several ion channels**,** lipid transporters and solute carriers (Mindell, 2012) that participate in the transport of sugars, nucleosides and other products of lysosomal degradation (Zoncu and Perera, 2022). Lysosomes also contain several heavily glycosylated membrane proteins called lysosome-associated membrane proteins or LAMPs that, among other functions, protect the membrane of lysosomes from degradation. Lysosomes perform multifaceted functions in mammalian cells some of which are summarized below:

1) Lysosomes as the signaling platform: The cytosolic face of lysosomes is the platform for the assembly of several signaling complexes that associate with lysosomes in response to cellular cues to such cellular nutrient status and other environmental stimuli and maintain cellular homeostasis, as discussed next.

Nutrient sensing and mTORC1 signaling: Stimulus such as nutrient status of the cells are sensed by the lysosomes through the nutrient regulated kinase complex called mechanistic target of rapamycin complex 1 (mTORC1) (Saxton and Sabatini, 2017). mTORC1 associates dynamically on the surface of lysosomes to initiate anabolic responses and to inhibit catabolic responses such as autophagy, for instance by phosphorylation of Unc-51-like kinase 1 (ULK1) (Hosokawa et al., 2009). In response to amino acids, mTORC1 is recruited and activated on lysosomes by the protein complex containing Rag GTPases and Ragulator (Sancak et al., 2010). Rag GTPases belong to the family of RAS related GTPases and are composed of 4 types, which are RagA, RagB, RagC and RagD. They function in the form of heterodimers formed by RagA or C and RagB or D. Ragulator is a big pentameric (LAMTOR1-5) protein complex located on the surface of lysosomes, it activates mTORC1 together with Rag GTPAses. Interestingly, in addition to sensing amino acids, the lysosome

surface also harbors the cholesterol transporter Niemann–Pick type C1 protein (NPC1) that, through the release of cholesterol, can activate mTORC1 (Castellano et al., 2017). Surface of lysosomes also acts as the platform for recruitment of transcription factors such as transcription actor EB (TFEB), to inactivate catabolic pathways like autophagy, which are transcriptionally regulated by TFEB (Settembre et al., 2013a). This recruitment also happens as a response to cellular nutrients (Martina and Puertollano, 2013). The machinery of mTORC1 assembly and activation is presented in the next section as the nutrient sensing function of lysosomes.

Calcium signaling: Lysosomes exhibit on their surface 3 main calcium channels, which are the transient receptor potential cation channels of the mucolipin family (TRPML), trimeric Ca2+ two-transmembrane channel P2X and the two-pore channels (TPC) (Morgan et al., 2011). Calcium release from lysosomes has been shown to be important for the fusion to endosomes, autophagosomes, plasma membrane, thus regulating trafficking pathways (Morgan et al., 2011). TRPML1 or mucolipin 1 is the most characterized calcium channel on lysosomes. Activation of TRPML1 happens during starvation or oxidative stress and results in release of calcium from lysosome to the cytosol (Wang et al., 2015). TRPML1 has been shown to be important for lysosomal adaptation functions through TFEB, because calcium release from TRPML1 is involved in activation and nuclear translocation of TFEB (Medina et al., 2015). Overexpression of TRPML1 and calcium release from lysosomes facilitates lysosomal exocytosis (Medina et al., 2011), which could provide membranes for phagocytosis of large particles (Samie et al., 2013). Additionally, TRPML1 activation facilitates migration of dendritic cells by activation of actin-dependent motor protein myosin 2 (Bretou et al., 2017).

2) Lysosomes in cellular adaptation: Cellular metabolism needs to be adapted according to the environmental conditions and requires lysosomes to change their functions accordingly. Lysosomal functions are regulated through a gene network termed as the ‘CLEAR’ network that stands for ‘coordinated lysosomal expression and regulation’, and TFEB was found to be a master regulator of this gene network (Sardiello et al., 2009; Settembre et al., 2011). TFEB belongs to the MiT/TFE family of transcription factors along with MITF (Microphthalmia-associated transcription factor), TFE3 (Transcription factor E3) and TFEC (Transcription factor EC), all of which are helix-loop-helix leucine zipper proteins (Hemesath et al., 1994). TFEB broadly

regulates genes involved in autophagosome biogenesis, autophagosome-lysosome fusion, lysosomal acidification, lysosomal exocytosis, lysosomal degradation, lysosomal biogenesis as well as lysosome positioning, and thus, broadly control autophagy and lysosomal functions (Medina et al., 2011; Palmieri et al., 2011; Sardiello et al., 2009; Settembre et al., 2011; Willett et al., 2017). Other members of this family of transcription factors have some overlapping functions with TFEB. For instance, TFE3 is known to regulate lysosomal biogenesis and autophagy. There is a redundancy in metabolic functions of TFEB and TFE3 (Martina et al., 2014; Pastore et al., 2017). Additionally, a recent report showed that both, TFEB and TFE3, regulated genes involved in maintaining the circadian rhythm (Pastore et al., 2017). TFEB, similar to its family members, is inactivated, and thus, regulated at the surface of lysosomes through phosphorylation by mTORC1. Activation of TFEB during starvation or cellular stress leading to nuclear translation of TFEB and activation of the CLEAR network genes forms the basis of lysosomal adaptation functions (Ballabio and Bonifacino, 2020). Mechanisms of regulation of TFEB are discussed in next sections in more details.

3) Lysosomal in organelle fusion: Lysosomal functions as degradation, require fusion of lysosomes with other organelles. Lysosomes can associate with several tethering complexes, soluble N-ethylmaleimide-sensitive factor attachment protein receptors (SNARE) proteins and small GTPases that facilitate these fusion events. SNAREs assemble on lysosomes as trans SNAREs, which are composed of 4 α-helix bundles. Depending on the residue in the layers of this bundle SNAREs can be either ‘Q’ or ‘R’ type. Organization of trans SNARE complex (with one R-SNARE and 2 or more Q-SNARE) requires release of calcium from lysosomes (Hesketh et al., 2018). The type of SNARE present on the lysosomes guides to which organelle lysosomes will fuse. For instance, lysosomal fusion is important for degradation of cargos. An important step in the degradation of endocytic vesicles is the fusion of late endosomes (LE) and lysosomes (**Fig 6**). This fusion is regulated by the small GTPase, Arf-like GTPase 8 (Arl8) and the hetero-hexameric tethering complex called mammalian homotypic fusion and vacuole protein sorting (HOPS), which together assemble the trans SNARE complex on lysosomes (Garg et al., 2011). This trans SNARE complex is formed of syntaxin 7 (Q-SNARE), syntaxin 8 (Q-SNARE), VTI1B (Q-SNARE) and Vesicle-associated membrane protein 7 and 8 (VAMP7/VAMP8) (R-SNARE) (Ballabio

and Bonifacino, 2020). Arl8 along with small GTPase Rab7 additionally, interact with another tethering complex PLEKHM1 (pleckstrin homology domain-containing protein family member 1) and promotes LE-lysosome fusion (Marwaha et al., 2017).

4) Lysosomal secretion via exocytosis: In addition to fusion with other organelles, lysosomes can fuse with the plasma membrane during exocytosis. Lysosomal exocytosis is required for plasma membrane repair (Reddy et al., 2001), secretion of lysosomal contents out of the cells to the extracellular milieu (Medina et al., 2011), for instance during bone reabsorption (Baron et al., 1988), or for the formation of invasive protrusions (Naegeli et al., 2017), of importance during cancer invasion. One trigger for lysosomal exocytosis is damage to the plasma membrane, which leads to a calcium influx into the cell (Reddy et al., 2001). Calcium influx is sensed by the synaptotagmin-VII (Syt-VII) on lysosomes that interacts with a trans SNARE complex. This trans SNARE complex is formed by VAMP7, (Vesicle-associated membrane protein 7, R-SNARE) localized on lysosomes, syntaxin-4 (Q-SNARE) and SNAP23 (synaptosome-associated protein 23 kDa, Q-SNARE) on the plasma membrane. Interestingly, the fusion of lysosomes to the plasma membrane secretes the lysosomal enzyme sphingomyelinase that converts sphingomyelin to ceramide (Tam et al., 2010). This forms curvature in damaged plasma membrane that is removed by endocytosis allowing resealing (Tam et al., 2010).

5) Lysosomal intra organelle contacts: Proteins present on lysosomes can facilitate non-fusion dependent functions such as lipid transports or regulating lysosomal positioning. These functions involve formation of membrane contact sites (MCS) between lysosomes and other organelles such as ER, the Golgi complex, mitochondria etc. ER-lysosome MCS are among the most characterized ones. These MCS facilitate transfer of lipids between lysosomes and other organelles. For instance, lysosomal cholesterol transporters Niemann–Pick type C1 and C2 proteins (NPC1 and 2) export cholesterol out of lysosomes. Cholesterol is taken up by the ER through the lipid transport protein ORP1L localized on lysosomes and interacting with ER membrane tethering proteins VAPA and VAPB (Luo et al., 2017). MCS also regulate lysosome positioning that is discussed in later sections as well as Ca^{2+} signaling.

Fig 7 shows an overview of the lysosome topology and respective functions that were briefly mentioned above. I will discuss lysosomal signaling pathways below as well as highlight few other lysosomal functions, which are important in cancer.

Ballabio and Bonifacino, 2020

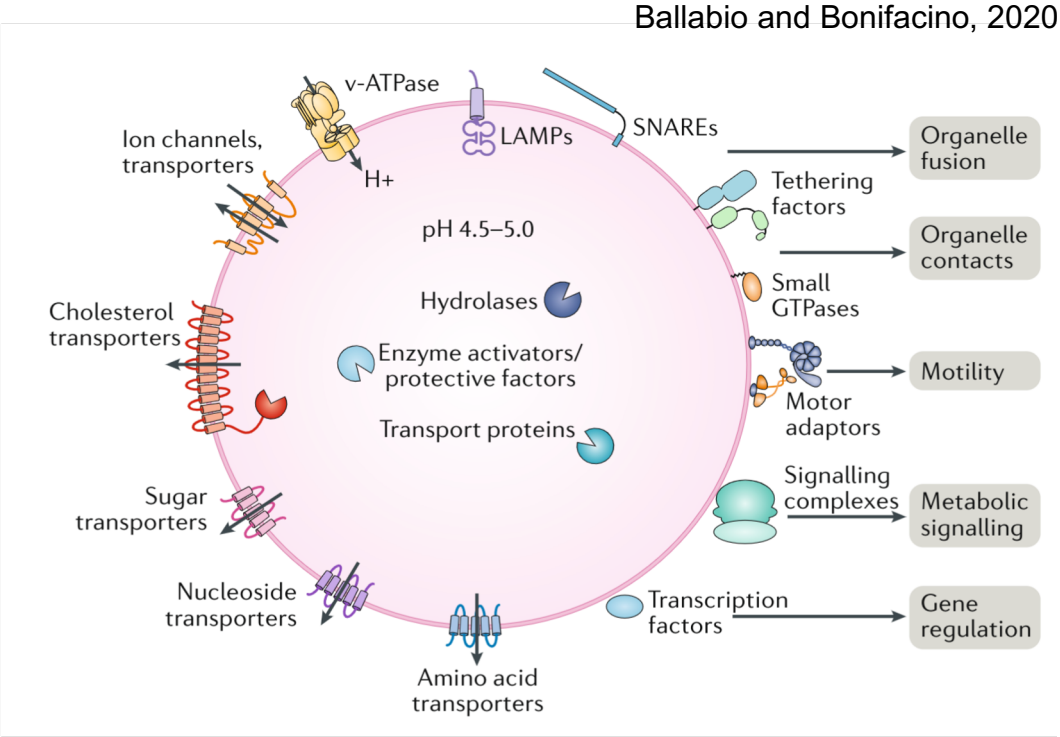

Fig 7. Lysosome topology and the associated functions.

Different activities of lysosomes are interconnected and tightly regulated in order to maintain homeostasis of mammalian cells. Thus, conditions that influence lysosomal components and their interconnected functions, either genetic, epigenetic or post translational in nature, could disturb the overall cell homeostasis, and thus, lead to development of diseases. Given the wide range of functions that lysosomes participate in, diseases originating from lysosomal dysfunctions are quite varied. Chief among them are the lysosomal storage disorders (LSDs). LSD are the best example of diseases that results from lysosome functional defects, and which result in complex multisystemic pathologies. LSD often result from defects in genes coding for lysosomal enzymes e.g., Pompe disorder is caused by deficiency of acid α-glucosidase and leads to accumulation of glycogen in cell. Some LSD result from defects in lysosome membrane proteins, e.g. mucolipidosis type IV is caused by mutations in TRPML1 calcium channel and causes defects in lysosomal trafficking (Bassi et al., 2000). Moreover, Niemann–Pick disease type C1 is caused by mutations in the cholesterol

channel NPC1 and leads to cholesterol accumulations in lysosomes (Platt, 2018). A secondary effect of LSD can be aberrant mTORC1 signaling, as seen in Niemann–Pick disease type C1, where accumulation of cholesterol causes mTORC1 overactivation (Bartolomeo et al., 2017). Other than LSDs, disruption of lysosomal functions have been observed in some common neurodegenerative diseases such as Parkinson's, Alzheimer's, Huntington's disorders etc. (Nixon, 2013). More recently, lysosomal dysfunctions have been implicated in cancers (Kimmelman and White, 2017).

Lysosomes are the nutrient sensors of the cell:

Fed state – Anabolic responses through mTORC1

Mechanistic target of rapamycin complex 1 (mTORC1) is a master regulator of cell anabolic responses, which assembles and signals from the surface of lysosomes. mTORC1 signaling is regulated by amino acids and growth factors. mTORC1 is a multi-subunit protein complex and has the following core components: the core kinase mTOR, the regulatory protein associated with mTOR (RAPTOR), Proline-rich Akt substrate of 40 kDa (PRAS40), DEP domain containing mTOR-interacting protein (DEPTOR) and mammalian lethal with Sec13 protein 8 (mLST8) (Hara et al., 2002; Peterson et al., 2009; Sancak et al., 2007). RAPTOR acts as a scaffold protein for subcellular localization of mTOR on lysosomes. mLST8 associates with the catalytic domain of mTOR and stabilizes interaction of mTOR and RAPTOR. PRAS40 and DEPTOR are inhibitors of the kinase activity of mTORC1 (Saxton and Sabatini, 2017) (**Fig 8**).

Saxton and Sabatini, 2017

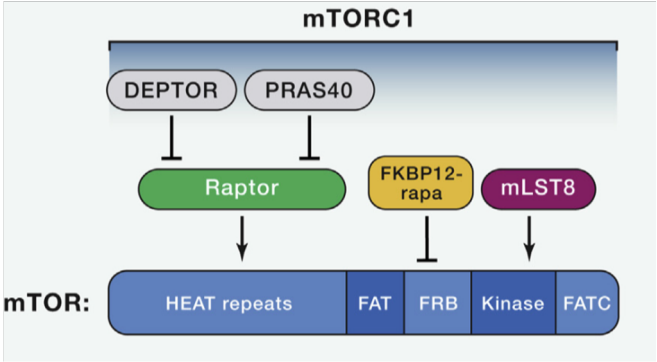

Fig 8. mTOR complex 1 sub-units

In response to nutrient rich conditions, mTORC1 is recruited to the surface of lysosomes. This recruitment is regulated by Rag GTPases, which function as heterodimers, the active form containing GTP-bound RagA or RagB and GDP- bound RagC or RagD. Amino acids have been shown to regulate guanine nucleotide state of the Rag GTPases (Kim et al., 2008; Sancak et al., 2008). In the presence of amino acids, RagA or B are loaded with GTP and RagC or D are loaded with GDP. This shuffling between GTP and GDP states is facilitated by specific GTPase-activating proteins (GAPs) and guanine nucleotide exchange factors (GEFs). Particularly, the pentameric scaffold protein called 'Ragulator' on lysosomes acts as the GEF for Rag GTPases and leads to GTP binding of RagA/B. Two GAP complexes that cause GTP hydrolysis to GDP have been characterized, GATOR1 and Folliculin. In the presence of leucine and arginine, GATOR2 inhibits GATOR1 and prevents its GAP activity on RagA/B. In contrast, Folliculin causes RagC/D to become GDP bound in the presence of amino acids, which is required for mTORC1 recruitment. Thus, Rag GTPases in their active form (RagA/B with GTP and RagC/D with GDP) bind to lysosomes via the 'Ragulator' and interact with RAPTOR to bring mTOR to the surface of lysosomes (Sancak et al., 2010) (Lim and Zoncu, 2016). v-ATPase, along with amino acid transporter SLC38A9, also regulate the activity of Ragulator at lysosomes in an amino acid dependent manner. Thus, lysosomes are not only the docking station for the mTOR kinase but connect cellular and lysosomal amino acids concentration to mTORC1 recruitment (Zoncu et al., 2011). At the surface of lysosomes, mTORC1 is additionally activated by the small GTPase Rheb (Ras homolog enriched in brain). Activity of Rheb is negatively regulated by the TSC1/2 complex (tuberous sclerosis complex 1 and 2) and TBC1D7 (TBC1 domain family member 7), which act as GAPs for Rheb (Puertollano, 2014). Activity of TSC1/2 complex is regulated by phosphorylation through the PI3K-Akt signaling pathway downstream of growth factors. Phosphorylation inactivates TSC1/2, and thus, reduces its inhibitory effect on Rheb leading to activation of mTORC1 (Demetriades et al., 2014). The activation of mTORC1 in response to amino acids and growth factors through the lysosome nutrient sensing machinery (LYNUS) is summarized in **Fig 9** (Lim and Zoncu, 2016). mTORC1 activity is also regulated by lysosome positioning.

Lim and Zoncu, 2016

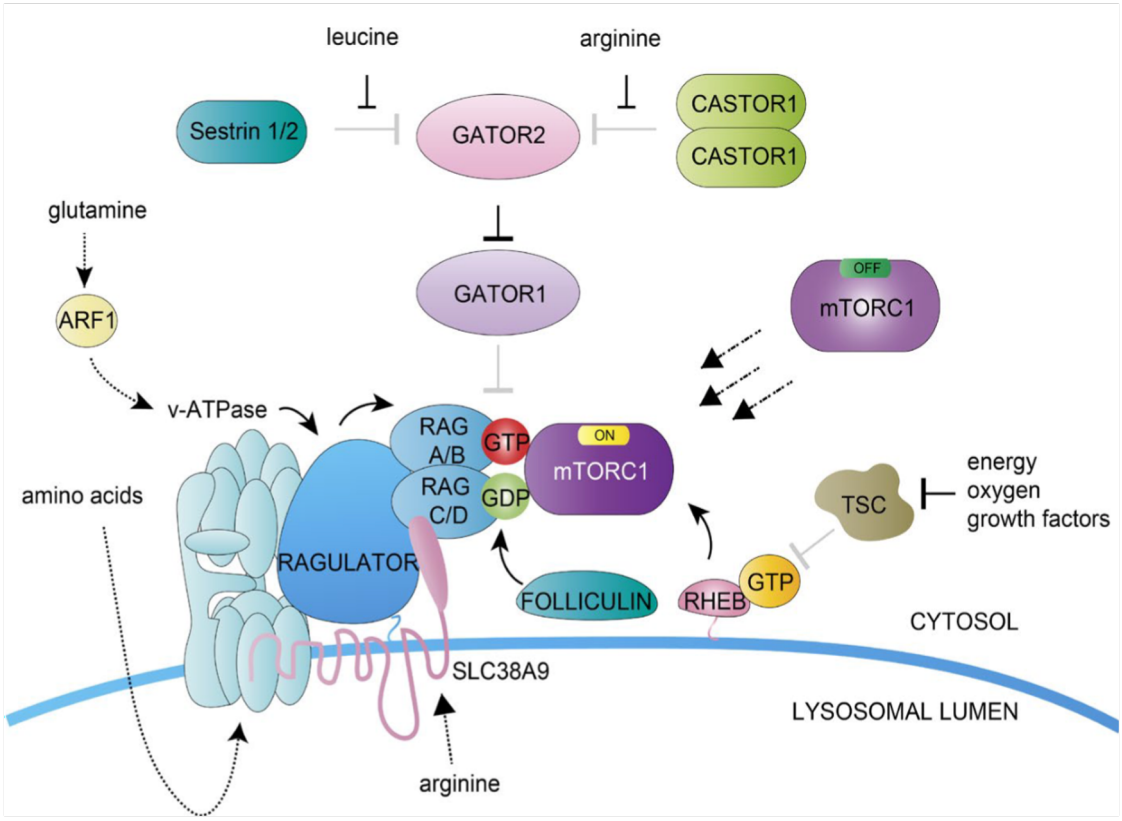

Fig 9. Lysosome nutrient sensing machinery (LYNUS): Activation of mTORC1 on lysosomes in response to amino acids (cytosolic and lysosomal) and growth factors.

Downstream pathways of mTORC1 activation:

mTORC1 is a master regulator of cell anabolism that controls cellular functions like: protein synthesis, protein turnover and lipid / nucleotide/ glucose metabolism (Saxton and Sabatini, 2017).

Protein synthesis is regulated by mTORC1-dependent phosphorylation of p70S6 kinase 1 (S6K1) and eIF4E Binding Protein (4EBP). mTORC1 kinase phosphorylates S6K1 at Thr389 and 4EBP at multiple sites (Gingras et al., 1999). Phosphorylation of S6K1 leads to its activation and thus downstream phosphorylation of different substrates which promote initiation of mRNA translation. S6K1 phosphorylates and activates eIF4B, which helps in binding of eIF4F to the 5' cap of mRNA to initiate translation (Holz et al., 2005). S6K1 also inhibits programmed cell death protein 4 (PDCD4) which is the negative regulator of eIF4B (Dorrello et al., 2006). mTORC1 substrate 4EBP is a negative regulator of translation. 4EBP binds to eIF4E and prevents translation by inhibiting the assembly of the translation initiation complex.

Phosphorylation of 4EBP by mTORC1 causes its inhibition and dissociation from eIF4F allowing 5' cap dependent translation (**Fig 10**)(Saxton and Sabatini, 2017).

Protein turnover regulation is another function of mTORC1. Active mTORC1 suppresses catabolic processes such as autophagy. One of the direct substrates of mTORC1 is Unc-51 Like Autophagy Activating Kinase 1 (ULK1) kinase, which when phosphorylated and inactivated, is unable to assemble complexes of autophagy initiation (Kim et al., 2011). Additionally, mTORC1 phosphorylates the transcription factor EB (TFEB), the master regulator of lysosomal biogenesis and autophagy genes. Phosphorylation of TFEB leads to its cytosolic retention, and thus, inactivation (Settembre et al., 2012). I will discuss in detail the function and regulation of TFEB in the next section (**Fig 10**).

Finally, mTORC1 regulates cellular biochemical pathways involved in lipid, glucose and nucleotide anabolism. mTORC1 controls lipid metabolism by activation of a lipid-sensitive transcription factor, the sterol responsive element binding protein (SREBP). SREBP regulates transcription of cholesterol and fatty acid biosynthesis genes (Porstmann et al., 2008). SREBP is activated when cells are under low cholesterol levels, but it has been shown that mTORC1 also activates this transcription factor through an undescribed mechanism dependent on S6K (Düvel et al., 2010). Additionally, mTORC1 phosphorylates and inactivates Lipin1 that inhibits SREBP, and thus again, mTORC1 activates lipid metabolism (Peterson et al., 2011). mTORC1 regulates glucose metabolism by increased translation of hypoxia-inducible factor 1-alpha (HIF1a) a transcriptional regulator of glycolytic enzymes such as phospho-fructo kinase (Düvel et al., 2010). Finally, mTORC1 regulates nucleotide metabolism by increasing activating transcription factor 4 (ATF4)-dependent expression of methylenetetrahydrofolate dehydrogenase/cyclohydrolase (MTHFD2). This enzyme provides one carbon units to the mitochondria tetrahydrofolate cycle for purine synthesis (Ben-Sahra et al., 2016). These substrates of mTORC1 involved in cellular metabolism are highlighted in **Fig 10**

Overall, mTORC1 signaling positively regulates cellular anabolic responses, which is typically expected as a response to nutrient rich conditions. Activation of anabolism leads to a 'fed' cellular state, increase in cell mass, which triggers cell proliferation.

Saxton and Sabatini, 2017

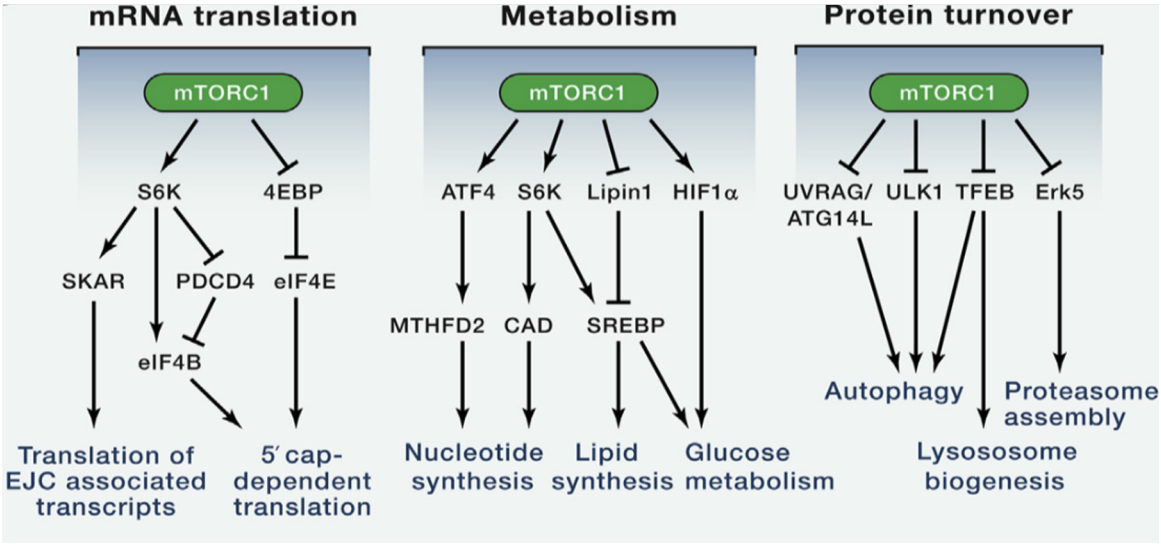

Fig 10. Downstream of mTORC1: Substrates phosphorylated by mTORC1 and their respective function

Lysosomal adaptation and catabolic response through TFEB:

TFEB is a MiT/TFE family transcription factor that regulates autophagy and lysosomal functions by regulating genes expression of the CLEAR (coordinated lysosomal expression and regulation) network genes. In this section, I focus on the regulation of TFEB and MiT/TFE transcription factor and downstream functions of TFEB that arise from expression of CLEAR network genes. Older studies have shown that during steady state or fed conditions, most of the TFEB is localized in the cytoplasm (Sardiello et al., 2009). In conditions of starvation or stress conditions such as infections, inflammation, exercise, mitochondrial damage etc., TFEB rapidly translocates to the nucleus (Gray et al., 2016; Mansueto et al., 2017; Nezich et al., 2015; Pastore et al., 2016; Visvikis et al., 2014). The central mechanism of regulation of TFEB, as well as other MiT/TFE family members, is their cytosolic localization and the phosphorylation status of certain serine residues of these proteins (Puertollano et al., 2018). In fed state, mTORC1 phosphorylates, and thus, inactivates TFEB and other MiT/TFE factors (Martina et al., 2012 ; Peña-Llopis et al., 2011 ; Roczniak-Ferguson et al., 2012 ; Settembre et al., 2012). Phosphorylation of TFEB leads to its retention in the cytoplasm there it remains bound to the protein 14-3-3 (Roczniak-Ferguson et al., 2012; Settembre et al., 2012). In conditions of starvation, mTORC1 is however inactivated, which prevents TFEB phosphorylation and results in TFEB nuclear

translocation. Interestingly, as TFEB is phosphorylated (at S211) by mTORC1 at the surface of lysosomes, it has been suggested that lysosomes regulate their own biogenesis by regulating TFEB (Settembre et al., 2013a). Other than mTORC1, extracellular signal-regulated kinase (ERK) and glycogen synthase kinase 3 (GSK3) also phosphorylate MiT/TFE factors, including TFEB (Marchand et al., 2015; Ploper et al., 2015). Interestingly, it has been shown that Rag GTPases that activate mTORC1 also bind to TFEB (Martina and Puertollano, 2013) suggesting that mTORC1 dependent phosphorylation and inactivation of TFEB happens on the surface of lysosomes. Whether ERK and GSK3 also phosphorylate MiT/TFE factors (and TFEB) on lysosomes is still not clear. Nuclear translocation of TFEB is also regulated through dephosphorylation by the phosphatase calcineurin (CaN). CaN is activated at lysosomes through calcium released from the lysosomal calcium channel TRPML1 (or mucolipin 1)(Medina et al., 2015), highlighting the importance of lysosomal calcium signaling in regulation of TFEB activity. Surprisingly, phosphorylation of TFEB at the residues S142 & S138 has been shown to be important for its nuclear export (Napolitano et al., 2018). However, the exact mechanism for this unexpected regulation remains unclear. Indeed, phosphorylation of TFEB at these sites would indicate the presence of mTOR in the nucleus, which has not yet been reported. **Fig 11** shows a summary of the regulation of TFEB and its shuffling between cytoplasm and nucleus.

Ballabio and Bonifacino, 2020

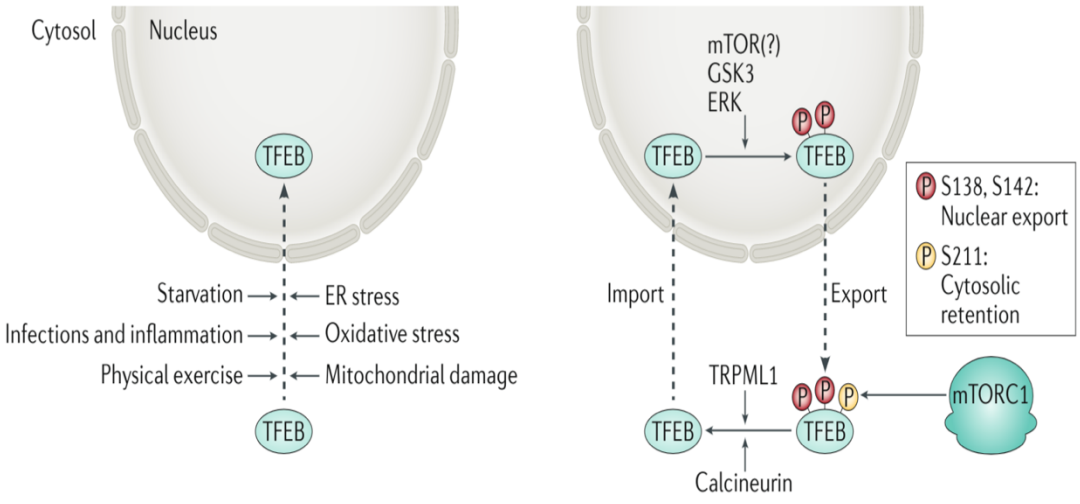

Fig 11. Factors regulating TFEB shuffling between cytosol and nucleus

Downstream pathways of TFEB activation:

Autophagy: Autophagy is the fundamental catabolic process in cells for the degradation of damaged organelles and misfolded proteins, and also plays a role in eliminating intracellular pathogens (Mizushima, 2007). Autophagy, particularly macroautophagy, proceeds through the following main steps: A) Formation of the isolation membrane during initiation, B) conjugation of ubiquitin like molecules, C) elongation of autophagosomal membranes, D) cargo recruitment to the autophagosomes, D) Fusion of autophagosomes to lysosomes. TFEB transcriptionally regulates multiple protein that are involved in these steps of autophagy. For instance, it regulates protein involved in initiation, such as Beclin-1 (BECN1), WD Repeat Domain Phosphoinositide Interacting 1 (WIPI1), autophagy related protein 9B (ATG9B), in membrane elongation, such as ATG5, LC3B, in cargo recruitment, such as, Sequestosome-1 (SQSTM1 or P62), and in autophagosome-lysosome fusion, such as Ras-related protein Rab-7 (Rab7), Vesicle Associated Membrane Protein 8 (VAMP8) etc. (Palmieri et al., 2011; Settembre et al., 2011). Thus, TFEB is a major regulator of autophagy, and TFEB activation induced this pathway in cells under starvation or stress.

Lysosomal biogenesis, membrane proteins and hydrolases: TFEB regulates a extended group of lysosome-specific genes, which all are a part of the CLEAR network. TFEB regulates lysosomal membrane proteins such as LAMP1 and Transmembrane protein 192 (TMEM192), Osteopetrosis-associated transmembrane protein1 (OSTM1), the calcium transporter TRPML1 implicated in TFEB dephosphorylation, and therefore, contributing to a feedback loop. TFEB also regulates transcription of lysosomal channels and transporters such as Chloride Voltage-Gated Channel 7 (CLC7), Proton-coupled amino acid transporter A (SLC36A) as well as subunits of v-ATPases that regulate lysosomal acidification. Several lysosomal hydrolases, e.g. Glucocerebrosidase (GBA), acid alpha-glucosidase (GAA), Beta-hexosaminidase (HEXB), are under the control of TFEB Thus, by regulating lysosome membrane proteins, transporters and channels, lysosomal acidification proteins and enzymes, TFEB is a master regulator of lysosome biogenesis and functions.

Endocytosis: TFEB has been shown to regulate genes involved in endocytosis (Nnah et al., 2019). Notably, clathrin, caveolin and EEA1 (Early Endosome Antigen 1) are CLEAR network genes. In fact, regulation of endocytosis and endocytic genes has

been shown to be a mechanism of mTORC1 re-activation after prolonged starvation (Nnah et al., 2019). This study proposes that starvation induces activation of TFEB that drives expression of endocytic genes. These contribute to endosome formation that shuttle the components of LYNUS, including p-AKT, to lysosomes that subsequently inactivates TSC complex via phosphorylation. Together, mTOR is recruited to lysosomes by the LYNUS machinery and is activated by the Rag GTPases. **Fig 12.** summarizes these steps of mTORC1 activation by TFEB driven endocytosis.

Nnah et al., 2019

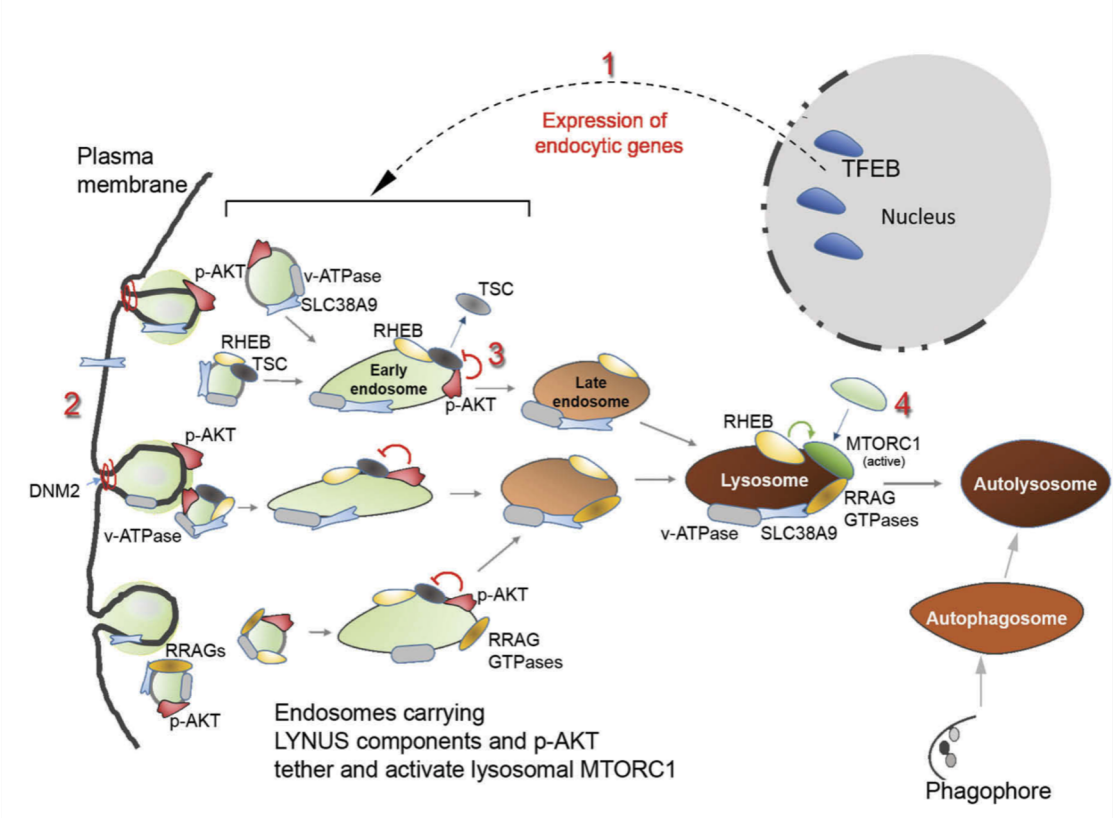

Fig 12. TFEB driven endocytosis regulates mTORC1 activation post starvation

Autoregulatory feedback loop: TFEB can bind to its own promotor, and thus regulates its own expression. In response to the lack of nutrients, there is a rapid transport of TFEB into the nucleus due to mTORC1 inactivation and loss of phosphorylation, which leads to auto-activation allowing a transcription-dependent, sustained, slower and longer response (Settembre et al., 2013b) This feedback and

autoregulation is a mediator for cells to adapt to starvation by inducing lipid catabolism through active TFEB (Settembre et al., 2013b).

Tissue specific functions of TFEB:

Liver (Lipid catabolism): Autophagy is crucial for breakdown of lipids as it shuffles lipid droplets to lysosomes where they can be broken down / hydrolyzed to free fatty acids (FFA) and glycerol. This particular kind of autophagy is termed as macrolipophagy (Singh and Cuervo, 2011; Singh et al., 2009). In contrast, the presence of high amounts of lipids can lead to switching off of autophagy (Rodriguez-Navarro et al., 2012). This can occur due to changes in the membrane proteins of lysosomes that prevent their fusion to autophagosomes, as seen by the loss of stability of LAMP2A during high fat diet. LAMP2A is a receptor on lysosomes whose loss leads to the inhibition of chaperon mediated autophagy (CMA) (Rodriguez-Navarro et al., 2012). Excess lipids can also turn off the expression of autophagic genes in liver and lead to autophagy inhibition (Yang et al., 2010). These observations showed that lysosomal and autophagic pathway, both of which are under TFEB regulation, affected cellular lipid metabolism. Transcriptome analysis performed on mouse liver after an overexpression of TFEB revealed that TFEB regulates expression of several genes involved in lipid catabolism including lipophagy, ketogenesis and fatty acid oxidation (Settembre et al., 2013b). In addition, it was found that TFEB induced protein expressions of the peroxisome proliferator-activated receptor γ coactivator 1α (PPARGC1A) and peroxisome proliferator-activated receptor α (PPARα) in a starvation induced manner (Settembre et al., 2013b). Both of these are key regulators of lipid metabolism in cells (Finck and Kelly, 2006; Lin et al., 2005).

Immune cells: TFEB and TFE3 have been implicated in regulating inflammatory and immune responses, because depletion of TFE3 and TFEB in macrophages resulted in impaired expression as well as secretion of pro-inflammatory cytokines such as Interleukin (IL)-1β, IL-6, tumor necrosis factor α (TNFα) etc. (Pastore et al., 2016). In T cells, depletion of both, TFE3 and TFEB, led to faulty antibody responses (Huan et al., 2006). In dendritic cells, TFEB was important for antigen presentation through the major histocompatibility complexes (MHC). These finding point towards a broad and important role of TFEB in cellular immune responses (Samie and Cresswell, 2015).

Bones: In osteoclasts, TFEB deletion has been shown to increase bone mass suggesting that TFEB might be important for bone reabsorption (Ferron et al., 2013).

Secretion from lysosomes: TFEB overexpression has been shown to induce lysosomal secretion/exocytosis (Palmieri et al., 2011). TFEB transcriptionally regulates the calcium channel TRPML1 that releases calcium from lysosomes to increase the cytoplasmic levels. Because calcium elevation is important for fusion of lysosomes to plasma membrane (Rodríguez et al., 1997), it was found that TFEB induced TRPML1 calcium release was important for lysosomal exocytosis (Medina et al., 2011). Additionally, overexpression of TFEB increased peripheral lysosomes and facilitated their docking to plasma membrane although the exact mechanism was undescribed (Medina et al., 2011).

mTORC1-TFEB regulatory loop: Recently, a novel regulatory axis of MiT/TFE family transcription factors regulating mTORC1 has been described. Di Malta et al. found that, when active during prolonged starvation, MiT/TFE transcription factors (and TFEB) led to upregulation of RRAGD and RRAGC (to a lesser extent), genes coding for RagD and RagC, respectively. Rag GTPases are involved in the activation of mTORC1 and constitutive activation of these transcripts lead to reactivation of mTORC1 once nutrients are available again (Di Malta et al., 2017). **Fig 13.** shows a brief summary of important functions driven by MiT/TFE transcription factors

In summary, the surface of lysosomes is a signaling hub. In response to varying nutrient conditions, multitude of signaling events occur at the surface of lysosomes. In the presence of nutrients, we see assembly of multiple regulators of mTORC1 that initiate protein biogenesis, a general anabolic response leading to cell mass accumulation and cell proliferation. Contrary, in conditions of starvation, catabolic mechanisms that rely on lysosomal degradation are initiated by TFEB-dependent transcriptional activation to meet the nutrient demands of starving cells. Next, I will present how these lysosomal nutrients signaling pathways are hijacked by cancer cells.

Perera et al., 2019

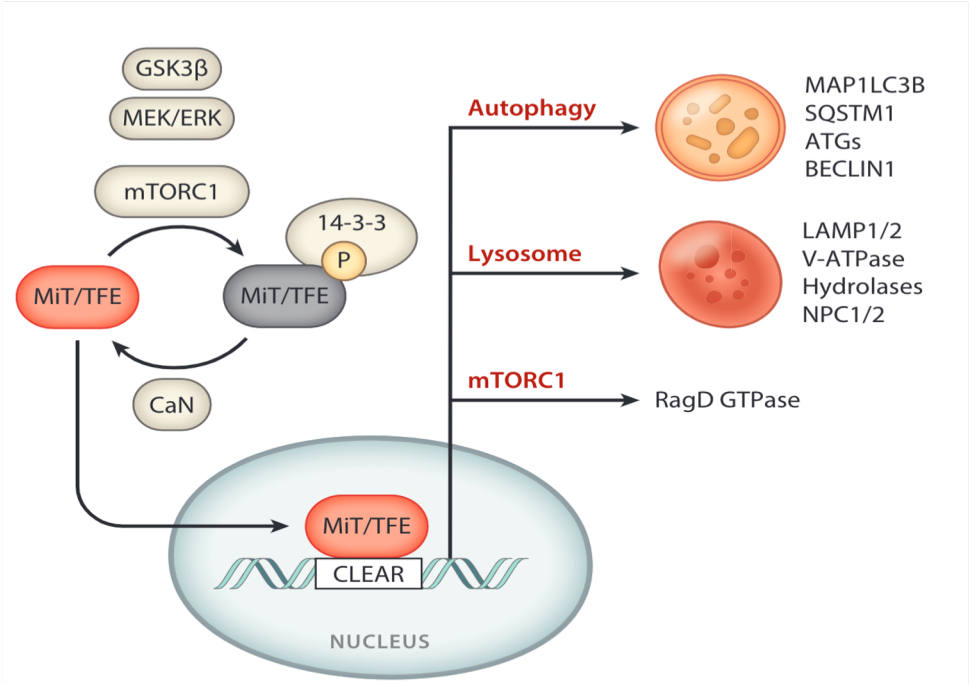

Fig 13. Important function of MiT/TFE transcription factors
CaN : Calcineurin

1.5 Implications of lysosomal signaling pathways (mTORC1 and TFEB) in cancer

Given the complexity of metabolic regulation by mTORC1 and TFEB at lysosomes and their integral role in protein homeostasis and cell proliferation, it is not surprising that these pathways are reprogrammed in cancers. Here, I summarize how cancer cells make use of lysosomal signaling complexes (mTORC1) and lysosome-dependent gene regulation by TFEB to sustain their energy demands and for rapid uncontrolled proliferation.

mTORC1 in cancer

Deregulation and hyperactivation of mTORC1 has been reported in several cancers such as lung cancer, gastric cancers, renal cell carcinomas, colorectal cancers, prostate cancers, bladder cancers etc. (Tian et al., 2019). Since PI3K/AKT and Ras/MAPK pathway mutations are common in cancers, including bladder cancers, and mTORC1 functions downstream of PI3K signaling, mTORC1 hyperactivation is

commonly seen in cancers with such mutations. Furthermore, mutations in proteins, which are components of the mTORC1 regulon, such as TSC1/2, Rag GTPases, GATOR or mTOR itself, are regularly found in cancer and are associated with mTORC1 hyperactivity (Saxton and Sabatini, 2017). GATOR1 complex mutations were found in low frequency in case of glioblastomas (Bar-Peled et al., 2013). Also, recurrent mTORC1 activating mutations in RagC were detected in follicular lymphomas (Okosun et al., 2016). mTOR gene mutations were also detected in a wide array of cancers particularly distinct in the cases of kidney cancers. This study highlighted a total of about 33 mutations in mTOR that could lead to mTOR hyperactivity detected in cases of different cancers (Grabiner et al., 2014). Substrates downstream of mTORC1 have also been implicated in cancers. Phosphorylation of 4EBP has been shown to drive prostate cancer and T cell lymphoma in mice (Hsieh et al., 2010). A study in bladder cancer has reported 4EBP to support cancer growth and to be a possible therapeutic target (Nawroth et al., 2011). However, it has been suggested that phosphorylation of 4EBP1 is independent of mTORC1 but is indirectly driven through PI3K.

Apart from a hyperactivity in the tumor cells, mTORC1 activity is also found to be important in regulating tumor microenvironment. For instance, mTORC1 signaling plays a role in tumor vasculature and is crucial for tumor angiogenesis (Guba et al., 2002). Tumor angiogenesis or formation of new blood vessels is important for oxygen and nutrient supply to tumor cells in situations of deprivation. Lack of oxygen, or hypoxia, is known to induce tumor angiogenesis through the transcription factor HIF (hypoxia inducible factor), which can be translationally regulated by mTORC1 (as mentioned before), especially in cancers (Hudson et al., 2002). HIF induces proteins involved in formation of new blood vessels, e.g. the vascular endothelial growth factor (VEGF), which can promote angiogenesis through binding to the VEGF receptors on vascular endothelial cells (Kim et al., 2017).

mTOR inhibitors used in cancers: Rapamycin is an mTORC1 specific inhibitor. Rapamycin and rapamycin-derived therapeutics have been approved for treatment of cancers. Temsirolimus and everolimus are derivatives of rapamycin, which were first approved for treatment of renal carcinomas in early 2000s. Use of everolimus has also been highlighted for treatment of bladder cancers, as discussed in earlier sections. However, mTORC1 inhibitors have not been very successful in pre-clinical models, which could be due to the inefficiency of the rapamycin derivatives to act equally on

all mTORC1 substrates (Choo and Blenis, 2009; Choo et al., 2008). Inactivation of mTORC1 induces autophagy, which could be additionally exploited by cancers.

TFEB and MiT/TFE family transcription factors in cancer:

Several cancers, including pancreatic cancers, renal carcinomas, melanomas and prostate cancers, have shown increased dependency on autophagic degradation and recycling pathways as nutrient scavenging alternatives (Kimmelman and White, 2017). MiT/TFE family members (MITF, TFE3, TFEB, TFEC) have been reported as oncogenes in several cancers (Haq and Fisher, 2011). For instance, about 5-20% of melanomas have genomic amplification of MITF (microphthalmia-associated transcription factor). TFEB and TFE3 nuclear translocations and gene rearrangements have been observed in renal cell carcinomas (RCC) and alveolar soft part sarcoma (ASPS) (Argani et al., 2001; Ramphal et al., 2006). In patient derived pancreatic ductal adenocarcinomas (PDA) cell lines, MiT/TFE family transcription factors are found to be upregulated (Perera et al., 2015a).

Some of the cancers dependent on MiT/TFE family transcription factors show a higher basal level of autophagy, e.g. PDA cancers (Yang et al., 2011). In PDA cell lines, an upregulation of MiT/TFE factors was necessary for maintaining a higher level of autophagy and lysosome biogenesis. In fact, in PDA, there was about a 12fold increase in lysosomal biogenesis. Additionally, the MiT/TFE factors escaped the mTORC1-dependent regulation and were found to be constitutively in the nucleus (Perera et al., 2015a). Moreover, in these cancers, an increase in MiT/TFE-dependen lysosomal catabolic activity has been shown to be important for meeting the amino acid demands. PDA cancers also performed a high rate of micropinocytosis. Micropinocytosis is known to facilitate the uptake of extracellular serum albumin and possibly other nutrients. In an experiment of carbon tracing with labelled albumin, it was found that micropinocytosis-dependent uptake of albumin was degraded in lysosomes to generate free amino acids. These amino acids were consumed in the cytoplasm (Commisso et al., 2013; Davidson et al., 2017; Kamphorst et al., 2015), although the exact role of MiT/TFE factors here remained unclear. Together, these observations suggest that MiT/TFE cancers utilize autophagic flux and lysosomal degradation for efficient cargo processing from autophagy and possibly also through micropinocytosis (Perera et al., 2019).

mTORC1-MiT/TFE feedback loop in cancer:

In cancers such as PDA, MiT/ TFE transcription factors have been reported to escape mTORC1 regulation and show constitutive nuclear translocation independent of nutrient conditions. Active MiT/TFE factors have shown to re-activate mTORC1 by transcriptional regulation of Rag genes, specifically RRAGD that encodes RagD (Di Malta et al., 2017). This finding suggests that constitutive activation of MiT/TFE factors in tumors could lead to mTORC1 hyperactivity by transcriptional regulation of RagD. In line, in tumors such as RCC, melanoma and PDA that are MiT/TFE factor malignancies a constitutive induction of RRAGD was reported (Perera et al., 2019). A positive correlation between MITF and RRAGD expression levels was also found in melanoma cell lines. Similarly, an increase in RRAGD was found in a renal cell carcinomas model upon TFEB overexpression and nuclear activation. Together, these findings depict that cancers driven by MiT/TFE transcription factors could maintain mTORC1 signaling (Di Malta et al., 2017). This activation pathway has been recently termed 'the non-canonical pathway of mTORC1' signaling (Napolitano et al., 2022). Additionally, alveolar soft part sarcoma (ASPS) were described to have a translocation of TFE3 resulting a chimeric transcription factor with the gene ASPSCR1 (that encodes the tether containing UBX domain for GLUT4 (TUG), i.e. ASPSCR1-TFE3 (Ladanyi et al., 2001). A transcriptome study showed that ASPS cells with overexpression of ASPSCR1-TFE3 had an elevated expression of RRAGD and other autophagy genes (Kobos et al., 2013). However, it remains to be tested whether this expression of RRAGD was important for mTORC1 activation in these cells.

In addition to the role of mTORC1 in supporting tumor vasculature, there are some evidences for a possible role of MiT/TFE factors in angiogenesis. However, this is not yet validated for MiT/TFE specific malignancies. The role of TFEB in angiogenesis was highlighted in an old study, in which TFEB knock down mice died prenatally due to defects in placental vasculature (Steingrimsson et al., 1998). A newer study found that endothelial cell (EC)-specific TFEB transgenic mice (with TFEB over expression) showed an increased blood perfusion, capillary density and better recovery post ischemia, whereas, the EC specific knockout mice did not have this phenotype (Fan et al., 2018). These findings again highlight that TFEB plays an important role in angiogenesis, but it not known if this occurs in TFEB-driven cancers. Additionally, MITF positively regulates angiogenesis, because it regulates the expression of HIF

transcription factor (Buscà et al., 2005) that induces angiogenesis in a VEGF dependent manner in conditions of hypoxia. Here again, it is not known if MiT/TFE factors play a role in cancer angiogenesis.

Finally, TFEB regulates lysosomal exocytosis by upregulating the expression of TRPML1. Lysosomal exocytosis is an important function in cancers, because the secretion of proteases allows cancer cells to breach the basement membrane and to metastasize to other organs (Olson and Joyce, 2015). Whether TFEB-driven cancers use this function of lysosomes for cancer progression remains however to be established. Interestingly, significant elevations in the expression of MiT/TFE-targeted 'CLEAR' genes, including TRPML1, have been recently reported in primary tumors of bladder carcinoma mutated in p53 in the Cancer Genome Atlas Research Network database, (TCGA).

In summary, mTORC1 and TFEB can be dysregulated in cancers. Both pathways converge at lysosomes and highlight the central role of lysosomes in tumorigenesis. Very little is known about mTORC1 and TFEB functions in bladder cells and bladder cancer. Notably, lysosomes are dynamic organelles, and lysosomal positioning has been shown to be involved in the complex regulation of lysosomal signaling. In the next section, I will summarize the current knowledge on the regulation and functions of lysosome positioning, in physiological conditions and in the context of cancer.

1.6. Regulators of lysosome positioning

Lysosomes are dynamic organelles, which move within the cells rapidly. Lysosomes have certain spatiotemporal characteristics which could influence their functions, for instance lysosomal pH in the peripheral lysosomes was reported to be less acidic. It was proposed that reduced v-ATPase activity, and thus reduced lysosomal acidification could indicate less proteolysis activity of these lysosomes (Johnson et al., 2016). Lysosomes are part of the endocytic system of the cell. When cargo or plasma membrane receptors enter the cell during endocytosis, they first traffick to early endosomes, where they can be either recycled back to the plasma membrane through recycling endosomes or assigned for breakdown in lysosomes (Bakker et al., 2017). Lysosomes are distributed throughout the cell, some of them can be assigned to a cloud around the perinuclear region, near to the MTOC (microtubule organizing center), which could fuse to the autophagosomes and give autolysosomes (Nakamura

and Yoshimori, 2017). Some lysosomes are observed in the cell periphery, close to the plasma membrane, which are more dynamic and proposed to account for plasma membrane repair and mTORC1 signaling (Encarnação et al., 2016; Korolchuk et al., 2011; Nakamura and Yoshimori, 2017). Several cellular factors and conditions can influence organization of lysosomes, for instance lysosome clustering can be observed during cell starvation (Korolchuk et al., 2011), drug induced apoptosis (Yu et al., 2016) or even in lysosome storage disorders (Li et al., 2016; Uusi-Rauva et al., 2012); whereas lysosomal dispersion or tubulation can be observed in maturation of dendritic cells to deliver the MHCII to the plasma membrane (Chow et al., 2002; Vyas et al., 2007). Additionally, cell acidity has been shown to rapidly disperse lysosomes, and alkalization to bring them back to their central localization (Heuser, 1989a). Positioning of lysosomes is regulated by different sets of proteins. Because lysosomes move in a 'stop and go' fashion, it has been suggested that their movement is constantly subjected to regulatory stimuli (Cabukusta and Neefjes, 2018). Next, I will highlight the machinery involved in lysosomal movements and different regulators of lysosome positioning.

Regulators of lysosome positioning:

Lysosome movements are performed by 3 main families of motor proteins, which are kinesins, dyneins and myosins. Kinesins and dyneins move lysosomes on microtubules, which leads to long-range directive movement. Mammalian cells express over 40 kinesin proteins (Hollenbeck and Swanson, 1990) but only one cytoplasmic dynein protein. Dynein works together with the dynactin complex for the movement of the 'cargo' (the organelle) (Harada et al., 1998). Myosins have been implicated in the tethering of lysosomes to the actin cytoskeleton (Cordonnier et al., 2001), and could also participate in short-range directed movements (Kapitein et al., 2013)

1) Microtubule-dependent movement

In a non-polarized cell, microtubules are often organized radially. Their 'minus' ends are located at the MTOC and their 'plus' ends are pointing toward the cell periphery (Sanders and Kaverina, 2015). Kinesins are motor proteins, most of them involved in movement of organelles (but here we focus on lysosomal movements only) to the plus

ends of microtubules, thus towards the cell periphery (anterograde movement). Contrary, dynein moves lysosomes to the minus ends, thus cell center (retrograde movement). Binding of these motor proteins to lysosomes are facilitated by small GTPases and their effector proteins as well as the phospholipid composition of the organelle (Bonifacino and Neefjes, 2017), lysosomes in this case.

Retrograde movement of lysosomes**:**

Retrograde or 'minus end' movement of lysosomes is mainly based on dynein. Dynein is a multimeric protein that is composed of 2 heavy chains, 2 intermediate chains and many light chains (Ishikawa, 2012). Dynein is shown to interact to another multimeric protein called dynactin, which is required for its association to lysosomes (Burkhardt et al., 1997). Dynein can be recruited to late endosomes and lysosomes by several mechanisms. Mainly, this recruitment is through the small GTPase Rab7 (Ras related protein 7). The GTP loading of this GTPase is under regulation of the Mon1–Ccz1 complex that acts as the guanine nucleotide exchange factors (GEF) (Nordmann et al., 2010). GTPase activation is performed by the TBC domain family member 15 (TBC1D15) (Zhang et al., 2005) and the TBC domain family member 2 (TBC1D2) (Frasa et al., 2010) ,which are the GAPs of Rab7. Rab7 interacts with several downstream effectors that couple dynein to lysosomes. One of these effectors is RILP (Rab interacting lysosomal protein) that interacts with the dynactin complex (specifically the $p150^{glued}$ subunit of this complex) (Johansson et al., 2007; Rocha et al., 2009) (**Fig 14 (A)**). Another effector of Rab7 is the oxysterol-binding protein-related protein 1 (ORP1L) that associates with Rab7 at ER-Lysosomes contact sites. Membrane contact sites (MCS) are an emerging topic of interest, because they represent sites of lipid exchanges between organelles as well as intracellular domains with several molecular functions, such as signaling and motor protein recruitment. The ER being the most spread out organelle, it has been show to form contacts with multiple organelles and the plasma membrane (Cabukusta and Neefjes, 2018). The ER forms contacts with lysosomes, which is important for regulating lysosomal cholesterol levels and also lysosome positioning. The protein critical for cholesterol transport and lysosome positioning is ORP1L. At high cholesterol levels in lysosomes, ORP1L associates to lysosomes through interaction with Rab7 as well as its PH (pleckstrin homology) domain, through which it interacts with phosphoinositides on lysosomes (Johansson et al., 2005). On lysosomes, ORP1L can also clamp onto

cholesterol through its cholesterol interacting domain ORD. ORPL1 and Rab7 together with RILP recruit dynein and move lysosomes retrograde (Johansson et al., 2007) (**Fig 15 A**). However, in conditions of low cholesterol, there is a conformational change in ORP1L, which exposes its FFAT motif, a protein motif that binds to the vesicle-associated membrane protein (VAMP)-associated ER protein A/B (VAPA/ VAPB) to tether it to the ER (Rocha et al., 2009). This interaction facilitates transfer of cholesterol from lysosomes to ER. It has been proposed that ER-lysosome contacts block retrograde transport of lysosomes in this context (**Fig 15 A**). ER-lysosome contacts also facilitate anterograde transport that is discussed in next section. Other mechanisms of retrograde transport of lysosomes include proteins JIP4 and ALG2 that interact with dynein. JIP4 is recruited by the lysosomal membrane protein TMEM55B. JIP4 is the adaptor of dynein-dynactin complex and leads to retrograde transport of lysosomes (Willett et al., 2017)(**Fig 14 (C)**). The ALG2 interaction to lysosomes is dependent on phosphatidylinositol-3,5,-bisphosphate ($PI(3,5)P_2$) and the lysosome calcium channel TRPML1. $PI(3,5)P_2$ activates TRPML1 and leads to calcium release from lysosomes. Calcium activates the calcium sensor ALG2, which forms a complex with TRPML1 on lysosomes and leads to interaction with dynein-dynactin complex for retrograde movement of lysosomes (Li et al., 2016) (**Fig 14 (B)**). Several other Ras related proteins (Rabs) have been shown to be involved in lysosome positioning. For instance, overexpression of Rab34 and Rab36 causes perinuclear clustering of lysosomes (Chen and Yu, 2013; Wang and Hong, 2002). Both Rabs can interact with dynein interacting protein RILP, however they are localized to the Golgi complex / trans Golgi network (TGN), so it is unclear how they regulate lysosome retrograde movement. However, it has been suggested that regulation could be through lysosomes and Golgi / TGN contacts (Pu et al., 2016).

Cabukusta and Neefjes, 2018

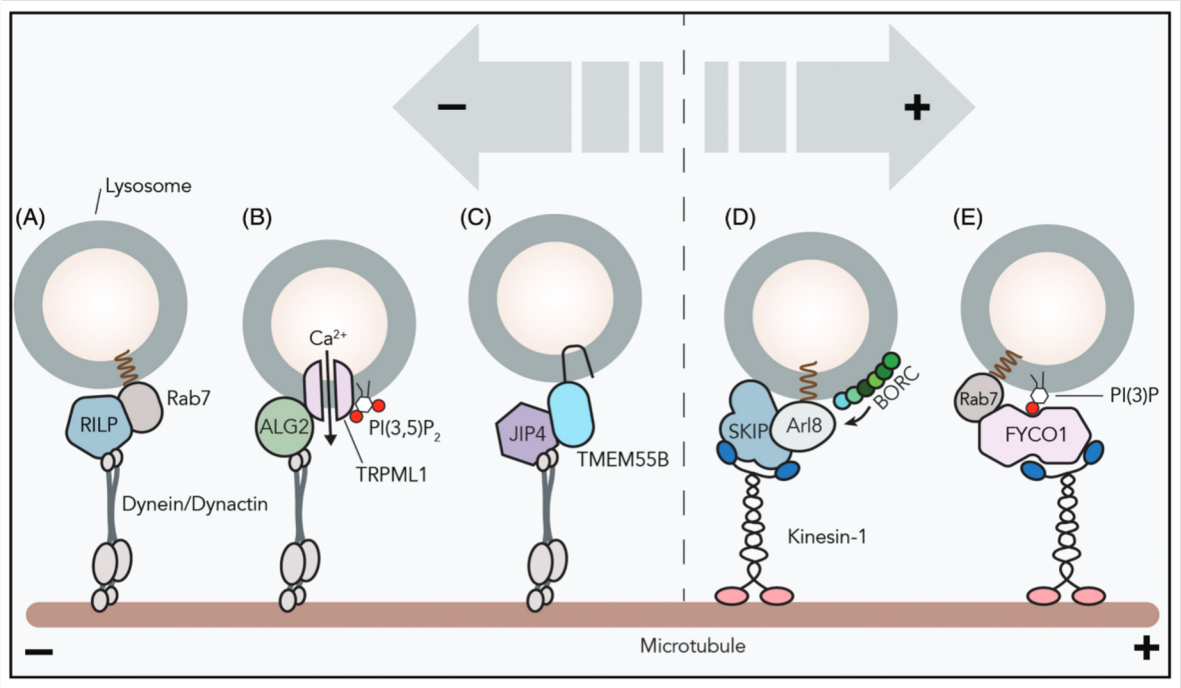

Fig 14. Multiple mechanisms of movement of lysosomes on microtubules

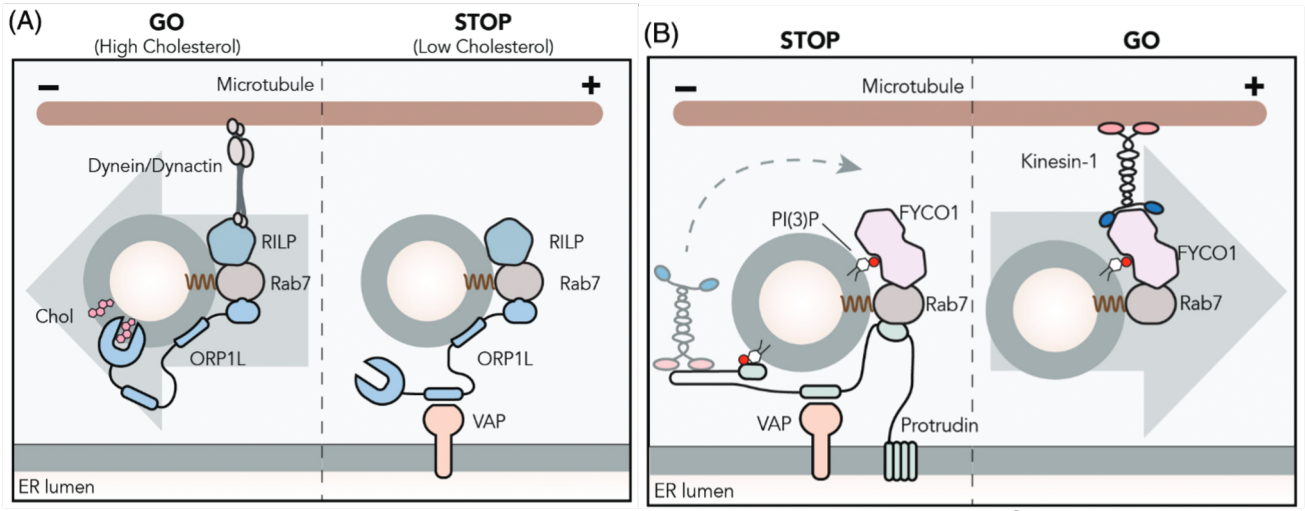

Fig 15. ER-Lysosome contacts regulate lysosome positioning Cabukusta and Neefjes, 2018

<u>Anterograde movement of lysosomes:</u>

Anterograde or 'plus end' movement of lysosomes is based on different kinesins that are recruited by several mechanisms. Mammalian cells have about 45 kinesin proteins (KIFs). Kinesins exhibit a globular motor domain that attaches to microtubules, and a tail domain that interacts with the cargos or adaptor proteins. Hydrolysis of ATP at the motor domain drives the movement of most kinesins to the '+' ends of microtubules

that are often found towards cell periphery. Exceptions are members of the kinesin-14 family that move in the opposite direction towards the '-' ends of microtubules (Hirokawa and Noda, 2008). Interestingly, movement of lysosomes is facilitated not by one but several kinesins including the kinesin-1 (KIF5A, KIF5B, KIF5C)(Nakata and Hirokawa, 1995; Rosa-Ferreira and Munro, 2011), kinesin-2 (KIF3) (Brown et al., 2005), kinesin-3 (KIF1A, KIF1B) (Korolchuk et al., 2011; Matsushita et al., 2004) and kinesin-13 (KIF2) (Santama, 1998) member proteins. It's unclear why so many different kinesins are involved in lysosomal movement, but it could be due to cell type specificity, functional redundancy, differential regulation, for different lysosomal functions, or because of preferential association to different microtubule tracks as a result of different post translational modifications (PTM) on tubulins, microtubule associated proteins (MAPs) etc. (Marx et al., 2006). For instance, kinesin-1 are shown to move faster on microtubules, which have acetylated and GTP bound tubulins (Reed et al., 2006). Loss of polyglutamylation on tubulins decreases kinesin-3 (KIF1A) association and movement on microtubules (Ikegami et al., 2007). Some MAPs on microtubules hinder the movement of kinesis, such as MAP protein tau hinders kinesin-1 movement (Dehmelt and Halpain, 2004). However, some others enhance recruitments of kinesins on microtubules, e.g. ensconsin (Sung et al., 2008). Kinesin-1 is the best described one for the movement of lysosomes. Kinesin-1 is composed of 2 heavy (KIF51, KIF5B or KIF5C) and 2 light chains (KLC1, KLC2, KLC3 or KLC4) to form a heterotetramer (DeBoer et al., 2008). Mechanisms of kinesin recruitment on lysosomes rely on BLOC-1-related complex (BORC), Arf-like small GTPase Arl8b, the Arl8 effector SifA and kinesin-interacting protein (SKIP) (Bagshaw et al., 2006; Hofmann and Munro, 2006; Pu et al., 2015). BORC is an octameric protein complex composed of the following subunits BLOS1, BLOS2, snapin, KXD1, MEF2BNB, myrlysin, lyspersin and diaskedin (Falcón-Pérez et al., 2002; Moriyama and Bonifacino, 2002; Pu et al., 2015). BORC associates to lysosomes through its myrlysin domain. On lysosomes, BORC can activate Arl8b (possible through being a GEF for Arl8 that remains unclear yet), which loads its effector SKIP. SKIP binds to Arl8 through its N-terminal RUN domain and recruits kinesin-1 to lysosomes (Rosa-Ferreira and Munro, 2011) (**Fig 14 (D)**. Arl8b/SKIP can actually recruit 2 kinds of kinesins to lysosomes. Kinesin-1 is recruited to more acetylated microtubules mostly found in perinuclear regions, and kinesin-3 is recruited to tyrosinated α-tubulin containing

microtubules, which are mostly found towards cell periphery (Guardia et al., 2016). This highlights the complexity and multistep regulation of lysosomal movement.

Another mechanism of lysosome anterograde transport is based on ER-lysosome contact sites. Protrudin is an ER anchored protein that simultaneously binds to Rab7 and to phosphatidylinositol-3-phosphate (PI3P) on lysosomes through its FYVE domain and establish ER-lysosomes (and late endosomes) contacts (**Fig 14 (E) and 15 B**). Protrudin then transfers kinesin-1 to the effector FYVE- and coiled-coil-domain-containing protein (FYCO1) on lysosomes. FYCO1 also associates to lysosomes through binding of its FYVE domain with PI3P on lysosomes. These interactions lead to anterograde lysosomal movement toward the cell periphery (Pankiv et al., 2010; Raiborg et al., 2015). This movement was found to be especially important for neurite growth (Raiborg et al., 2015). Interestingly, this anterograde trafficking mechanism involving PI3P, protrudin, Rab7 and FYCO was shown to be important for mTORC1 activation in response to nutrients, discussed next.

2) Cellular nutrients regulate lysosome positioning:

Lysosomes have been shown to change their positioning depending on the cellular nutrients status (Korolchuk et al., 2011). It has been proposed that positioning changes are part of the cellular mechanisms to coordinate catabolic and anabolic signaling through mTORC1**.** Indeed, lysosome positioning has been shown to regulate mTORC1 signaling (Korolchuk et al., 2011). Experimental induction of peripheral dispersion of lysosomes was shown to induce mTORC1 activity, whereas experimental induction of perinuclear clustering of lysosomes reduced mTORC1 activity.

Perinuclear clustering of lysosomes in starvation is attributes to changes in internal pH (pHi) of the cell, among one proposed mechanism (Korolchuk et al., 2011). This study showed that starvation increased pHi and reduced binding of Arl8b, thus decreasing kinesin recruitment on lysosomes and inhibiting their anterograde movement. This suggested that increased pHi is capable of displacing Arl8 from lysosomes (Korolchuk et al., 2011). Old observations show that low pHi can disperse lysosomes (Heuser, 1989a). Additionally, starvation in normal cells inactivates mTORC1 and removes it from lysosomes due to the absence of amino acids and growth factors, which are required for activation of mTORC1 machinery. Additionally, in absence of amino acids, Ragulator complex interacts with BORC on lysosomes which prevents Arl8B/SKIP/

kinesin-1 dependent peripheral movement of lysosomes (Filipek et al., 2017; Pu et al., 2017). Finally, lysosomes clustering to the perinuclear region upon starvation, has been shown to be anchored to the Golgi complex through lysosome-Golgi contact sites for immobilization (Starling et al., 2016). This contact site has been shown to be between RILP, the Golgi-associated Rab34 and FLCN (folliculin) (Starling et al., 2016). Thus, although lack of nutrients leads to lysosomal retrograde movement, the underlying mechanisms are not completely clear. (**Fig 16**).

Upon addition of amino acids and in presence of growth factors, lysosomes are found to be dispersed to the cell periphery that actives mTORC1. Addition of amino acids disrupts BORC-Ragulator interaction and activates Arl8b/SKIP/Kinesin-1 facilitated lysosome movement to cell periphery (Filipek et al., 2017).

Also, amino acids have been shown to activate Class III PtdIns3 kinase (PI3KC3) VPS34 (Nobukuni et al., 2005), which increases phosphatidylinositol-3-phosphate (PI3P) on lysosomes. This facilitates ER-lysosome contacts through ER protein protrudin and the recruitment of FYCO, the kinesin-1 adaptor for peripheral movement of lysosomes (Hong et al., 2017; Raiborg et al., 2015). Increased activity of mTORC1 on peripheral lysosomes was also attributed to it closeness to growth factor signaling at the plasma membrane, which activates AKT and leads to full activation of mTORC1 (Hong et al., 2017; Korolchuk et al., 2011; Raiborg, 2018) (**Fig 16**).

3) TFEB dependent regulation of lysosome positioning:

Starvation induces TFEB activation and nuclear translocation. Starvation also leads to perinuclear lysosome clustering. Indeed, two TFEB-dependent mechanisms were proposed to induce lysosomal retrograde movement. Firstly, TFEB has been found to induce the expression of lysosomal membrane protein TMEM55B. TMEM55B has been shown to recruits JIP4 to lysosomes, which is a dynein adaptor and leads to lysosomal retrograde transport (Willett et al., 2017).

Additionally, TFEB has been shown to increase the activity of lysosomal calcium channel TRPML1 (Palmieri et al., 2011). Activated TRPML1 channel and subsequent Ca^{+2} release during starvation leads to the activation of ALG2, which then leads to its interaction with the dynein-dynactin complex and retrograde movement of lysosomes (Li et al., 2016) (**Fig 16**). This function is however surprising, given the role of the TRPML1 calcium channel in supporting lysosomal exocytosis and TFEB overexpression resulting in peripheral lysosomes that was reported before by Medina

et al. (Medina et al., 2011). Because lysosomes are found at the cell periphery during exocytosis, the authors propose that differences in effector proteins downstream Ca^{+2} release could be a reason for these contradictory observations (Li et al., 2016). **Fig 16**. summarizes the nutrient dependent regulation of lysosome positioning.

Together, these findings indicate that TFEB could regulate anterograde or retrograde movement of lysosomes depending on the cell context and the downstream effectors. Next, I focus on highlighting the cancer supporting functions of lysosome positioning.

Raiborg, 2018

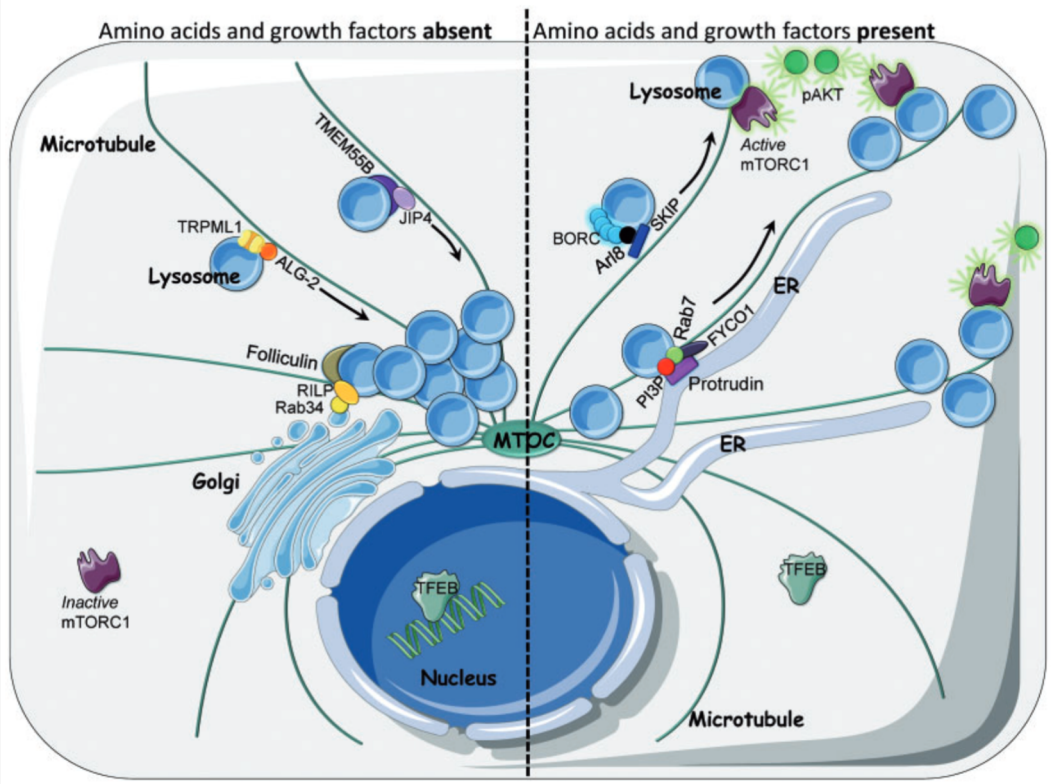

Fig 16. Lysosome positioning pathways in fed and starvation conditions

1.7. Functions of lysosome positioning in cancer progression

Having established the different mechanisms that regulate lysosome positioning, I will now introduce how lysosome positioning changes in cancer, and how this could support carcinogenesis.

Lysosomal dispersion to the cell periphery has been reported in several cancers. For instance, breast cancer cells have been reported to show peripheral distribution of lysosomes in late 1900s and early 2000s (Nishimura et al., 1998, 2003; Sameni et al., 1995). One proposed mechanism for lysosomal dispersion in cancer cells is the acidity

of tumor microenvironments (Glunde et al., 2003). This study proposes that the acidity of tumor microenvironment can lead to lysosomal dispersion which probably supports lysosomal exocytosis. Another proposed mechanism for lysosomal dispersion is the over-expression of genes regulation lysosomal anterograde transport, such as kinesin-1 (Cardoso et al., 2009). Another study reported decrease in the levels of Rab7 resulting in peripheral lysosomal dispersion and more invasiveness in prostate cancer (Steffan et al., 2014). However, given the complexity in the regulation of lysosomal organization, the drivers of lysosomal dispersion remain widely unexplored.

Lysosomal exocytosis and ECM degradation

Lysosomal exocytosis is one of the proposed functions of peripheral lysosomes in cancer. Lysosomal exocytosis is a Ca^{+2} driven process that requires lysosomal trafficking and docking to the plasma membrane (PM) to release their content outside the cells (LaPlante et al., 2006; Rodríguez et al., 1997). Briefly, fusion of lysosomes to the plasma membrane is initiated by synaptotagmin VII, a Ca^{+2} sensor that upon release of calcium from lysosomes or calcium influx from PM, interacts with SNARE protein VAMP7 on lysosomes, syntaxin 4 and SNAP23 (synaptosomal associated protein 23) on PM and leads to lysosomal fusion and exocytosis (Martinez et al., 2000). One evidence of lysosomal exocytosis in cancers has been the presence of lysosomal membrane proteins on the PM. For instance, in case of breast cancers, LAMP1 and LAMP2 that are markers of lysosomal membranes have been found at the PM (Damaghi et al., 2015; Machado et al., 2021). Lysosomal exocytosis could perform several functions to support cancer progression. Lysosomal exocytosis is important for remodeling of the extracellular matrix (ECM) to facilitate cancer cell evasion. In prostate cancers and melanomas, lysosomal redistribution to the cell periphery leads to increased release of proteases, such as cathepsins, that supports invasion. In line with these results, it has been shown in breast cancer that increased lysosomal exocytosis leads to secretion of HSP90s (Heat shock protein 90a) and activation of MMP9 (Matrix metalloprotease 2) leading to ECM degradation and tumor invasion (Hendrix et al., 2010; Quintero-Fabián et al., 2019). Another function of increased lysosomal exocytosis in malignancies is to send oncogenic signals (such as growth factors, cytokines, etc.) to cancer cells in proximity. This has been observed in rhabdomyosarcoma cells, which were found to have fully sialylated LAMP1 lysosomes that release exosomes and send out oncogenic signals to neighboring cancer cells (Machado et al., 2015). Moreover, these signals promote transformation of

macrophages and fibroblasts around cancers cells into CAFs (Cancer associated fibroblasts) and TAMs (Tumor associated macrophages). Increased lysosomal exocytosis has also been shown to contribute towards drug resistance of cancer cells (Machado et al., 2015). Cancer cells trap lysomotropic drugs in their endosomes and could release these drugs through lysosomal exocytosis. Finally, increased lysosomal exocytosis could lead to changes in the composition of the plasma membrane of cancer cells. In some cancers, increased accumulation of LAMP1 on the PM of cancer cells was proposed to help survive the acidic tumor micro environment, as LAMP1 could forms a protective glycocalyx against the acidity of microenvironment (Damaghi et al., 2015). Additionally, LAMP1 on PM could also contribute to acidification of tumor microenvironment. These functions of lysosomal exocytosis in cancer progression are highlighted in **Fig 17**.

Changes that lead to peripheral lysosomes in cancer are also proposed to be hijacked by cancer cells to support increased lysosomal exocytosis. For instance, cancers driven by hyperactivity of MiT/TFE family members could have increased lysosomal exocytosis, as this process is regulated by TFEB through transcriptional regulation of lysosomal calcium release through TRPML1 channel (Medina et al., 2011).

Machado et al., 2021

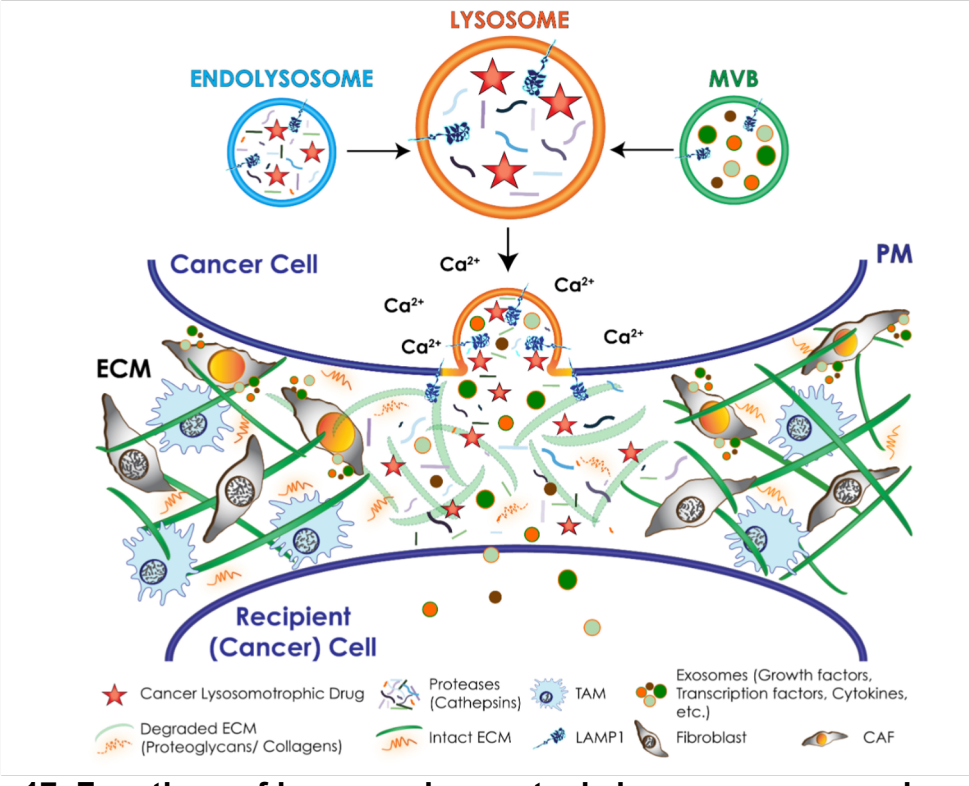

Fig 17. Functions of lysosomal exocytosis in cancer progression

Peripheral lysosomes in cell adhesion:

Another function of peripheral lysosomes is their role as a regulator of actin-based adhesion structures, such as focal adhesions. Repeated formation and dissolution of focal adhesion is pivotal in cell migration in 2D (Kim and Wirtz, 2013). It has been shown that LAMTOR2/3-positive lysosomes (component of Ragulator protein involved in mTORC1 activation, **Fig 8**) localize at focal adhesions (FA) at the cell periphery. This accumulation of LAMTOR 2/3 positive lysosomes was dependent on Arl8b and kinesin-1. Peripheral lysosomes disturbed the stability of focal adhesions and promoted cell motility (Schiefermeier et al., 2014). This observation of LAMTOR positive lysosomes associated with focal adhesions supports the idea of active mTORC1 in the proximity of focal adhesions due to the presence of its activator LAMTOR. This was recently confirmed and focal adhesions were shown to be sites of mTORC1 activation (Rabanal-Ruiz et al., 2021). This study also showed that lysosome positioning could be dispensable for mTORC1 that was already targeted to and activated at the focal adhesions, however it is unclear where the active mTORC1 would be localized once activated if not the lysosomes (Rabanal-Ruiz et al., 2021). These observations add focal adhesions as another axis for the activation mTORC1 in addition to lysosome positioning and cellular nutrients. Additionally, peripheral lysosomes have shown to be involved in integrin trafficking supporting invasion. For instance, active α5β1 integrins that are targeted to lysosomes have been shown not to be degraded, but instead targeted to the site of cancer invasion that promoted release of cancer cell from the matrix (Dozynkiewicz et al., 2012). Peripheral lysosomes have been shown to regulate the activity of FAK (Focal adhesion kinases). It has been proposed that lysosomal cathepsins degrade FAK Src and Talin, the activator of integrins, and disturb focal adhesions in cancer cells, thus resulting in tumor invasion (Akkari et al., 2014; Jevnikar et al., 2013). Whether cathepsins are released from lysosomes for the degradation of these substrate is unclear yet (Olson and Joyce, 2015).

To summarize, peripheral lysosome could be implicated in lysosomal exocytosis, ECM degradation, mTORC1 signaling, propagation of oncogenic signals to cancers cells in proximity, cell adhesion dynamics and providing drug resistance against lysomotropic drugs. Because many different functions of lysosomes converge on their positioning, the cellular landscape of lysosomes could be a biomarker of predicting underlying

molecular changes in cancer development. The complexity and the ability of lysosomes to use different molecular mechanisms to adapt and perform cellular functions could be used in cancer cells. The question remains to which extend tumors depend on lysosomes. Although several independent studies have tackled the difficult task of understanding the integrated functions of lysosome positioning in cancers, the phenotype of lysosomal dispersion in the context of cancer has not been exploited for treatment.

1.8. Phosphatidylinositol Phosphates: regulators of cellular lysosomal functions

I will next introduce the importance of phosphatidylinositol (PI) phosphates (PIPs) in regulating the various functions of lysosomes. I have briefly mentioned the involvement of phosphatidylinositol-3-phosphate in regulating lysosome positioning, in this section, I will summarize the current knowledge on how PIPs underly the previously discussed functions of lysosomes.

PIPs are minor phospholipids which define organelle membrane identity. In eukaryotes, 7 species of PIPs and 90 kinases and phosphatases that regulate their interconversions have been identified. 7 species of PIPs result from addition of phosphate group to the 3-, 4-, and 5- OH group of the inositol ring of the phosphatidylinositol. These 7 PIPs can be monophosphorylated, bisphosphorylated or triphosphorylated. Monophosphorylated PIPs are: PI3P, PI4P, and PI5P; bisphosphorylated PIPs are: $PI(3,4)P_2$, $PI(3,5)P_2$, and $PI(4,5)P_2$ and the triphosphorylated one is: $PI(3,4,5)P_3$. These species are interconvertible, which is regulated by specific PI kinases or phosphatases (Balla, 2013; Di Paolo and De Camilli, 2006; Stahelin et al., 2014).

In brief, PI can be phosphorylated at 4-OH position by PI4K (PI 4 kinase) to give PI4P. PI4P can again be phosphorylated by PIP5K to give $PI(4,5)P_2$. $PI(4,5)P_2$ can further be phosphorylated by the class I PI3K to yield the triphosphorylated $PI(3,4,5)P_3$. Similarly, PI can also be phosphorylated at 3-OH positioning by the class II or class III PI3K enzymes to give the monophosphorylated PI3P. This PI3P when phosphorylated by the enzyme PIKFYVE results in formation of the bisphosphorylated $PI(3,5)P_2$. **Fig 18** Gives a brief highlight of these interconversions and the kinases and phosphatases involved.

Wallroth and Haucke, 2017

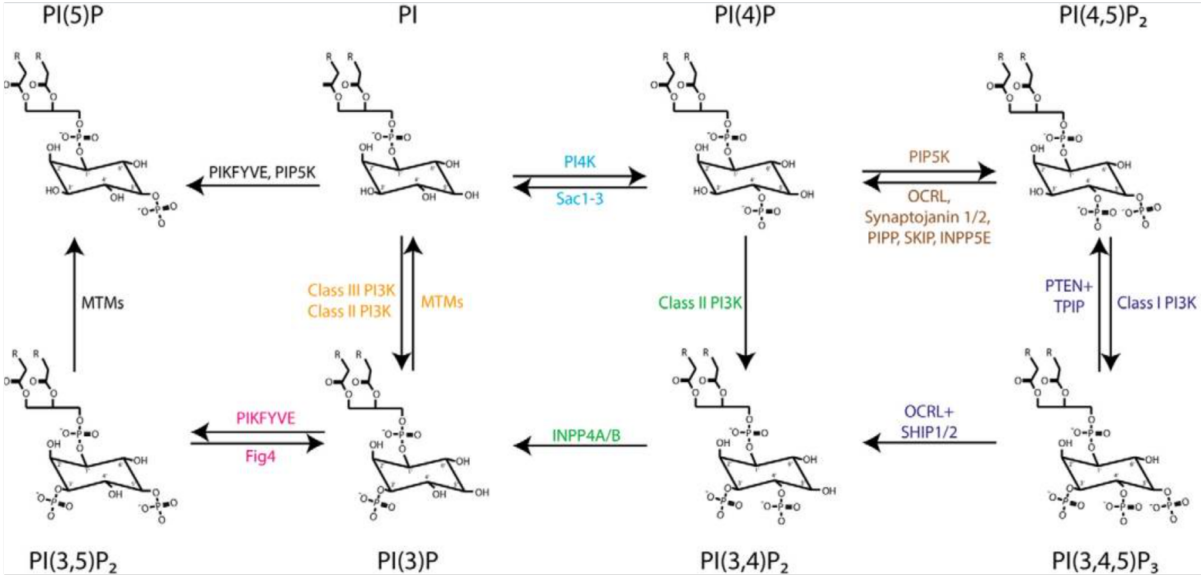

Fig 18. Kinases and phosphatases in PIP interconversions

Proteins that bind to organelle membranes recognize different phosphoinositides on them through their specific domains such as Pleckstrin Homology (PH) domain, Phox homology (PX), Fab1, YOTB, Vac1, and EEA1 (FYVE) domains, protein kinase C (PKC) conserved 2 (C2) domain, AP180 amino-terminal homology (ANTH) domain, epsin amino-terminal homology (ENTH) domain, PROPPIN domain etc. (Stahelin et al., 2014). FYVE domain proteins, for instance EEA1, recognize the PI3P on endomembranes (Lemmon, 2008). Additionally, some PX proteins have also been shown to bind to PI3P on membranes. C2 domain proteins such as synaptotagmins bind to phosphoinositides PI(4,5)P_2 and some other PIPs (Stahelin et al., 2014).

Different species of PIPs are found enriched on different organelles, which also contribute to regulating their functions. They are considered as determinants for the interactions and binding of proteins (involved in signaling, motility etc.) (Di Paolo and De Camilli, 2006; Posor et al., 2022; Wallroth and Haucke, 2018). PI4 phosphates such as PI4P are mostly concentrated at the Golgi complex, trans Golgi network (TGN) and also some at the plasma membrane. Contrastingly, PI3P is found at endosomes mostly including late endosomes, lysosomes and multi vescicular bodies (MVBs). PI(3,5)P_2 is mostly found at lysosomes and MVBs. PIPs have been shown to be

important for several lysosomal functions, as regulators of lysosomal signaling pathways, lysosome mobility, autophagosome lysosome fusion, and lysosomal homeostasis (Wallroth and Haucke, 2018). **Fig 19**. gives a concise overview of the different PIP species found on different organelles.

Posor et al., 2022

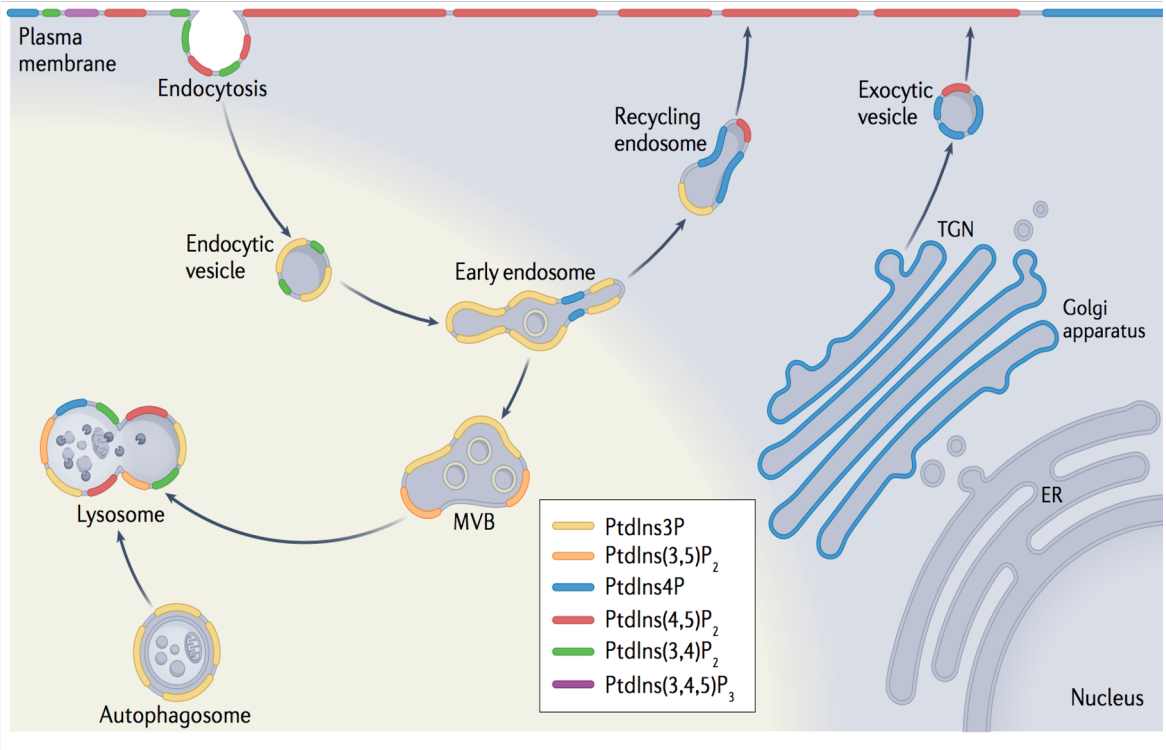

Fig 19. An overview of different species of PIPs present on different cellular compartments

Interestingly, lysosomes can contain many species of PIPs. Lysosomes harbor phosphatidylinositol-3-phosphate (PI3P), which is prominently present on endocytic vesicles. At endosomes, PI3P is crucial for the binding of the FYVE domain containing proteins, such as for instance EEA1 (Lawe et al., 2000). Lysosomes also contain phosphatidylinositol-3,5-bisphosphate ($PI(3,5)P_2$), and phosphatidylinositol-5-phosphate (PI5P), which are considered as PIPs specific to late endosomes and lysosome related organelles. A small fraction of Golgi-specific (PI4P) and plasma membrane-specific PIPs ($PI(4,5)P_2$) are also observed on lysosomes (Ebner et al., 2019). Given the understanding that different PIPs perform different functions, presence of so many different species of PIPs on lysosomes could possibly have a role on regulating different functions of lysosomes and a change in the balance of

specific PIP species could determine the prominent role of lysosomes in a given functional state or in response to a particular stimulus (Ebner et al., 2019).

PIPs can act as regulators of mTORC1 and TFEB signaling through lysosome positioning. Several metabolizing enzymes of PIPs have been implicated in the regulation of these pathways as well as also lysosome dynamics. Particularly, I will highlight 3 species of PIPs: PI3P, PI(3,4)P_2,and PI(3,5)P_2, which have been shown to play a regulatory roles in lysosomal functions.

PIPs regulate lysosome dynamics, mTORC1 and TFEB signaling:

1) **PI3P (Phosphatidylinositol-3-phosphate):** PI3P is generated predominantly by the class III PI3 kinase (PIK3C3) or VPS34 but also to a minor extent by class II PI3 kinase (e.g. PI3KC2 α) (Devereaux et al., 2013; Franco et al., 2014). Class III PI3K forms 2 distinct complexes. One complex functions with the autophagy vesicles VPS34/ VPS15/ Beclin1 /ATG14 (Itakura et al., 2008) during autophagy and the other one at the endosomes and lysosomes that is formed of VPS15/ VPS34/ Beclin 1/ UVRAG/ BIF-1 (Thoresen et al., 2010). Dephosphorylation of PI3P is performed by the myotubularin family phosphatases (MTMs), which include MTM1 and myotubularin related proteins (MTMR), i.e. MTMR1, MTMR2, MTMR4.

Vps34 is important for mTORC1 re-activation during starvation or refeeding (Nobukuni et al., 2005; Yoon et al., 2011). It has been proposed that this is through generation of PI3P. PI3P is required for the formation of ER-lysosome contacts through ER protein protrudin, Rab7 and FYCO1 on lysosomes. This contact leads to anterograde transport of lysosomes to cell periphery, through recruitment of kinesin-1 to the adaptor FYCO1 on lysosomes (**Fig 14, 15** shown in previous section and **Fig 20)**. Additionally, this translocation has been shown to be crucial for mTORC1 activation through growth factor signaling dependent activation (Hong et al., 2017). Depletion of PI3P phosphatase MTMR4 that leads to more PI3P on lysosomes did not increase mTORC1 activity but led to TFEB nuclear translocation (Pham et al., 2018). This suggested that PI3P regulates TFEB activation in a mTORC1-independent, undescribed mechanism.

2) **PI(3,4)P_2 (Phosphatidylinositol-3,4-bisphosphate):** PI(3,4)P_2 plays a role in mTORC1 inhibition. PI(3,4)P_2 is generated on lysosomes by class II PI3 kinase (PI3KC2β). In starvation conditions, PI3KC2β associates to the mTORC1 subunit

Raptor and converts PI4P to PI3,4P_2 on lysosomes. Increase in the levels of PI3,4P_2 leads to binding of protein 14-3-3 to Raptor and to mTORC1 inactivation (Marat et al., 2017). Additionally, increased PI(3,4)P_2 levels on lysosomes activate lysosomal ORP1L and facilitate cholesterol transport from lysosome to ER (Dong et al., 2019). Low cholesterol in lysosomes inactivate mTORC1 signaling and induce nuclear translocation of TFEB (Castellano et al., 2017). Finally, perinuclear accumulation of lysosomes is observed upon increase in PI(3,4)P_2 levels but the exact mechanism of the retrograde movement remains unknown (Marat et al., 2017) .

3) **PI(3,5)P_2 (Phosphatidylinositol-3,5-bisphosphate):** PI(3,5)P_2 is generated by the kinase PIKfyve. PI(3,5)P_2 has been shown to activate the calcium channel TRPML1 (or MCOLN1) on lysosomes during starvation (Dong et al., 2010). Release of calcium from this channel leads to activation of TFEB dephosphorylation by the phosphatase calcineurin and TFEB nuclear translocation (Medina et al., 2015) (**Fig 20**). Thus, formation of PI(3,5)P_2 on lysosomes in starvation leads to activation of TFEB. Contrastingly, in yeast, PI(3,5)P_2 in fed conditions, leads to mTORC1 activation by binding to Raptor subunit of mTORC1 (Bridges et al., 2012). **Fig 20.** summarizes the regulations of lysosome functions by PIPs discussed above.

PIPs regulate sterol transfer at lysosome contact sites:

I have introduced how lysosome-ER contact sites influence lysosome positioning and mTORC1 signaling. These contact sites also are known for non-vesicular transfer of sterols from lysosomes to ER and PIPs are important in this transport. LDL-cholesterol that reached lysosomes through the endocytic pathway is degraded here to give rise to free cholesterol. This free cholesterol is transported to the lysosome membrane via the cholesterol transporter NPC1/2 (Pfeffer, 2019). From there, cholesterol is transferred to the ER via the ORP1L by formation of ER-lysosome contact sites. Interestingly, this transport is stimulated by PI(3,4)P_2 and impaired when cells were depleted of PI3KC2β kinase, which is required for generation of PI(3,4)P_2 at lysosomes (Dong et al., 2019; Marat et al., 2017). In addition, PIPs also regulate sterol transfer through proteins for e.g., Oxysterol-binding protein (OSBP) interacts with golgi PI4P through its PH domain and with ER protein VAPA through its FFAT domain. This contact site enables transfer of cholesterol from ER to golgi in exchange for PI4P(Mesmin et al., 2013). Another example would be the oxysterol-binding protein

related protein 2 (ORP2). ORP2 shows affinity of binding to the plasma membrane $PI(4,5)P_2$ and it facilitates transport of cholesterol to plasma membrane in exchange for $PI(4,5)P_2$ (Koponen et al., 2019; Wang et al., 2019) .

In summary, PIPs are integral components of organelle membranes and define their identity and functions. I have here highlighted the functions of PIPs in mTORC1 and TFEB signaling on lysosomes as well as lysosome positioning. Lysosomes contain several PIP species, which could indicate that they regulate several lysosomal functions. PIPs can regulate different proteins by affecting their activity or binding on the lysosomes. In the course of this project, I will study the role of PIPs on lysosomes in bladder cancer.

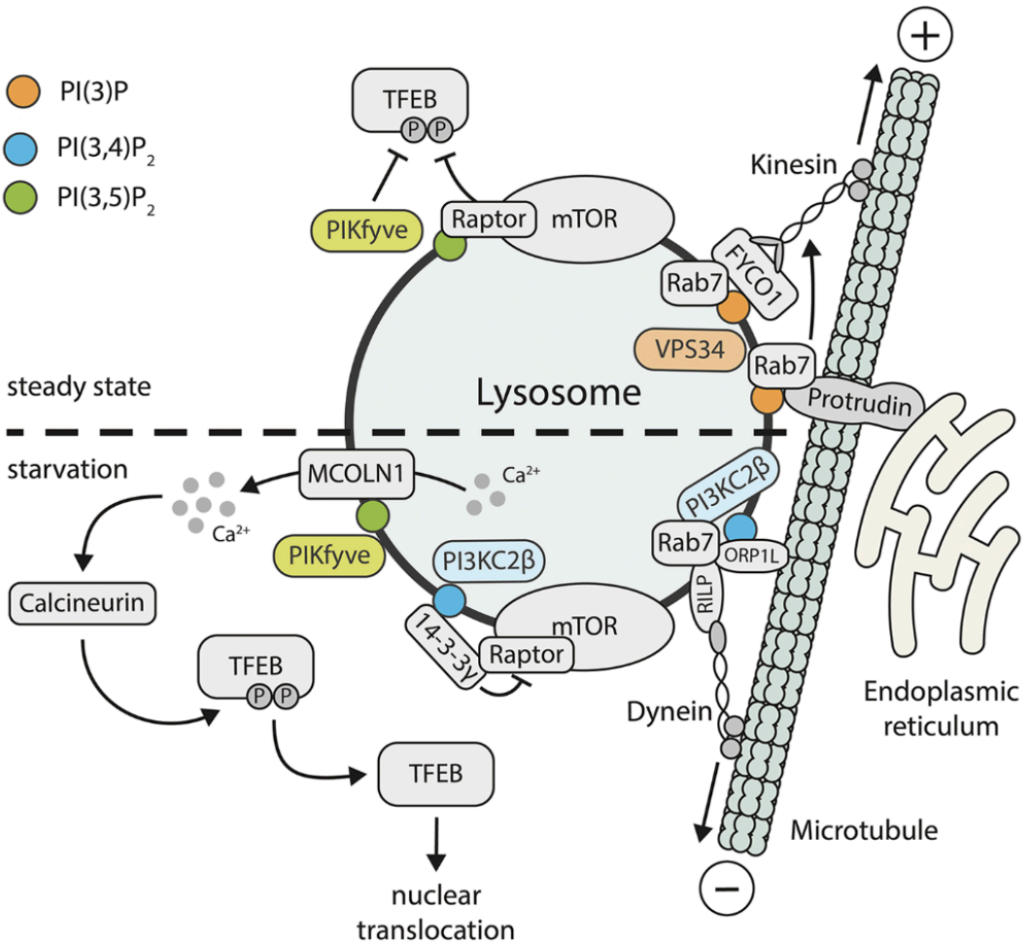

Fig 20. Role of PIPs in regulation of mTORC1, TFEB signaling and lysosome positioning

1.9. TFEB, cancer cell metabolism and functions of lysosome membrane contact sites

I have introduced the central role of lysosomes in cellular nutrient homeostasis and how this balance is disrupted in cancer. Because TFEB plays a crucial role in cellular metabolic pathways, alterations in its regulation at lysosomes could be exploited by cancer cells to rewire the cellular metabolism. In this section, I focus on our current knowledge of the role of TFEB in regulating cancer cell metabolic pathways. Because membrane contact sites emerge as important players in cancer cell metabolism, I will also mention contact sites formed by lysosomes and their relevance in cancer progression.

Cancer cell metabolism and metabolic rewiring is established as a crucial hallmark of cancer (Pavlova and Thompson, 2016). This is highlighted by the pivotal finding of Otto Warburg that cancer cells depend on glucose instead of the more energy generating oxidative phosphorylation (Warburg, 1925, 1956). The major pathways of glucose uptake in cells is through stimulation of growth factor signaling by molecules such as PDGF (Platelet Derived Growth Factor) or EGF (Epidermal Growth Factor) (Thompson, 2011). Growth factors stimulate the PI3K-Akt signaling axis, which leads to more expression and plasma membrane localization of the glucose uptake receptor GLUT-1 facilitating cellular glucose uptake (Wieman et al., 2007). Activity of the enzyme hexokinase, which is important for the phosphorylation of glucose and its utilization in glycolysis, is also elevated in cells with increased Akt signaling supporting increased glycolysis (Rathmell et al., 2003). In cancer cells, deregulation of EGFR signaling and activating mutations in PI3K or inactivating mutations in PTEN that negatively regulates PI3K pathway are usually observed, including bladder cancers. This leads to upregulated glucose uptake and metabolism in tumor cells. Other than this mechanism, other factors such as degradation of the ECM components, for instance hyaluronic acid, has recently been shown to regulate glucose uptake as well as utilization (Pavlova et al., 2022; Sullivan et al., 2018). Interestingly, TFEB has been reported to control several genes involved in glucose uptake and metabolism (Mansueto et al., 2017). It has been shown in skeletal muscles that during exercise/ starvation activated TFEB regulated glucose uptake and metabolism. TFEB directly binds to the promotor of GLUT1/4 and increases their expression resulting in higher

glucose uptake. TFEB overexpression also correlated with increased expression of hexokinase, the enzyme of glycolysis that regulates glucose metabolism (Mansueto et al., 2017). These observations could suggest that in malignancies, which dependent of TFEB hyperactivity, TFEB could be responsible for driving glucose uptake and metabolism.

Other than glucose, glutamine dependency has been observed in many cancers. Glutamine is an important source of nitrogen for cancer cells and is important for nucleotide synthesis and the production of non-essential amino acids. It has been shown that glutamine is also important for the uptake of essential amino acids such as leucine, which cannot be synthesised by the cells and are acquired by external sources. Efflux of glutamine was shown to be coupled to the activity of plasma membrane localized amino acid anti-transporter (LAT1) for the uptake of essential amino acids like leucine. This also regulated mTORC1 activity, which was dependent on amino acids (Nicklin et al., 2009). Glutamine has been shown to control mTORC1 and autophagy pathways through other mechanisms as well (Durán and Hall, 2012). Glutamine can be substituted as a carbon source to fuel the TCA cycle by the process of anaplerosis, in which the TCA cycle proceeds through non-conventional alternative substrates in stress conditions or malignancies. Glutamine is deaminated and converted to alpha-KG (alpha-ketoglutarate) by the enzyme GLS (glutaminase) and GLUD1 (glutamate dehydrogenase). Thus, the TCA cycle is sustained through formation of alpha-KG instead of citrate. Alpha-KG formed in mitochondria through glutamine can be transported to the cytosol and increase GTP loading of Rag GTPases. This activates mTORC1 (Durán and Hall, 2012) and inhibits autophagy and TFEB. Interestingly, glutaminolysis produces ammonia, which when diffused to the tumor microenvironment and taken up by stromal cells, facilitates autophagy. This way, increased autophagy in stromal cells provides support and growth advantage to tumor cells in a co-dependent manner. This shows that glutamine can stimulate the TCA cycle, activate mTORC1 and induce autophagy in cancer-surrounding stromal cells. This could underly the coactivation of mTORC1 and autophagic pathways observed in certain cancers (Villar et al., 2015).

Glutamine metabolising enzymes, such as GLS (glutaminase), have been recently shown to be under the control of TFEB in a recent study of pancreatic MiT/TFE family driven cancers. TFEB knockdown in these cells resulted in reduced glutamine metabolism and reduced growth, whereas supplementation of growth medium with

glutamate recovered the growth inhibition by TFEB depletion (Kim et al., 2021). Together these findings point toward an important role of TFEB in cancer cell metabolism, increased glucose and glutamine utilization being one of the functional axis. Although many studies independently have characterized the role of TFEB in metabolism in mouse models, cancer specific studies are very few. Particularly, the integration between different roles of TFEB and its functional importance in cancers is an interesting area of malignancies driven by TFEB.

Another interesting role of TFEB is mitochondrial biogenesis. Shown in skeletal muscles, TFEB depletion significantly led to abnormal mitochondria, which also affected their activity. Contrary, when TFEB was overexpressed in skeletal muscles, it increased mitochondrial respiration and ATP production. TFEB regulates the activity of PPAR gamma co-activator 1 alpha, (PGC1a) by directly binding to its promotor (Settembre et al., 2013b). PGC1a regulates lipid metabolism along with PPAR gamma, however, PGC1a is also a master regulator of mitochondrial biogenesis and functions. Thus, TFEB regulates mitochondrial biogenesis through PGC1a. However, in the study of skeletal muscles, TFEB regulates mitochondrial biogenesis independent of PGC1a, instead it regulates the expression of NRF1/2 and Tfam, both of which can regulate mitochondrial biogenesis in muscles (Mansueto et al., 2017) (**Fig 21**).

Since proper mitochondrial functions are important in meeting the high energy demands of cancer cells, this opens another interesting area of studying the role of TFEB in cancer cell metabolism through mitochondrial quality control (Wang et al., 2020).

Wang et al., 2020

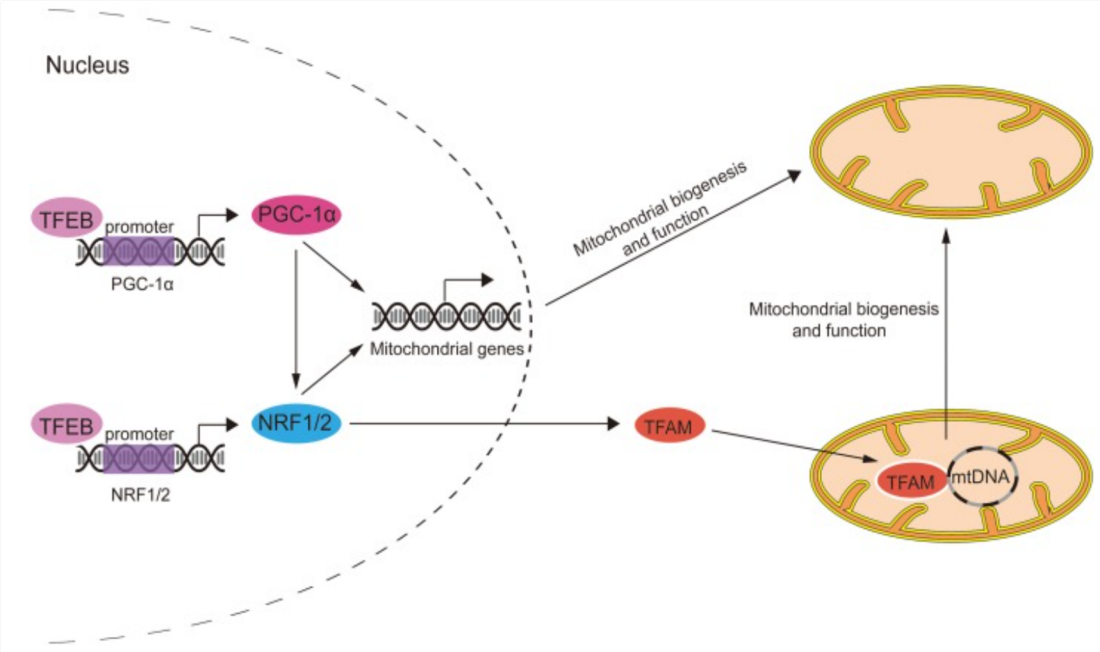

Fig 21. TFEB regulates mitochondrial biogenesis and functions

Lysosomes membrane contact sites in cancer:

Membrane contact sites formed between lysosomes and cellular organelles are important for the regulation of their positioning but could also be a consequence of lysosome positioning alterations observed in some cancers. This however is a prospective area of research, and our current knowledge in this regards remains limited. Below we introduce some of the known functions of lysosome membrane contact sites in cancer progression.

ER-Lysosomes MCS: Lysosome-ER membrane contact sites were presented in the context of lysosome anterograde trafficking that rely on ER protein protrudin and Rab7 that recruit kinesin-1 through the adaptor FYCO1. Interestingly, this contact has been shown to facilitate invasion (Pedersen et al., 2020). In a study of breast cancer, protrudin overexpression led to transport of late endosomes/lysosomes to invadopodia in 3D cell cultures, which facilitated exocytosis of MMP14 and invasion (Pedersen et al., 2020).

Other proteins forming ER-lysosomes contacts are VAPA/B on ER and ORP1L on lysosomes. In addition to ORP1L, ER resident VAPA/B also have been shown to interact with STARD3 (steroidogenic acute regulatory protein-related lipid transferdomain protein 3) (Prinz et al., 2020). Although the function of STARD3 was previously shown to be the redistribution of cholesterol to the plasma membrane, this correlated with FAK/Src signaling and was shown to be elevated in cancers (Vassilev

et al., 2015). It could be speculated that ER-lysosome contact sites through STARD3 could contribute to this phenotype in cancers (Machado et al., 2021).
Finally, ER-Lysosome contacts have been described to maintain calcium transfer in these organelle. These contacts involve IP3R (Inositol 1,4,5-trisphosphate receptor) that are localized at ER and release calcium from ER. Although IP3R does not form a tether of the MCS, calcium is up-taken by lysosomes due to the close opposition between lysosomal and ER membranes. This activity controls lysosome dynamics and positioning. As lysosomes disperse to the cell periphery, the uptake of calcium could potentially decrease, probably due to disturbed ER-lysosome contacts as hypothesised in the study (Machado et al., 2021). It has been speculated that these ER-lysosomes contacts might be crucial for mTORC1 constitutive activation in cancers and help tumor cells to evade calcium mediated cell death (Machado et al., 2021).

Mitochondria-lysosome contact sites: A relative new and mostly uncharacterized MCS are whose between mitochondria and lysosomes. Although their function in cancer is not yet clear, a role of GTP loaded Rab7 has been described in the formation of these lysosome-mitochondria contacts. The mitochondrial TBC1D15, which is a GAP for Rab7, functions in untethering of these contacts between lysosome and mitochondria. Mitochondria-lysosomes contacts regulate lysosome dynamics: indeed, TBC1D15 activates hydrolysis of Rab7-GTP (Wong et al., 2018) that could lead to dissociation of Rab7 from lysosomes and affect lysosomes trafficking (retrograde and anterograde) through RILP or FYCO (**Fig 22A**). Additionally, mitochondria-lysosomes contacts regulate mitochondrial dynamics, because lysosomes have been shown to mark the sites of mitochondrial fission, and disruption of these contacts lead to decreased mitochondrial fission (Wong et al., 2018) (**Fig 22B**). Mitochondria-lysosomes contact sites are speculated to be the sites of metabolite transfer such as lipids, calcium etc. Recently it has been shown that lysosomal calcium channel TRPML1 is important at these contact sites for calcium flux from lysosomes into mitochondria. This transport was found to be disturbed in patients with lysosomal storage disorder mucolipidosis type IV (Peng et al., 2020; Wong et al., 2019) and remain of potential interest in other pathologies (**Fig 22C**). **Fig 22** summarizes these interesting functions of the mitochondria-lysosome contacts.
In summary, intra-organelle contacts formed by lysosomes regulate not only their positioning in the cells but also certain metabolic processes. TFEB appears as in

interesting driver of this process, as it lies at the centre of lysosomal functions, cell metabolism and lysosome organization. Establishing the connection between these various multifaceted functions of TFEB and how it converges on lysosome positioning presents a very interesting area of research.

Wong et al., 2019

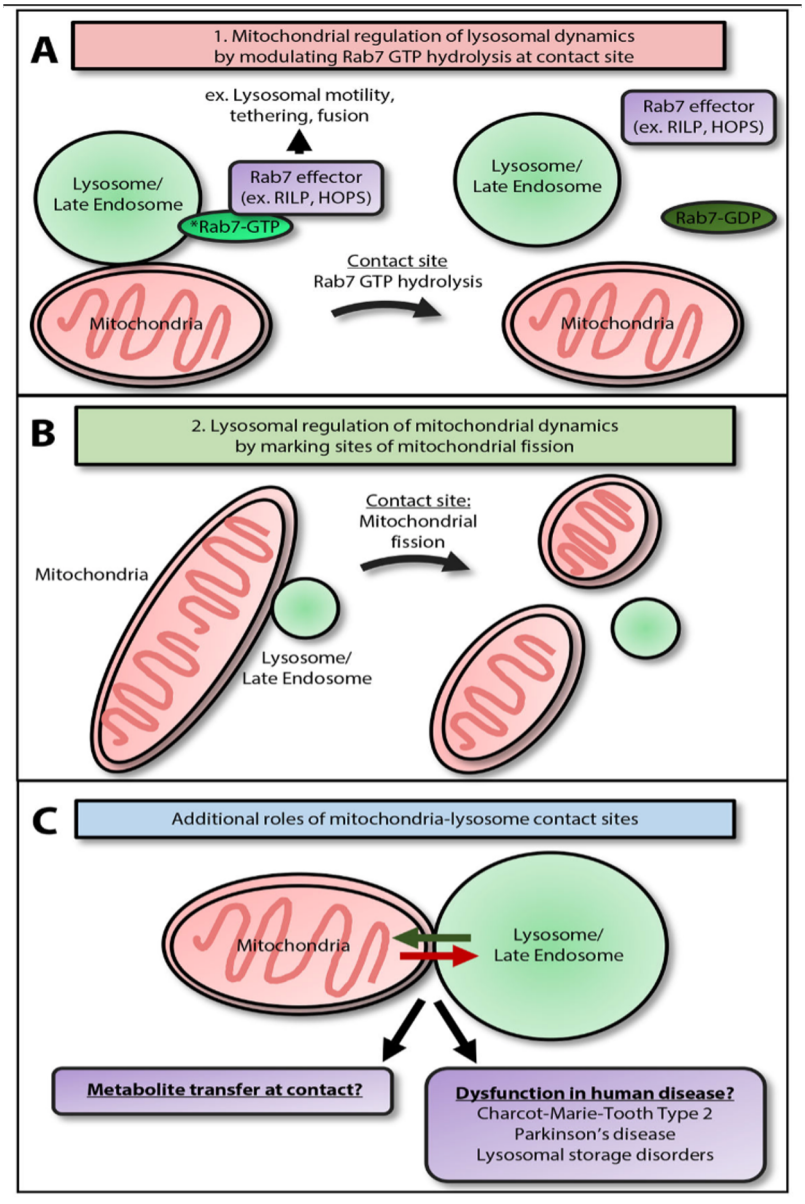

Fig 22. Multiple functions of mitochondria-lysosome contact sites

Chapter 2

Aims and Objectives

2.1 Premise and preliminary results

Intra-organelle cross talks are an emerging area of interest in tumorigenesis studies. Organelles were earlier considered as membrane limited structures acting as independent units within the cells, with specialized and well-defined functions. This perception changed with advanced microscopy techniques revealing reproducible contact sites between several organelles in mammalian cells. Studies have revealed that organelles interact with each other through membrane contact sites (MCS), formed by specialized proteins. MCS regulate a wide range of cellular functions such as metabolism, immune responses, organelle identity and integrity, cell responses to external stimulus and cell death (Patergnani et al., 2021). All these functions are of crucial importance in the development of cancers as they form some of the cancer hallmarks. Thus, intra organelle organization could be an important pre-determinant of cellular functions and an interesting area of study to understand how perturbations in the organization of organelles could lead to pathologies such as cancers. Since organelle organization and positioning is an important element for the contacts formed and potentially their functions, the interest of our lab is to study organelle landscape in normal and bladder cancer cells, which is our model of study.

Previous investigations in the laboratory have focused on the organelle landscape in bladder cancers and have revealed important, consistent changes in the organization of lysosomes between NHU (Normal Human Urothelium) and bladder cancer cell lines (MGHU3, RT112, KU19-19, JMSU1) that represent different aggressiveness of cancer. They had employed the technique of cell culture on adhesive micropatterns of defined geometry that allow normalization of cell shape and compared the positioning of lysosomes between the bladder cancer cell lines mentioned above. The results have shown that, when compared on these normalized cultures on micropatterns, lysosomes are found to be perinuclear, in the cell centre, in normal cells and cancer cell lines representing low grade, but peripheral in cell lines representing high grades (**Fig 23A**). Concomitantly, the Nearest Neighbour Distance (NND) between lysosomes significantly increased in more aggressive bladder cancer cells as compared to normal cells (**Fig 23B**).

To verify the importance of lysosome positioning in bladder cancer invasion, 3D spheroid invasion assays were performed in conditions inducing either peripheral scattering or central clustering (**Fig 24A)**. Preliminary experiments demonstrated that

in the cell line RT112 central lysosomes, after knockdown of Arl8b GTPase, slowed down invasion from 3D spheroids (**Fig 24C**), whereas, Rab7 knockdown, which scattered lysosomes toward the cell peripheral, led to faster invasion from 3D spheroids (**Fig 24B**). These result indicated that changing lysosome positioning alone was enough to regulate cancer progression in RT112 bladder cancer cells. Together these results pointed toward the hypothesis that lysosomal homeostasis was potentially disrupted in bladder cancers. During my PhD project, I have tested this hypothesis and have defined the following aims.

2.2 Aims

1. Investigation of the crosstalk between lysosome positioning and lysosomal signalling pathways:
    a) Role of altered lysosome positioning in mTORC1-dependent signaling
    b) Role of lysosomal signaling pathways in the regulation of lysosome positioning
2. Molecular mechanisms regulating lysosomal dispersion in bladder cancer cells
3. Implications of lysosomal signaling and positioning in bladder cancer progression
4. Role of lysosome positioning in bladder cancer metabolism

2.3 Objectives

Aim 1. Investigation of the crosstalk between lysosome positioning and lysosomal signalling pathways

Lysosomes act as a sensitive monitor of cellular nutrient status by providing a platform for the signalling of mTORC1 kinase. mTORC1, in response to cellular nutrient availability, can initiate anabolic or catabolic pathways from the surface of lysosomes. Since lysosome positioning has been established as an important regulator of signaling through mTORC1, I have investigated whether the inherent phenotypic lysosome positioning changes observed in aggressive bladder cancer cell lines result in alterations in mTORC1 signaling. Additionally, I have tested the reverse, how inducing changes in lysosome positioning in different bladder cancer cell lines regulates mTORC1 signaling.

Aim 2. Molecular mechanisms regulating lysosomal dispersion in bladder cancer cells

I have focussed on the molecular mechanisms that regulate lysosome positioning. Firstly, I have studied the transcription factor EB (TFEB), a downstream target of mTORC1 that regulates not only lysosomal biogenesis and autophagy but also lysosome positioning (Sbano et al., 2017; Willett et al., 2017). Secondly, I have focused on phosphatidylinositol-3-phosphate (PI3P) that is a phospholipid enriched on endosomes that is an key factor in the recruitment of proteins for lysosome intracellular transport (Ebner et al., 2019)

Aim 3. Implications of lysosomal signaling and positioning in bladder cancer progression

I have studied the impact of lysosome alterations during 3D invasion. I have monitored lysosomal secretion, cell proliferation and migration to provide insights on the role of lysosomal changes in cancer-supporting phenotypes.

Aim 4. Role of lysosome positioning in bladder cancer metabolism

Finally, I have started to explore how metabolism is influenced by lysosomal changes in different bladder cancer cell lines. Lysosomes are known to respond to cellular nutrient status, and thus, they could contribute to metabolic rewirering in cancer.

Fig 23

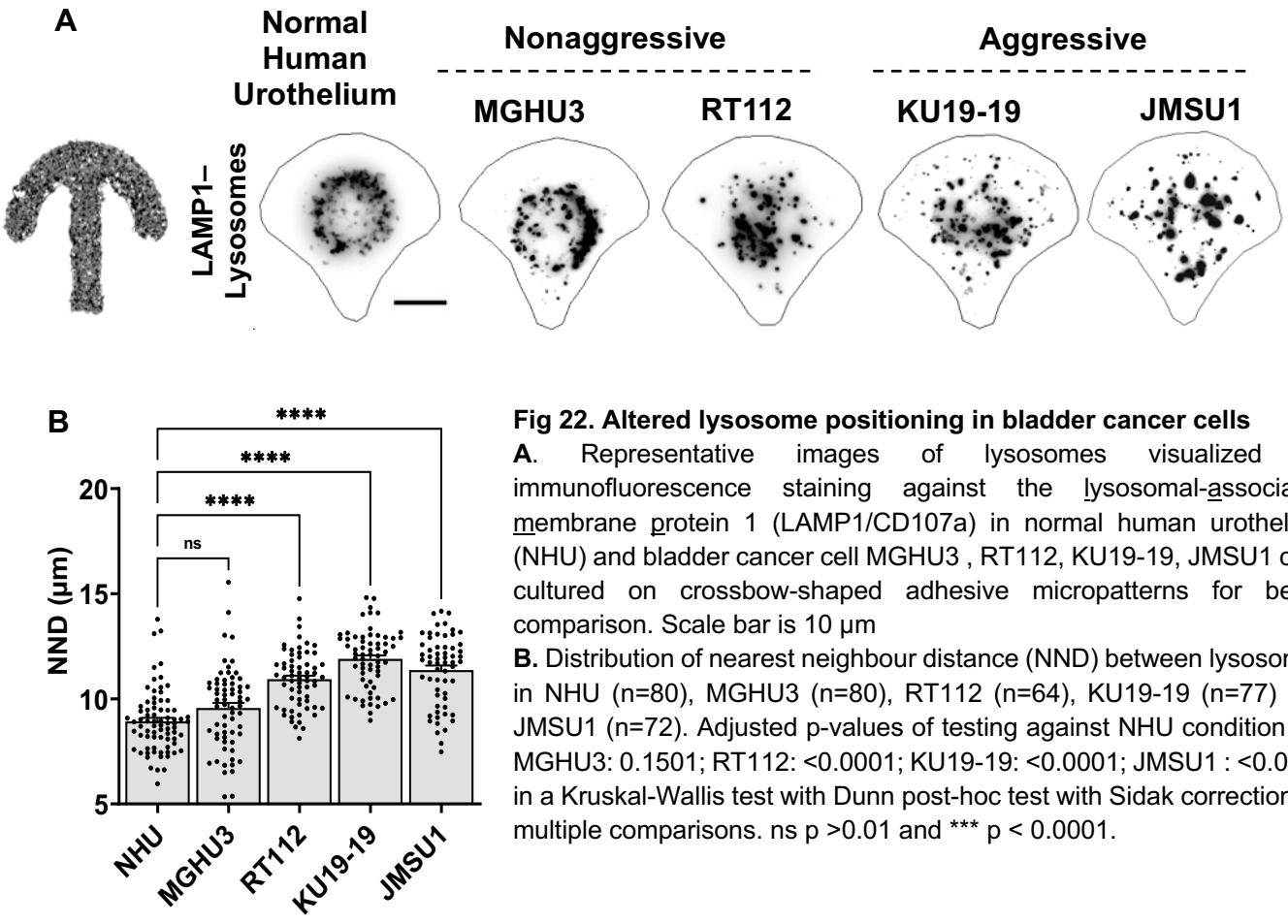

Fig 22. Altered lysosome positioning in bladder cancer cells

A. Representative images of lysosomes visualized by immunofluorescence staining against the lysosomal-associated membrane protein 1 (LAMP1/CD107a) in normal human urothelium (NHU) and bladder cancer cell MGHU3 , RT112, KU19-19, JMSU1 cells cultured on crossbow-shaped adhesive micropatterns for better comparison. Scale bar is 10 µm

B. Distribution of nearest neighbour distance (NND) between lysosomes in NHU (n=80), MGHU3 (n=80), RT112 (n=64), KU19-19 (n=77) and JMSU1 (n=72). Adjusted p-values of testing against NHU condition are MGHU3: 0.1501; RT112: <0.0001; KU19-19: <0.0001; JMSU1 : <0.0001 in a Kruskal-Wallis test with Dunn post-hoc test with Sidak correction for multiple comparisons. ns p >0.01 and *** p < 0.0001.

Fig 24

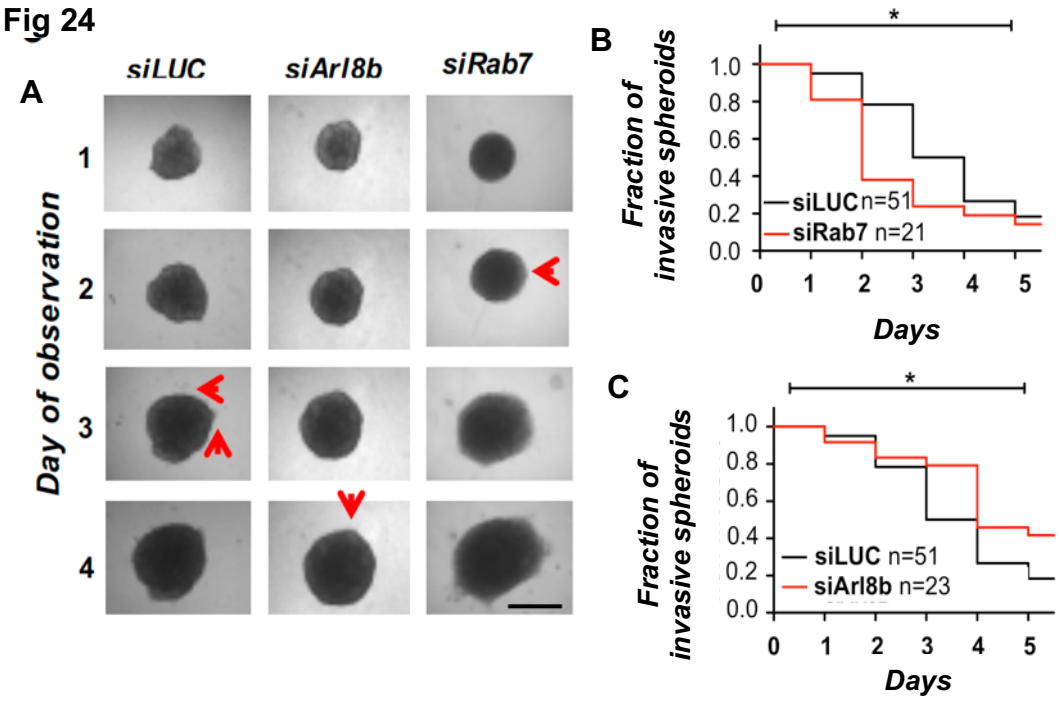

Fig 23. Lysosome positioning regulates 3D invasion in non-aggressive cancer cells

A. 3D invasion of RT112 spheroids into collagen I matrix in control conditions (siLUC) or after siRNA targeting of Arl8b (siArl8b) or Rab7 (siRab7). Red arrows represent invading cells. Scale bar is 0.5 mm. **B**. Invasion rate of RT112 siLUC (black, n=51) and RT112 siRab7 (red, n=21) spheroids as a function of the time (observed at the interval of 1d). * p < 0.05 in a logrank test. **C**. Invasion rate of RT112 siLUC (black, n=51) and RT112 siArf8b (red, n=23) spheroids as a function of the time (observed at the interval of 1d). * p < 0.05 in a logrank test

Chapter 3

Experimental Procedures

We have used the following four cell lines representing different bladder cancer aggressiveness:

	Cell line	Stage	Subtype	Prominent Mutation
1	MGHU3 (non-aggressive)	Ta/T1	Luminal	FGFR3 Mutant
2	RT112 (non-aggressive)	T2	Luminal	FGFR3 Mutant
3	KU19-19 (aggressive)	T3b	Basal	NRAS Mutant
4	JMSU1 (aggressive)	T4	Mixed type	P53 Mutant

(Justin et al., 2020; Zuiverloon et al., 2018)

Table 1: Bladder cancer cell lines used and underlying prominent mutations

3.1 Cell culture and treatments

Bladder cancer cells lines MGHU3, RT112, KU19-19, JMSU1 were grown in RPMI-1640 medium (Life Technologies, Carlsbad, CA, USA), supplemented with 10% Fetal Bovine Serum (FBS; Eurobio, Courtaboeuf, France). RT112 and JMSU1 cells stably expressing Lamp1-mCherry-FKBP and BicD2-HA-FRB were obtained via viral transduction previously in the lab. For A/C heterodimerizer induced endolysosome clustering in cells stably expressing the FKBP-FRB system, 0.5 µM of A/C heterodimerizer (635056; Takara) was added in complete media for 1 hour at 37 ºC. For experiments with inhibitors, as per the experiment either the day after cell seeding or after transfection respective drugs were added for incubation time of 24 h or as indicated and cells were incubated, at 37ºC. The concentration of inhibitors used were as follows: rapamycin (10 µM), wortmannin (1 µM, 2 h), ML-SI1 (20 µM, 3 h), BAPTA AM (10µM, 3 h) and cycloheximide (20 µg/mL). For starvation experiments, the day after cell seeding, the medium was removed and cells were washed once with EBSS (Earle's Balanced Salt Solution) and incubated in EBSS for 4 or 24 h, as per the experiment, before lysate preparation or cell fixation with 4% PFA.

3.2 Cell transfection

For RNA interference studies, 200,000 cells were transfected in 12 well plate with 50nM siRNA. SiRNA used were : siTFEB : ON-TARGETplus Human TFEB, L-009798-00-0005, Dharmacon™; si4EBP1: ON-TARGETplus Human EIF4EBP1, L-003005-

00-0005, Dharmacon™; siLuc: 5'-CGTACGCGGAATACTTCGA-3'; siRab7: 5'-CACGTAGGCCTTCAACACAAT-3' and 5'-CTGCTGCGTTCTGGTATTTGA-3'; siArl8b: 5'-GAUAGAAGCUUCCCGAAAU-3'; Sigma-Aldrich.Transfection was performed using Lipofectamine RNAiMAX Transfection Reagent (1:30; Life Technologies). Cells were incubated 72 h at 37°C prior to further manipulation or drug treatment. Efficiency of gene silencing was verified by western blot of cell lysate after three days of transfection.

For plasmid transfection, 200,000 cells were transfected in a 12 well plate. Transfection was performed using Lipofectamine LTX with Plus reagent (Invitrogen) using 1 µg of plasmid. pEGFP-N1-TFEB plasmid was a gift from Shawn Ferguson (Addgene plasmid # 38119; http://n2t.net/addgene:38119; RRID:Addgene_38119n (Roczniak-Ferguson et al., 2012), EGFP-2X FYVE plasmid (kind gift from B. Payrastre, Toulouse))(Gillooly et al., 2000), or VAMP7. 48 h post transfection, cells were trypsinized and transferred to sterilized coverslips (12 mm) in 1 mL medium in 12 well plate. Cells were fixed with 4%PFA 72 h after transfection and used for immunofluorescence and imaging.

3.3 Micropatterned coverslips preparation and cell seeding

Micropattern production was as previously described (Duong et al., 2012; Schauer et al., 2010a) using photo-lithography methods. Briefly, coverslips were coated with Poly-L-Lysine(20)-grafted[3.5]-Polyethyleneglycol(2) (PLL-g-PEG) from SuSoS (Dübendorf, Switzerland) at a final concentration of 0.1 mg/mL in 10 mM HEPES (pH 7,3) solution. Coverslips were exposed to deep UV during 5 min using a photomask containing arrays of crossbows (37 µm diameter, 7 µm thick). Prior to cell seeding, the patterned surface was incubated for 1 h with a mixture of 50 µg/mL fibronectin (Sigma-Aldrich, St. Louis, MO, USA), 5 µg/mL concanavalin A (Sigma-Aldrich, St. Louis, MO, USA) and 1 µg/mL fibrinogen–Cy5 (Invitrogen). Cells were seeded on micropatterns in RPMI medium supplemented with 20 mM HEPES (Life Technologies) for 4 h prior the experiment.

3.4 Invasion assay

Cells were trypsinized and re-suspended in RPMI medium containing 10% FBS and 1% Penicillin-Streptomycin (Life Technologies) in concentration of 100,000 cells/mL.

Then 100 µl of cell suspension was plated in 96-well plates previously coated with 1% agarose (left at room temperature (RT) after coating for 1h) (Life Technologies) and incubated for 3 days. In each well, a spheroid was formed from 10,000 cells. Next, the spheroids were plated on the 8 well Lab-Tek chambered slides (Sigma), in a 15µL drop containing a mixture of collagen I from rat tail (Corning) at a final concentration of 2 mg/ml, 1X PBS, sodium hydroxide (NaOH, 0.05M) and serum-free medium. The spheroid in the collagen mix was left undisturbed until collagen was polymerized (about 20-30min at RT). 400µL of complete media was added to each 8 well of the chambered slide with the spheroid, carefully as to not disturb the collagen drop that contained the spheroid at incubated at 37°C (**Fig 25**). The spheroids were monitored for 3-4 consecutive days by using the EVOS FL microscope with camera device using 4x objective. For invasion assay after TFEB depletion, siRNA knock down was performed, as described before, prior to formation of spheroid and siTFEB was added to the mixture during collagen coating in the serum free media (50nM) that was the component of the collagen mix.

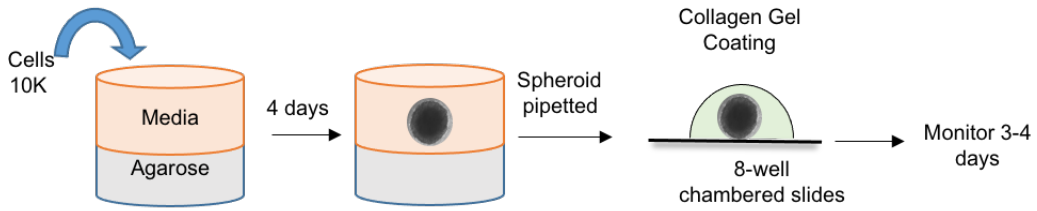

Fig 25. Invasion assay protocol

3.5 Immunofluorescence

Cells were fixed with 4 % formaldehyde for 15 min at room temperature, washed three times with PBS and permeabilized in PBS containing 0.2% BSA and 0.05% saponin. Cells were then incubated with the primary antibodies (mouse monoclonal antibody against Lamp1/CD107a (1:1000, 555798, BP Pharmingen™), rabbit mAb against mTOR (1:1000, 7C10, #2983, Cell Signaling Technology), EEA1 (1:200; 610456, BD Biosciences), protrudin / ZFYVE27 (1:500; 12680-1-AP, Proteintech) and Alexa Fluor 488 (1:400), or Alexa Fluor 647 (1:400) or Cy3-coupled (1:400) secondary antibodies (Jackson ImmunoResearch) for 1 h. Actin was visualized by FluoProbes 547H (557/572nm) coupled Phalloïdin (Interchim) and nuclei with 0.2 µg/mL 4',6-diamidino-

2-phenylindole (DAPI; Sigma-Aldrich). Coverslips were mounted in Mowiol (Sigma-Aldrich).

3.6 Western blot

250,000 cells were seeded in a 12 well plate one day prior to the experiment. Drug treatments or knock-down experiments were performed as mentioned before. Equal volumes of lysate from each cell line was loaded on a 10% or 12% polyacrylamide gel, resolved by SDS-PAGE and electrotransferred to nitrocellulose membranes. Membranes were incubated with primary antibodies at 4ºC overnight: Phospho P-70 (Thr389)-S6K (CST: 9205S, 1:1000 in 5% BSA in TBST), P-70 S6K (CST: 9202S, 1:1000 in 5% milk in TBST), GAPDH (Sigma: G9545, 1:10,000 in 5% milk in TBST), EEA1(610456, BD Biosciences, 1:500 in 5% milk in TBST), protrudin (ZFYVE27, Proteintech 12680-1-AP) and species specific HRP secondary antibodies (1:10,000) for 1 hour at room temperature, following ECL western blotting substrate.

3.7 Image acquisition

Images for immunolabelled cells on micropatterns were acquired with an inverted wide field Deltavision Core Microscope (Applied Precision) equipped with highly sensitive cooled interlined charge-coupled device (CCD) camera (CoolSnap Hq2, Photometrics). Z-dimension series were acquired every 0.5 µm.

Images for non-pattered immuolabelled cells were acquired with a spinning disk confocal microscope (Inverted Eclipse Ti-E (Nikon) + spinning disk CSU-X1 (Yokogawa) integrated with Metamorph software by Gataca Systems). Cells were imaged as z-stacks with 0.2 µm distance and 12 µm total height.

3.8 Image processing and analysis

For cells on micropatterns, several tens of single cell images were aligned using the coordinates of the micropattern (determined on ImageJ (Bethesda, MD, USA) as previously described (Grossier et al., 2014; Schauer et al., 2010b). To extract the 3D spatial coordinates of lysosomes, images were segmented with the multidimensional image analysis (MIA) interface on MetaMorph (Molecular Devices, Sunnyvale, CA, USA) based on wavelet decomposition.

Image analysis for colocalization results was done using CellProfiler (version: 3.1.9) on one-plane of the images. The pipelines for different analysis were prepared as follows:

To detect the total and membrane bound intensities of protein of interest (labelled as total integrated intensity or spots/total, respectively, in the figures) or intensities of co-localized proteins the pipeline was created as follows:

Step 1: Module '*EnhanceorSuppressFeatures*' was applied to channels where the objects needs to be segmented, either to obtain their intensities or objects for the intensities of co-localized proteins, to get sharp and defined objects which makes segmentation easier (for eg. On channels with LAMP1 or EEA1 or GFP-FYVE).

Step 2: Nucleus was identified in the DAPI channel using the '*IndentifyPrimaryObject*' module

Step 3: Module '*IndentifyPrimaryObject*' was used again on the images obtained from Step 1 to segments objects whose measurements are required (such LAMP1, EEA1, EGFP-FYVE)

Step 4: Cells were segmented using the '*IdentifySecondaryObject*' module with nucleus as the 'primary object' (identified in step 2) and using phalloidin or another cytoplasmic protein channel to recognize the cell boundaries.

Step 5: Module '*RelateObjects'* was used to relate the objects obtained in step 3 to each cell obtained in Step 4. Output of this channel was saved as another object which gives the objects of protein of interest per cell.

Step 6: Objects from step 3 were masked on the channel whose co-location or membrane bound fraction had to be calculated using the '*MaskImage*' module. (for eg: to calculate EGFP-FYVE on lysosomes in Fig. 4B, Lysosomes were segmented in step 3 and the output objects were masked on EGFP-FYVE channel or to calculate membrane bound EGFP-FYVE, segmentation of EGFP-FYVE objects from step 3 was masked on EGFP-FYVE channel)). Output of this step was saved as a new image in the pipeline.

Step 7: '*MeasureObjectIntensity*' module was used to obtain total 'per cell intensity' and 'intensity on spots' of protein of interest. Intensities were picked from images from step 6 and raw images of channel of interest using cells from step 4 as the objects.

Step 8: Cell size was obtained using the module '*MeasureObjectSizeandShape*' on the cells segments in Step 4 as the objects

Step 9: Finally, all the measurements were exported to the excel sheet using the

module '*ExporttoSpreadsheet*'

Step 10: The final values were exported to a csv file named 'cell'. This file had the values of cell size (in pixels), total intensity of protein of interest per cell, intensity of protein of interest on spots and intensity of co-localized protein on the object of interest (eg: GFP-FYVE on lysosomes). Integrated intensities were used for the analysis and to plot the graphs.

3.9 Statistical analysis

The statistical analysis of endolysosome volume, number and normalized NND was performed with R (3.6.0). For NND analysis, the centroids distance between structures was calculated from a constant number of lysosomes that was randomly sampled from each cell. Therefore, variation in NNDs cannot be imputed to variation in the number of lysosomes but to bona-fide variation of their spatial organization. The statistical analysis was a Kruskal-Wallis test with Dunn test for multiple comparisons correction. For all experiment, a large number of cells were monitored from 3 to 6 independent experiments. Two-sided Mann-Whitney U test were performed for 2 conditions comparisons. For multiple comparisons, a Kruskal-Wallis has been used with Dunn's test for multiple comparisons. Additionally, to compare the global distribution of cell population, χ^2 tests were performed (R function "chi-square()") and Benjamini-Hochberg multiple comparison correction has been applied. For the statistical analysis on the data from CellProfiler, Prism was used. Mann-Whitney U test was applied for the two conditions comparison or Kruskall-Wallis test with Dunn test for multiple comparison.

3.10 Seahorse assay for cell metabolism:

Seahorse assays were performed as per the commercial kit protocols. Either Cell Phenotype Assay was performed or the Mito Fuel Flex test was performed.

Cell Phenotype assay: This assay measures mitochondrial respiration and rate of glycolysis as the OCR (oxygen consumption rate) and ECR (extracellular acidification rate) respectively. This assay uses a mixture of 2 drugs: Oligomycin, that blocks mitochondrial ATP synthase and causes compensatory increase in glycolysis to meet the energy demand in the cells; and FCCP that depolarizes mitochondrial membranes and facilitates the cells to consume more oxygen as mitochondrial membrane potential

is restored. The readings are taken before and after drug addition to assess the baseline and stressed metabolic phenotype of the cell.
Detailed protocol for the Cell Phenotype Assay is described at:
(https://www.agilent.com/cs/library/usermanuals/public/XF_Cell_Energy_Phenotype_Test_Kit_User_Guide.pdf)

Mito Fuel Flex test: This assay measures the rate of consumption of different fuels in the cells namely, glucose (pyruvate), Glutamine (glutamate) and fatty acids (FA). It measures mitochondrial respiration (OCR) in cells by using drugs in different combinations to block pathways specific to each fuel and asses the dependency of cells on specific type of fuel and flexibility to use alternative fuel when they cannot utilize the others. The drug used in this assay are UK5099, that block consumption of pyruvate in oxidative phosphorylation by blocking mitochondrial pyruvate carrier; BPTES, block consumption of glutamine in oxidative phosphorylation by blocking the enzyme Glutaminase (GLS) the prevents conversion of glutamine to glutamate; and Etomoxir blocks consumption of FA in mitochondrial beta oxidation by inhibiting carnitine palmitoyl-transferase 1A (CPT1A) that is required for transport of FA to mitochondria.
Detailed protocol for the Mito Fuel Flex test is described:
(https://www.agilent.com/cs/library/usermanuals/public/XF_Mito_Fuel_Flex_Test_Kit_User_Guide%20old.pdf)

Steps of the assays were as follows:
1) One day before the seahorse assay, bladder cancer cells were seeded in a 96 well seahorse plate, 20,000 cells per well each in 80uL media. The cartridge was hydrated (it contains the sensors which go to each well of the assay plate) as per the protocol, seal and incubate it overnight at 37°C
2) On the day of the assay assay medium DMEM provided by Agilent was supplemented as follows (for 50mL media)

- 1mM Pyruvate (100mM Stock) - 0.5mL
- 2mM Glutamine (200mM Stock) - 0.5mL
- 10mM Glucose - 90mg; pH was adjusted if required to 7.4 with 0.1M NaOH

3) Cells were washed in assay media multiple times as follow

- Remove: 60µL
- Add: 160µL
- Remove: 160µL
- Add: 160µL
- Remove: 180µL; Add: 180µL and incubate cells in CO_2 free incubator at 37°C.

4) **For the Cell Phenotype Assay**: Working solutions (10X) for the drugs FCCP and Oligomycine were prepared to get the following concentrations in the wells: FCCP 0.5µM, Oligomycine 1µM diluted from a previously prepared stock solutions (stock solutions were 100X, working solution was 10X to get 1X in each well when added to cells with 200 µL media).

For the Mito Fuel Flex test : Working solutions for the drugs BPTES, Etomoxir, UK5099 were as follows: BPTES (3 µM), Etomoxir (4 µM), UK5099 (2 µM) diluted from previously prepared stock solutions (stock solutions were 100X, working solution was 10X to get 1X in each well when added to cells with 200 µL media).

5) 20µL of drugs were loaded to the ports of the cartridge using the guide plate. Sensors of the cartridge were still in the calibrant plate.

For **Cell Phenotype Assay** 20uL already contained the mixture of oligomycin and FCCP.

For **Mito Fuel Flex test**, each of the 3 drugs were added to the ports of the cartridge in different combinations which is described in the commercial protocol.

6) Guide plate was removed and the cartridge with calibrant plate was inserted in the seahorse machine to run the calibration and to enter the cell plate layout and the assay parameters for the run cycle in WAVE software.

8) After calibration: The cell plate is inserted in the machine after removing the calibrant plate (cartridge is retained in the machine after calibration)

9) Assay was run and the results were exported to excel .

3.11 Matrix metalloproteinases (MMP) assay

MMP assay was performed using the SensoLyte® 520 Generic MMP Assay Kit (Cat No. AS-71158). It detects a variety of MMPs and is based on fluorescence detection after proteolysis of the generic MMP substrate when incubated with samples containing MMPs. The kit uses a generic MMP substrate tagged with a quencher i.e. 5-FAM/QXL™520. When intact the 5-FAM is quenched by QXL™520, however when

cleaved by the MMPs in the samples the quencher releases the (-FAM and its fluorescence can be detected at excitation/emission wavelengths of 490nm / 520nm (**Fig 26**). The fluorescence was measured using the microplate reader CLARIOstar (BMG LABTECH).

The detailed protocol can be found at (https://www.anaspec.com/assets/2410244f-dac2-4150-9887-21f80b5f4a98/tds-en-as-71158-sensolyte-520-generic-mmp-activity-kit-fluorimetric.pdf).

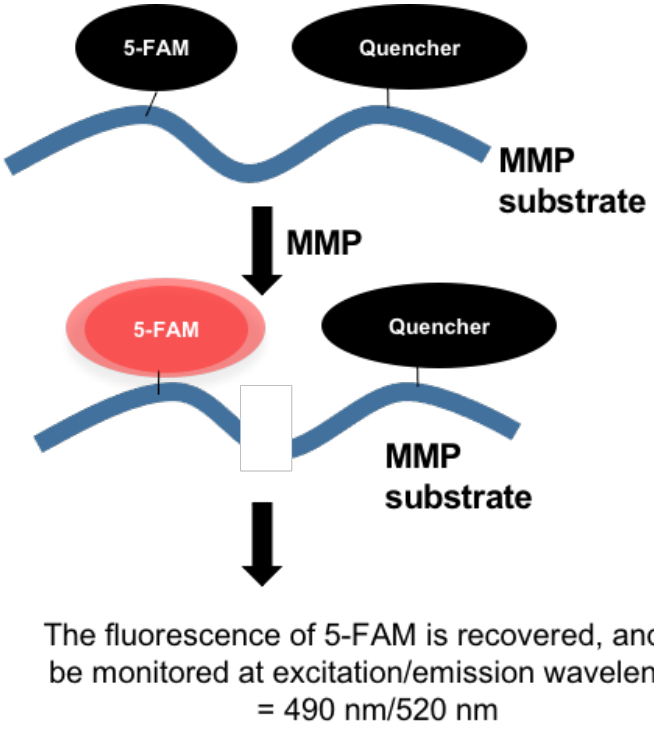

Fig 26. Working principle of MMP assay

Calibration using the standards : Before the assay, instrument calibration was performed using the 5-FAM reference standard (5-FAM-Pro-Leu-OH) provided with the kit. Standards were diluted serially in a 2-fold manner to obtain the concentrations 2.5, 1.25, 0.625, 0.3125, 0.156 and 0.078µM in a assay buffer included with the kit in a volume of 50µL. 50µL of standards were added to a 96 well plate and fluorescence reading were taken using the microplate reader (490nm / 520nm). A linear standard curve was plotted to get the line equation (**Fig 27**)

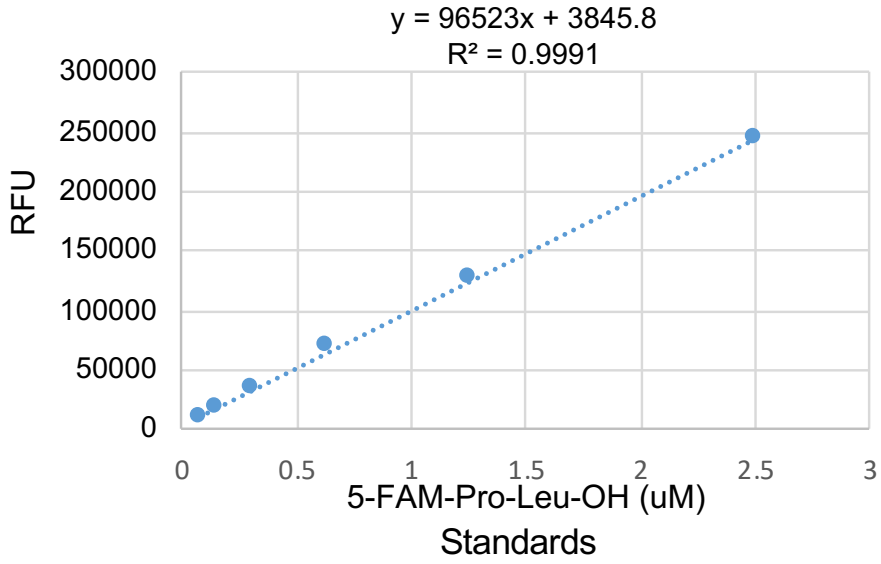

Fig 27. MMP assay standard curve

Assay protocol:

1) Equal number of cells (200,000/ well) were seeded in a 12 well plate 24h before the experiment and incubated at 37°C

2) 200µL of media supernatant was collected from each well in ice and centrifuged at 1000xg at 4°C

3) Samples were incubated with 1mM AMPA (4-aminophenylmercuric acetate) provided with the kit to activate the MMPs in the samples and incubated at 37°C for 3h.

4) After 3h of incubation, 50µL of sample was added to wells of a 96 well plate (4 replicated were recorded for each sample from the 200µL sample collected in step 2).

5) 50µL of MMP substrate (5-FAM/QXL™520), diluted 1:100 in assay buffer (provided with the kit) was added to each sample well in the 96 well plate.

6) Fluorescence reading were taken at time intervals of 5h, 18h and 24h post addition of MMP substrate using the microplate reader at the wavelength 490nm / 520nm.

3.12 Glutamine uptake assay

Glutamine uptake in bladder cells was detected using the protocol of the commercial kit - Megazyme L-Glutamine/Ammonia Assay Kit (product code: K-GLNAM). Glutamine in the samples is detected in two steps:

Step1: Glutamine is first converted to glutamate by addition of the enzyme Glutaminase to the samples. This reaction generated ammonium ions ($NH4^+$) in addition to glutamamte.

Step2: Reduced nicotinamide-adenine dinucleotide phosphate (NADPH) and the enzyme glutamate dehydrogenase (GIDH) are then added to the samples (provided in the kit) . GIDH converts glutamate formed in step1 to 2-oxoglutarate. $NH4^+$ formed in step1 reacts with 2-oxogultarate to convert NADPH to $NADP^+$. Absorbance of samples is taken before and after GIDH addition at wavelength of 340nM to calculate decrease in NADPH levels. Amount of $NADP^+$ formed is stoichiometric to the amount of glutamine in the sample.

The detailed protocol can be found at:

(https://www.megazyme.com/documents/Assay_Protocol/K-GLNAM_DATA.pdf)

Assay protocol

1) Equal number of cells (200,000/ well) were seeded in a 12 well plate 24h before the experiment and incubated at 37°C

2) 100µL of media supernatant was collected from each well and added to plastic cuvettes. To 100 µL of test sample, 200µL of solution 1 buffer and 200µL of suspension 4 (glutaminase) was added from the kit. To the blank reading no sample was added but just the other 2 components.

3) Mix was incubated at room temperature (RT) for 5mins

4) To both the test and sample cuvette, 1.5mL of distilled water, 300µL of solution 2 buffer and 200µL of solution 3 (NADPH) was added and after 4 min, absorbance (A1) was taken at 340nm using a spectrophotometer.

5) 20µL of suspension 5 (GIDH) was added to both the cuvettes and after 5mins of reaction at RT, absorbance (A2) was taken at 340nm using a spectrophotometer.

6) Glutamine concentration was calculated using the formula described in the kit.

3.13 Total Internal Reflection Microscopy (TIRF) and analysis

Bladder cancer cells were transfected with VAMP7-pHluorin after described before. For TIRF assay with cells having TFEB knockdown, siRNA transfection was performed and then subsequent transfection with VAMP7-pHluorin was performed, as per the protocol described before. One day before the experiment the cells with transfections were seeded on 35mm glass bottom fluorodishes. Secretion from cells was imaged using the Nikon Super Resolution TIRF/STORM-PALM microscope. Movies were

imaged for about 1-2mins and secretion events were calculated manually by counting the burst of fluorescence observed on the plasma membrane of the cells.

3.14 Cytoplasmic pH testing:

Cells (200,000) were seeded in 35mm Fluorodishes and stained with pHRodo Green (Invitrogen) according to the manufacturer's protocol along with 50nM LysoTracker Deep Red (Invitrogen) and incubated at 37ºC for 1 hour. Cells were washed with complete RPMI media and imaged live using an inverted wide field Deltavision Core Microscope. For calculating the RFU (Relative Fluorescence Unit) of cytoplasmic pH, 25,000 cells were seeded in black bottom 96 well cell culture plates and stained with pHRodo Green as before for 1 hour at 37ºC. Cells were then washed with complete RMPI 1640 media and readings were taken using CLARIOstar plate reader (BMG LABTECH) using excitation/emission of 509/533.

3.15 Cell proliferation and migration analysis through lens free microscope

We used the lens free microscope setup called Cytonote (from Iprasense, Montpellier, France) to obtain videos of cells over 3 days to monitor their proliferation and migration in different treatment conditions. Cytonote images cells over a wide field of view (FOV) of area of 29.4 mm^2. This microscope uses RBG (Red, Green and Blue) illumination delivered by LEDs through a pinhole that is about 5cm above the cells / samples. Cytonote is equipped with a CMOS image sensor, cell culture plates are placed above the CMOS sensor in the setup of the assay and the whole setup is compact enough to fit inside the cell culture incubator to monitor different cellular parameters in live cells. When cells are illuminated, the CMOS sensor receives the holographic interphase pattern formed by the scattering of light by the cells and light passing through directly from the source to the sensor, which is recorded as images/videos. These images of the cells are then reconstructed through holographic reconstruction method which involved back propagating the light intensity recorded by the sensor. (Allier et al., 2017). The assay was performed in collaboration with Dr. Cédric Allier (CEA LETI, Grenoble) who performed the reconstruction of images obtained from Cytonote and the analysis of the data.

Assay protocol:

1) 6 well glass bottom plates were coated in fibronectin (30µg / mL, Sigma-Aldrich, St. Louis, MO, USA) for 1h at room temperature. After which the fibronectin solution was removed the cells were seeded

2) One day before the imaging in Cytonote, cells were seeded at a concentration of 3000 cells / well and incubated at 37°C overnight.

3) Next day, siTFEB or siLuc was added to the cells (50nM) and the plate was placed on the Cytonote fixed inside the cell culture incubator.

4) Cytonote was connected to the computer outside the incubator where the images are recorded, one image is recorded every 5 min for a total duration of 3 days.

3.16 Cell fragmentation

1) 1.5 million cells were seeded in a 10cm dish 2-3 days before the experiment and allowed to grow

2) After 3 days cells were washed once in ice cold PBS, pH 7.4 and scrapped using a plastic scrapper in 1.5mL ice cold PBS

3) Cells were centrifuged for 10sec in a tabletop pop-spin centrifuge and the supernatant were discarded

4) The pellet was resuspended in 1.2mL of ice cold 0.1% NP40 (Sigma Aldrich) in PBS and 400µL of mix was removed as the whole cell lysate. 100µL of 5X laemmli buffer was added and the sample was boiled for 1 min

5) Rest of the sample was centrifuged as above and 400µL of supernatant was collected as the cytosolic fraction. 100µL of 5X laemmli buffer was added and the sample was boiled for 1 min. Rest of the supernatant was discarded

6) Pellet containing the nuclear fraction was resuspended in 400µL of 1X laemmli buffer and the sample was boiled for 1 min

3.17 DQ BSA uptake assay

1) 100,000 cells were seeded on a coverslip in 1mL media in a 12 well plate one day before the uptake assay.

2) Next day, DQ BSA (50µg/mL) was added to the cells in the cell culture media and the cells were incubated for required time points at 37°C in the cell culture incubator

3) Cells were fixed with 4% PFA and imaged

For siTFEB treatment, the transfection was performed as per the protocol described before 1 day before and on the 2nd day cells were transferred to coverslips in a 12 well plate. On 3rd day the DQ BSA staining was performed as described above.

Chapter 4

Results and Conclusions

(Note: Results of aims 1 and 2 correspond to a complete story under revision in Communications Biology)

Results Aim 1- Investigation of the crosstalk between lysosome positioning and lysosomal signaling pathways

4.1. Signaling from lysosomes – mTORC1 signaling in different bladder cancer cell lines

Because mTORC1 activity has been shown to be regulated by the positioning of lysosomes, we first tested whether the alteration in lysosome positioning that we see in the different bladder cancer cell lines are also reflected by changes in mTORC1 signaling. To test this, we monitored mTORC1 activity by studying the two steps crucial for the activation of mTORC1, the recruitment of mTOR to the surface of lysosomes and the phosphorylation of mTORC1 substrates. First, we analyzed mTOR localization by co-visualizing it with LAMP1 by immunofluorescence and measuring the fraction of mTOR that localized on the LAMP1-positive compartment. We found that about 15-20 % of mTOR signal was found on lysosomes in different cell lines. Although RT112 showed slightly but significantly more mTOR on lysosomes, the levels of mTOR on lysosomes were comparable between the tested cell lines (**Fig 28**). Next, we tested mTORC1 activity by monitoring the phosphorylation of the direct downstream substrates. We analysed eIF4E Binding Protein (4EBP1) and p70-S6 Kinase 1 (S6K1) that are phosphorylated by mTORC1 to activate protein synthesis. Interestingly, phosphorylation of 4EBP1 was high in KU19-19 and JMSU1 cells that represent the aggressive cancer cell lines as compared to MGHU3 and RT112 cells that represent non-aggressive cancers (**Fig 29**). Contrary, phosphorylation of S6K1 was opposite: we detected low phosphorylation of S6K1 in aggressive KU19-19 and JMSU1 cells but high levels of phosphorylation in non-aggressive MGHU3 and RT112 cells (**Fig 30**). Increase of 4EBP1 phosphorylation correlated with an increase of total levels of 4EBP1 (**Fig 29**), whereas the total protein levels of S6K1 remained the same in all cell lines (**Fig 30**).

Fig 28

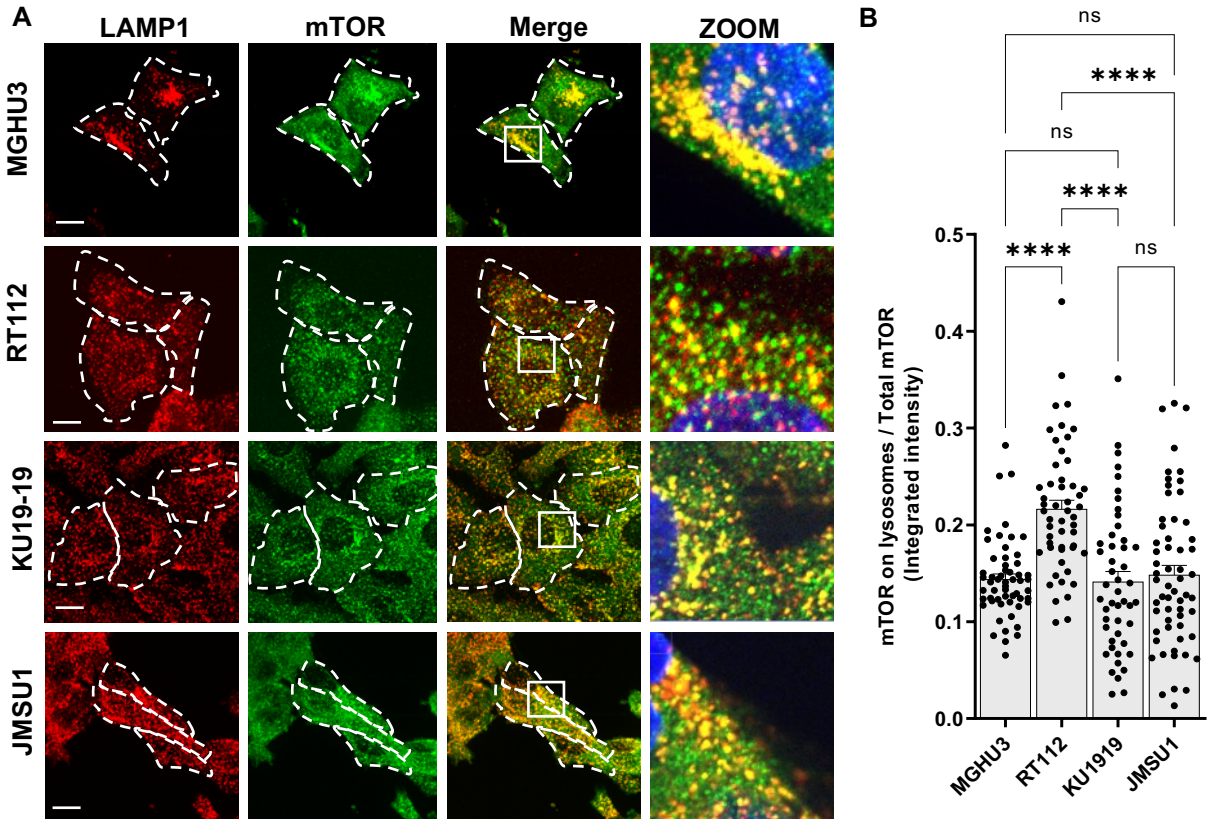

Fig 28: mTORC1 localization on lysosomes in bladder cancer cells

A. Immunofluorescence staining of the lysosomal-associated membrane protein 1 (LAMP1, CD107a) and mTOR in MGHU3, RT112, KU19-19 and JMSU1. The zoom shows the merged image for both proteins of the area in white box. Scale bars equal 15 µm. **B**. Quantification of mTOR intensity on lysosomes normalized to total cellular mTOR (approximately 50 cells) for each cell line; **** p <0.0001; Kruskal-Wallis test with Dunn post-hoc test with Sidak correction

Fig 29

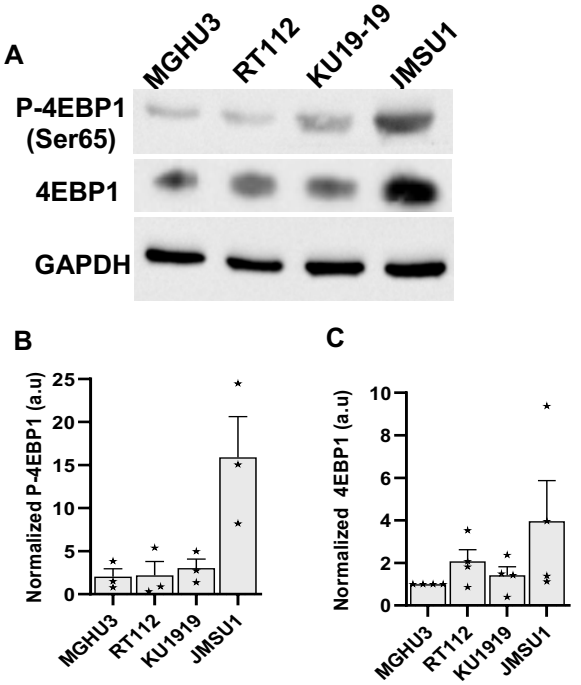

Fig 29. 4EBP1 analysis

A. Western blot analysis of phosphorylated p70-S6 Kinase 1 (P-4EBP1 Ser65) and total 4EBP1 as well as GAPDH loading control in MGHU3, RT112, KU19-19 and JMSU1 cells and quantification of **B.** P-4EBP1 and **C**. 4EBP1 levels from multiple experiments, error bars are SEM.

Fig 30

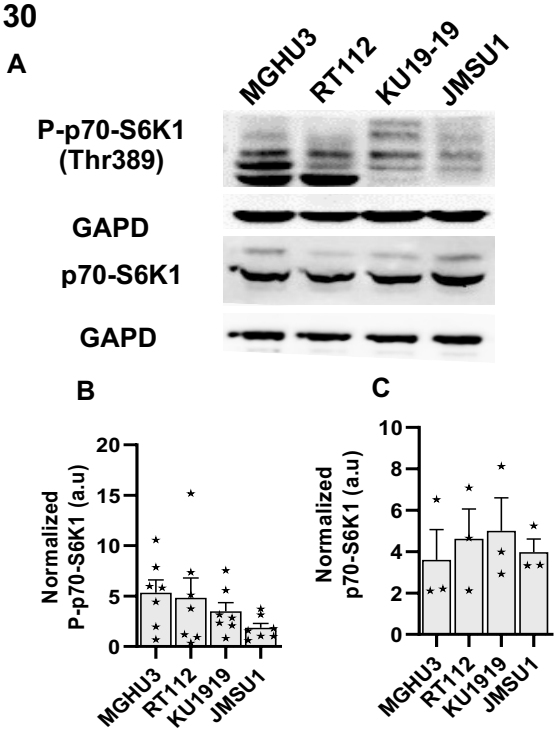

Fig 30. p70-S6K analysis

A. Western blot analysis of phosphorylated p70-S6 Kinase 1 (P-p70-S6K1 Thr389) and total p70-S6K1 as well as GAPDH loading control in MGHU3, RT112, KU19-19 and JMSU1 cells and quantification of **B.** P-p70-S6K1 **C.** and p-70-S6K1 levels from multiple experiments, error bars are SEM.

Fig 31

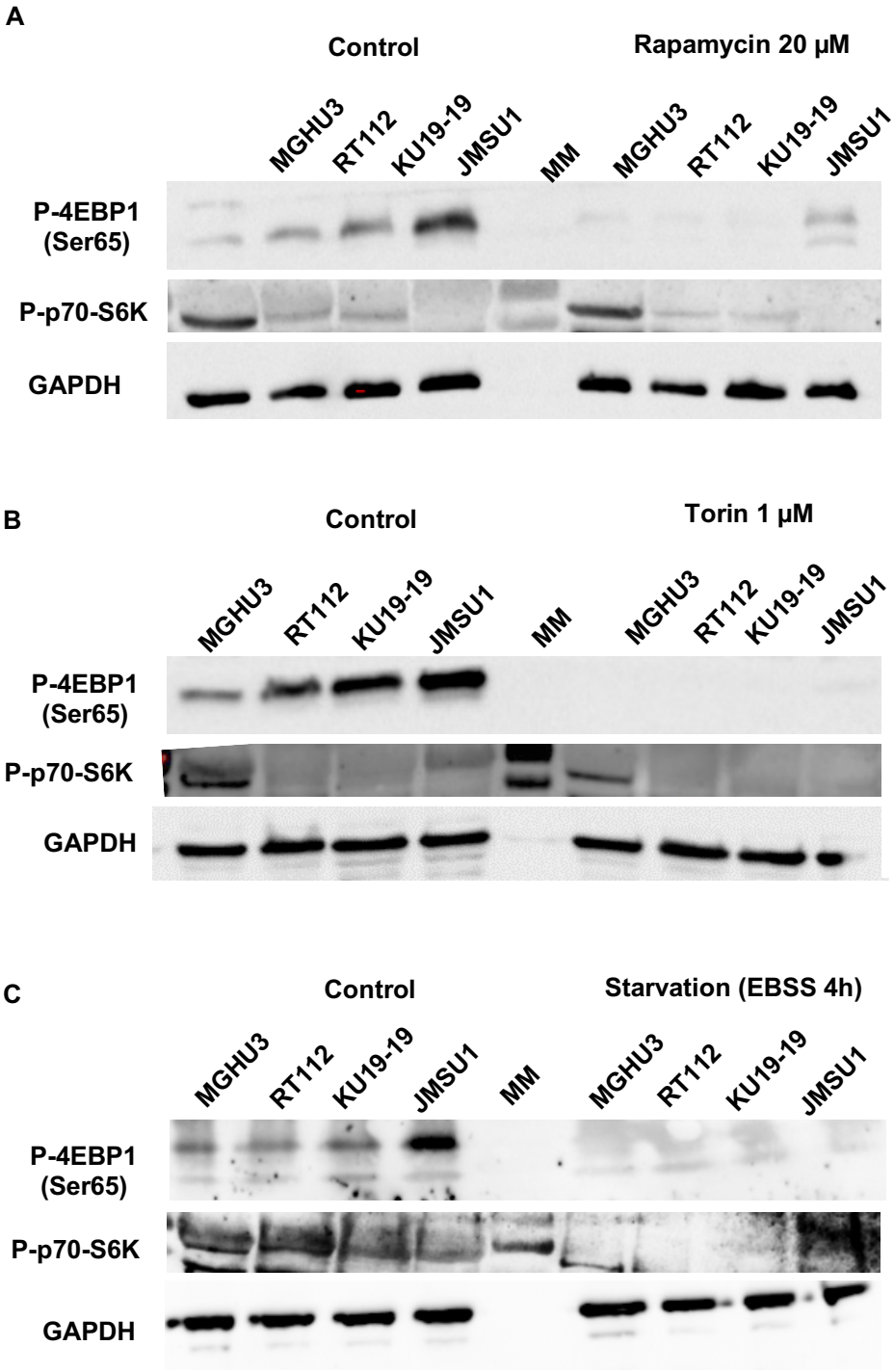

Fig 31. mTORC1 substrate phosphorylation after mTORC1 inhibition
Western Blot analysis of 4EBP1 phosphorylation (P-4EBP1 Ser65) and p70-S6 Kinase 1 (S6K1) phosphorylation (P-p70-S6K Thr389) in MGHU3, RT112, KU19-19 and JMSU1 in control conditions (full media) and after treatment with **A**. Rapamycin at 20µM for 2 h. **B**. Torin at 1µM for 2 h. **C**. starvation in EBSS for 4h. Along with the loading control GAPDH.

We confirmed that the phosphorylation of these substrates was mTORC1 specific in all bladder cancer cell lines employing the well-established inhibitors of mTORC1 kinase, rapamycin and torin (Dumont and Su, 1995; Liu et al., 2010). As expected, both treatments decreased phosphorylation of both 4EBP1 and S6K1 (**Fig 31 A, B**) Additionally, complete starvation (in EBBS) of bladder cancer cells that also switches off mTORC1, decreased both 4EBP1 and S6K1 phosphorylation confirming that both substrates were under the control of mTORC1 (**Fig 31C**)**.**

Conclusion: Our results of mTORC1 activity assays showed that mTORC1 is active in the four bladder cancer cell lines tested. This indicated that the phenotypic differences in lysosome positioning did not correlate with a loss of overall mTORC1 activity. mTORC1 was active in all cell lines tested and was sensitive to nutrient availability, because we observed a loss of mTORC1 dependent substrate phosphorylation upon starvation. We observed that peripheral dispersion of lysosomes in aggressive bladder cancer cell lines did not increase mTORC1 activity as has been described in previous reports. However, we found surprising differences in mTORC1 downstream substrate specificity, indicating that certain substrates of mTORC1 are preferentially phosphorylated in aggressive versus non-aggressive bladder cancer cell lines.

4.2 Regulation of mTORC1 by lysosome positioning

Next, we asked whether lysosome positioning regulates mTORC1 signaling in these cancer cells. To test this, we specifically altered lysosome positioning via recruitment of motor proteins to lysosomes in full media conditions. Dynein is the retrograde motor required for lysosomal transport towards the cell center (Pu et al., 2016). To cluster lysosomes in the cell center, we thus induced recruitment of dynein on them employing the FKBP/FRB heterodimerization by the A/C heterodimerizer, a strategy that has been previously validated (van Bergeijk et al., 2015). We used our previously engineered RT112 and JMSU1 cells, representing non-aggressive and aggressive cell lines, respectively, that stably expressed FKBP-fused to LAMP1-mCherry and FRB-fused to the dynein adaptor BicD2. In these cell lines, addition of A/C heterodimerizer to the culture medium induced lysosomes to cluster at the cell center (**Fig 32**). We ensured that the overexpression of LAMP1-mCherry and FRB-BicD2 did not disrupt the lysosomal degradation of cell surface receptors such as EGFR (Epidermal Growth

Factor Receptor). For this, we added EGF (Epidermal Growth Factor) for different time intervals to cells. EGF binds to the EGFR and is endocytosed before being degraded in lysosomes. Our western blot results showed that EGFR degradation was similar between control cells and cells expressing the BicD2 system (**Fig 33**) in both, RT112 and JMSU1. We further confirmed that mCherry specifically labelled lysosomes in engineered cells by performing immunofluorescence (IF) in JMSU1 cells with LAMP1 and CD63, markers of lysosomes and multi-vesicular bodies, respectively. IF showed colocation of both LAMP1 and CD63 to mCherry-positive compartments indicating that Lamp1-mCherry was labelling lysosomes and MVBs (**Fig 34**). We then monitored mTORC1 activity in these cells by visualizing phosphorylation of 4EBP1 and S6K1. We found that A/C-induced clustering of lysosomes in RT112 cells drastically decreased 4EBP1 and S6K1 phosphorylation (**Fig 35 A-D**). Contrary, clustering of lysosomes in JMSU1 cells did not change 4EBP1 phosphorylation levels but did reduce phosphorylation of S6K1 (**Fig 36 A-D**). To further confirm these results, we altered lysosome positioning via siRNA knockdown (**Fig 37**) by targeting the small GTPases Arl8b or Rab7, which regulate the recruitment of molecular motors on lysosomes, Arl8b recruits kinesins for anterograde transport (Pu et al., 2016), and thus, gene silencing of Arl8b leads to retrograde movement of lysosomes to the cell center. Silencing of Rab7 prevents recruitment of dynein, and thus, anterograde movement of lysosomes to the cell periphery in these cells. Similar to the A/C-induced clustering of lysosomes, siArl8b decreased phosphorylation of 4EBP1 in RT112 but not in JMSU1 cells (**Fig 38, 39**). However, increasing peripheral lysosomes by siRab7 did not change the levels of phosphorylated 4EBP1 in either cell line (**Fig 38, 39**). To better understand mTORC1 activity after lysosome clustering in RT112 and JMSU1 cells we monitored mTOR recruitment to lysosomes in these cells. Consistent with our previous results, we found that upon A/C-induced clustering mTOR was lost from lysosomes in RT112 cells (**Fig 40**). Contrary, in JMSU1 cells, mTOR remained on clustered lysosomes (**Fig 41**).

Conclusion: Lysosome positioning is an important regulator of mTORC1 activity in non-aggressive RT112 cells, because central clustering of lysosomes induces loss of mTOR and decreases downstream phosphorylation. However, in aggressive JMSU1 cells, lysosome positioning changes do not impact mTOR recruitment or activity.

Fig 32

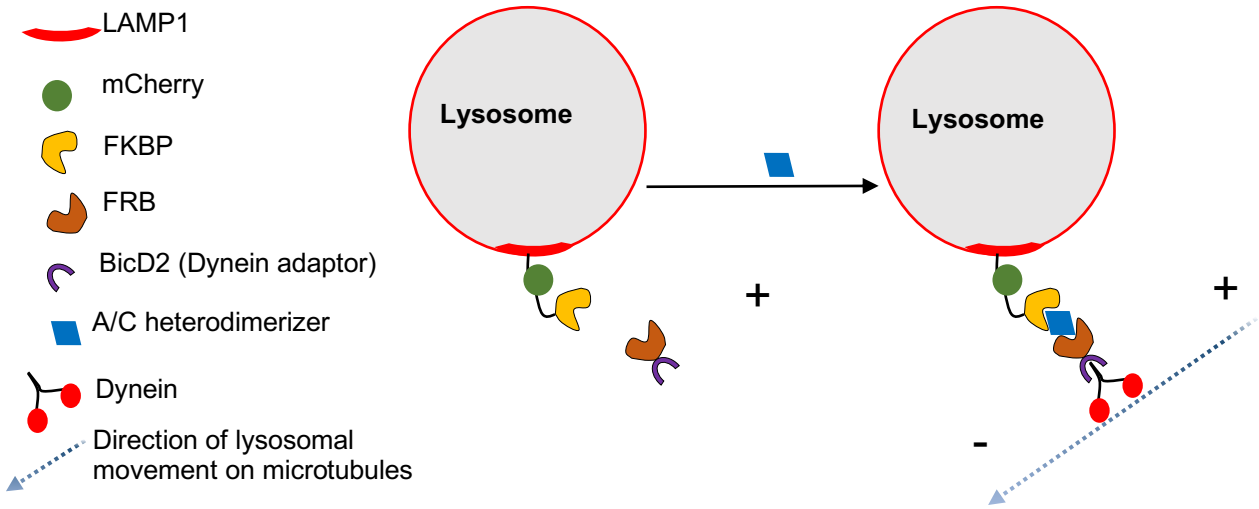

Fig 32. Schematic of lysosome clustering using the BicD2 dimerization system

Fig 33

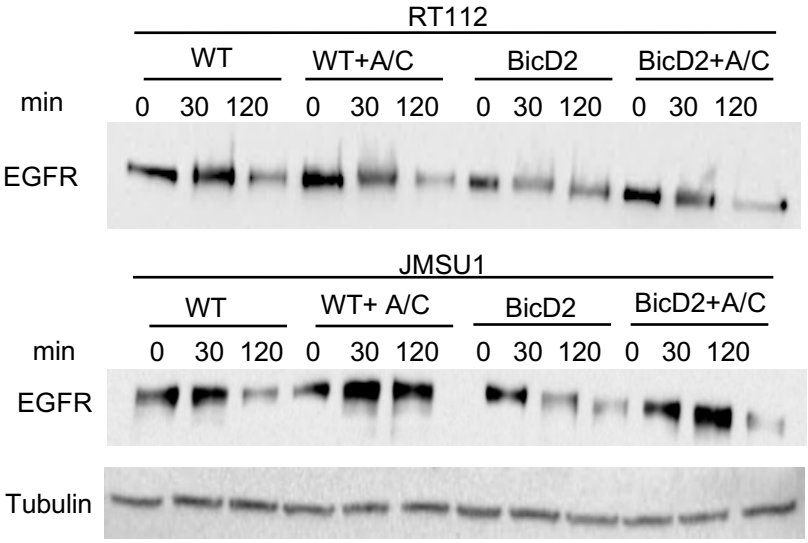

Fig 33. EGFR degradation in lysosomes in RT112 and JMSU1 cells WT: represents the Wild type cells; BicD2: cells with the Bicd2 dimerization system; A/C: Cells treated with the A/C heterodimerizer; Min: represents the minutes after EGF addition. Tubulin is the loading control.

Fig 34

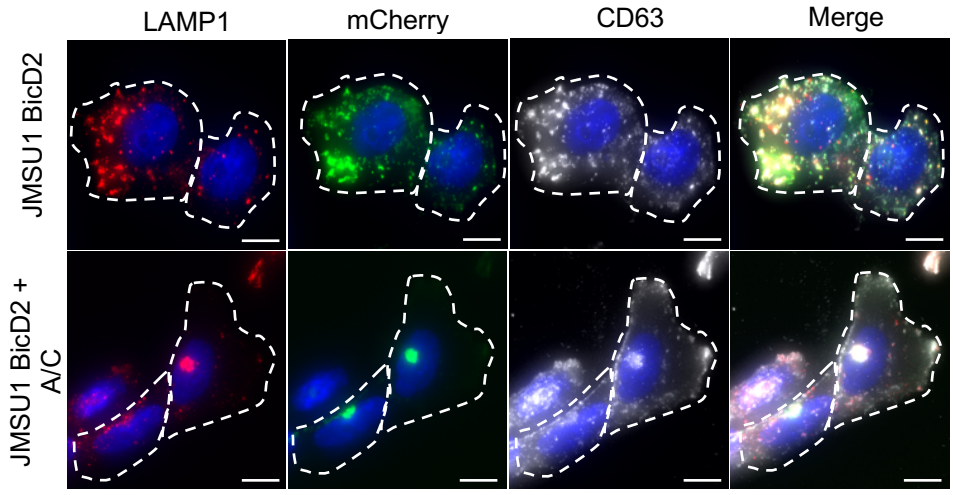

Fig 34. Localization between LAMP1, mCherry-LAMP1 and CD63 in cell lines with BicD2 heterodimerization system

Fig 35

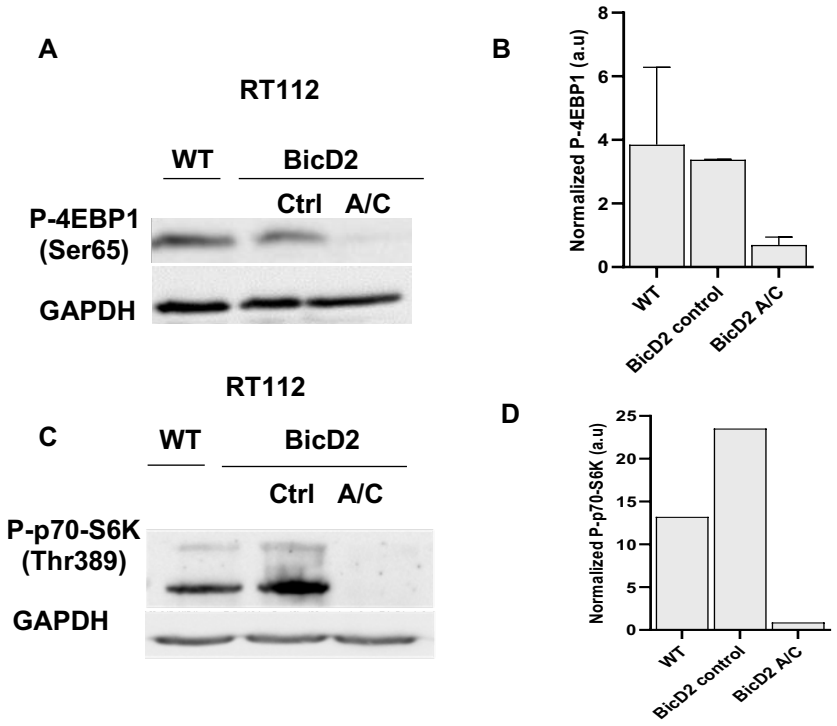

Fig 35. mTORC1 substrate phosphorylation in RT112 cells with BicD2dimerization system
A. Western Blot analysis of 4EBP1 phosphorylation (P-4EBP1 Ser65) in WT RT112 cells and RT112 cells with BicD2 dimerization system in control condition (DMSO Ctrl) and after addition of A/C heterodimerizer (A/C) and **B**. quantification of relative phosphorylated P-4EBP1 normalized to GAPDH levels. Error bars show s.d. of three independent experiments. **C**. Western Blot analysis of p70-S6 Kinase 1 (S6K1) phosphorylation (P-p70-S6K Thr389) in WT RT112 cells and RT112 cells with BicD2 dimerization system in control condition (DMSO, Ctrl) and after addition of A/C heterodimerizer (A/C) and **D**. quantification of relative phosphorylated P-p70-S6K1 normalized to GAPDH levels.

Fig 36

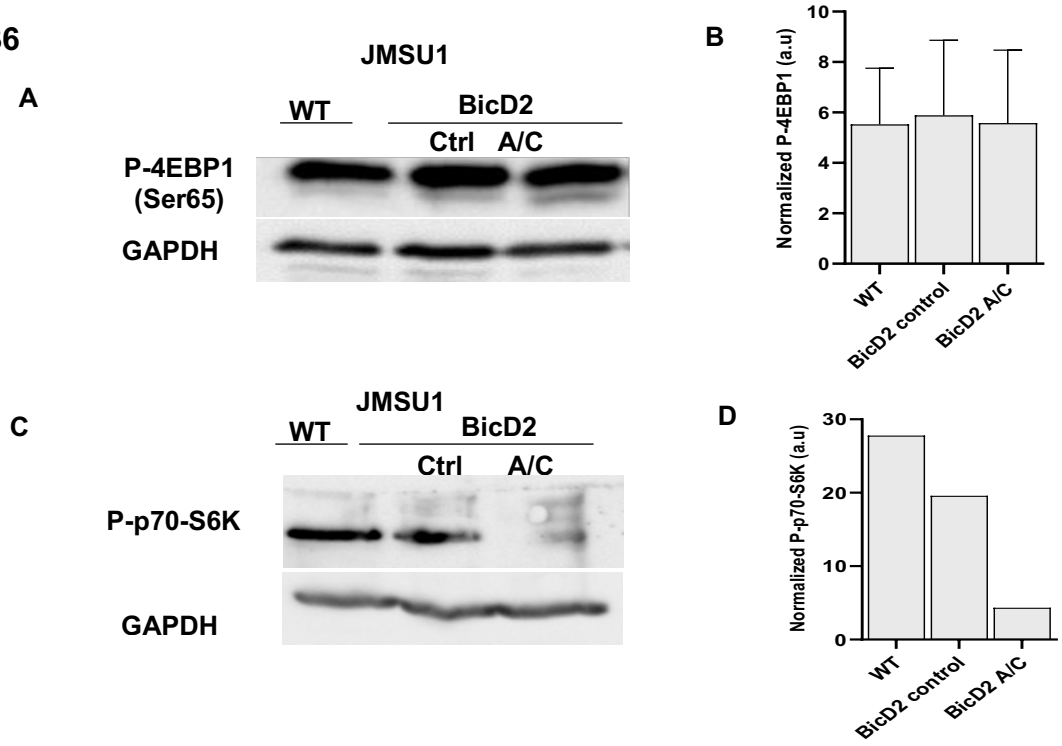

Fig 36. mTORC1 substrate phosphorylation in JMSU1 cells with BicD2dimerization system
A. Western Blot analysis of 4EBP1 phosphorylation (P-4EBP1 Ser65) in WT RT112 cells and RT112 cells with BicD2 dimerization system in control condition (DMSO Ctrl) and after addition of A/C heterodimerizer (A/C) and **B**. quantification of relative phosphorylated P-4EBP1 normalized to GAPDH levels. Error bars show s.d. of three independent experiments. **C**. Western Blot analysis of p70-S6 Kinase 1 (S6K1) phosphorylation (P-p70-S6K Thr389) in WT RT112 cells and RT112 cells with BicD2 dimerization system in control condition (DMSO Ctrl) and after addition of A/C heterodimerizer (A/C) and **B**. quantification of relative phosphorylated P-p70-S6K1 normalized to GAPDH levels.

Fig 37

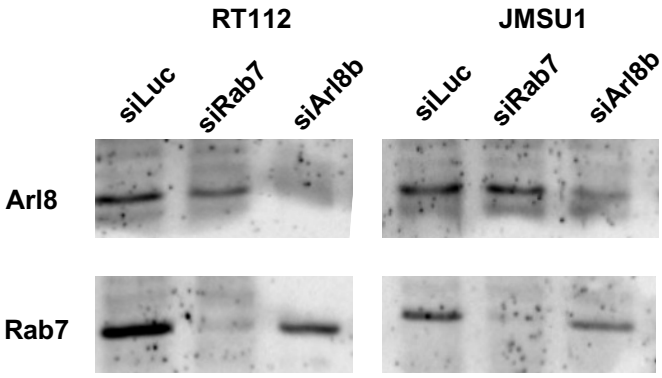

Fig 37. Western blot of Rab7 and Arl8b after siLUC, siRab7 and siARl8b conditions in RT112 and JMSU1 cells

Fig 38

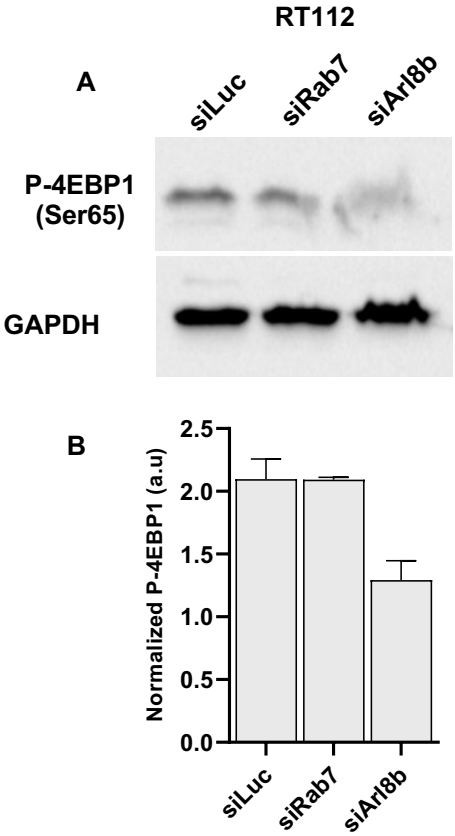

Fig 38. mTORC1 substrate phosphorylation in RT112 cells with Rab7 and Arl8 knockdown

A. Western Blot analysis of phosphorylation (P-4EBP1 Ser65) in RT112 cells in control condition (siLUC) and upon targeting of Rab7 (siRab7) or Arl8b (siArl8b) and **B.** quantification of relative phosphorylated P-4EBP1 to GAPDH levels. Error bars show s.d. of three independent experiments.

Fig 39

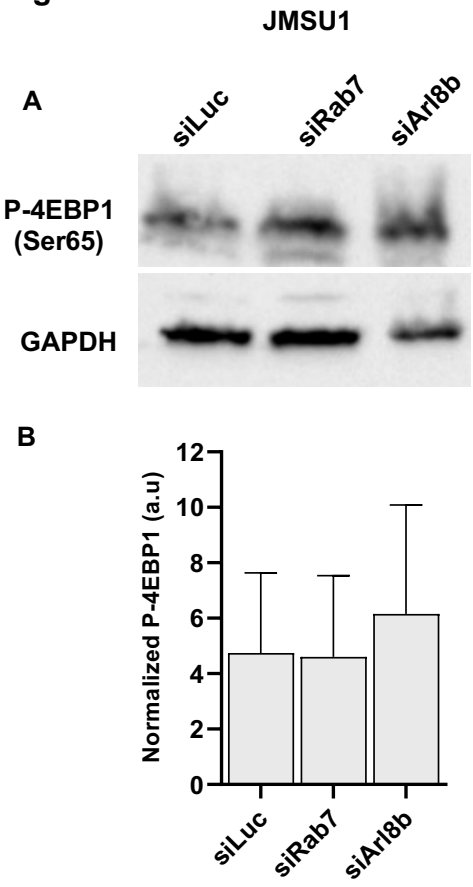

Fig 39. mTORC1 substrate phosphorylation in JMSU1 cells with Rab7 and Arl8 knockdown

A. Western Blot analysis of phosphorylation (P-4EBP1 Ser65) in JMSU1 cells in control condition (siLUC) and upon targeting of Rab7 (siRab7) or Arl8b (siArl8b) and **B.** quantification of relative phosphorylated P-4EBP1 to GAPDH levels. Error bars show s.d. of three independent experiments.

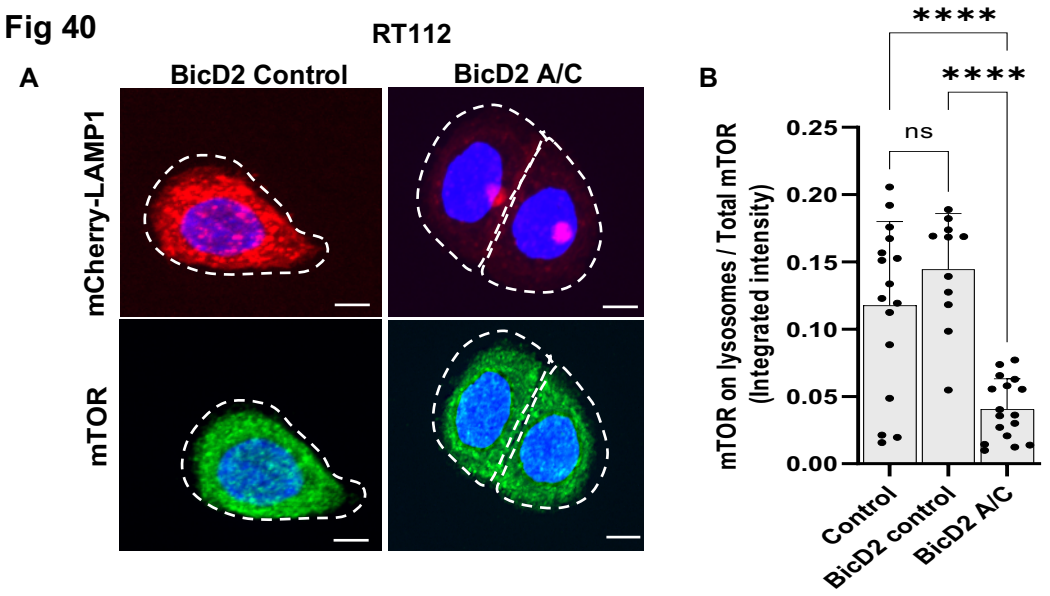

Fig 40. mTORC1 localization on lysosomes in RT112 cells with BicD2dimerization system

A. Representative images of mCherry-LAMP1 lysosomes and mTORC1 in RT112 BicD2 cells in control condition (DMSO, Ctrl) and after addition of A/C heterodimerizer (A/C). Scale bars are 5 μm. **B**. Quantification of mTOR intensity on lysosomes normalized to total cellular mTOR in RT112 WT (control) and RT112 BicD2 cells in control (DMSO, Ctrl) and after addition of A/C heterodimerizer (A/C). Error bards are s.d. **** p <0.0001; Kruskal-Wallis test with Dunn post-hoc test with Sidak correction

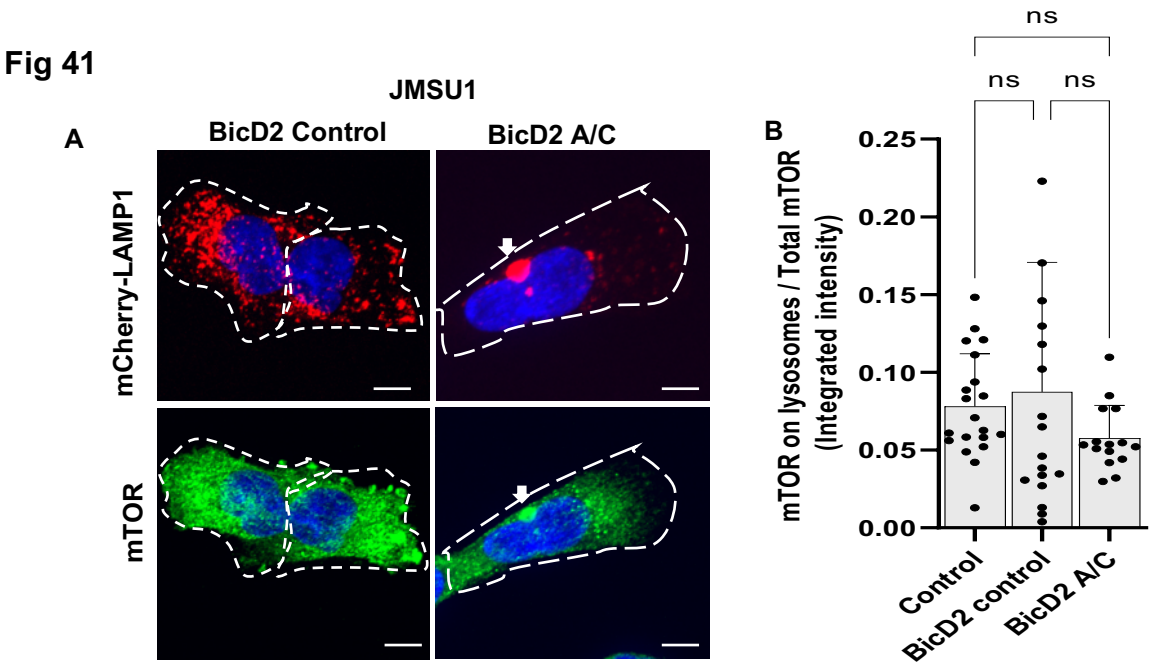

Fig 41. mTORC1 localization on lysosomes in JMSU1 cells with BicD2dimerization system

A. Representative images of mCherry-LAMP1 lysosomes and mTORC1 in JMSU1 BicD2 cells in control condition (DMSO, Ctrl) and after addition of A/C heterodimerizer (A/C). Scale bars are 5 μm. **B**. Quantification of mTOR intensity on lysosomes normalized to total cellular mTOR in JMSU1 WT (control) and RT112 BicD2 cells in control (DMSO, Ctrl) and after addition of A/C heterodimerizer (A/C). Error bards are s.d. ns; Kruskal-Wallis test with Dunn post-hoc test with Sidak correction

Results Aim 2- Molecular mechanisms regulating lysosomal dispersion in bladder cancer cells

4.3 TFEB status and regulation in bladder cancer cells

Because our results showed differences in mTORC1 substrate phosphorylation in bladder cancer cells, we tested the status of another well-established substrate of mTORC1, the Transcription Factor EB (TFEB). TFEB is a key regulator of autophagy, lysosomal functions through regulation of genes involved in these pathways. Interestingly, TFEB has been shown to regulate lysosome positioning (Sbano et al., 2017; Willett et al., 2017). Because phosphorylation of TFEB retains this transcription factor in the cytosol, whereas the active, non-phosphorylated form is nuclear, we monitored TFEB localization in bladder cancer cells by expressing TFEB-GFP. Whereas TFEB-GFP showed cytosolic localization in MGHU3 and RT112 cells (40% of mean TFEB-GFP intensity was found in the nucleus), more than 70% of the mean intensity of TFEB-GFP was found in the nucleus of KU19-19 and JMSU1 cells (**Fig 42 A, B**). Next, we tested if this cytosolic retention in MGHU3 and RT112 cells was mTORC1 dependent. For this, we transfected cells with TFEB-GFP and then treated them with rapamycin, an inhibitor of mTORC1. We observed that nuclear fraction of TFEB-GFP increases upon inhibition of mTORC1 (**Fig 42 C, D**) indicating that TFEB cytosolic retention in non-aggressive MGHU3 and RT112 cells was mTORC1 dependent. No change was observed in KU19-19 and JMSU1 cells (**Fig 42 C, D**). Together these results indicated that TFEB was under the control of mTORC1 in non-aggressive bladder cancer cells and nuclear, thus probably active, in aggressive cells. To confirm the results of overexpressed TFEB-GFP, we performed cell fractionation and separated the nuclear and cytosolic fractions, in which endogenous TFEB was monitored by western blotting. We used LaminB, component of the nuclear lamina that is part of the nuclear envelope, as the nuclear marker and GAPDH as the cytosolic marker to ensure the efficiency of fractionation (**Fig 43A**). Consistent with the TFEB-GFP results, we observed that nuclear fraction of JMSU1 was enriched in TFEB, whereas the in RT112 cells, TFEB was predominantly found in the cytosol (**Fig 43A, B**).

We next used the RT112 and JMSU1 cells with the BicD2 dimerization system (explained before) to test if changing lysosome positioning regulates TFEB localization. Because TFEB is a substrate of mTORC1, its phosphorylation, and thus, cytosolic retention could be regulated by mTORC1 recruitment on lysosomes. Indeed, we observed that A/C-induced lysosome clustering promoted TFEB-GFP nuclear translocation in RT112 cells (about 70% of the mean intensity of TFEB-GFP was found in the nucleus), consistent with our results of loss of mTORC1 substrate phosphorylation upon lysosome clustering in this cell line (**Fig 44 A, B**). Contrary, no difference in TFEB-GFP localization before or after clustering of lysosomes was observed in JMSU1 cells (**Fig 45 A, B**).

To confirm our observation that TFEB is active in aggressive JMSU1 cells, we monitored the levels of Microtubule-associated protein light chain 3 I and II (LC3I and LC3II) in bladder cancer cells in control and bafilomycin treatment conditions. Detection of LC3 by western blots is a common method of studying autophagy. Endogenous LC3 is detected in two forms in western blot, LC3I is the cytosolic form of the protein whereas LC3II is the lipidated form that is conjugated with phosphatidylethanolamine (PE) and is localized to autophagosomes. LC3II however is degraded by lysosomes upon autophagosome - lysosome fusion, making it difficult to monitor the autophagic flux in the cells. Thus, BafilomycinA1, an inhibitor of vATPase on lysosomes and thus inhibitor autophagosome-lysosome, is used to prevent LC3II degradation and monitor the autophagic flux in the cells (Mizushima and Yoshimori, 2007). Our results showed that while the levels of LC3I and LC3II were comparable in control conditions in the four cell lines tested, the levels of LC3II were found to be higher in aggressive KU19-19 and JMSU1 cells upon bafilomycin-dependent inhibition of vATPase that is important for the fusion of autophagosomes to lysosomes. This indicated that autophagosome maturation (or autophagic flux) was increased in aggressive cells, consistent with the hypothesis of active TFEB in these cell lines (**Fig 46**). Additionally, since RRAGD, that codes for the protein RagD (required for mTORC1 activation) (Di Malta et al., 2017) is regulated by TFEB and we monitored the mRNA levels of RRAGD in the transcriptome of the four bladder cancer cell lines (MGHU3, RT112, KU19-19 and JMSU1). We found that nuclear translocation of TFEB also correlated with upregulation of RRAGD aggressive cell lines KU19-19 and JMSU1 (**Fig 47A**).

Fig 42

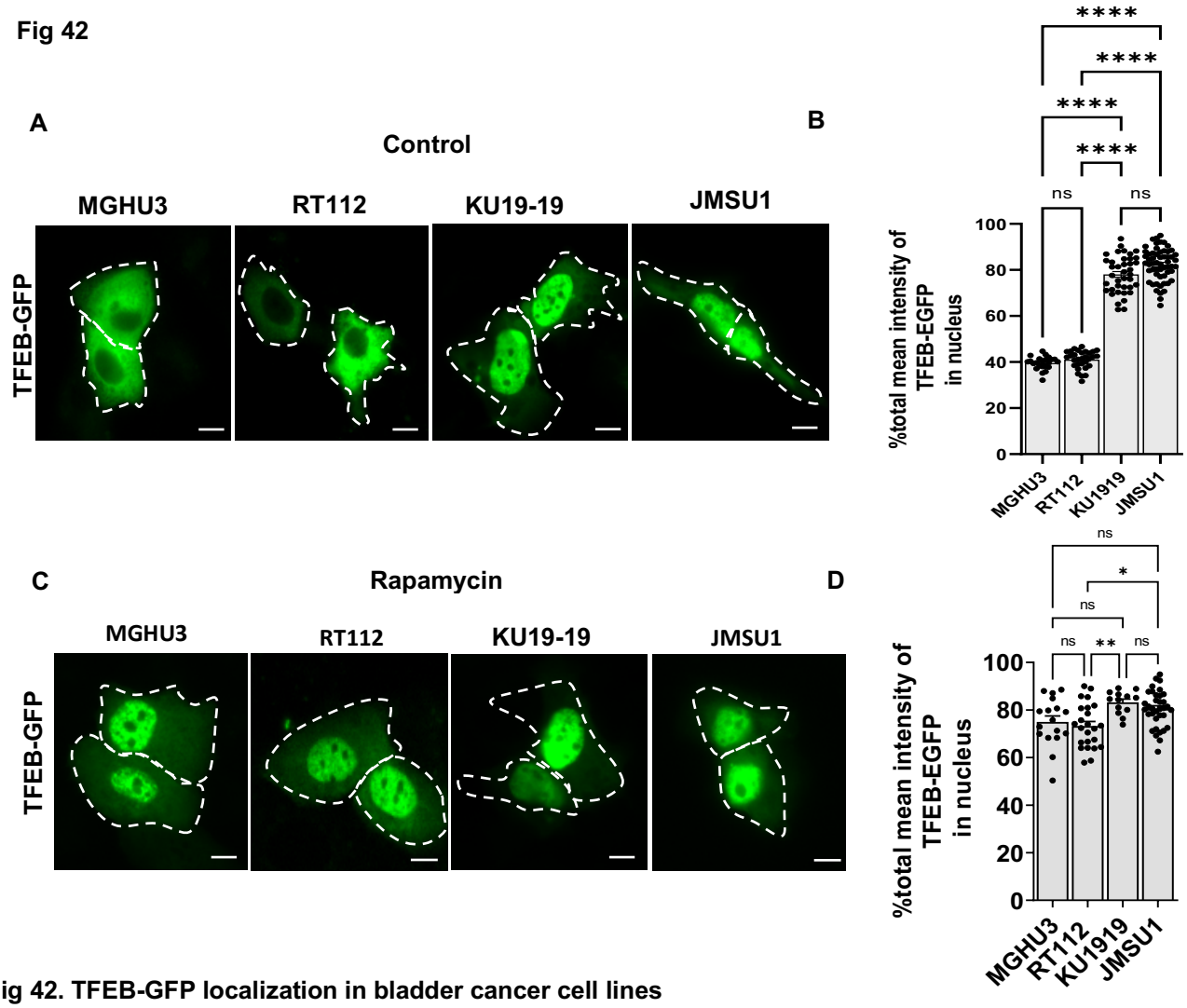

Fig 42. TFEB-GFP localization in bladder cancer cell lines
Representative images of MGHU3, RT112, KU19-19 and JMSU1 cells transfected with TFEB-GFP for 72 h **A**. control (full media) condition. **C.** treated with 10 μM rapamycin for 2 h Scale bars equal 5 μm. Quantification of the nuclear fraction of the total mean TFEB-EGFP fluorescent intensity in MGHU3, RT112, KU19-19 and JMSU1 in **B.** control (full media) condition and **D.** treated with 10 μM rapamycin for 2 h. n>20 cells in each condition. Data are depicted as mean ± SEM. * p<0.05, ** p<0.01, **** p<0.0001 Kruskal-Wallis test with Dunn post-hoc test with Sidak correction

Fig 43

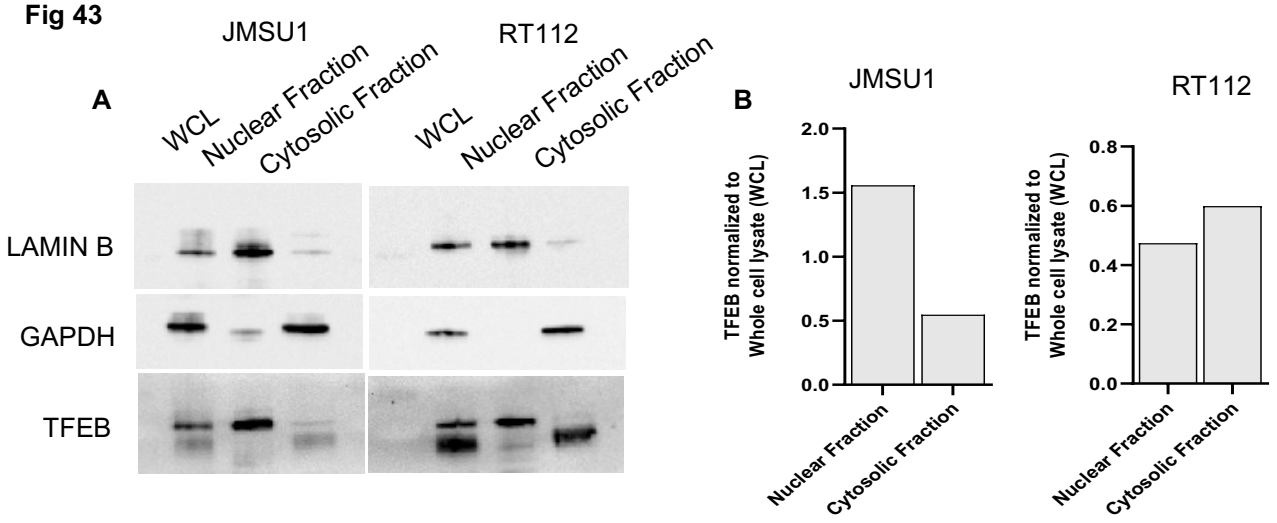

Fig 43. Endogenous TFEB localization in RT112 and JMSU1 bladder cancer cell lines
A. Western blot analysis of TFEB in RT112 and JMSU1 cells in Whole Cell Lysate (WCL), Nuclear fraction and cytosolic fraction. LAMIN B blot represents the nuclear fraction marker and GAPDH as the cytosolic fraction marker. **B**. Quantification of TFEB in nuclear and cytosolic fraction in RT112 and JMSU1 normalized to TFEB in the WCL.

Fig 44

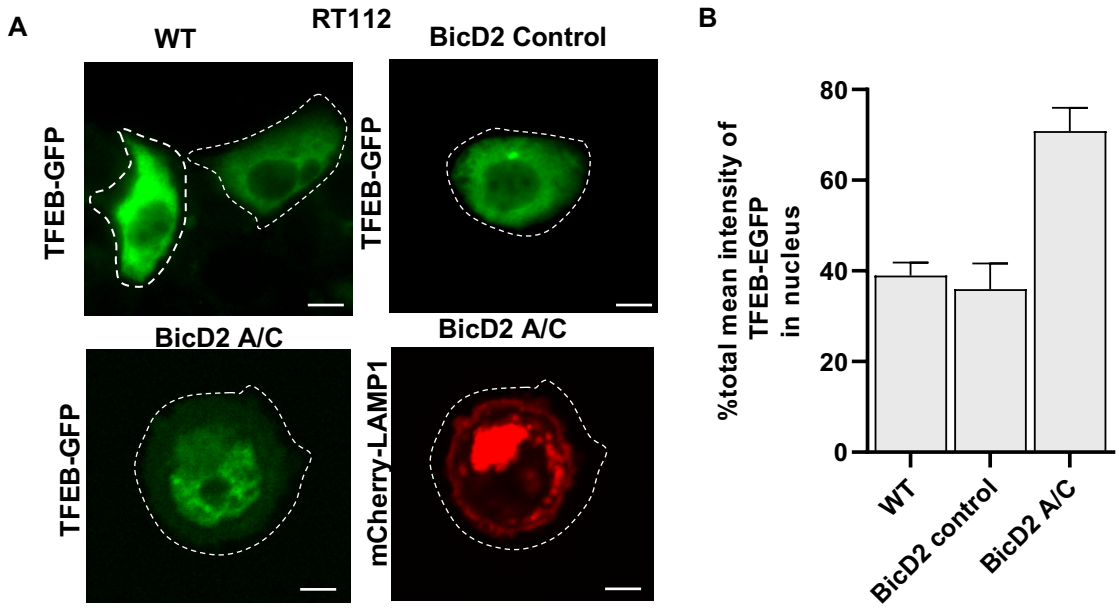

Fig 44. TFEB-GFP localization in RT112 cells with BicD2dimerization system
A. Representative images of RT112 WT transfected with TFEB-GFP (green) for 72h and BicD2 cells transfected with TFEB-GFP (green) for 72h in control condition (DMSO, Ctrl) and after addition of A/C heterodimerizer (A/C). In red, representation image of clustering of mCherry-LAMP1 tagged lysosomes after addition of A/C heterodimerizer. **B**. Quantification of the nuclear fraction of the total mean TFEB-EGFP fluorescent intensity in RT112 WT cells and RT112 BicD2 cells in control condition (DMSO, Ctrl) and after addition of A/C heterodimerizer (A/C). Scale bars are 10 μm. Error bars show s.d. of three independent experiments

Fig 45

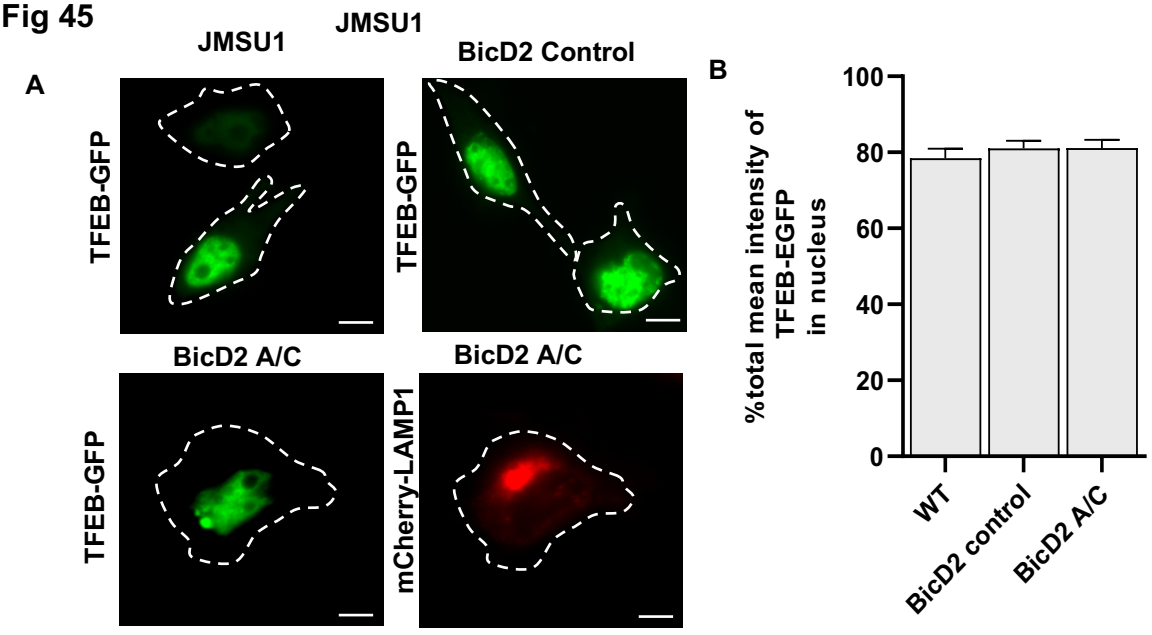

Fig 45. TFEB-GFP localization in JMSU1 cells with BicD2dimerization system
A. Representative images of JMSU1 WT transfected with TFEB-GFP (green) for 72h and BicD2 cells transfected with TFEB-GFP (green) for 72h in control condition (DMSO, Ctrl) and after addition of A/C heterodimerizer (A/C). In red, representation image of clustering of mCherry-LAMP1 tagged lysosomes after addition of A/C heterodimerizer. **B**. Quantification of the nuclear fraction of the total mean TFEB-EGFP fluorescent intensity in JMSU1 WT cells and RT112 BicD2 cells in control condition (DMSO, Ctrl) and after addition of A/C heterodimerizer (A/C). Scale bars are 10 μm. Error bars show s.d. of three independent experiments

Fig 46

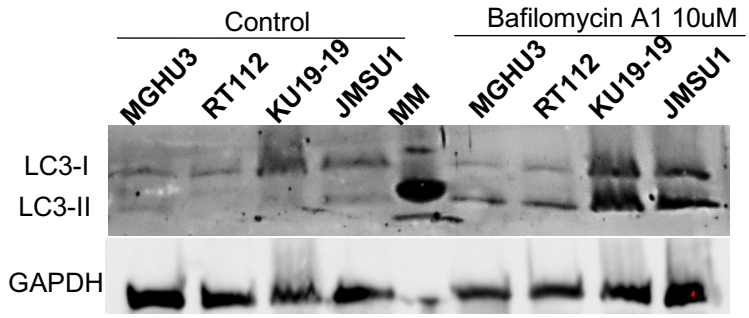

Fig 46. Autophagic flux in bladder cancer cells
Western blot analysis of LC3I and LC3II in control and Bafilomycin (10μM, 2h) treatment conditions in MGHU3, RT112, KU19-19 and JMSU1. GAPDH blot shows the loading control

Fig 47

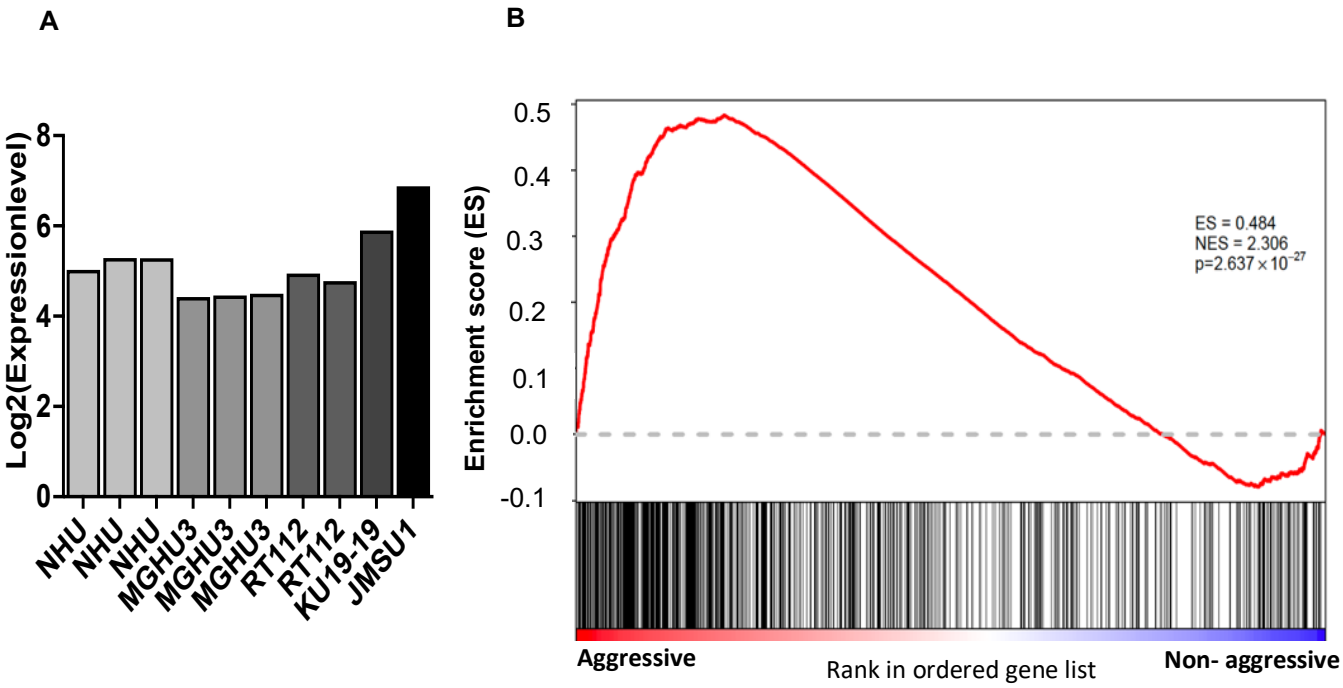

Fig 47. Transcriptome analysis for TFEB regulated genes in bladder cancer cells
A. Normalized Log2 RNA expression levels of TFEB regulated genes RRAGD in NHU, MGHU3, RT112, KU19-19 and JMSU1. **B.** Gene set enrichment analysis (GSEA) of the CLEAR network genes in the transcriptome of aggressive (KU19-19 and JMSU1) vs non-aggressive bladder cancer cell lines (MGHU3 and RT112). ES shows the enrichment score; p represents the p value of the analysis.

Finally, to further test whether TFEB activity is different between cancer cell lines, we performed a GSEA (Gene Set Enrichment Analysis) of their transcriptome. We compared the TFEB regulated CLEAR network genes in transcriptome of non-aggressive (MGHU3 and RT112) vs aggressive (KU19-19 and JMSU1) cell lines. This data showed significant enrichment of TFEB genes in aggressive KU19-19 and JMSU1 cells compared to the non-aggressive MGHU3 and RT112 cells and strongly indicated that TFEB is active in aggressive bladder cancer cells (**Fig 47B**).

Conclusion: The bladder cancer cells MGHU3 and RT112 have a more cytosolic, and hence presumably inactive TFEB, whereas aggressive cell lines KU19-19 and JMSU1 have a more nuclear/active TFEB. Our results indicate that cytosolic retention of TFEB-GFP in RT112 cells is mTORC1-dependent. We find that autophagic flux and expression of RRAGD is upregulated in aggressive cells (KU19-19 and JMSU1). Because TFEB is a crucial transcriptional regulator of autophagy, this indicates a TFEB hyperactivity in aggressive bladder cancer cells. Finally, our results of GSEA analysis on the transcriptome of different bladder cancer cells vs NHU also showed enrichment of TFEB genes in aggressive cell lines.

4.4 Regulation of TFEB in aggressive bladder cancer cells

We next focused on the understanding of the mechanisms behind TFEB activity / nuclear translocation in aggressive cancer cells. As mentioned before, we observed an upregulation of total protein level of 4EBP1 in these cells (KU19-19 and JMSU1). Because both TFEB and 4EBP1 are substrates of mTORC1, we tested whether TFEB nuclear translocation could be due to substrate competition for mTORC1 dependent phosphorylation between 4EBP1 and TFEB. We depleted 4EBP1 in JMSU1 cells by siRNA knockdown (**Fig 48A**) and compared TFEB-GFP cellular localization between control and si4EBP1 conditions. We did not observe any change in the localization of TFEB-GFP in these cells (**Fig 48B**), TFEB-GFP remained mostly nuclear.

An important step of nuclear translocation of TFEB involves its dephosphorylation by the phosphatase Calcineurin. Calcineurin activation has been shown to be dependent on calcium release from lysosomes through the lysosomal calcium channel TRPML1 (MCOLN1) (Medina et al., 2015). Thus, we inhibited TRPML1 in JMSU1 cells using

GW-405833 (ML-SI1) or incubated cells with the calcium chelator BAPTA (1,2-bis(o-aminophenoxy)ethane-N,N,N′,N′-tetraacetic acid). Both treatments led to the cytoplasmic translocation of TFEB-GFP (**Fig 49 A, B**). This indicated that increased dephosphorylation of TFEB by calcineurin in response to lysosomal calcium release strongly contributes to the nuclear accumulation of TFEB in aggressive bladder cancer cells.

Conclusion: Our results indicated that activation / nuclear translocation in JMSU1 cells could be due to increase lysosomal calcium signaling. Previous reports have shown that TFEB increases peripheral lysosomes and regulates calcium homeostasis (Sbano et al., 2017) proposing the hypothesis that TFEB activation could be an important regulator of lysosomal dispersion in aggressive bladder cancer cells.

4.5 mTORC1-TFEB feed-back loop in aggressive bladder cancer

Our results indicated that there is concurrent activation of mTORC1 and TFEB in aggressive cell lines, JMSU1 and KU19-19. It has been previously shown that TFEB induces RagD-mediated mTORC1 recruitment to lysosomes and its activation in cancers such as melanomas, renal carcinomas and pancreatic adenocarcinomas with upregulated MiT/TFE genes (Di Malta et al., 2017). We tested if mTORC1 activity is TFEB-dependent in bladder cancer cells. For this, we depleted TFEB in JMSU1 cells and monitored mTORC1 phosphorylation of its substrates, 4EBP1 and S6K1. We observed no change in 4EBP1 phosphorylation, but a very slight decrease in S6K1 phosphorylation (**Fig 50A**). Next, we tested if TFEB regulated the recruitment of mTOR to lysosomes. For this, we performed an immunofluorescence staining of LAMP1 and mTOR in JMSU1 cells in control and siTFEB conditions. We observed a decrease in mTOR localization on lysosomes after siTFEB (**Fig 50B**) indicating that mTORC1 recruitment to lysosomes is regulated by TFEB possibly through inducing expression of RagD which we find upregulated in these aggressive cells. However, no significant change in phosphorylation of mTORC1 substrate S6K1 and 4EBP1 could indicate presence of compensatory mechanisms in absence of mTORC1.

Conclusion: These results suggest that nuclear TFEB in aggressive bladder cancer cell lines could be important for mTORC1 activation. This phenotype has been

reported in several other cancers and is required for hyper cell proliferation and cancer growth (Di Malta et al., 2017). However, a role of TFEB has not been reported in bladder cancers yet, and thus could be of interest for further investigations.

Fig 48

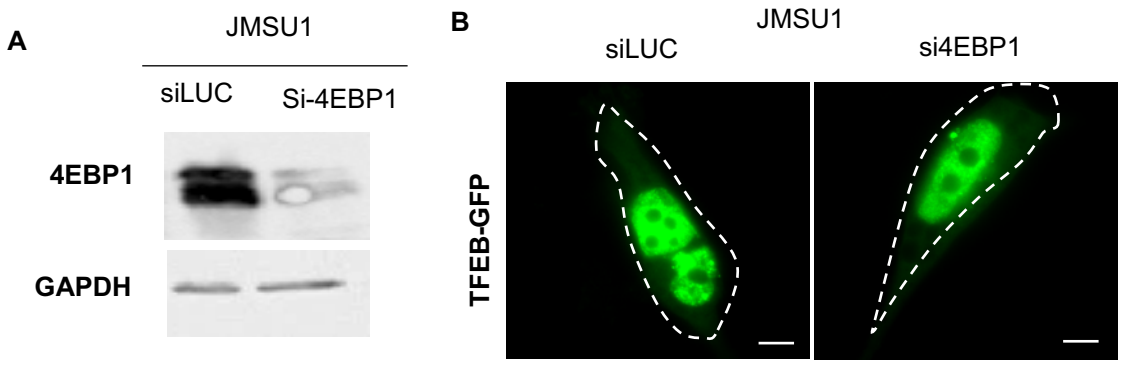

Fig 48. TFEB-GFP in JMSU1 after 4EBP1 depletion

A. Western blot analysis of 4EBP1 in siLUC and si4EBP1 conditions in JMSU1 cells, GAPDH represents the loading control. B. Representative images of JMSU1 cells transfected with TFEB-GFP in siLUC and si4EBP1 conditions after 72h siRNA knockdown. Scale bar is (5µm)

Fig 49

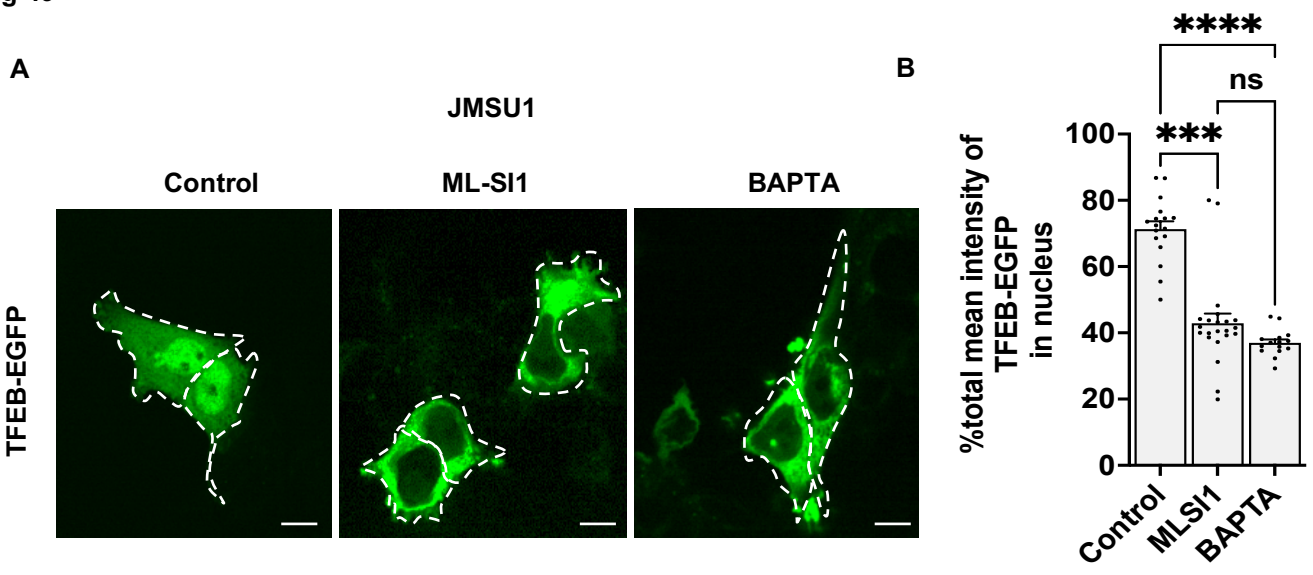

Fig 49. TFEB-GFP in JMSU1 cells after inhibition of lysosomal calcium signaling calcium chelation in cells

A. Representative images of JMSU1 cells transfected with TFEB-EGFP for 72 h and treated with ML-SI1 or BAPTA AM for 3 h. Scale bars equal 10 µm. **B**. Quantification of the nuclear fraction of the total mean TFEB-EGFP fluorescent intensity in control, ML-SI1 and BAPTA AM treatment conditions (for >15 cells in each condition). Data are depicted as mean ± SEM. *** $p<0.001$, **** $p<0.0001$ Kruskal-Wallis test with Dunn post-hoc test with Sidak correction

Fig 50

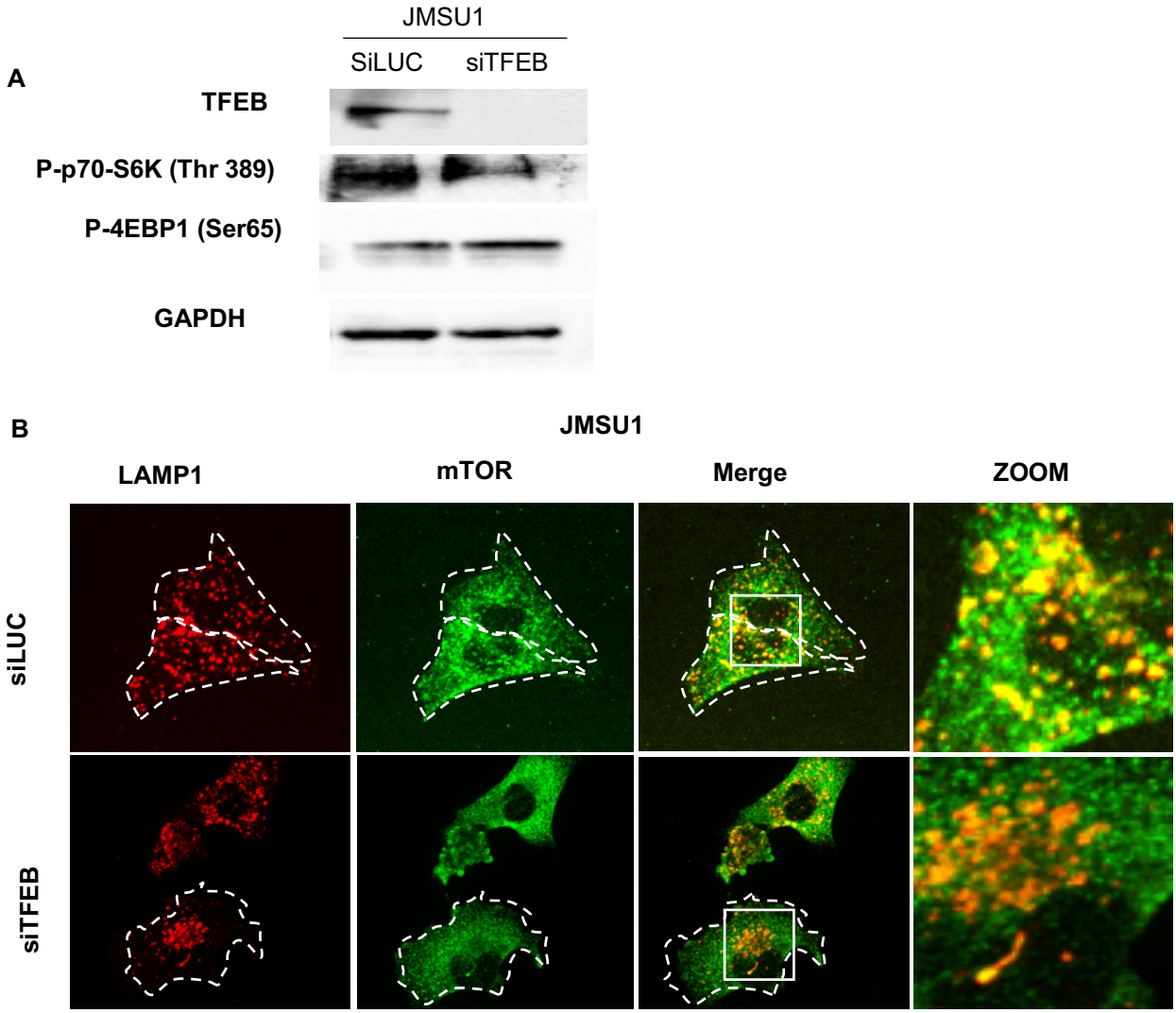

Fig 50. mTORC1 substrate phosphorylation and localization on lysosomes after TFEB depletion

A. Western blot analysis of phosphorylated p-70-S6K1 (P-p70-S6K1) and phosphorylated 4EBP1 (P-4EBP1) in siLUC and siTFEB conditions in JMSU1 cells

B. Immunofluorescence staining of the lysosomal-associated membrane protein 1 (LAMP1, CD107a) and mTOR in MGHU3, RT112, KU19-19 and JMSU1. The zoom shows the merged image for both proteins of the area in white box. Scale bars equal 15 µm.

4.6 Regulators of lysosome positioning in bladder cancer cells lines

Because nuclear TFEB localization correlated with lysosome dispersion in bladder cancer cells, we further investigated the role of TFEB in lysosome positioning. First, we tested whether inducing nuclear translocation of TFEB in cells with cytoplasmic TFEB (RT112) triggered anterograde lysosome movements. RT112 cells were treated with rapamycin (4h) to induce TFEB nuclear translocation (**Fig 42C, D**), and lysosomes were visualized by immunofluorescence against LAMP1. Inspection of classically cultured cells revealed recurrent accumulation of lysosomes at the cell periphery (**Fig 51A**). To better quantify lysosome positioning changes, we cultured cells on adhesive micropatterns and calculated the nearest neighbor distance (NND) of lysosomes in RT112 cells. Lysosomes were more dispersed after rapamycin treatment in micropatterned cells (**Fig 51B**), and the average NND was significantly increased as compared to untreated controls (**Fig 51C**). We additionally tested the effect of TFEB activation by starvation (4h) in classically cultured RT112 cells. Starvation induced nuclear translocation of TFEB in RT112 cells (**Fig 52A, B**) and lysosomal dispersion post starvation (**Fig 52 C**).

Next, we targeted TFEB by siRNA depletion in JMSU1 cells, where TFEB was mostly nuclear. Silencing of TFEB by either a pool of four siRNAs or four individual siRNAs significantly reduced TFEB protein levels after 3d and reversed the scattered lysosome phenotype in classically cultures JMSU1 cells (**Fig 53 A-C**). Quantification of lysosome positioning on micropatterns revealed a significant decrease in the average NND of lysosomes (**Fig 54A, B**) confirming TFEB-dependent regulation in these high-grade bladder cancer cells.

Fig 51

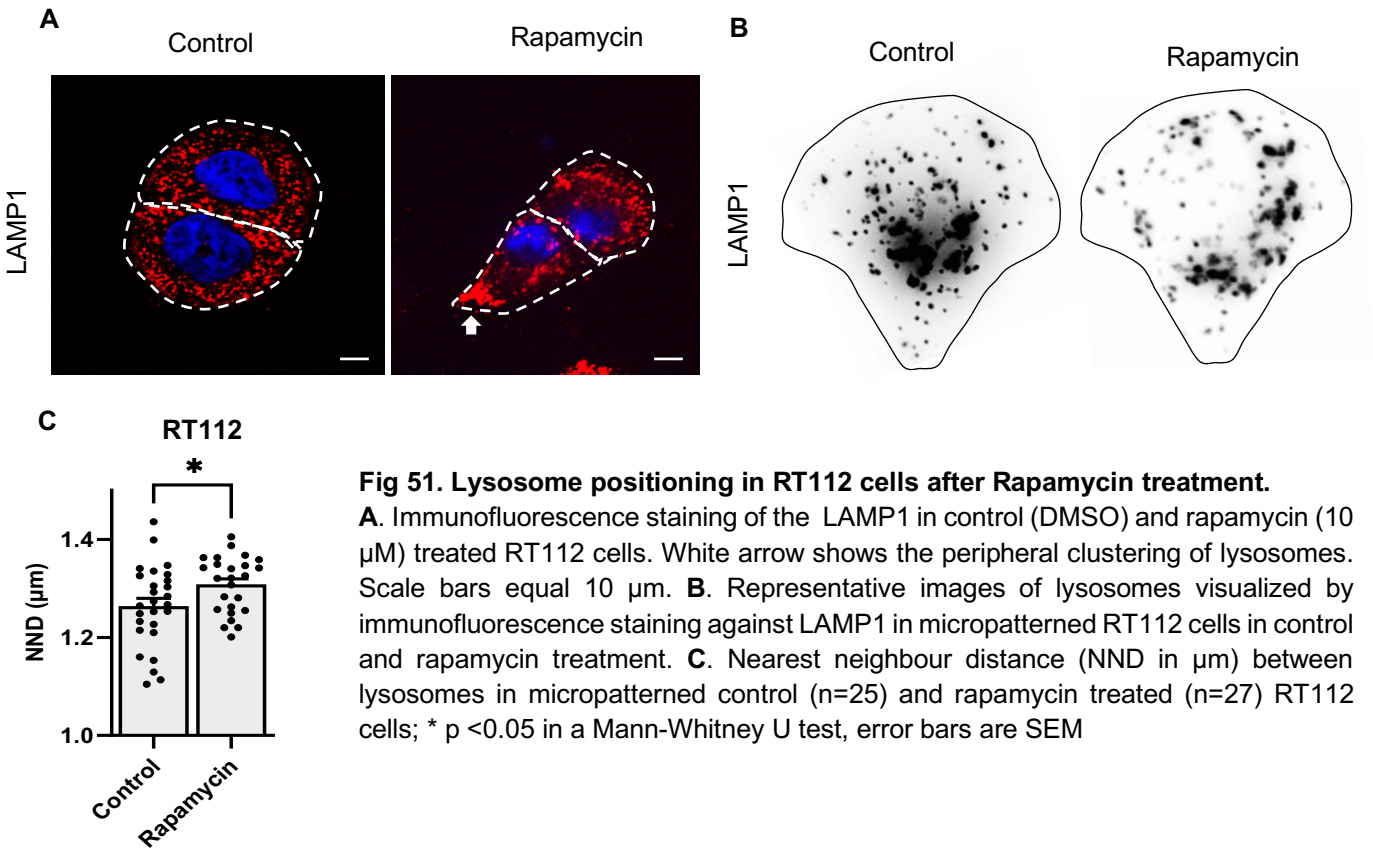

Fig 51. Lysosome positioning in RT112 cells after Rapamycin treatment.
A. Immunofluorescence staining of the LAMP1 in control (DMSO) and rapamycin (10 µM) treated RT112 cells. White arrow shows the peripheral clustering of lysosomes. Scale bars equal 10 µm. **B**. Representative images of lysosomes visualized by immunofluorescence staining against LAMP1 in micropatterned RT112 cells in control and rapamycin treatment. **C**. Nearest neighbour distance (NND in µm) between lysosomes in micropatterned control (n=25) and rapamycin treated (n=27) RT112 cells; * p <0.05 in a Mann-Whitney U test, error bars are SEM

Fig 52

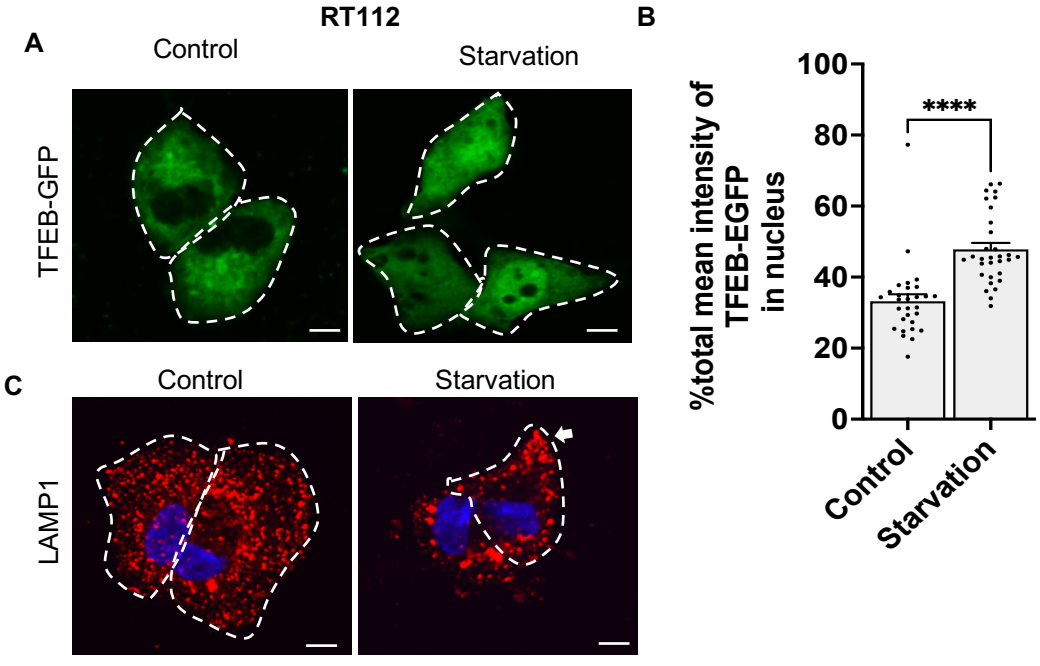

Fig 52. TEFB-GFP localization and lysosome positioning in RT112 cells after starvation
A. Representative images of RT112 cells transfected with TFEB-GFP for 72h in control and starvation (EBSS,4h) conditions. **B**. Quantification of total mean intensity of TFEB-GFP in nucleus in RT112 cells in control and starvation conditions. **** p<0.0001 in a Mann-Whitney U test, error bars are SEM **C**. Immunofluorescence staining of the LAMP1 in control and starvation treated RT112 cells. White arrow shows the peripheral clustering of lysosomes. Scale bars equal 10 µm.

Fig 53

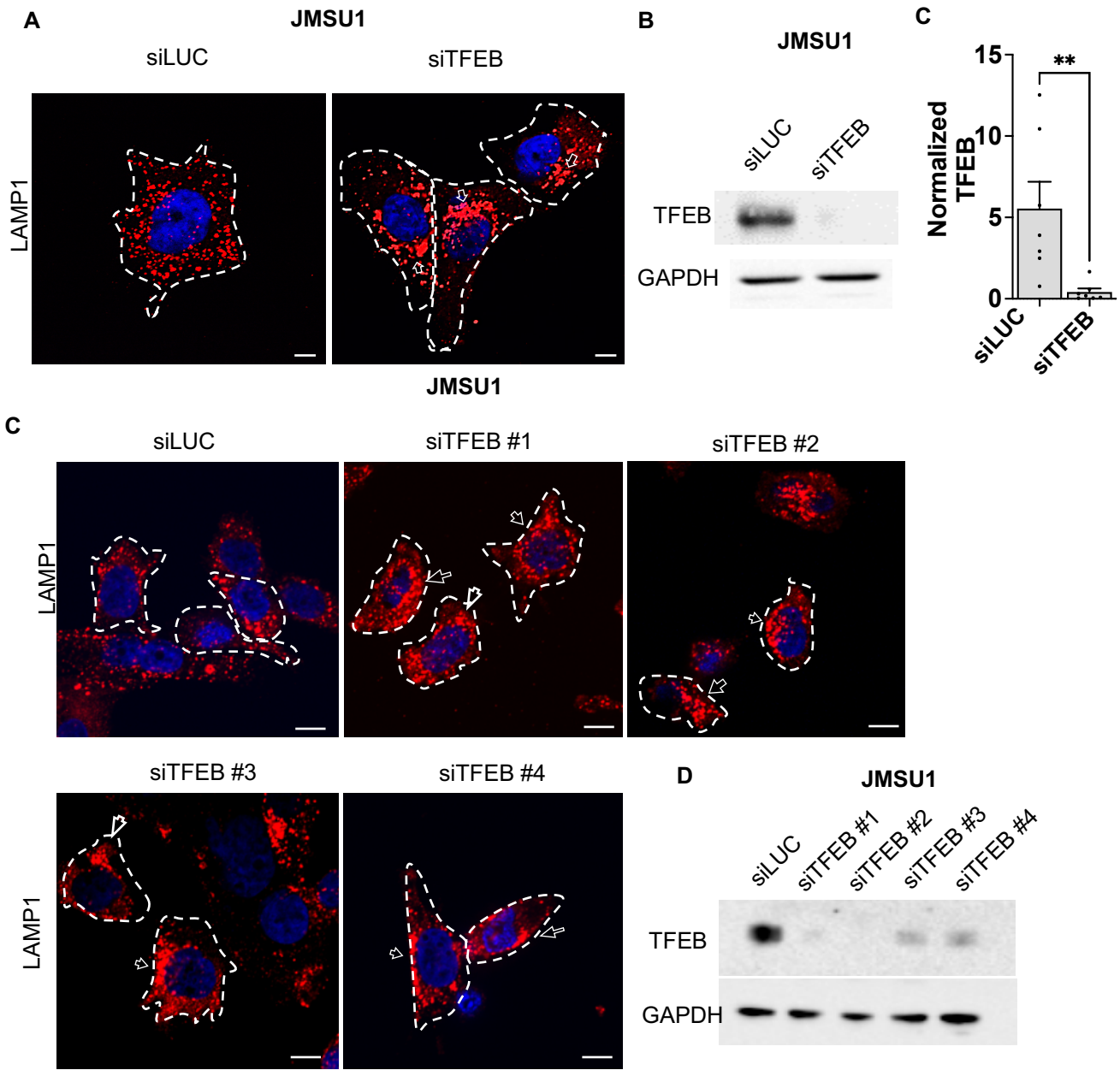

Fig 53. Lysosome positioning in JMSU1 cells after TFEB depletion
A. Immunofluorescence staining of LAMP1 in JMSU1 cells treated with siLUC and siTFEB for 72 h. Arrow shows the perinuclear clustering of lysosomes. Scale bars equal 10 µm. **B.** Western blot analysis of siTFEB (72 h, with siRNA pool) in JMSU1 cells and quantification of TFEB levels normalized to GAPDH. Error bars are SED of 7 independent experiments. ** $p < 0.005$ in a Mann-Whitney U test, error bars are SEM **C**. Immunofluorescence staining against the lysosomal-associated membrane protein 1 (LAMP1, CD107a) in JMSU1 cells after TFEB knockdown with individual siTFEB RNAs (72 h). Arrows show the perinuclear clustering of lysosomes. Scale bar is 15 µm. **D**. Western blot of TFEB knockdown with individual siTFEB RNAs (72 h).

Fig 54

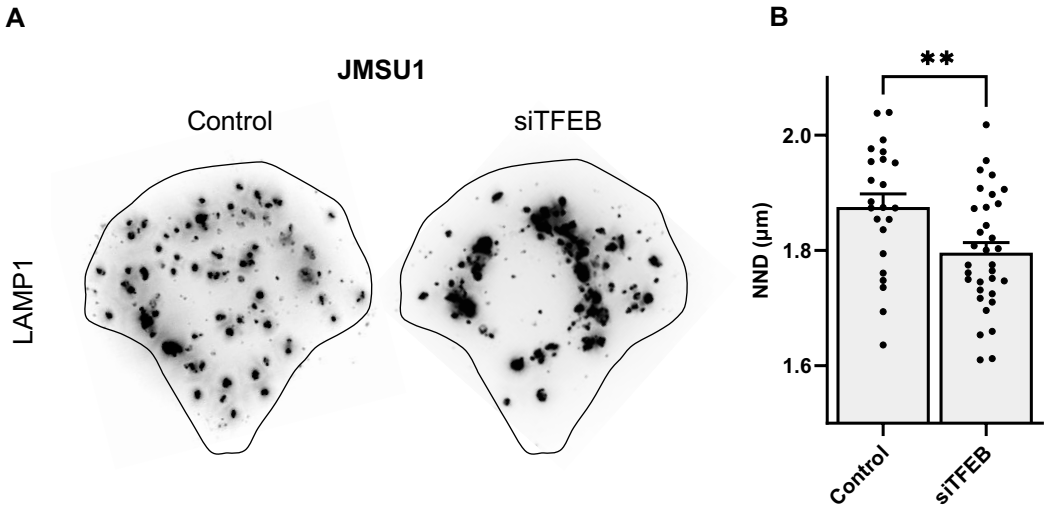

Fig 54. Lysosome positioning on micropatterns in JMSU1 cells after TFEB depletion
A. Representative images of lysosomes visualized by immunofluorescence staining against LAMP1 in micropatterned JMSU1 cells in control and siTFEB treatment conditions. **B**. Nearest neighbor distance (NND in µm) between lysosomes in micropatterned control (n= 23) and siTFEB (n= 34) treated JMSU1 cells; ** $p < 0.01$ in a Mann-Whitney U test, error bars are SEM

Fig 55

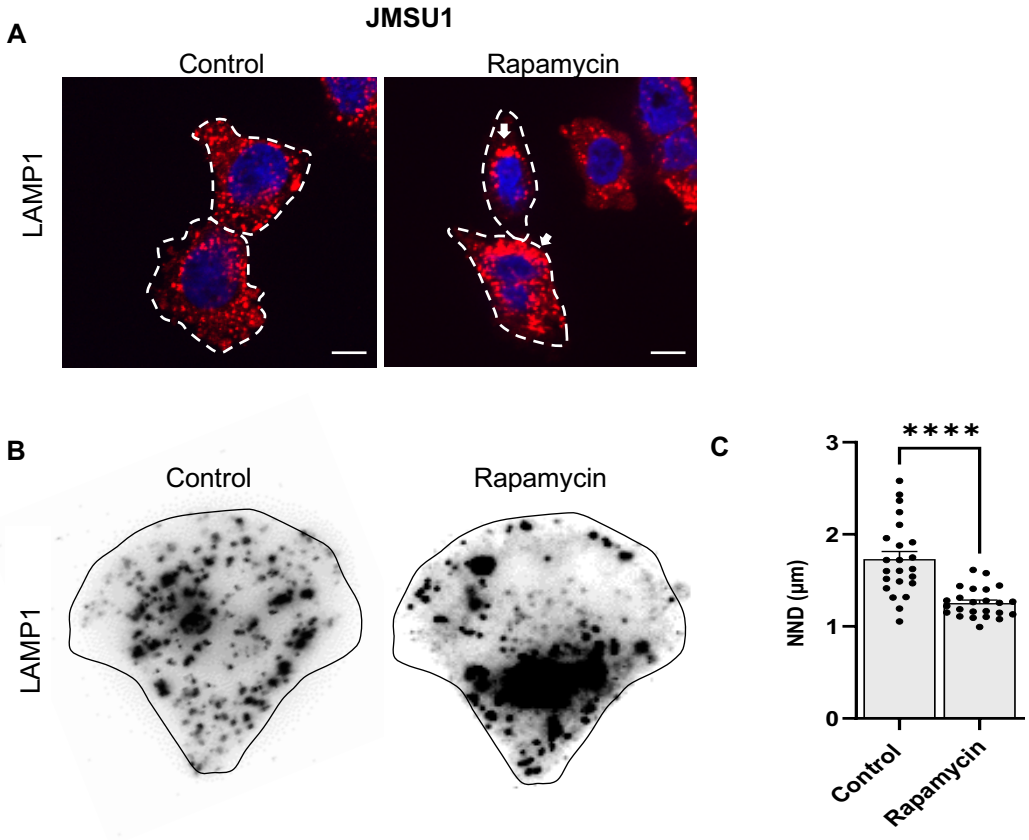

Fig 55. Lysosome positioning in JMSU1 cells after Rapamycin treatment.
A. Immunofluorescence staining of the LAMP1 in control (DMSO) and rapamycin (10 µM) treated JMSU1 cells. White arrow shows the peripheral clustering of lysosomes. Scale bars equal 10 µm. **B**. Representative images of lysosomes visualized by immunofluorescence staining against LAMP1 in micropatterned JMSU1 cells in control and rapamycin treatment. **C**. Nearest neighbour distance (NND in µm) between lysosomes in micropatterned control (n=25) and rapamycin treated (n=24) JMSU1 cells; **** $p < 0.0001$ in a Mann-Whitney U test, error bars are SEM

Additionally, we tested the effect of rapamycin treatment on lysosome positioning in JMSU1 cells. As shown before, rapamycin treatment in these cells led to inhibition of mTORC1 activity. Because our results indicate that both, mTORC1 and TFEB, are active in these cells, and TFEB is important for lysosomal dispersion, we aimed to test if mTORC1 regulates lysosomal dispersion in these cells. After rapamycin-dependent inhibition of mTORC1, lysosomes were visualized by LAMP1 IF in JMSU1 cells. Classically cultured cells revealed accumulation of lysosomes at the cell center (**Fig 55A**). We also quantified this by culturing JMSU1 cells on micropatterns and calculated the nearest neighbor distance (NND) of lysosomes. Lysosomes were more clustered after rapamycin treatment in micropatterned cells (**Fig 55B**), and the average NND was significantly increased as compared to untreated controls (**Fig 55C**).

Conclusion: TFEB regulates lysosomal dispersion in JMSU1 cells, because lysosomal clustering is observed upon TFEB silencing in these cells. This suggests that TFEB nuclear translocation drives lysosomal dispersion in these cells. In addition, we reveal that mTORC1, which we find active in JMSU1 cells, is important for lysosomal dispersion, because lysosomal clustering is observed upon mTORC1 inhibition. It seems that both, the TFEB and mTORC1 pathways, are active and together participate in anterograde lysosome movement in aggressive bladder cancer cell lines. Potentially, this could support the hyper proliferation of these cell lines. Interestingly, treatment of less aggressive RT112 cells with rapamycin or nutrient depletion inhibits mTORC1, translocate TFEB into the nucleus and induces lysosomal scattering. The specificity of TFEB is investigated in the next section.

4.7 TFEB-dependent mechanism of lysosome dispersion in RT112 cells

It has been shown that lysosomes translocate to the cell periphery upon overexpression of protrudin, and conversely, cluster perinuclearly upon protrudin depletion (Hong et al., 2017). Protrudin has been shown to form ER-lysosome contacts, which helps in loading of kinesisn-1 to the motor adaptor FYCO1 on lysosomes for anterograde trafficking (Raiborg et al., 2015) (**Fig 59A**). Thus, we next tested whether recruitment of protrudin to lysosomes is TFEB-dependent. Again, we

first induced nuclear translocation in RT112 cells, and thus, activation of TFEB by rapamycin treatment and visualized protrudin by immunofluorescence. Because protrudin is an ER-localized protein and only is found on lysosomes at ER-lysosome contact sites, we measured the fraction of protrudin that is found on LAMP1-positive lysosomes. We either treated RT112 cells with rapamycin or starved them (in Earle's Balanced Saline Solution, EBSS) for 4h, two conditions that induce nuclear TFEB. We then monitored colocalization between LAMP1 and protrudin. We found that treatment with rapamycin or starvation, significantly increased the fraction of protrudin found on lysosomes (**Fig 56 A, B**). Next, we checked for the presence of colocalization in these cells after a 24h treatment of rapamycin or starvation. This was done to confirm that the observed colocalization was maintained at longer time intervals and could be supported by the activation of transcription factor EB and downstream translation. We found that treatment with rapamycin or starvation, significantly increased the fraction of protrudin found on lysosomes after 24h of treatments (**Fig 57 A, B**). We next investigated if the increased protrudin colocalization at lysosomes could be a result of increased protein levels of protrudin induced by activated TFEB. We found no changes in the total level of protrudin in RT112 cells after treatment of rapamycin or starvation, either at 4h or 24h (**Fig 58**). However, starvation induced increased cell death in RT112 cells, as observed by low signals of housekeeping protein GAPDH.

Recruitment of protrudin to lysosomes is regulated by the binding of its FYVE (Fab 1, YOTB, Vac 1, and EEA1) domain to phosphatidylinositol-3-phosphate (PI3P) found on endomembranes (Hong et al., 2017) (**Fig 59A**). We thus tested whether TFEB regulated recruitment of another well-characterized FYVE domain protein, EEA1 (Early Endosome Antigen 1). EEA1 is recruited to early endosomes through binding of its FYVE domain to PI3P on the early endosome membrane (Lawe et al., 2000) (**Fig 59B**). Consistent with protrudin results, we found a significant increase of EEA1 on endomembranes upon treatment of RT112 cells with rapamycin as well as starvation, both conditions which induce nuclear TFEB. In case of starvation, both 4h and 24h treatment significantly induced more membrane bound EEA1 (**Fig 60, 61**) in RT112 cells. However, treatment with rapamycin showed no change in the levels of membrane bound EEA1 at 4h and only significant increase in membrane bound EEA1 after 24h treatment (**Fig 60, 61**). No change was observed in the total protein levels of EEA1 after treatments with rapamycin or starvation at either 4h or 24h time points in RT112 cells (**Fig 62**).

Fig 56

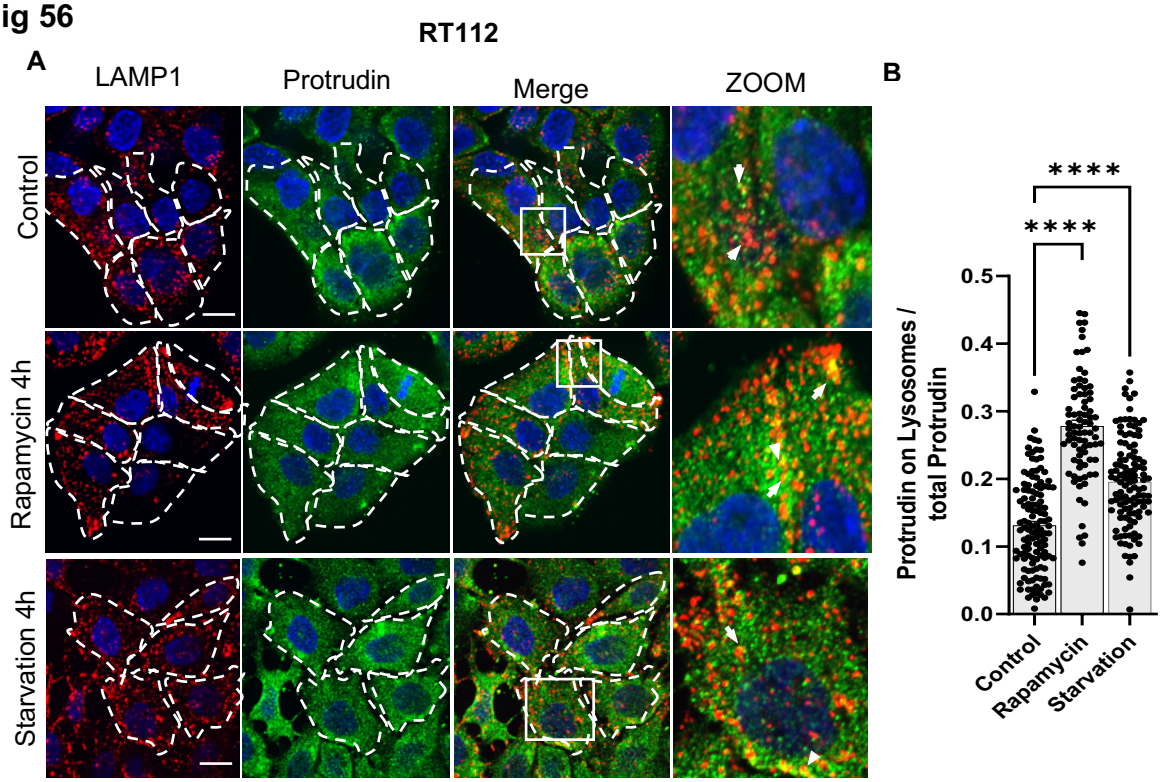

Fig 56. Protrudin colocalization on Lysosomes after 4h of rapamycin or starvation in RT112 cells
A. Immunofluorescence staining of LAMP1 (red) and protrudin (green) in control, rapamycin (10 μM, 4h) and starvation (EBSS, 4h) treated RT112 cells. Zoom shows the merged image of both proteins in the white box. White arrow shows the colocalization between LAMP1 and protrudin. Scale bars are 15 μm. **B**. Quantification of protrudin integrated intensity on lysosomes normalized to total cellular protrudin, in control, rapamycin and starvation treated RT112 cells; **** p<0.0001 Kruskal-Wallis test with Dunn post-hoc test with Sidak correction

Fig 57

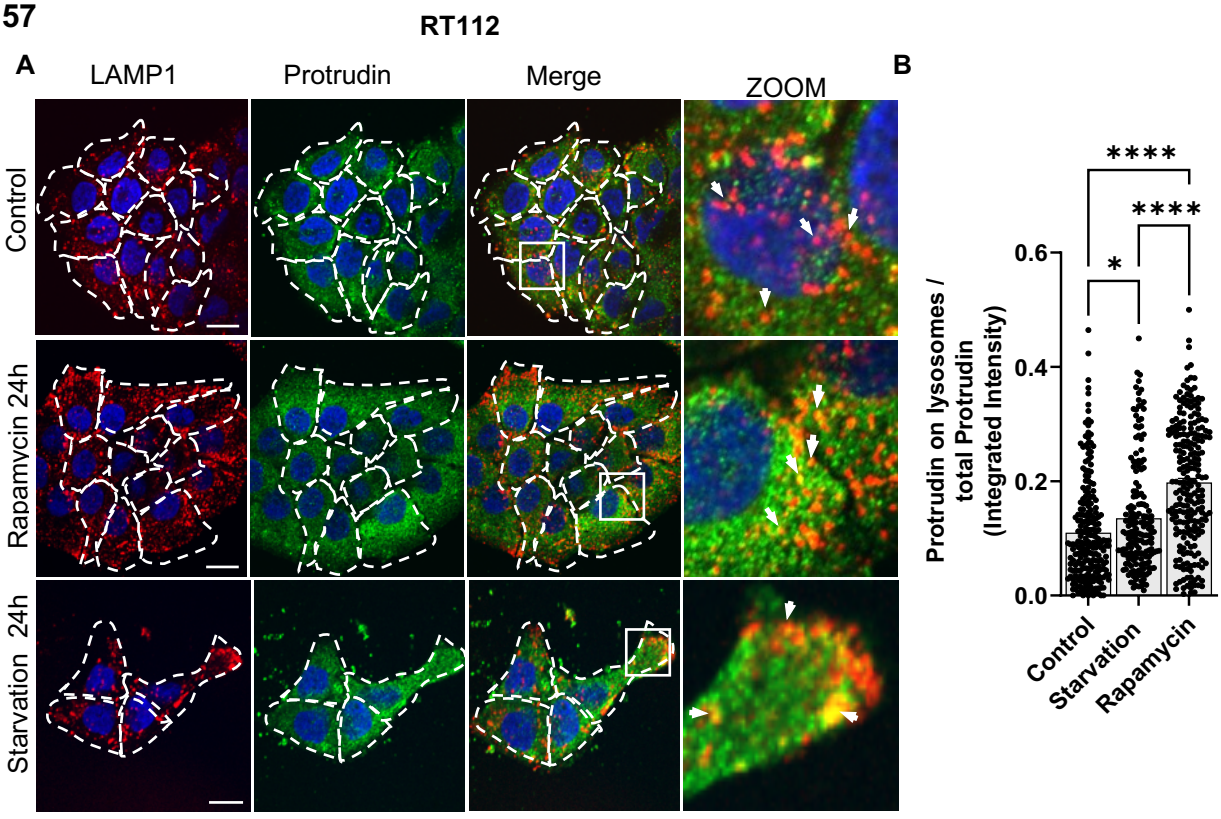

Fig 57. Protrudin colocalization on Lysosomes after 24h of rapamycin or starvation in RT112 cells
A. Immunofluorescence staining of LAMP1 (red) and protrudin (green) in control, rapamycin (10 μM, 24h) and starvation (EBSS, 24h) treated RT112 cells. Zoom shows the merged image of both proteins in the white box. White arrow shows the colocalization between LAMP1 and protrudin. Scale bars are 15 μm. **B**. Quantification of protrudin integrated intensity on lysosomes normalized to total cellular protrudin, in control, rapamycin and starvation treated RT112 cells; * p<0.05, **** p<0.0001 Kruskal-Wallis test with Dunn post-hoc test with Sidak correction.

Fig 58

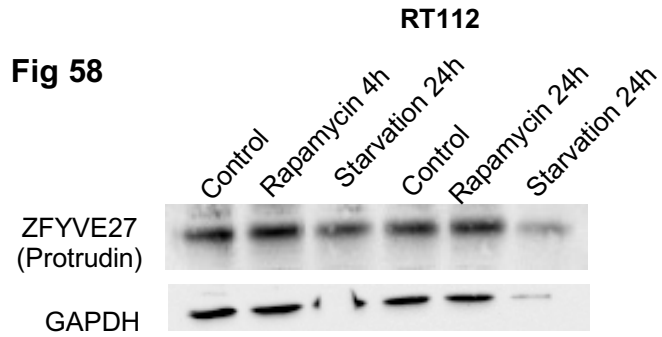

Fig. 58. Total protrudin in RT112 cells after Rapamycin or starvation treatments
Western blot analysis of Protrudin in control, Rapamycin (10 µM, 4h and 24h)and starvation treatments (EBSS, 4h and 24h) in RT112 cells. GAPDH represents the loading control.

Fig 59

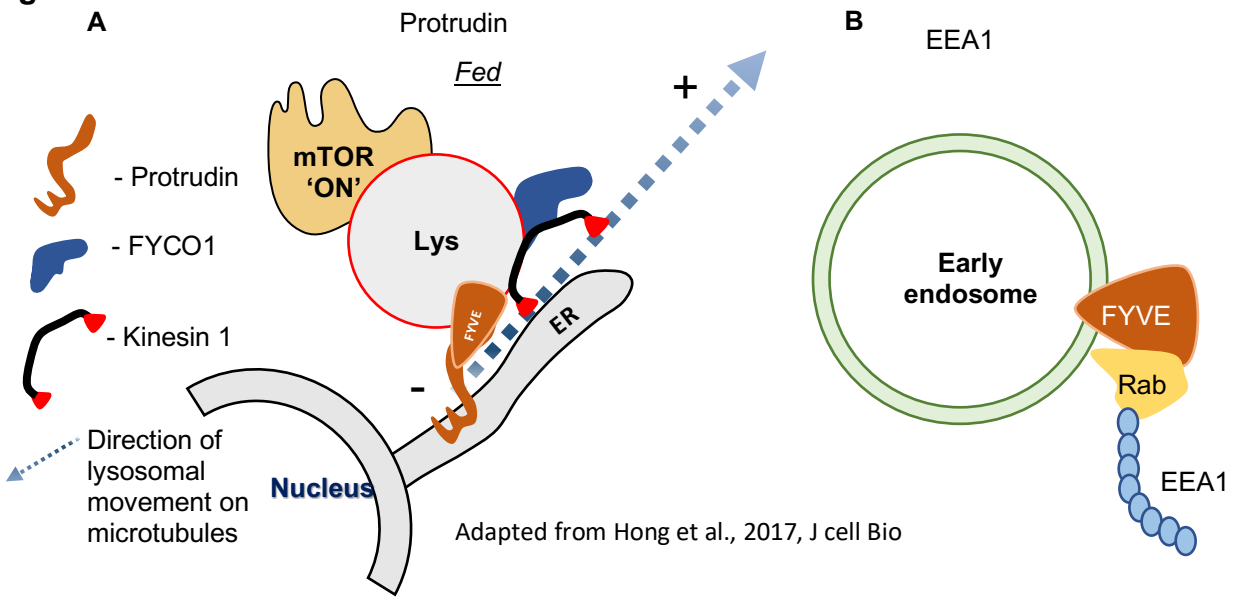

Fig 59. Schematic showing binding of protrudin and EEA1 to lysosome and endosome
A. Schematic showing binding of protrudin to lysosomes through its FYVE domain and lysosome anterograde movement through kinesin-1. **B.** Binding or EEA1 to early endosomes through its FYVE domain

Fig 60

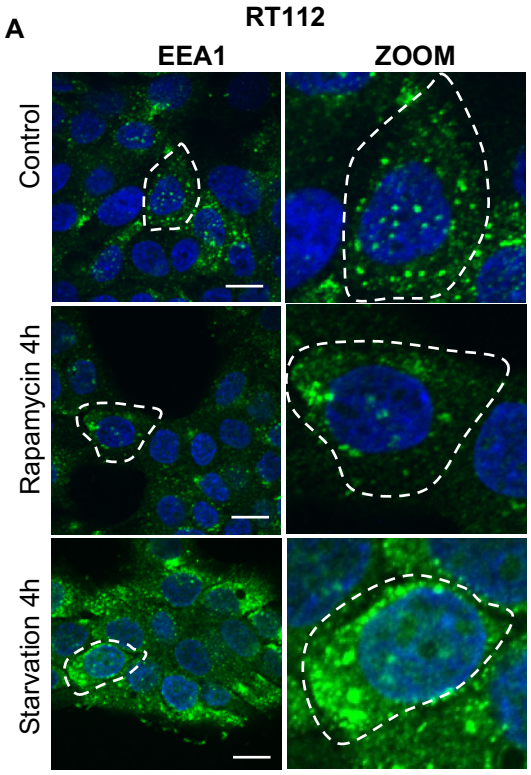

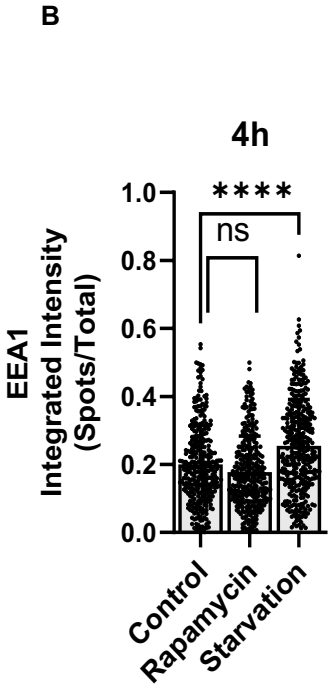

Fig 60. EEA1 localization on endomembranes after 4h of rapamycin or starvation in RT112 cells
A. Representative images of EEA1 staining in RT112 cells in control rapamycin (10 µM, 4h) and starvation (EBSS, 4h) conditions. Zoom shows one single cell. Scale bars are 15 µm. **B**. Quantification of EEA1 integrated intensity on segmented spots normalized to total cellular EEA1, in control, rapamycin and starvation conditions in RT112 cells; ns p>0.1, ****p<0.0001 in a Kruskal-Wallis test with Dunn post-hoc test with Sidak correction, error bars are SEM.

Fig 61

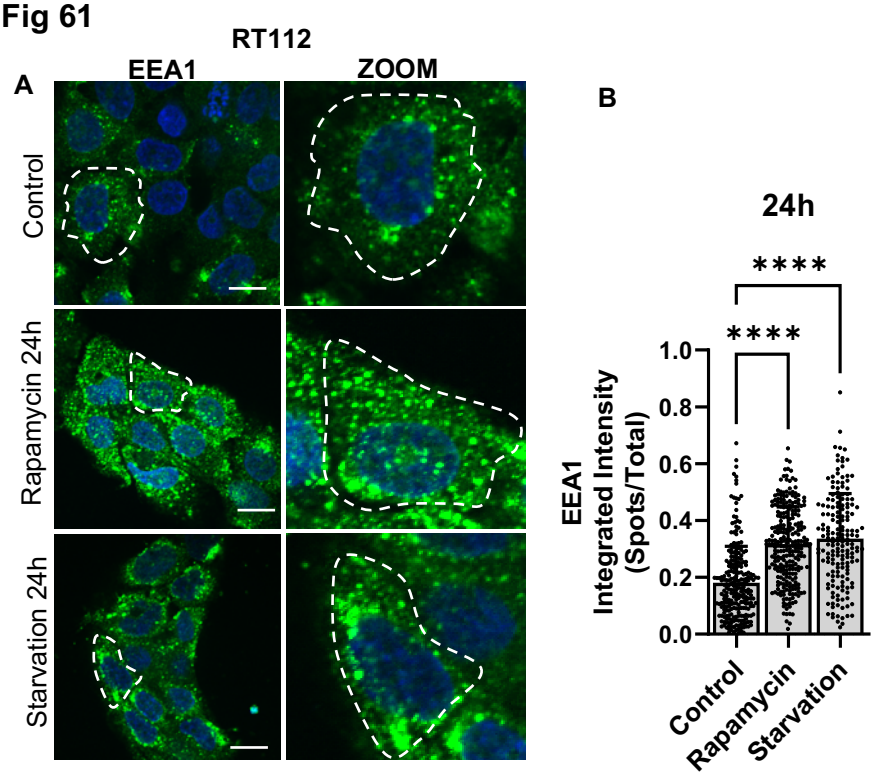

Fig 61. EEA1 localization on endomembranes after 24h of rapamycin or starvation in RT112 cells
A. Representative images of EEA1 staining in RT112 cells in control rapamycin (10 µM, 24h) and starvation (EBSS, 24h) conditions. Zoom shows one single cell. Scale bars are 15 µm. **B**. Quantification of EEA1 integrated intensity on segmented spots normalized to total cellular EEA1, in control, rapamycin and starvation conditions in RT112 cells; ****p<0.0001 in a Kruskal-Wallis test with Dunn post-hoc test with Sidak correction, error bars are SEM.

Fig 62

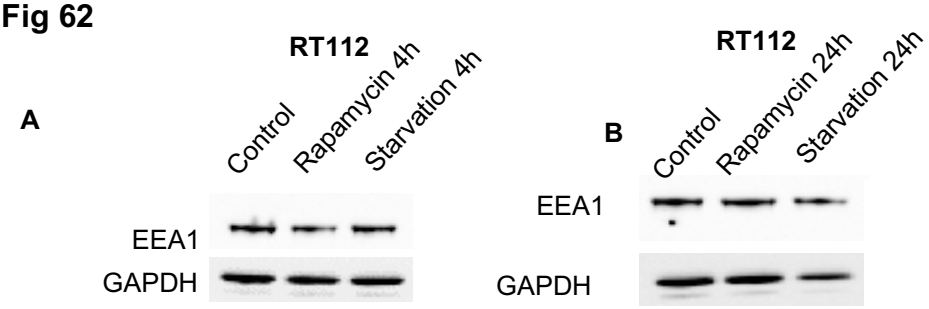

Fig. 62. Total EEA1 in RT112 cells after Rapamycin or starvation treatments
A. Western blot analysis of Protrudin in control, Rapamycin (10 µM, 4h) and starvation treatments (EBSS, 4h) in RT112 cells. GAPDH represents the loading control. B. Western blot analysis of Protrudin in control, Rapamycin (10 µM, 24h) and starvation treatments (EBSS, 24h) in RT112 cells. GAPDH represents the loading control

TFEB being a transcription factor, we checked if the accumulation of these two FYVE domain proteins on lysosomes was translation dependent. We treated RT112 cells with rapamycin for 24h, either in the presence or absence of the translation inhibitor cycloheximide (CHK). We monitored localization of protrudin on lysosomes and levels of membrane bound EEA1 by immunofluorescence and colocalization with Lamp1. In the presence of translation inhibitor CHK, EEA1 binding to endomembranes decreased in cells treated with rapamycin (**Fig 64 A, B**). Recruitment of protrudin to lysosomes however showed no decrease after treatment of RT112 cells with CHK. Rapamycin induced recruitment of protrudin to lysosomes was maintained even after blocking of translation with CHK (**Fig 63 A, B**), As before, no changes in the total levels of protrudin or EEA1 was observed after treatment with rapamycin or rapamycin along with cycloheximide when compared to control RT112 cells (**Fig 65 A, B**)

Finally, we tested whether the phenotype of increased recruitment of FYVE domain proteins to endomembranes, namely protrudin and EEA1, was TFEB dependent. We performed TFEB depletion through a siRNA approach (72h) in RT112 cells and monitored recruitment of protrudin or EEA1 to lysosomes in control, rapamycin 24h, siTFEB + rapamycin24h and only siTFEB conditions. We observed an increase in the levels of protrudin and EEA1 on lysosomes after 24h treatment of rapamycin, (**Fig 66 A, B; Fig 67A, B**). Whereas TFEB depletion significantly decreased the fraction of membrane bound EEA1 (**Fig 67 A, B**), we did not observe differences in protrudin levels on lysosomes after siTFEB (**Fig 66 A, B)**. Additionally, siTFEB treatment in RT112 cells (without any rapamycin activation) significantly decreased membrane bound EEA1 compared to control (**Fig 67 A, B**). siTFEB treatment (without any rapamycin activation) gave no change in recruitment of protrudin on lysosomes and the fraction of protrudin found on lysosomes was comparable to control RT112 cells (**Fig 66 A, B**). As before, we also monitored levels of total EEA1 and protrudin protein after siTFEB treatment and found very slight decrease in the levels of both EEA1 and protrudin after TFEB depletion in RT112 cells (**Fig 68 A-C**).

Fig 63

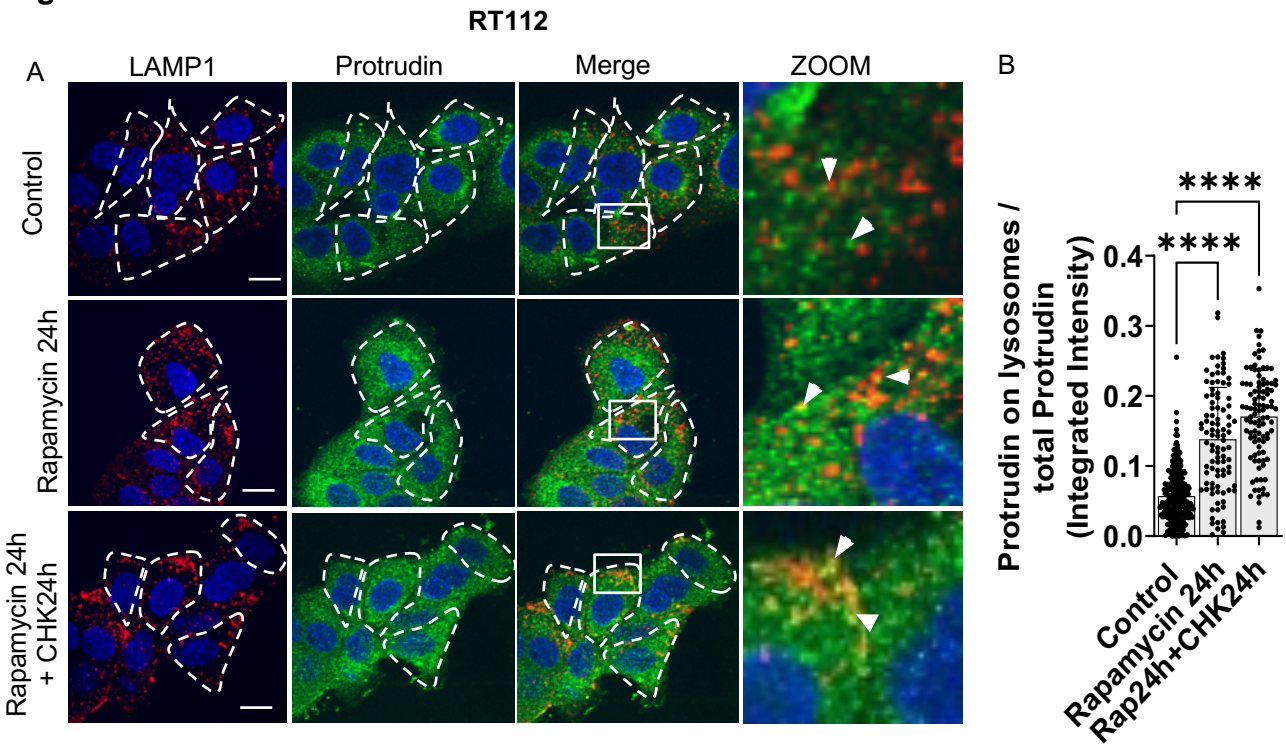

Fig 63. Protrudin localization on lysosomes after rapamycin and rapamycin + CHK treatment in RT112 cells

A. Immunofluorescence staining of LAMP1 (red) and protrudin (green) in control (DMSO), rapamycin (10 µM, 24 h) and cycloheximide (20 µg/mL, 24 h) conditions. Zoom shows the merged image of both proteins in the white box. White arrow shows the colocalization between LAMP1 and protrudin. Scale bars are 15 µm. **B**. Quantification of protrudin integrated intensity on lysosomes normalized to total cellular protrudin in control, rapamycin and cycloheximide treatment conditions in RT112 cells; ****p<0.0001in a Kruskal-Wallis test with Dunn post-hoc test with Sidak correction, error bars are SEM)

Fig 64

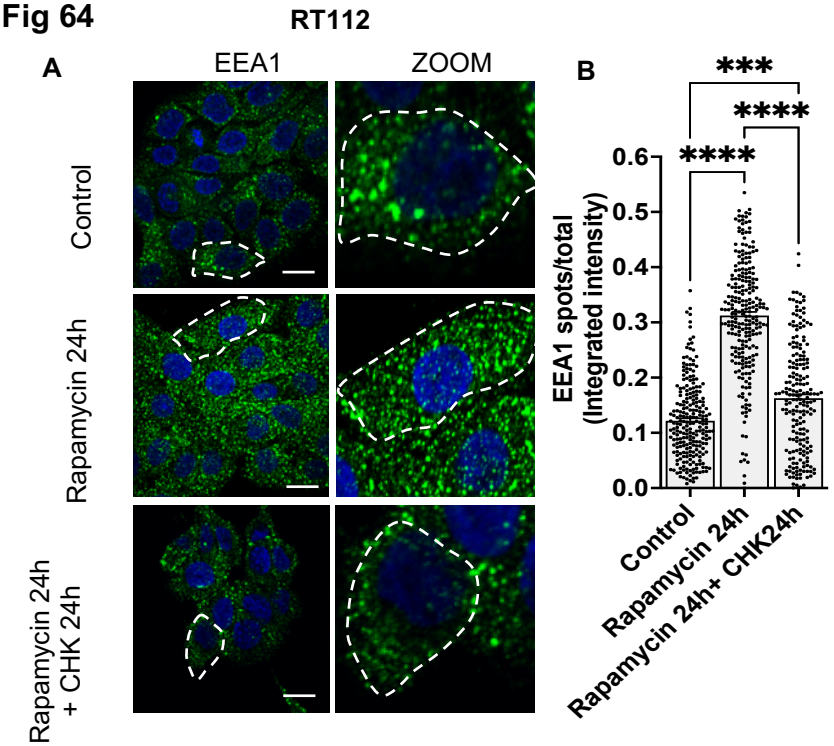

Fig 64. EEA1 localization on endomembranes after rapamycin and rapamycin + CHK treatment in RT112 cells

A. Representative images of EEA1 staining in RT112 cells in control (DMSO), rapamycin (10 µM, 24 h) and cycloheximide (20 µg/mL, 24 h) conditions. Zoom shows one single cell. Scale bars are 15 µm. **B**. Quantification of EEA1 integrated intensity on segmented spots normalized to total cellular EEA1, in control, rapamycin and cycloheximide treatment conditions in RT112 cells; ****p<0.0001, ***p<0.001 in a Kruskal-Wallis test with Dunn post-hoc test with Sidak correction, error bars are SEM)

Fig 65

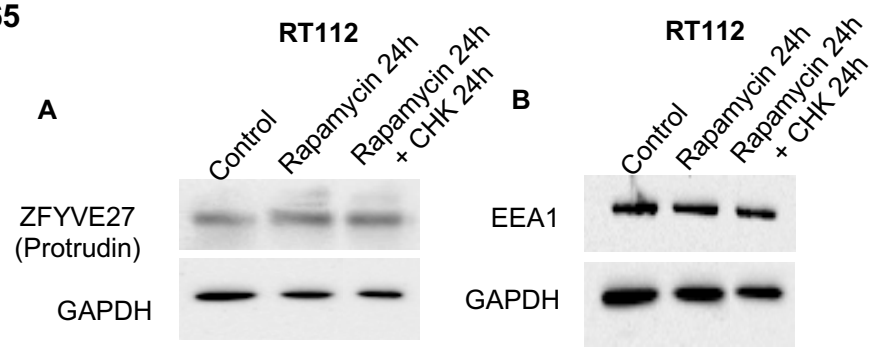

Fig. 65. Total EEA1 and protrudin in RT112 cells after Rapamycin and rapamycin CHK treatments

A. Western blot analysis of Protrudin in control, Rapamycin (10 µM, 24h) and Rapamycin + CHK (20 µg/mL, 24 h) treatments in RT112 cells. GAPDH represents the loading control. **B.** Western blot analysis of EEA1 in control, Rapamycin (10 µM, 24h) and Rapamycin + CHK (20 µg/mL, 24 h) treatments in RT112 cells. GAPDH represents the loading control.

Fig 66

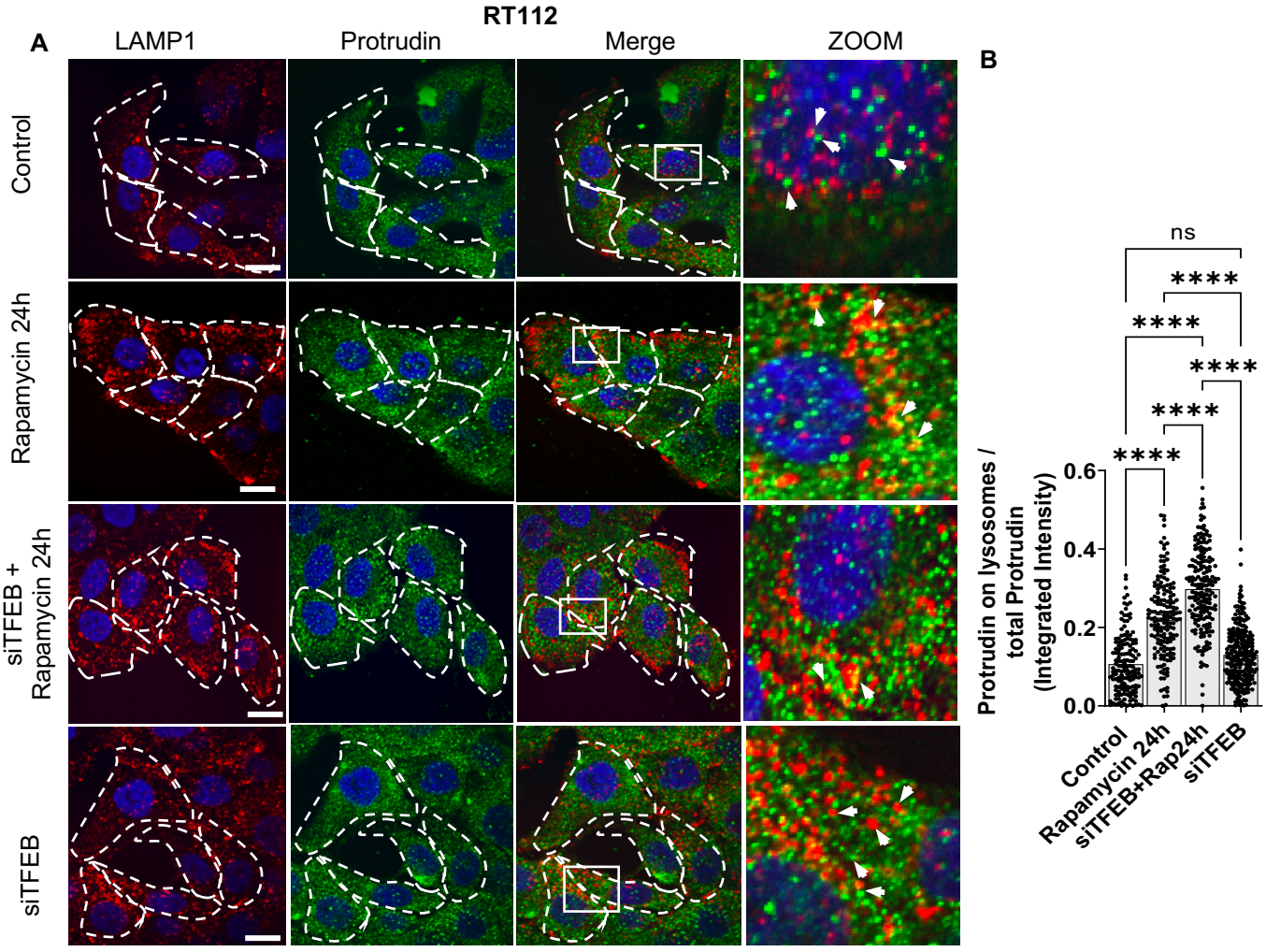

Fig 66. Protrudin localization on lysosomes after rapamycin and siTFEB + rapamycin treatment in RT112 cells

A. Immunofluorescence staining of LAMP1 (red) and protrudin (green) in control, rapamycin (10 µM, 24 h), siTFEB (72h) + Rapamycin and siTFEB (72h) conditions in RT112 cells. Zoom shows the merged image of both proteins in the white box. White arrow shows the colocalization between LAMP1 and protrudin. Scale bars are 15 µm. **B**. Quantification of protrudin integrated intensity on lysosomes normalized to total cellular protrudin in control, rapamycin, rapamycin + siTFEB and siTFEB treatment conditions in RT112 cells; ****p<0.0001in a Kruskal-Wallis test with Dunn post-hoc test with Sidak correction, error bars are SEM)

Fig 67

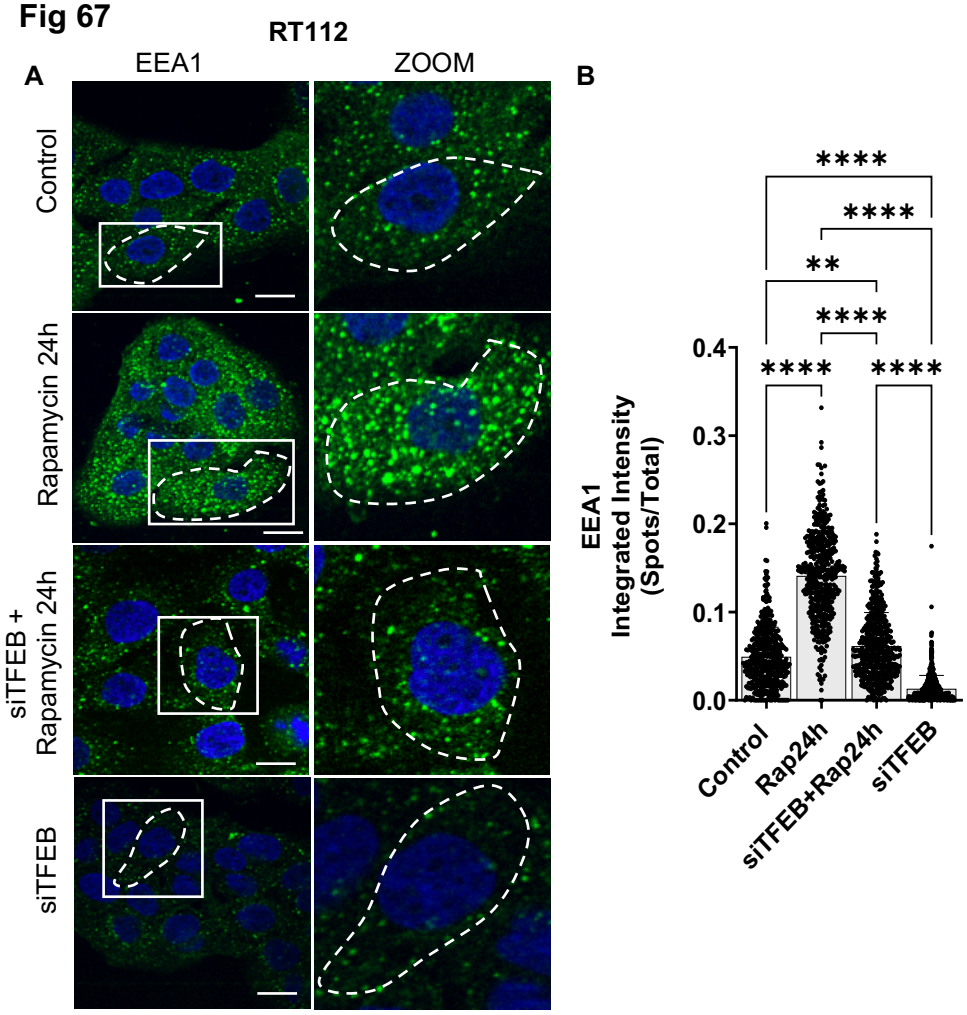

Fig 67. EEA1 localization on endomembranes after rapamycin and siTFEB + rapamycin treatment RT112 cells

A. Representative images of EEA1 staining in RT112 cells in control, rapamycin (10 µM, 24 h), siTFEB (72h) + Rapamycin and siTFEB (72h) conditions. Zoom shows one single cell. Scale bars are 15 µm. **B**. Quantification of EEA1 integrated intensity on segmented spots normalized to total cellular EEA1, in control, rapamycin (10 µM, 24 h), siTFEB (72h) + Rapamycin and siTFEB (72h) conditions in RT112 cells; ****p<0.0001, **p<0.01 in a Kruskal-Wallis test with Dunn post-hoc test with Sidak correction, error bars are SEM)

Fig 68

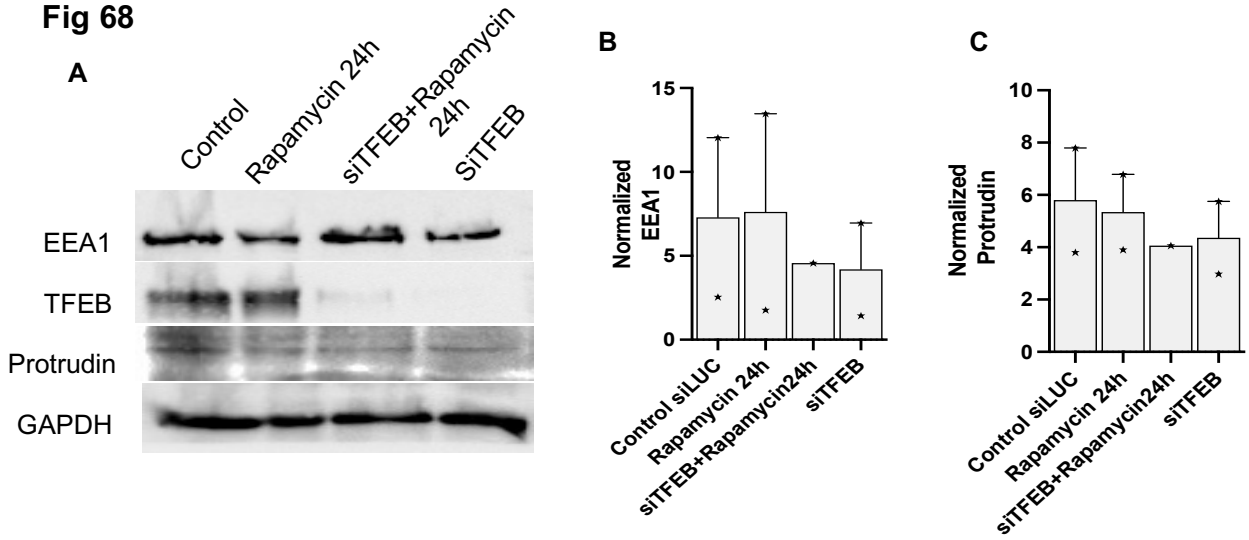

Fig. 68. Total EEA1 and protrudin in RT112 cells after rapamycin and siTFEB + rapamycin treatment

A. Western blot analysis of Protrudin, EEA1 and TFEB in control, rapamycin (10 µM, 24 h), siTFEB (72h) + Rapamycin (24h) and siTFEB (72h) conditions in RT112 cells. GAPDH represents the loading control. **B.** Western blot quantification of EEA1 and **C**. protrudin in control, rapamycin (10 µM, 24 h), siTFEB (72h) + Rapamycin (24h) and siTFEB (72h) normalized to GAPDH in RT112 cells. Error bars represent the s.d of multiple experiments

Conclusion: Our results showed that in RT112 cells, treatment of rapamycin or starvation induced nuclear TFEB and significantly induced recruitment of protrudin to lysosomes required for lysosomal dispersion. Since recruitment of protrudin to lysosome is through its FYVE domain, we also tested if TFEB was important for recruitment of another classic FYVE domain protein, EEA1. We found that similar to protrudin EEA1 recruitment to endomembrane was significantly increased upon TFEB nuclear induction by rapamycin or starvation. This indicated that TFEB activation regulated binding of FYVE domain protein to lysosomes, and in general to endomembranes, and thus, regulated lysosomal dispersion. We tested the specific role of TFEB in recruitment of these FYVE domain proteins by inhibition of translation post TFEB nuclear induction or by depletion of TFEB by siRNA. We observed no decrease in fraction of protrudin on lysosome that was induced by rapamycin treatment after concurrent treatments with cycloheximide (CHK) or siTFEB. This indicated that recruitment of protrudin could also be maintained by TFEB-independent mechanisms. In case of EEA1, we observed that the fraction of membrane bound protein after rapamycin treatment was decreased when concurrently treated with either translation inhibitor or siTFEB. Because the FYVE domain specifically binds PI3P at endomembranes, we hypothesize that TFEB regulated PI3P levels that we further investigated.

4.8 TFEB-dependent mechanism of lysosome dispersion in JMSU1 cells

Building on our results from RT112 cells, we next tested whether TFEB regulates PI3P levels in JMSU1 cells. We performed TFEB depletion in these cells through siRNA interference. We then observed through immunofluorescence the recruitment of protrudin and EEA1 to lysosomes between control and siTFEB conditions. We found that depletion of TFEB (72h) significantly reduced the fraction of protrudin and EEA1 on lysosomes (**Fig 69A, B**) (**Fig 70A, B**). Again, we tested if this phenotype was a result of changes in the total levels of protrudin or EEA1 after TFEB depletion and found no major changes in the total levels of these two FYVE domain proteins (**Fig 71A, B**).

Fig 69

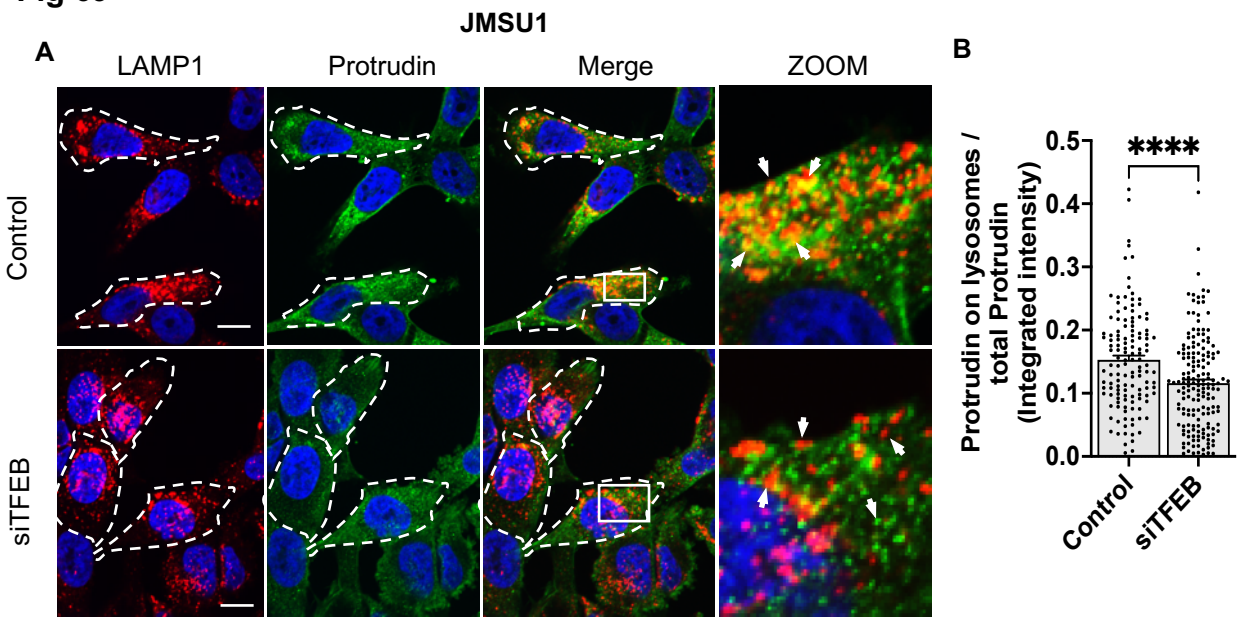

Fig 69. Protrudin colocalization on Lysosomes after TFEB depletion in JMSU1 cells
A. Immunofluorescence staining of LAMP1 (red) in and protrudin (green) in JMSU1 cells in control (siLUC) and siTFEB (72 h) treatment conditions. Zoom shows the merged image of the two proteins in the white box. White arrow shows the colocalization between LAMP1 and protrudin. Scale bars are 15 µm. **B**. Quantification of protrudin integrated intensity on lysosomes normalized to total cellular protrudin, in control (siLUC) and siTFEB in JMSU1 cells; p<0.0001 in a Mann-Whitney U test, error bars are SEM

Fig 70

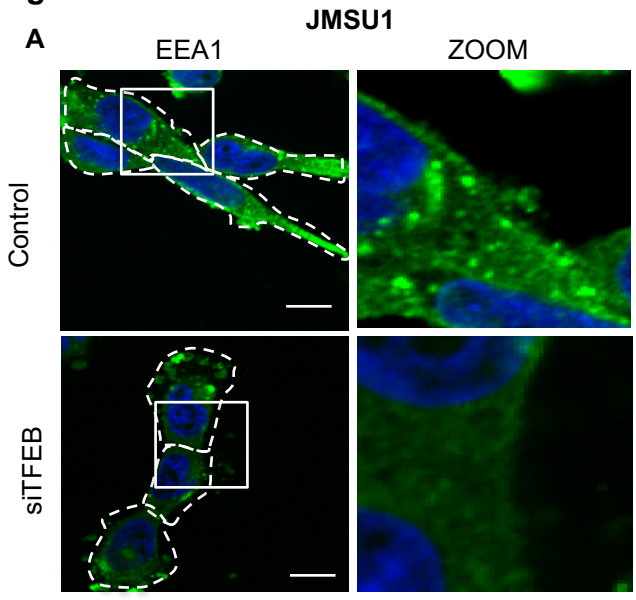

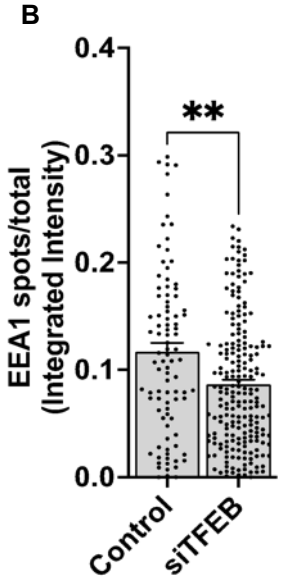

Fig 70. EEA1 localization on endomembranes after TFEB depletion in JMSU1 cells
A. Representative images of EEA1 staining in JMSU1 cells in control (siLUC) and siTFEB (72 h) conditions. Zoom shows area in white box. Scale bars are 15 µm. **B**. Quantification of EEA1 integrated intensity on segmented spots normalized to total cellular EEA1, in control (siLuc) and siTFEB in JMSU1 cells; ** p<0.01 in a Mann-Whitney U test, error bars are SEM

Fig 71

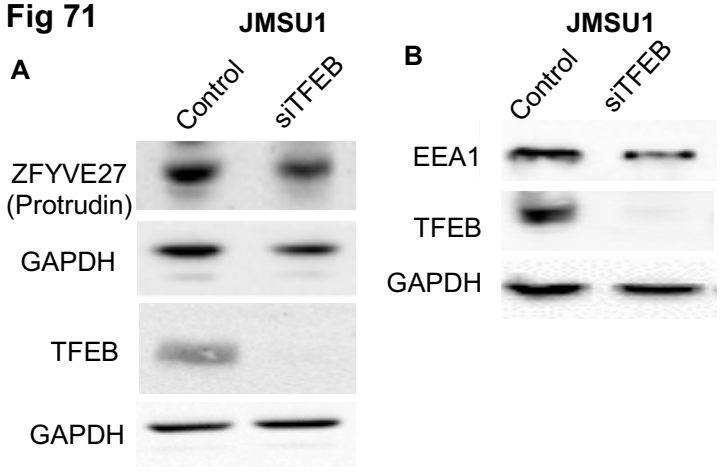

Fig. 71. Total protrudin and EEA1 and JMSU1 cells siTFEB
A. Western blot analysis of Protrudin in control (siLuc) and siTFEB (72h) in JMSU1 cells. GAPDH represents the loading control. B. Western blot analysis of EEA1 in control (siLuc) and siTFEB (72h) in JMSU1 cells. GAPDH represents the loading control

Conclusion: In JMSU1 cells, TFEB regulates recruitment of FYVE domain proteins such as protrudin and EEA1. Since FYVE domains specifically bind PI3P (Phosphatidylinositol-3-phosphate), our results indicated that TFEB could potentially regulate PI3P levels.

4.9 Regulation of Phosphatidyl inositol 3-phosphate in JMSU1 cells

We then studied levels of PI3P in JMSU1 cells in the presence and absence of TFEB. To monitor PI3P, we transiently expressed a cellular probe consisting of the PI3P-binding FYVE domain from the human homologue of the hepatocyte growth factor-regulated tyrosine kinase substrate Hrs, duplicated in tandem as an EGFP fusion construct (EGFP-FYVE)(Gillooly et al., 2000). We expressed EGFP-FYVE in JMSU1 cells and monitored the fraction of this construct (normalized to its total expression) on LAMP1-positive lysosomes upon knock down of TFEB. Most PI3P is found to be on early and late endosomes, thus as expected, EGFP-FYVE showed an endosomal staining and only partially colocalized with lysosomes (**Fig 72A, B**). Silencing of TFEB by siRNA significantly decreased the normalized fraction of EGFP-FYVE found on LAMP1-positve lysosomes in JMSU1 cells (**Fig 72A, B**). Moreover, we measured a significant reduction of membrane-bound EGFP-FYVE (normalized to total cellular expression levels) after knock-down of TFEB (**Fig 73A, B**). As a control, membrane-bound EGFP-FYVE was lost after treated with Wortmannin, an inhibitor of class II and class III PI3 kinases, which reduces the cellular levels of PI3P. Moreover, levels of EGFP-FYVE on LAMP1-positive lysosomes were significantly decreased after wortmannin treatment in JMSU1 cells (**Fig 74A, B**). To confirm the role of PI3P in in lysosomal dispersion, we cultured JMSU1 cells in classic cultures and on micropatterns and treated them with wortmannin. We observed that this significantly reversed the scattered lysosome phenotype (**Fig 75A, B**). Quantification on micropatterns revealed a significant decrease in the average NND of lysosomes (**Fig 75C**) confirming a PI3P-dependent lysosome scattering in these cells.

Finally, we investigated whether TFEB regulates class III PI3 kinase (PIK3C3 / VPS34). PIK3C3 is important for the localized conversion of phosphatidylinositol (PI) to phosphatidylinositol-3-phosphate at endosomes, which is important for fusion of lysosomes and autophagosomes (Bechtel et al., 2013). We performed TFEB knock

Fig 72

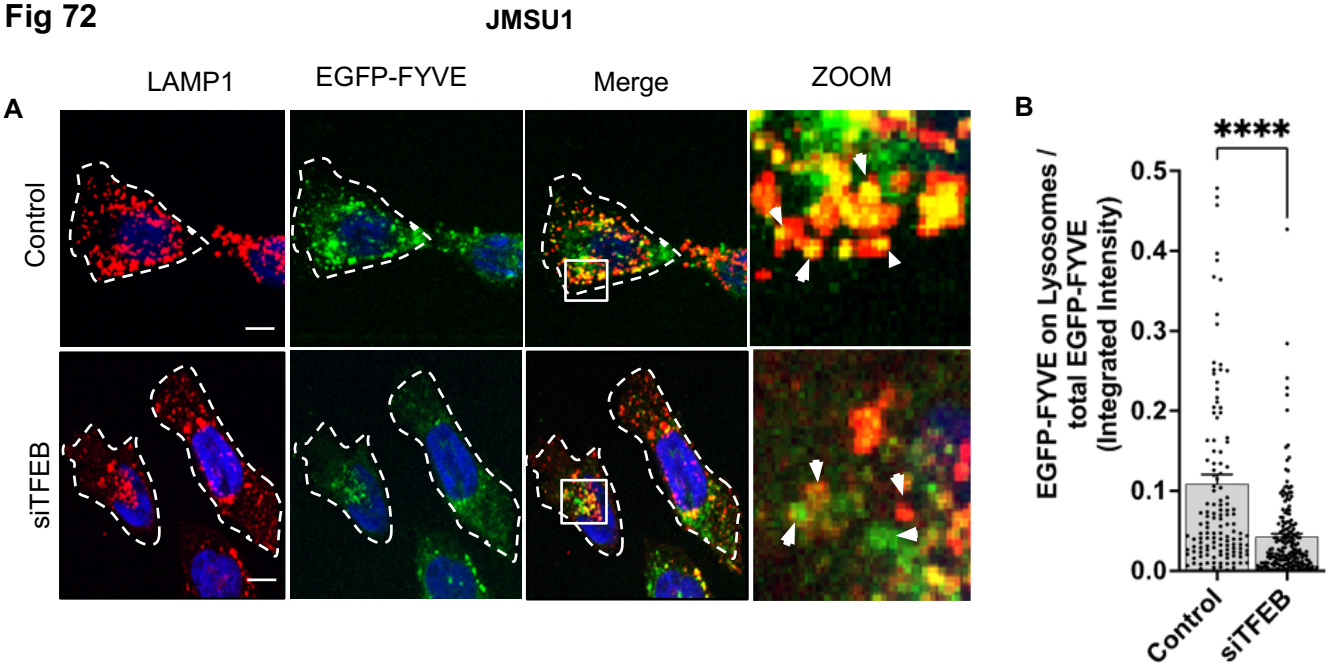

Fig 72. EGFP-FYVE colocalization on lysosomes after siTFEB in JMSU1 cells.
A. Immunofluorescence staining of LAMP1 (red) in control (siLUC) and siTFEB (72 h) treated JMSU1 cells transfected with EGFP-FYVE (green). Zoom shows the merged images of LAMP1 and EGFP-FYVE in white box. White arrow shows the colocalization between LAMP1 and EGFP-FYVE. Scale bars equal 10 µm. **B**. Quantification of EGFP-FYVE integrated intensity on lysosomes normalized to total cellular EGFP-FYVE, in siLUC and siTFEB treated JMSU1 cells; $p<0.0001$ in a Mann-Whitney U test, error bars are SEM.

Fig 73

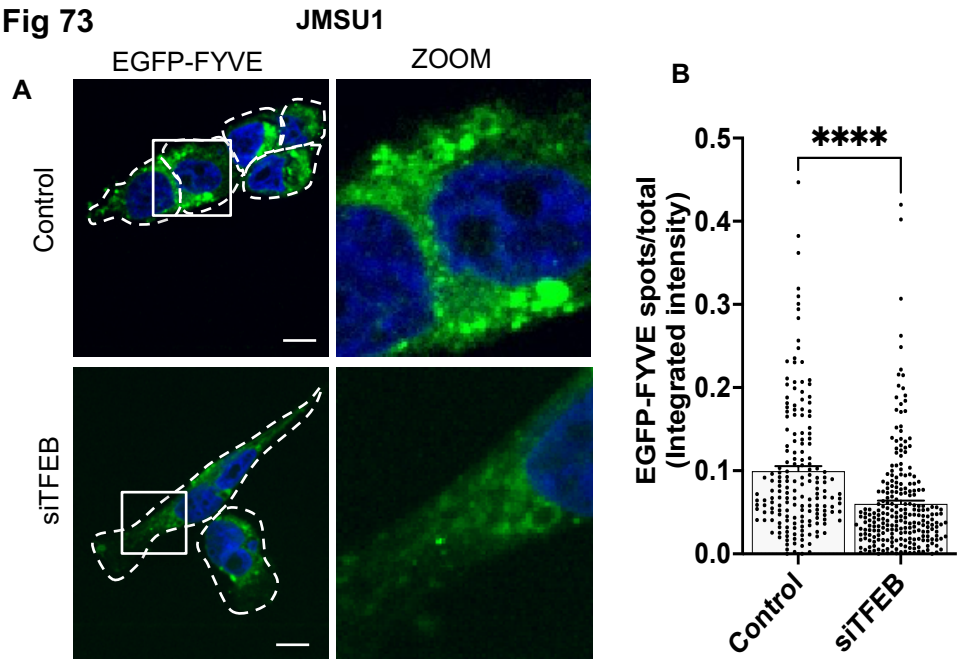

Fig 73. EGFP-FYVE localization on endomembranes after siTFEB in JMSU1 cells
A. Representative images of control (siLUC) and siTFEB (72 h) treated JMSU1 cells expressing EGFP-FYVE. Zoom shows EGFP-FYVE in white box. Scale bars equal 15 µm. **D**. Quantification of EGFP-FYVE integrated intensity on segmented spots normalized to total cellular EGFP-FYVE, in siLUC and siTFEB JMSU1 cells; $p<0.0001$ in a Mann-Whitney U test, error bars are SEM

Fig 74

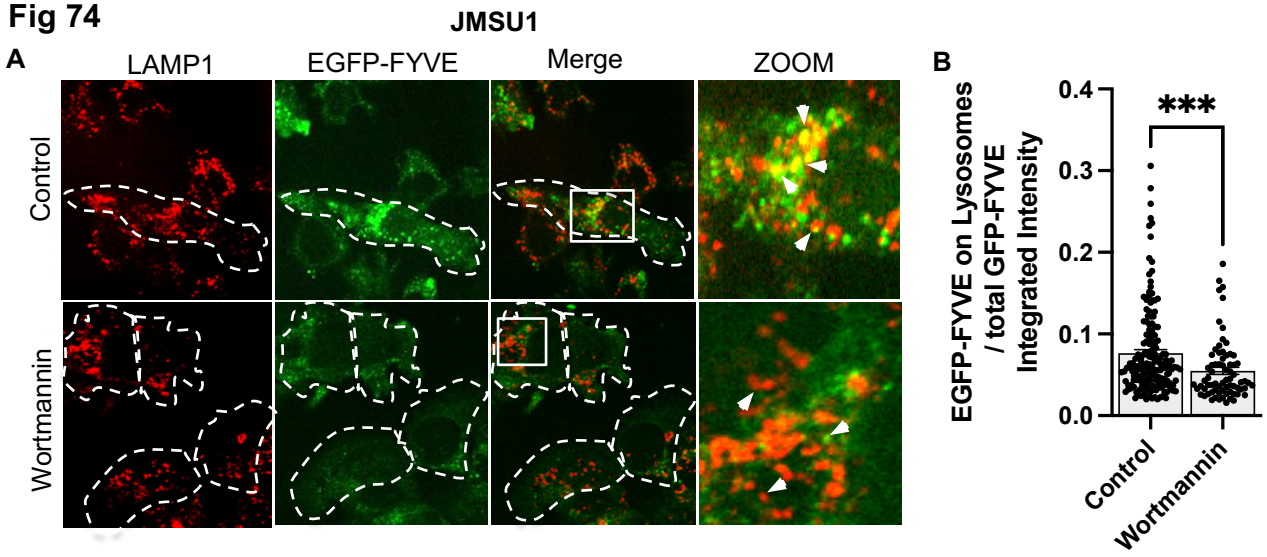

Fig 74. EGFP-FYVE localization on lysosomes after wortmannin treatment in JMSU1 cells

A. Immunofluorescence staining of LAMP1 (red) in control (DMSO) and Wortmannin($1\mu M$) treated JMSU1 cells transfected with EGFP-FYVE (green). Zoom shows the merged images of LAMP1 and EGFP-FYVE in white box. White arrow shows the colocalization between LAMP1 and EGFP-FYVE. Scale bars equal 10 µm. **B**. Quantification of EGFP-FYVE integrated intensity on lysosomes normalized to total cellular EGFP-FYVE, in control and wortmannin treated JMSU1 cells; ***p<0.001 in a Mann-Whitney U test, error bars are SEM

Fig 75

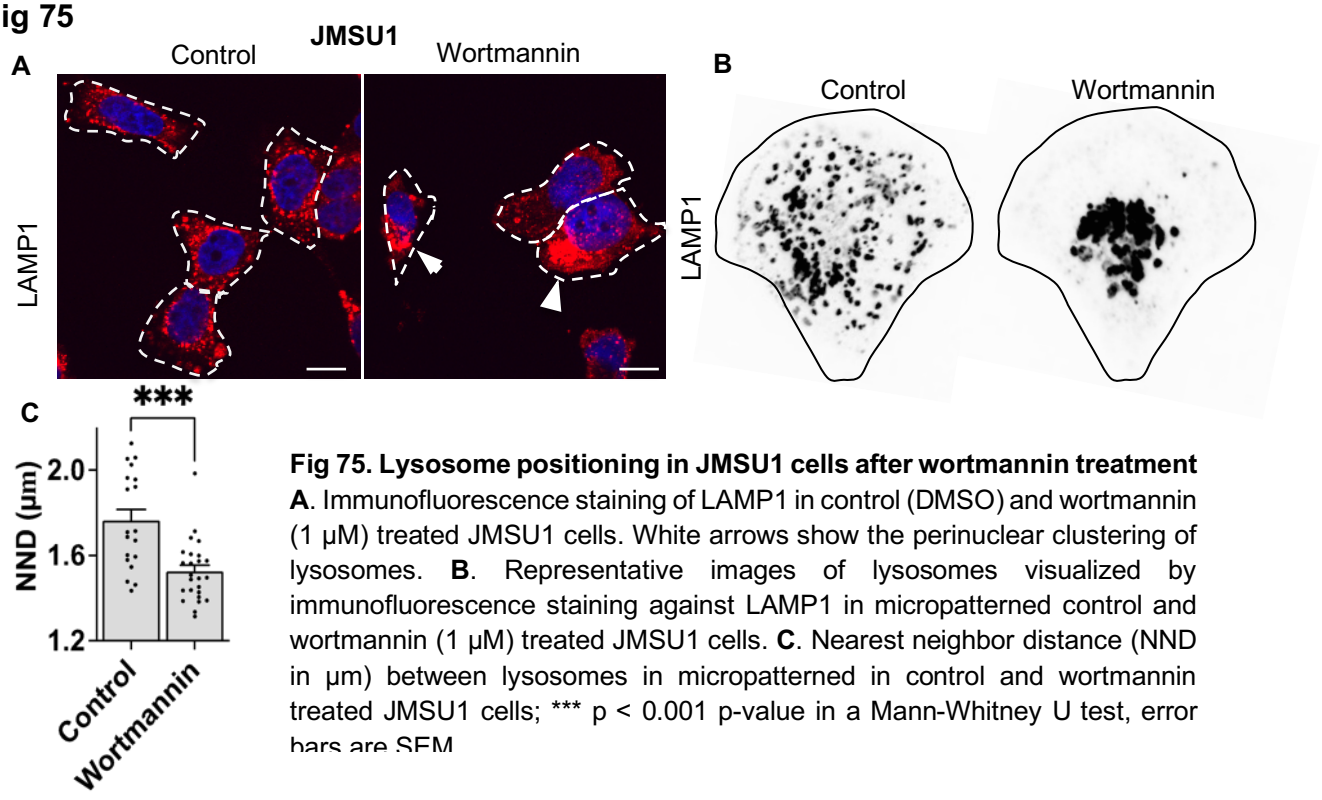

Fig 75. Lysosome positioning in JMSU1 cells after wortmannin treatment

A. Immunofluorescence staining of LAMP1 in control (DMSO) and wortmannin (1 µM) treated JMSU1 cells. White arrows show the perinuclear clustering of lysosomes. **B**. Representative images of lysosomes visualized by immunofluorescence staining against LAMP1 in micropatterned control and wortmannin (1 µM) treated JMSU1 cells. **C**. Nearest neighbor distance (NND in µm) between lysosomes in micropatterned in control and wortmannin treated JMSU1 cells; *** p < 0.001 p-value in a Mann-Whitney U test, error bars are SEM

Fig 76

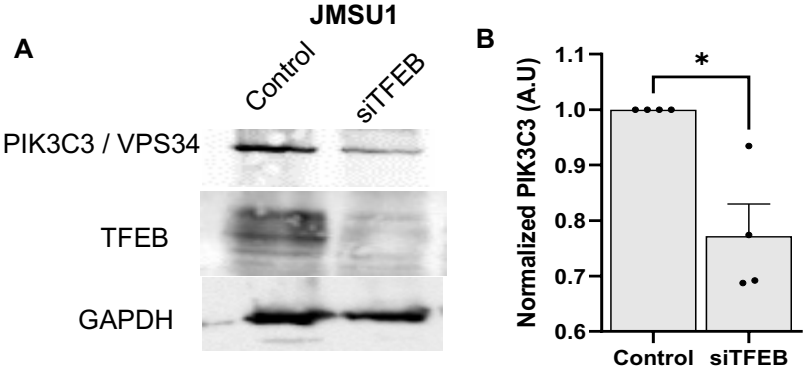

Fig 76. PIK3C3 levels in JMSU1 after siTFEB

Western blot analysis of PIK3C3/VPS34 in JMSU1 cells in control (siLuc) and siTFEB conditions. GAPDH represents the loading control B. Quantification of PIK3C3 in JMSU1 normalized to GAPDH from multiple experiments. *P< 0.05 in a paired t- test, error bars are SEM.

down in JMSU1 cells and monitored PIK3C3 levels by western blotting. We found that TFEB depletion significantly decreased protein levels of PIK3C3 in JMSU1 cells (**Fig 76A, B**). This indicated that expression of this PI3 kinase is under the regulation of TFEB in this aggressive bladder cancer cell line.

Conclusion: Our results indicate that TFEB regulates PI3P levels on lysosomes, which is required for lysosomal dispersion. This proposes that increased cellular PI3P levels in JMSU1 downstream of TFEB activation could results in a scattered lysosome phenotype observed in this cell line.

Results Aim 3 - Implications of lysosomal signaling and positioning in bladder cancer progression

4.10 Regulation of lysosome-dependent secretion and invasion in bladder cancer cells

Lysosomal exocytosis is known to facilitate secretion (release) of matrix metalloproteinases (MMPs) and cathepsins, which degrade the tumor extracellular matrix and support cancer invasion. Since role of peripheral lysosomes in cancer has been implicated in lysosomal secretion/exocytosis, we studies whether dispersion of lysosomes in bladder cancer cell lines correlates with increased secretion from these cells. We monitored the secretion of matrix metalloproteinase (MMPs) by measuring the MMP enzymatic activity in the supernatant from same number of cells after overnight culture. We used a MMP activity assay kit that employs a generic MMP peptide substrate tagged with 5-FAM (5-Carboxyfluorescein) and a quencher so that it does not fluoresce, however, when cleaved by MMPs in the samples, it emits a fluorescence that can be monitored to estimate the MMPs activity. Our results indicated that JMSU1 cells showed MMP activity of about 0.6 µM at the end of the 24h reaction / degradation of the MMP substrate, this was higher than those of the other three cell lines that had comparable MMP activity of about 0.4 µM after the 24h reaction (**Fig 77A**). To investigate if MMP secretion was dependent on the lysosome positioning, we used RT112 cells and JMSU1 cells with the BicD2 dimerization system cluster lysosomes. We performed the MMP activity assay from the media collected from these cell lines growing for 24h in control conditions or with A/C heterodimerizer.

We found no difference in the MMP activity between the cells without or with A/C-induced lysosome clustering, in either of the two cell lines (**Fig 77B, C**). This indicated that lysosome clustering did not impact the total MMP secretion in these cells. However the differences could be more subtle, thus, we next monitored the direct fusion of a lysosomal Soluble N-ethylmaleimide-sensitive-factor Attachment protein REceptor (SNARE), namely the Vesicle-associated membrane protein 7 (VAMP7) by TIRF (Total Internal Reflection Microscopy). VAMP7 was tagged with pHluorin and transiently expressed in the bladder cancer cell lines. The pHluorin signals are quenched in the acidic lysosomal lumen, but upon fusion of lysosomes to the plasma membrane, protons are released from the lumen that leads to a rapid increase in fluorescence (**Fig 78A, C**). We observed that non aggressive MGHU3 and RT112 cell lines had barely any of lysosomal exocytosis (**Fig 78B**). The KU19-19 and JMSU1 cell lines however showed events of lysosomal exocytosis (**Fig 78B**). The mean rate of exocytosis was about 5 secretion events / min in KU19-19 cells and about 20 secretion events/ min in JMSU1 cells (**Fig 78B**). We next investigated if VAMP7-facilitated exocytosis was dependent on lysosomal positioning. For this, we used JMSU1 cells stably expressing the BicD2 dimerization system for lysosomal clustering (**Fig 79A, B**), which transiently expressed VAMP7-pHluorin. We found the rate of lysosomal exocytosis per minute to be reduced by about half upon clustering of lysosomes than compared to the control cells. This indicated that lysosome positioning regulated secretion in JMSU1 cells.

Next, we investigated if TFEB-dependent lysosomal changes impacted invasion. We performed 3D spheroid invasion assays after treating JMSU1 cells with siLuc or siTFEB. Cells were siRNA transfected before formation of spheroids, which took about 4 days, and again once spheroids were embedded in collagen gel and grown at 37°C. We observed that invasion started from both, siLUC and siTFEB-treated spheroids, within 24h of collagen embedding, with no differences between the two conditions (**Fig 80A**). However, after monitoring the spheroids in the subsequent days (upto 3 days), we found that the spheroids with a TFEB knock down did not invade as much as the control (siLUC) spheroids (**Fig 80A**). We quantified the area of invasion by segmentation of all cells (in yellow, **Fig 80A**) and found significant decrease in the area of invasion after siTFEB (**Fig 80B**).

Finally, we tested whether TFEB regulated cell proliferation and cell migration in this aggressive cell line employing the technique of lens-free microscopy. We transfected JMSU1 cells with siTFEB or siLuc and captured movies of a big field of view ($29.4m^2$) for 3 days. Cell proliferation was measured by monitoring the increase in the number of cells as a function of time (over 3 days) in either of the treatment conditions. Cell migration was measured by tracking individual cells in siLuc and siTFEB conditions to calculate the speed of cell migration (μm/hour). Cells proliferated in logarithmic manner in control siLuc condition, reaching a peak (confluency) at around 3days, but the proliferation was significantly slower in cells treated with siTFEB. (**Fig 81A**). Cell migration in most of the cells of control siLuc condition was about 0.2μm / hour and which was reduced to almost zero post TFEB knockdown (**Fig 82B**).

Conclusion: JMSU1 and KU19-19 cells show more lysosomal exocytosis as compared to MGHU3 and RT112 cells. MMP activity in media from growing bladder cancer cells correlates to secretion rates found by TIRF imaging. However, although VAMP-7-dependent secretion was reduced after lysosomal clustering by A/C heterodimerizer, no changes in MMP activity were detected. Depletion of TFEB in JMSU1 cells leads to less VAMP7- pHluorin exocytosis and decreased invasion from 3D spheroids.

Fig 77

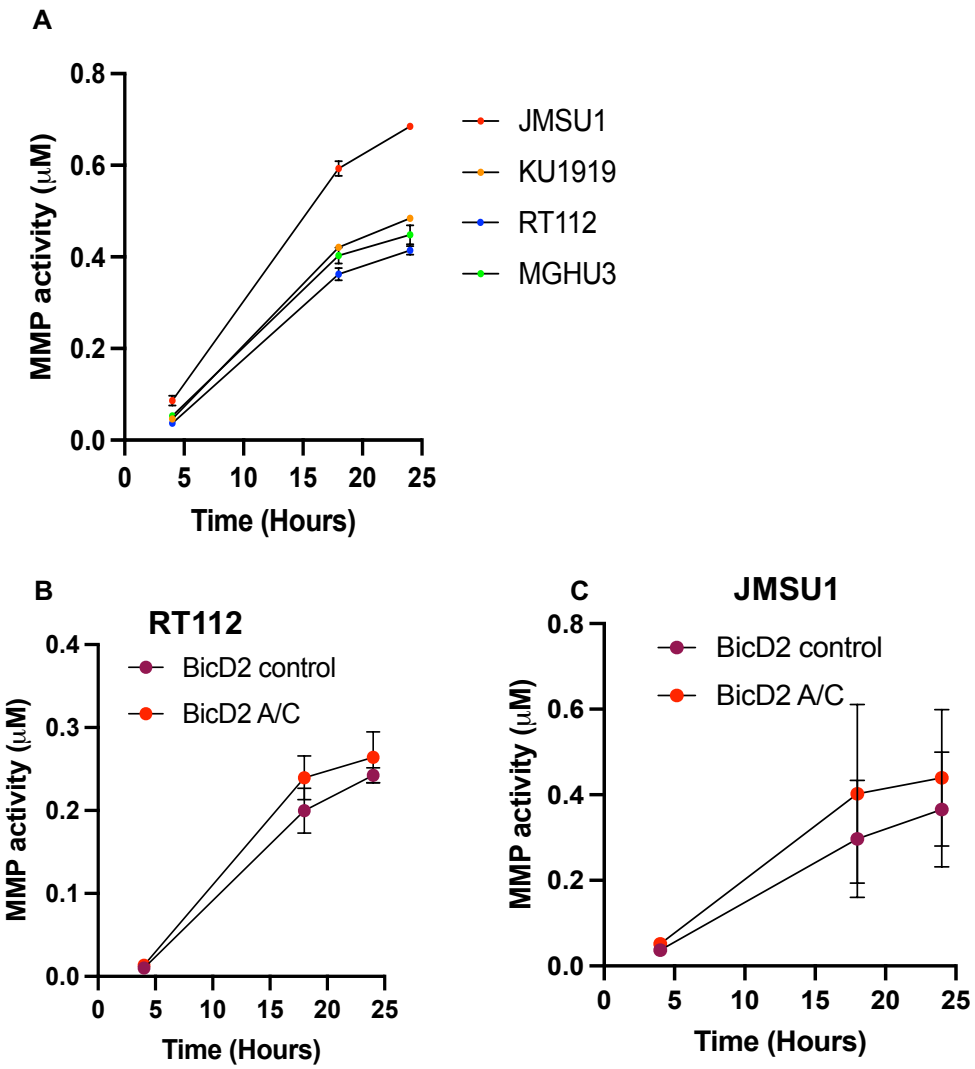

Fig 77. MMP secretion in bladder cancer cells

A. MMP activity (μM) in MGHU3, RT112, KU19-19 and JMSU1 cells over 24h of reaction with MMP substrate . Data represented as mean and s.d of 3 independent experiments.

B. MMP activity (μM) in RT112 cells with BicD2 dimerization system in control (DMSO) and with A/C heterodimerizer treatment condition, over 24h of reaction with MMP substrate. Data represented as mean and s.d of 3 independent experiments. **C.** MMP activity (μM) in JMSU1 cells with BicD2 dimerization system in control (DMSO) and with A/C heterodimerizer treatment condition, over 24h of reaction with MMP substrate. Data represented as mean and s.d of 3 independent experiments

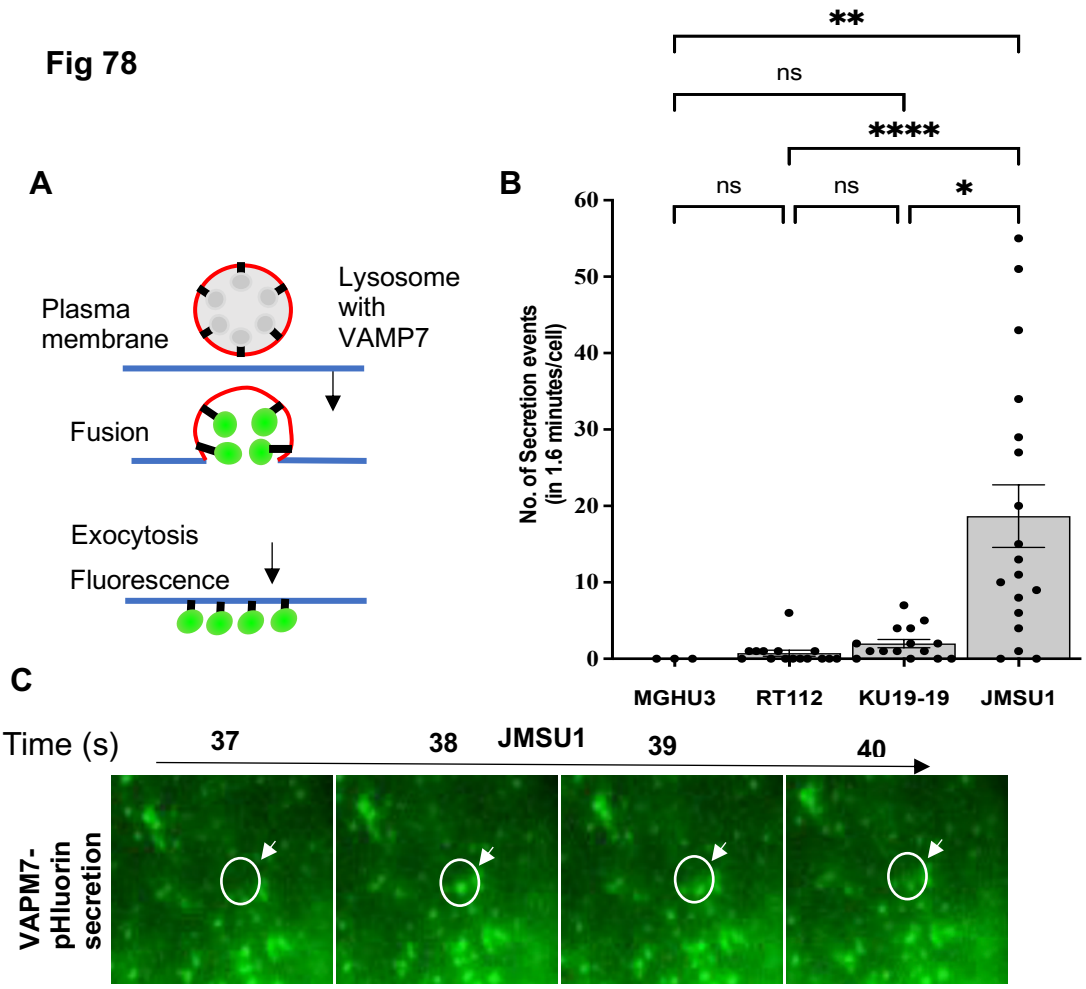

Fig 78. Lysosomal exocytosis in bladder cancer cells

A. Schematic of VAMP7-pHluorin tagged lysosomes exocytosis and fluorescence detection. **B.** Quantification of VAMP7-pHluorin tagged lysosome exocytosis in MGHU3, RT112, KU19-19 and JMSU1.* p value<0.05, ** p value <0.01, **** p value <0.0001 in a Kruskal-Wallis test with Dunn post-hoc test with Sidak correction, error bars are SEM.) **C**. Representative images showing appearance of VAMP7-pHluorin tagged lysosome and its exocytosis in subsequent time frames (in seconds). White circle and arrow mark the region of exocytosis.

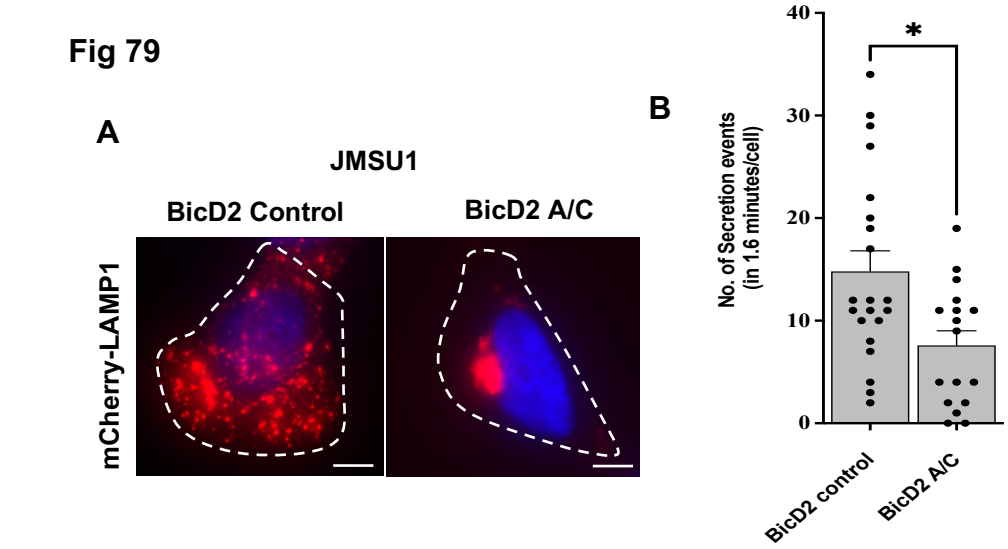

Fig 79. Lysosomal exocytosis in JMSU1 after lysosome clustering

A. Representative image of mCherry-LAMP1 tagged lysosomes in JMSU1 cells with the BicD2 dimerization system in control (DMSO) or A/C heterodimerizer treated conditions. Scale bar is 5µm. **B.** Quantification of VAMP7-pHluorin tagged lysosome exocytosis in mCherry-LAMP1 tagged lysosomes in JMSU1 cells with the BicD2 dimerization system in control (DMSO) or A/C heterodimerizer treated conditions. * p value < 0.05 in a Mann-Whitney U test, error bars are SEM

Fig 80

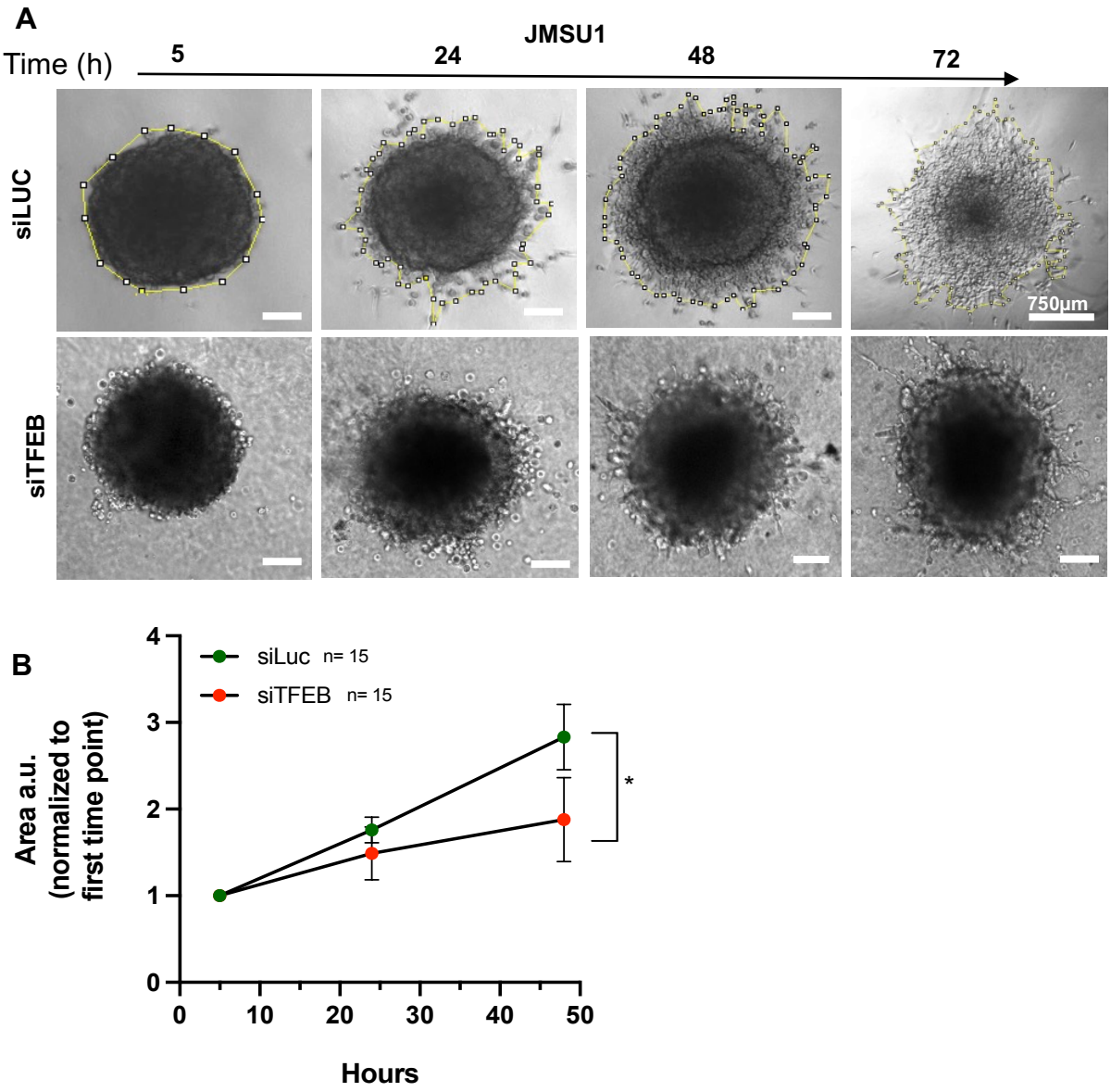

Fig 80. Spheroid invasion assay in JMSU1 cells in control (siLuc) and siTFEB conditions
A. 3D invasion of JMSU1 spheroids into collagen I matrix in control conditions of control (siLUC) or siTFEB. Scale bar is 300µm (unless stated otherwise) Yellow border around the spheroid represents the area of segmentation for analysis of area of invasion. B. Quantification of the area of invasion of 3D spheroids of JMSU1 in control (siLuc, n=15) or siTFEB (n=15) conditions. * p value< 0.05 in a Mann-Whitney U test, error bars are SEM.

Fig 81

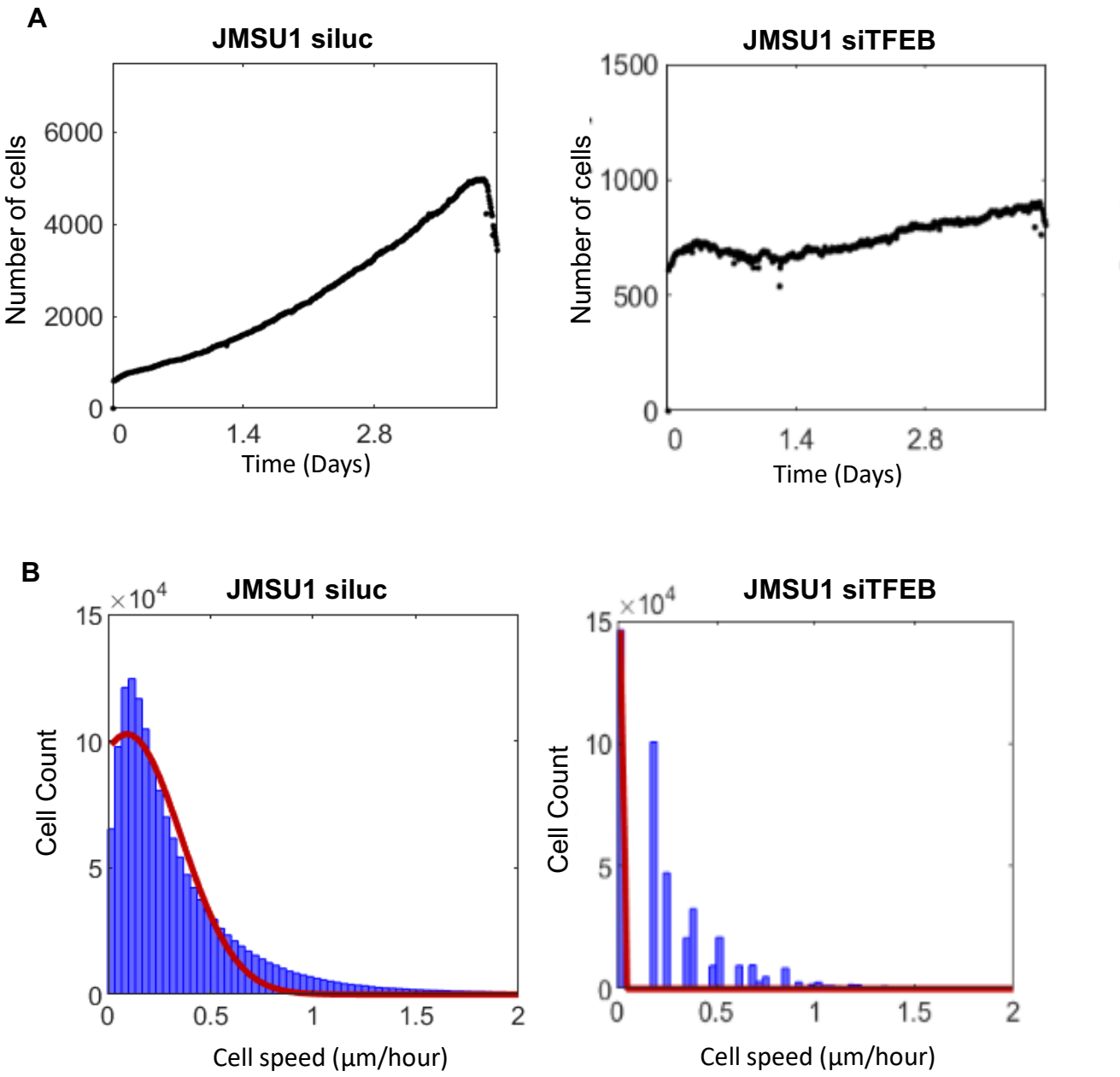

Fig 81. JMSU1 cell proliferation and migration after TFEB depletion

A. Proliferation of JMSU1 cells analysed as the increase in the number of cells in the treatment with siLuc or siTFEB over a course of 3 days.

B. Migration of JMSU1 cells analysed as the number of cells moving at a particular cell speed (µm/hour) in the treatment with siLuc or siTFEB. Area under the curve of the red line represents the distribution of the cell population as a function of their speed.

Results Aim 4 – Role of lysosome positioning in bladder cancer metabolism

4.11 Role of lysosome positioning in bladder cancer metabolism

Since TFEB is a well-established regulator of cellular metabolism (Mansueto et al., 2017) the question emerges if lysosome positioning impacts cancer cell metabolism. Altered cell metabolism is an important hallmark of cancer (Pavlova and Thompson, 2016). Cancer cells are known to use opportunistic ways of nutrient accumulation and depict an increased dependency on nutrients such as glucose, glutamine etc. for cell proliferation. Glutamine addiction has been observed in several cancers and has been established as an important cancer characteristic (Wise and Thompson, 2010). Glutamine serves not only as a nitrogen source for nucleotide synthesis, but also is used by cancer cells as a substrate for mitochondrial tricarboxylic acid (TCA) cycle (Pavlova and Thompson, 2016). Bladder cancers have shown dependency on glutamine under conditions of glucose depletion (Whyard et al., 2016). We thus first tested the rate of glutamine consumption in different cell lines (MGHU3, RT112, KU19-19 and JMSU1). We performed glutamine measurements in the media collected from equal number of cells growing for 24h in standard cell culture conditions and compared it to the cell culture media without the cells. Cell culture media contained about 200 mg/L (0.2g/L) of glutamine and the concentration of glutamine in the media collected from bladder cancer cells reduced gradually between non aggressive MGHU3 to aggressive JMSU1 cells (**Fig 82**). This showed that cells with more peripheral lysosomes, consumed more glutamine compared to whose with central lysosomes.

We next employed the Seahorse Mito Fuel Flex assay which measure the cellular fuel preference for mitochondrial respiration. This assay uses a combination of inhibitors to study the dependency and flexibility (in stress conditions when the consumption of alternative nutrient is blocked) of cells to oxidize the 3 basic substrates for mitochondrial oxidation, namely glucose (which is converted to pyruvate at the end of glycolysis and used for mitochondrial TCA cycle), glutamine and fatty acids (FA). We performed this assay with non-aggressive RT112 and aggressive JMSU1 cells and found that the reliance on glucose (or pyruvate) for mitochondrial respiration was similar between these (**Fig 83**). However, JMSU1 cells had more flexibility of consuming glutamine and FA in stress conditions compared to the RT112 cells (**Fig**

83). These results indicated that the JMSU1 cells were better adapted to upregulate mitochondrial respiration and energy production by switching to alternative fuels in stress conditions compared to RT112 cells. Cancer cells are known to drastically increase the uptake of glucose and to rely on glycolysis for energy production rather than the more energetic mitochondrial respiration pathway, an effect termed the Warburg effect (Warburg, 1956). We thus analyzed the cell energetic phenotype of all bladder cancer cells to understand the preferred energetic pathways employed using the Seahorse Cell Energy Phenotype assay. This assay calculates cellular glycolysis by monitoring the Extra Cellular Acidification Rate (ECAR), because glycolysis generates H^+ ions and leads to cellular and extracellular acidification. Mitochondrial respiration/oxidative phosphorylation is calculated in terms of Oxygen Consumption Rate (OCR). Our results indicated that aggressive KU19-19 and JMSU1cells exhibited a higher rate of glycolysis and oxidative phosphorylation than the non-aggressive RT112 and MGHU3 cells (**Fig 84A, B**). Additionally, the cell energetic phenotype showed that all four bladder cancer cell lines were capable of upregulating both glycolysis and mitochondrial respiration under stress conditions, although at a widely different scale (**Fig 84C**).

To better understand the role of lysosome positioning for cell metabolism we further monitored cellular pH in bladder cancer cells. Lysosomes change their positioning as a response to changes in the cytosolic pH and acidic conditions disperse the lysosomes to cell periphery in a rapid and reversible manner (Korolchuk et al., 2011) (Heuser, 1989b). Changes in cellular pH could be a downstream phenotype of cellular metabolism such as glycolysis, which decreases cytoplasmic pH by generation of H^+ ions. Thus, we asked whether peripheral positioning in bladder cancer cell lines is correlated with acidification of the cytoplasm. To test this, we incubated cells with the commercially available dye pHrodo-green, whose fluorescence intensity increases with decreasing pH. We found that cytoplasmic pH was indeed decreased in KU19-19 and JMSU1 as compared to MGHU3 and RT112. JMSU1 cells showing the lowest pH as observed by highest fluorescence of pHRodo-green (**Fig 85A, B**).

Next, we tested if the TFEB-dependent lysosomal scattering in JMSU1 cells could result from changes in cellular pH. To test this, we performed TFEB depletion in JMSU1 cells and monitored cell pH by incubating the cells with pHrodo-green in control (siLuc) and siTFEB conditions (**Fig 86A**). Quantification of pHrodo-green signals showed that TFEB knock down in JMSU1 cells increases the cell pH observed,

because pHrodo-green fluorescence intensity decreased in cells with TFEB depletion (**Fig 86B**).

Mammalian cells are surrounded by different kinds of nutrients such as glucose, amino acids and other micronutrients which need to be internalized via the endosomal pathway for cells to utilize metabolize them and meet their energy demands (Palm and Thompson, 2017). Because TFEB has been shown to regulate endocytic genes, one of the most prominent pathways of nutrient acquisition in mammalian cells, we monitored endocytosis in RT112 and JMSU1 cells. We performed the DQ BSA (Dye Quenched-Bovine Serum Albumin) uptake assay: DQ BSA is endocytosed and delivered to the lysosomes, where it is lysed by lysosomal proteases and allows to releases the quencher for fluorescence. We first compared the rate of DQ BSA uptake between RT112 and JMSU1 cells by incubating the cells with the dye at 37°C for different timepoints, 2h, 3h and 5h (**Fig 87A**). We observed that the JMSU1 cells had more uptake of DQ BSA, which increased over the timepoints. In RT112 cells, the uptake of DQ BSA was lower compared to JMSU1 cells and showed almost no change between the time points (**Fig 87B**). These results showed that JMSU1 cells performed more endocytosis of DQ BSA than RT112 cells. To check the role of TFEB in regulating DQ BSA uptake, and hence endocytosis of nutrients, we performed TFEB depletion in both RT112 and JMSU1 cells before incubation with DQ BSA at 37°C for 3h. We observed that while there was no difference in the DQ BSA signals between siLuc and siTFEB treatments (**Fig 88A, B**) in RT112 cells, there was a slight but significant decrease in DQ BSA signals after siTFEB in JMSU1 cells (**Fig 88C, D**). Together these results indicated that nuclear TFEB in JMSU1 cells increased endocytosis.

Conclusion: We found that aggressive KU19-19 and JMSU1 cells reveal an upregulation of both, glycolysis and oxidative phosphorylation, compared to less aggressive cells. Interestingly, lysosomal dispersion correlated with lower cytosolic pH in aggressive cells. However, TFEB depletion that reversed the lysosomal dispersion in high grade JMSU1 cells did not decrease intracellular pH, as expected, but showed the contrary phenotype of pH increase. This indicated that there is a more complex regulation between cellular pH, metabolism, TFEB and lysosomal positioning. Additionally, we found that endocytosis, the pathway of acquiring nutrients, was also upregulated in JMSU1 cells and was under regulation of TFEB. The connection

between TFEB activation and metabolic dysregulation in cancer requires further experimentation.

Fig 82

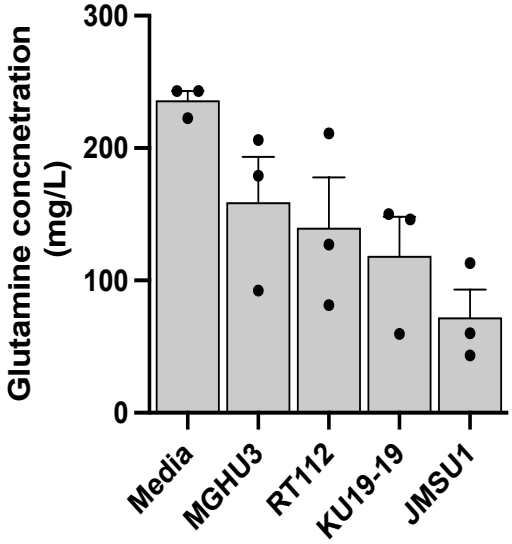

Fig 82. Glutamine utilization by bladder cancer cells
Measurement of glutamine concentration in the media taken from equal number of bladder cancer cells (MGHU3, RT112, KU19-19, JMSU1) growing at 37°C for 24h compared to the concentration of complete media control. Data is represented as mean and s.d of 3 independent experiments.

Fig 83

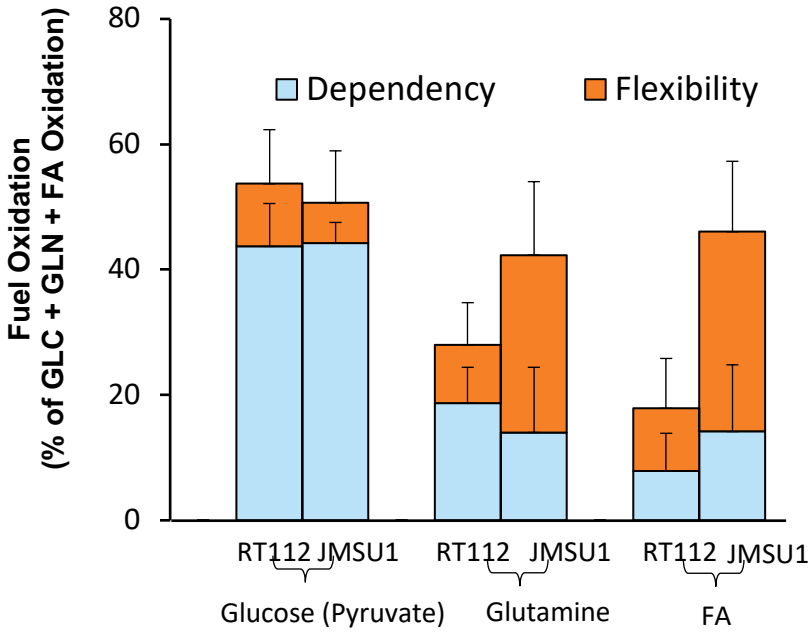

Fig 83. Seahorse Mito Fuel Flex assay in RT112 and JMSU1 cells
Analysis of percentage of dependency and percentage of flexibility of consumption of glucose, glutamine or Fatty acids (FA) for mitochondrial respiration in RT112 and JMSU1 cells. Data represented as mean and s.d of the cell population.

Fig 84

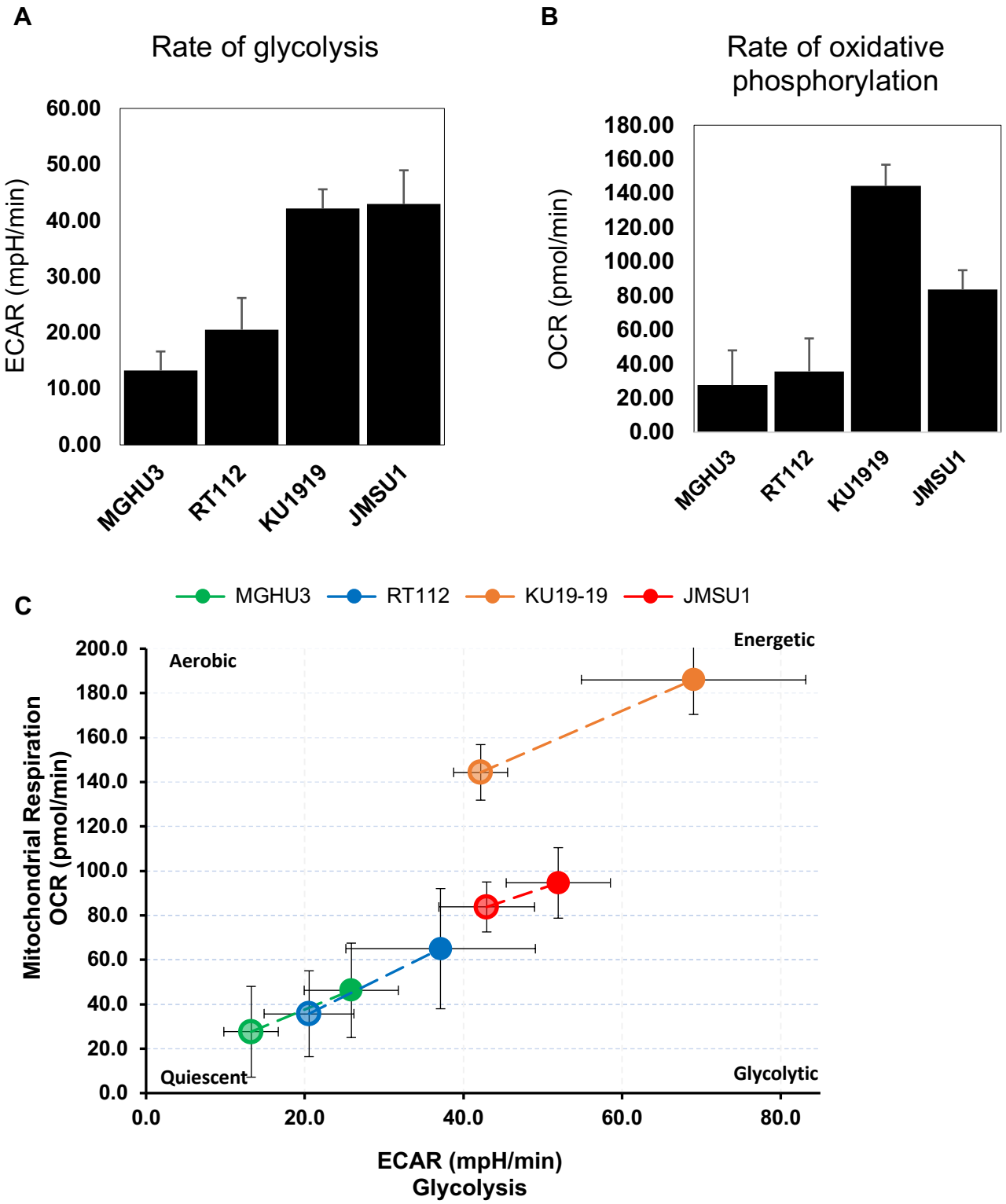

Fig 84. Seahorse Cell Phenotype assay in bladder cancer cells
A. Graph showing glycolysis in MGHU3, RT112, KU19-19, and JMSU1 cells measured as the extra cellular acidification rate (ECAR) (mpH/min). Data represented as mean and s.d. of the cell population **B.** Graph showing mitochondrial oxidative phosphorylation in MGHU3, RT112, KU19-19, and JMSU1 cells measured as the oxygen consumption rate (OCR) (pmol/min). Data represented as mean and s.d. of the cell population. **C**. Graph depicting the cell energy phenotype of MGHU3, RT112, KU19-19, and JMSU1 cells. For each cell lines, relative utilization of glycolysis and oxidative phosphorylation is represented at baseline condition (Lighter circle) and stressed condition (solid circle). Data is represented at the mean and s.d. of the cell population.

Fig 85

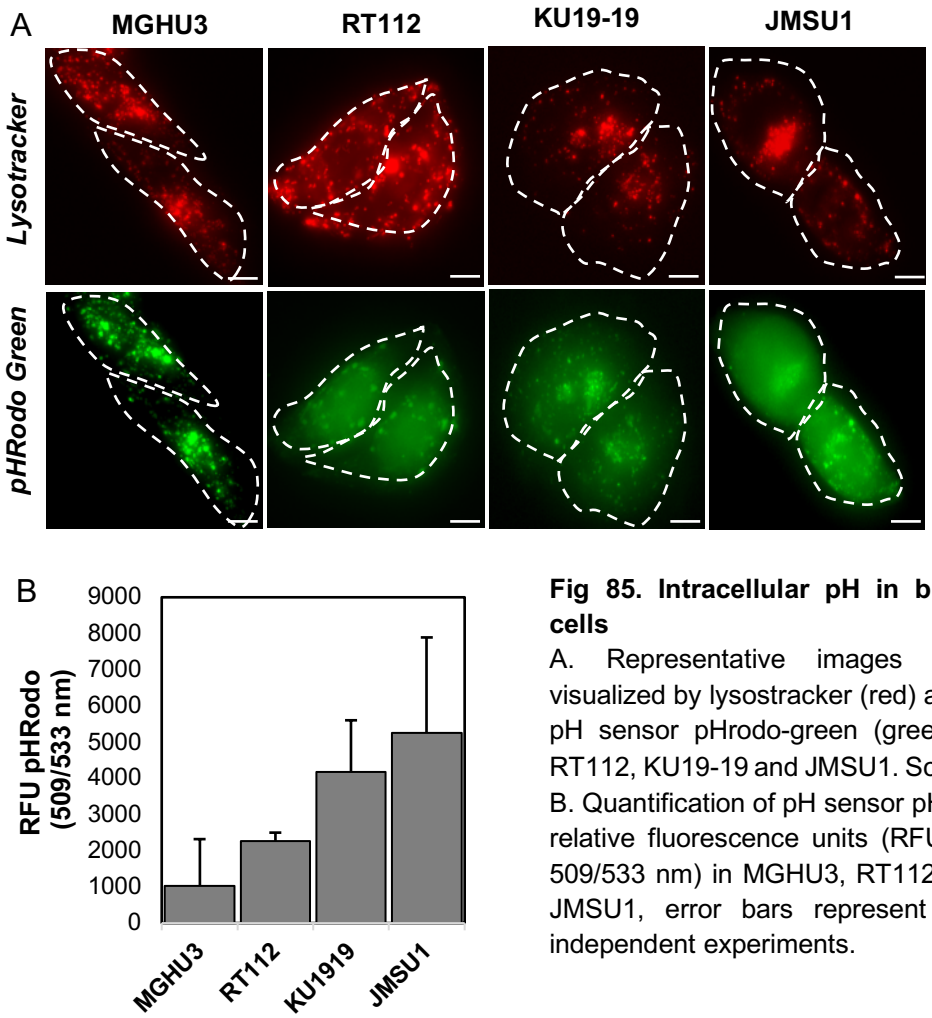

Fig 85. Intracellular pH in bladder cancer cells

A. Representative images of lysosomes visualized by lysostracker (red) and intracellular pH sensor pHrodo-green (green) in MGHU3, RT112, KU19-19 and JMSU1. Scale bar is 5 μm. B. Quantification of pH sensor pHrodo-green (in relative fluorescence units (RFU), emission at 509/533 nm) in MGHU3, RT112, KU19-19 and JMSU1, error bars represent s.d. of three independent experiments.

Fig 86

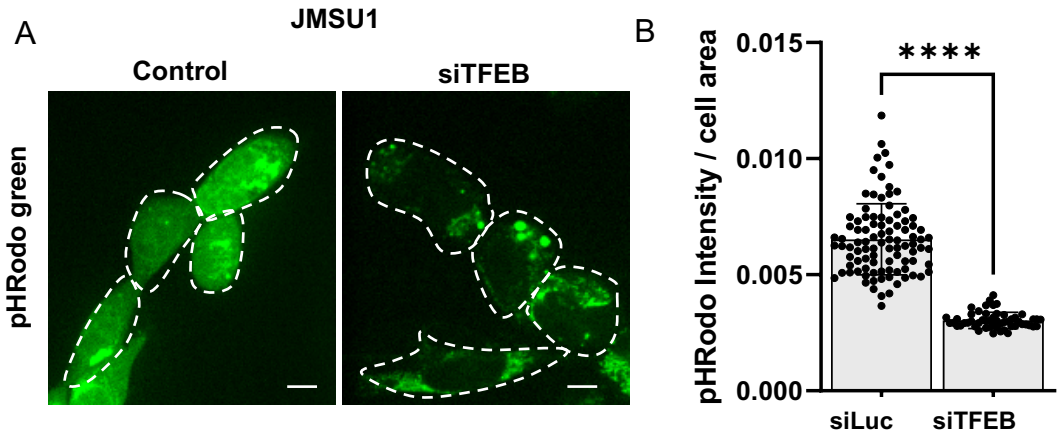

Fig 86. Intracellular pH in JMSU1 after siTFEB

A. Representative images of intracellular pH sensor pHrodo-green (green) in JMSU1 cells in control (siLuc) and siTFEB treatment conditions. Scale bar is 5 μm. B. Quantification of pH sensor pHrodo-green (a.u) normalized to cell area in JMSU1 in control (siLuc) and siTFEB treatment conditions. **** p value < 0.0001 in a Mann-Whitney U test, error bars are SEM.

Fig 87

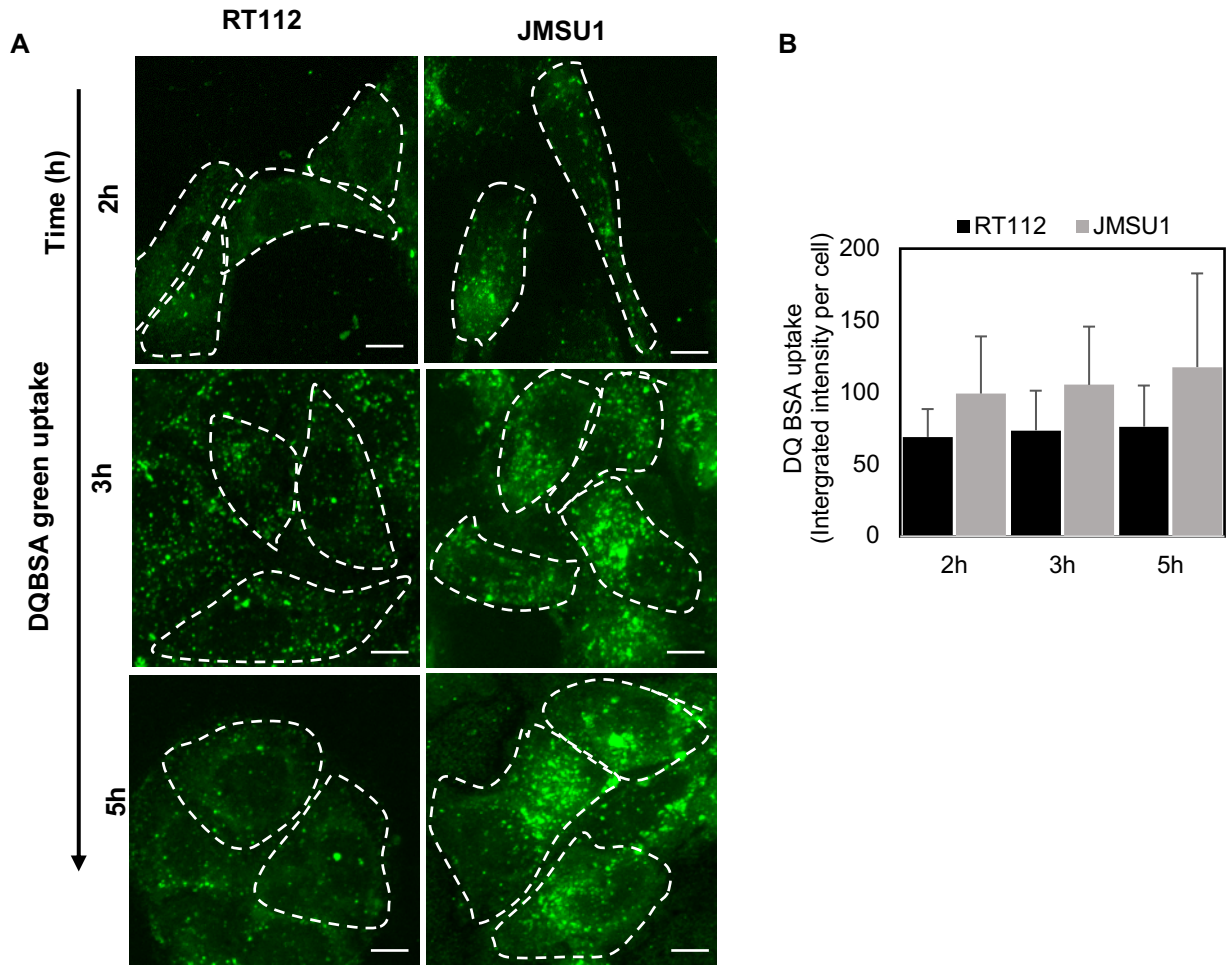

Fig 87. DQ BSA (Dye Quenched-Bovine Serum Albumin) uptake assay in RT112 and JMSU1
A. Representative image of DQBSA staining in RT112 and JMSU1 cells after 2h, 3h and 5h of DOBSA addition to the cells. Scale bar are 10µm. **B**. Quantification of the mean DQBSA intensity per cell in RT112 and JMSU1 after 2h, 3h and 5h of uptake. Error bars are the s.d.

Fig 88

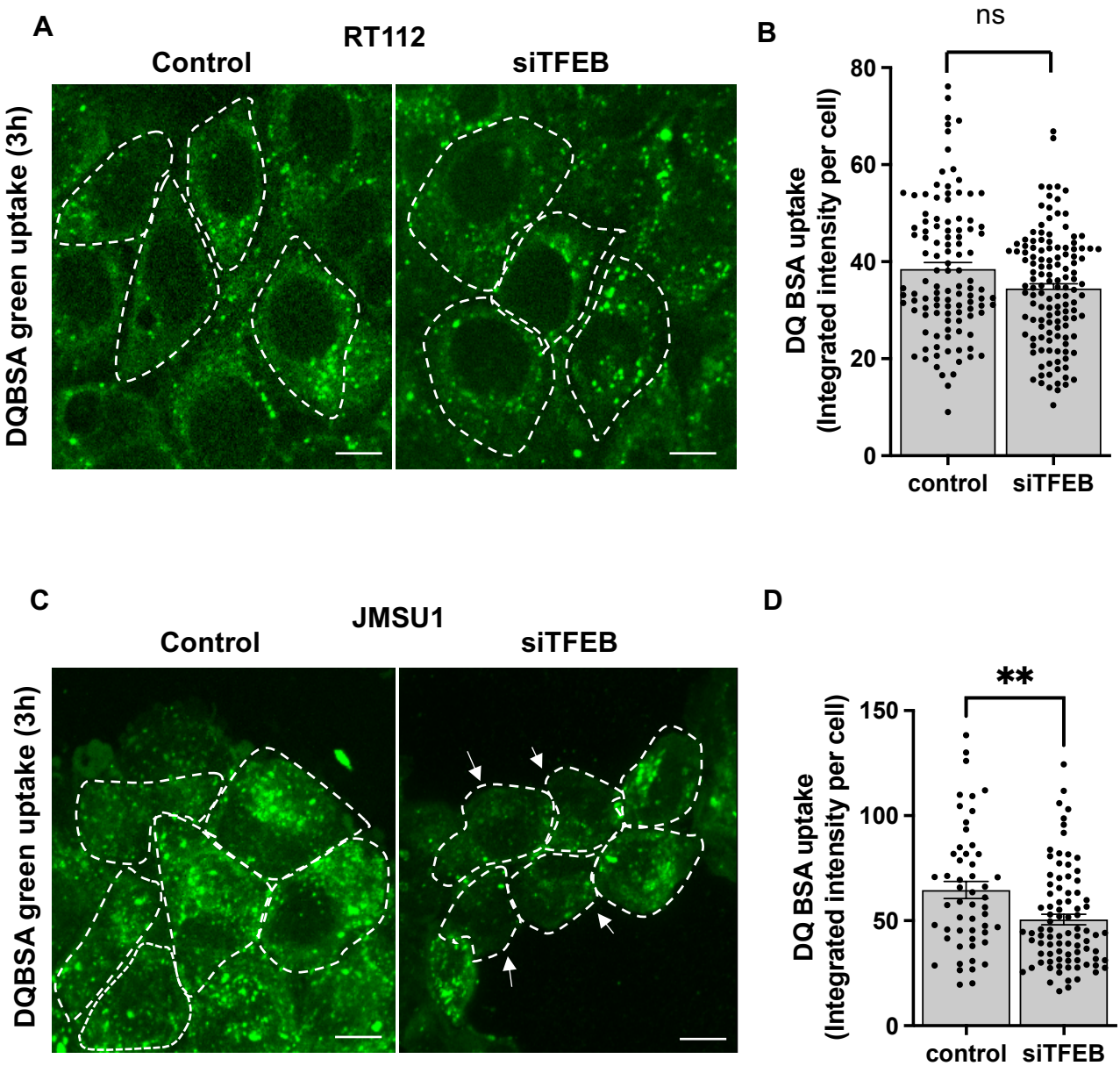

Fig 88. DQ BSA (Dye Quenched-Bovine Serum Albumin) uptake assay in RT112 and JMSU1 after siTFEB

A. Representative image of DQBSA staining in RT112 cells after 3h of DOBSA addition to the cells in control (siLuc) and siTFEB conditions (72h). Scale bar are 10µm. **B**. Quantification of the mean integrated DQBSA intensity per cell in RT112 in control (siLuc) and siTFEB treatment conditions. Ns p value> 0.05 in a a Mann-Whitney U test, error bars are SEM. **C.** Representative image of DQBSA staining in JMSU1 cells after 3h of DOBSA addition to the cells in control (siLuc) and siTFEB conditions (72h). Scale bar are 10µm. **D**. Quantification of the mean integrated DQBSA intensity per cell in JMSU1 in control (siLuc) and siTFEB treatment conditions. ** p value < 0.01 in a Mann-Whitney U test, error bars are SEM.

Chapter 5

Discussion and Perspectives

Discussion and perspectives:

Previous results in the lab have shown that lysosomes disperse towards the cell periphery in aggressive bladder cancer cell lines that represent high grade tumors, a phenotype that was not seen in normal human urothelium cells. The objective of this project was to study lysosomal functional changes that accompany the lysosomal dispersion, and the mechanism that sustain this phenotype.

5.1 Impact of lysosome dispersion on mTORC1 signaling

mTORC1 signaling takes place at the surface of lysosomes, and mTORC1 has been shown to assemble on peripheral lysosomes in response to cellular nutrients (Hong et al., 2017; Korolchuk et al., 2011). Thus, we first studied whether intrinsic lysosomal dispersion in aggressive cancer cell lines could activate mTORC1. We found that mTORC1 was localized on lysosomes in all cell lines analyzed, non-aggressive (MGHU3, RT112) and aggressive (KU19-19 and JMSU1) cells. Additionally, we revealed that both classical substrate of mTORC1, namely p70-S6K1 and 4EBP1, were phosphorylated, indicating that mTORC1 was active in all bladder cancer cell lines. We confirmed the specificity of these substrates by using mTORC1 inhibitors such as rapamycin, torin and starvation, which abolished the phosphorylation of these substrates. Interestingly, we observe a differential substrate specificity between cell lines. Whereas non-aggressive cell lines MGHU3 and RT112 showed high phosphorylation of p70-S6K1, aggressive cell lines, KU19-19 and JMSU1 showed higher phosphorylation of 4EBP1. It should be noted, that the total levels of 4EBP1 were increased in aggressive cell lines. We also studies TFEB, which is a substrate of mTORC1 kinase and whose phosphorylation leads to its cytosolic retention and thus inactivation. We found that while TFEB was mostly cytosolic and inactive in non-aggressive cell lines, TFEB was translocated to nucleus despite an active mTORC1 in aggressive cell lines. Altogether, our results did not show an increase in mTORC1 activity correlating with more peripheral lysosomes. The differential mTORC1 substrate phosphorylation that we observed was however quite interesting. 4EBP1 overexpression was shown to be associated with an unfavourable prognosis in a meta-analysis of different cancers (Zhang et al., 2017). 4EBP1 is a

negative regulator of protein translation, and an overexpression of this protein in cancers should decrease translation. However, an active mTORC1 inactivates it, and thus induces protein translation. Since 4EBP1 has been reported to show a higher affinity towards mTORC1 (Choo and Blenis, 2009), we tested whether decreasing 4EBP1 levels by siRNA could increase the phosphorylation of other substrates, such as TFEB or p70-S6K1. This was not the case in JMSU1 cells, where depletion of 4EBP1 did not change the nuclear localization of TFEB. Thus, overexpression of 4EBP1 seems not to be a strategy of bladder cancers to leave other substrate such as TFEB less phosphorylated. Although the exact function of 4EBP1 overexpression in cancers remains unknown, some studies have shown that overexpression of 4EBP1 correlated with increased infiltration of cancer associated fibroblasts (CAFs), including bladder cancers, and resulted in poor prognosis (Du et al., 2022). In breast cancers, knock down of 4EBP1 in overexpressing cancer cells was shown to result in significantly decreased proliferation, and thus, pointed to the role of 4EBP1 in cell proliferation distinct from its role as a regulator of translation (Rutkovsky et al., 2019).

It has been shown that peripheral movement of lysosomes in the presence of nutrients was required for mTORC1 activation, possible through the close proximity to growth factor receptors that are localized on the plasma membrane (Hong et al., 2017). We thus studied whether lysosome positioning alone was sufficient to regulate mTORC1 signaling in different bladder cancer cell lines. In the non-aggressive cell line RT112, we found that central clustering of lysosomes via enforced recruitment of dynein or through depletion of Arl8b, which recruits kinesin-1 for lysosomal dispersion, leads to loss of mTORC1 from lysosomes and attenuation of mTORC1 substrate phosphorylation (S6K and 4EBP1). Indeed, displacement of lysosomes to the cell center often correlates with mTORC1 dissociation from lysosomes in nutrient deficient or starvation conditions (Korolchuk et al., 2011; Perera and Zoncu, 2016). However, we performed the experiments in complete nutrient conditions, and thus, our results indicated that lysosome positioning can regulate mTORC1 signaling independent of nutrient status in RT112 cells. Contrary, we found that mTORC1 signaling is specifically decoupled from lysosome positioning in aggressive JMSU1 cells. Interestingly, we did not observe a loss of mTORC1 from clustered lysosomes in these cells. Because nutrient status and lysosome positioning are often tightly linked (Korolchuk et al., 2011), the loss of the spatial compartmentalization of mTORC1 signaling may help cancer cells to evade metabolic checks on anabolism and

proliferation. Future studies are required to elucidate the mechanisms by which mTORC1 is retained on central lysosomes in the aggressive bladder cancer cell line JMSU1.

We next studied the mTORC1-dependent regulation of TFEB. We found that inactivating mTORC1 with rapamycin induced nuclear translocation of TFEB in the bladder cancer cell lines MGHU3 and RT112. Additionally, starvation that also inactivates mTORC1 induced nuclear TFEB in RT112 cells. Some studies have reported TFEB as a rapamycin insensitive substrate (Roczniak-Ferguson et al., 2012; Settembre et al., 2011), however other studies have observed nuclear TFEB translocation upon rapamycin treatment (Martina et al., 2012; Peña-Llopis et al., 2011). From our results, we concluded that in MGHU3 and RT112 cells TFEB was regulated by mTORC1. Interestingly, we found that in the aggressive cell lines, KU19-19 and JMSU1, TFEB was translocated to nucleus although mTORC1 was active, suggesting that the mTORC1-dependent TFEB regulation was non-functional or non-important. Deregulation of mTORC1 signaling and MiT/TFE family hyper-activation parallels previous studies in other cancer types (Bar-Peled et al., 2013; Di Malta et al., 2017; Haq and Fisher, 2011; Kauffman et al., 2014; Perera et al., 2015b). Nuclear translocation of TFEB with an active mTORC1 indicated a TFEB hyperactivity in these aggressive bladder cancer cell lines, which has not yet been reported for bladder cancer. Additionally, these results also point towards a possible role of other MiT/TFE family transcription factors (such as MITF) in bladder cancer progression that remains to be tested. Gene set enrichment analysis (GSEA) on the expression of CLEAR network genes (regulated by TFEB) correlated with aggressiveness of bladder cancer cell lines supporting TFEB hyperactivity in these cells.

We found that inhibition of lysosomal calcium channel, TRPML1, resulted in cytosolic retention of TFEB. Since Ca^{+2} release from the lysosomes through TRPML1 has been shown to activate the TFEB dephosphorylating phosphatase calcineurin (Medina et al., 2015), the observed increased TFEB nuclear translocation could be a result of its increased dephosphorylation by calcineurin. A previous study has reported that, upon starvation, nuclear translocation and activation of TFEB induced mTORC1 reactivation. This was achieved by TFEB directly regulating the expression of RRAGD (gene that codes for protein RagD) that is important for mTORC1 recruitment to lysosomes, and thus, subsequent activation (Di Malta et al., 2017). We found an increase in the expression of RRAGD (mRNA levels) in KU19-19 and JMSU1 cells

and thus tested whether nuclear TFEB could sustain mTORC1 recruitment and signaling through RagD in these cells. We observed that depletion of TFEB in JMSU1 cells reduced mTORC1 localization on lysosomes showing that nuclear TFEB regulated mTORC1 recruitment. However, we did not see a major decrease in the phosphorylation of mTORC1 substrates S6K and 4EBP1, although a slight decrease of S6K phosphorylation could be observed. One possible explanation of this could be that, although both these substrates are mTORC1 specific (also confirmed by us before), alternative mechanism of phosphorylating may exist. For instance, it has been reported that in bladder cancers 4EBP1 can be phosphorylated indirectly through PI3K, bypassing mTORC1 (Nawroth et al., 2011).

5.2 Mechanism that sustain lysosome dispersion observed in aggressive bladder cancer cell lines

Reports that TFEB regulated lysosome positioning (Medina et al., 2011; Willett et al., 2017) and the fact that peripheral lysosomes correlated with a hyperactivate, nuclear TFEB phenotype, led us to investigate if TFEB regulated lysosome positioning in bladder cancer cells. We found that knockdown of TFEB in JMSU1 cells that showed nuclear TFEB, induced perinuclear clustering of lysosomes. Investigating the molecular mechanisms by which TFEB controls lysosome positioning, we discovered that TFEB transcriptionally regulates phosphatidylinositol-3-phosphate (PI3P) levels by regulating the expression of the class III PI3 kinase PIK3C3 / VPS34 in JMSU1 cells. Increased levels of PI3P on endosomes lead to enhanced recruitment of FYVE-containing proteins such as EEA1 or protrudin. Interestingly, protrudin is known to bind to PI3P at lysosome-ER membrane contact sites and to recruit kinesin-1 to lysosomes through the motor adaptor FYCO1. FYCO1-kinesin-1 have been shown to promote the microtubule-dependent translocation of lysosomes to the cell periphery (Raiborg et al., 2015).

In line with these results, we also observed that induction of nuclear TFEB by rapamycin or starvation in RT112 cells promoted lysosomal dispersion. These conditions also increased the recruitment of FYVE domain proteins such as EEA1 and protrudin to lysosomes indicative of an increase of PI3P in these cells upon TFEB activation. Interestingly, rapamycin treatment in the absence of TFEB (upon siRNA-

mediated depletion) did not reduce binding of protrudin to lysosomes, whereas binding of EEA1 was decreased. This suggested that rapamycin could regulate recruitment of protrudin to lysosomes independent of TFEB. One possible explanation could be as follows: VPS34, which produces PI3P, can exist in different complexes depending on the function in the cells. On late endosomes/ lysosomes, PI3P can be produced by VPS34 in a complex with VPS34/ VPS15/ Beclin 1/ UVRAG/ BIF-1 that is required for binding of protrudin (Hong et al., 2017; Thoresen et al., 2010). However, during the formation of autophagy vesicles, VPS34 exists in a complex with VPS34/ VPS15/ Beclin 1/ ATG14 (Itakura et al., 2008). Interestingly, rapamycin has been shown to activate the lysosomal calcium channel TRMPL1 (Zhang et al., 2019), and activation of TRMPL1 has been shown generates PI3P for autophagy vesicles formation through the VPS34/ VPS15/ Beclin 1/ ATG14 complex. Thus, our results that rapamycin treatment maintains protrudin on lysosomes even in absence of TFEB could be explained by the possibility of overlapping functions of the different VPS34 complexes. Indeed, VPS34/ VPS15/ Beclin 1/ ATG14 could be involved in the formation of PI3P on lysosomes upon TRPML1 activation by rapamycin, independent of TFEB. This interesting hypothesis however remains to be tested. However, our results indicate that EEA1 is more membrane bound upon TFEB nuclear translocation in RT112 cells, and specifically dependent on TFEB, because siRNA-dependent depletion significantly inhibits recruitment. This suggests differences between the recruitment of FYVE domain containing proteins that need to be further investigated.

Several pathways for anterograde lysosome trafficking have been described that all require endosomal PI3P, and could be exploited by cancer cells. The alternative kinesin-1 adaptor SKIP (also known as PLEKHM2) also contains three lipid-binding pleckstrin homology (PH) domains that conceivably could bind to lysosomal PI3P. Moreover, KIF16B, a highly processive kinesin-3 family member that participates in the trafficking of endosomes along microtubules contains a PX (Phox homology) motif binding PI3P (Pyrpassopoulos et al., 2017).

In addition to anterograde transport, it has been shown that endosomal PI3P levels regulate mTORC1 recruitment and signaling. For instance, this can be achieved via stimulation of class III PI3K/Vps34-mediated PI3P synthesis by amino acids (Gulati and Thomas, 2007). Moreover, PI3P facilitates lysosomal recruitment of phospholipase D1 (PLD1) via its PX domain that produces phosphatidic acid, which triggers dissociation of the inhibitory DEPTOR subunit from mTORC1 (Song and

Yoon, 2016). Additionally, the PI3P-phosphatase MTMR3 interacts with mTORC1, and overexpression of this enzyme inhibits mTORC1 activity (Hao et al., 2016). Finally, the formation of phosphatidylinositol-3,5-bisphosphate ($PI3,5P_2$) from PI3P regulates mTORC1 via raptor (Bridges et al., 2012). As increased endosomal PI3P levels globally activate mTORC1 that deactivates TFEB, we speculate that PI3P could be part of a feedback loop in the mTORC1/TFEB signaling axis.

5.3 Role of peripheral lysosomes in cancer supporting phenotypes

We finally started to test the role of peripheral lysosomes in cancer supporting phenotypes. Our results revealed a correlation between lysosomal dispersion, the secretion of matrix metalloproteinases and lysosomal exocytosis. Lysosomal exocytosis has been the most explored function of peripheral lysosomes (Machado et al., 2021) with an established role of TFEB. Studying lysosomal exocytosis via VAMP7-pHluorin dynamics at the plasma membrane in TIRF microscopy revealed that increased lysosomal exocytosis correlated with TFEB nuclear translocation/ activation in bladder cancer cell lines. TFEB overexpression has been shown to induce expression of lysosomal calcium channel TRPML1, to increase intracellular calcium and the docking of lysosomes to the plasma membrane in order to facilitate cell clearance. Activation of this pathway was exploited in lysosomal storage disorders such as multiple sulfatase deficiency (MSD) and reduced pathological signatures of this diseases (Medina et al., 2011). Our results indicate that this pathway could be active in JMSU1 cells, in which we observed an increased activity of TRPML1, required for TFEB nuclear translocation and activation. Indeed, TFEB-regulated lysosomal exocytosis could be possible through a feedback regulation on the expression of TRPML1 on lysosomes that could increase their docking to plasma membrane. Additionally, we observed that TFEB regulates cell migration in JMSU1 cells. A recent report showed that TFEB driven transcriptional regulation of Rab5a induces the endocytosis of α5β1 integrins and the disassembly of focal adhesions to promote migration and metastasis in pancreatic cancer (He et al., 2019). Pancreatic cancers have characteristic hyperactivation if MiT/TFE transcription factors, which regulate metabolism and drive cancer progression (Perera et al., 2015b). These results propose to study integrin trafficking in JMSU1 cells that show nuclear

translocation in TFEB and TFEB dependent migration. However, the exact mechanism of migration regulation by TFEB remained to be studied.

Metabolic imbalance and opportunistic acquisition of nutrients is a hallmark of cancers (Pavlova and Thompson, 2016; Pavlova et al., 2022). We found some evidences that hyperactivation of TFEB correlates with differential cellular metabolism. Firstly, we found that aggressive JMSU1 cells perform higher rate of endocytosis as compared to less aggressive RT112 cells. Moreover, we evidenced that TFEB regulated endocytosis in JMSU1 cells, as seen from decreased DQ BSA uptake upon TFEB depletion. TFEB has been shown to regulate expression of several endocytic proteins (such as EEA1, clathrin, Rab5) and to induce endocytic vesicles which assemble mTORC1-regulating machinery on lysosomes. This increase in endocytosis leads to a reactivation of mTORC1 after starvation (Nnah et al., 2019). This is an alternative mechanism for mTORC1 activation by nuclear TFEB in aggressive JMSU1 cells (in addition to the once discussed previously). Indeed, an increase in endocytosis would also help cancer cells to acquire nutrients to drive pathways of cellular energetics. Secondly, we find that lysosomal dispersion and TFEB nuclear translocation in aggressive bladder cancer cell lines correlates with increased glutamine uptake. A role of TFEB in glutamine metabolism by regulating the expression of Glutaminase (GLS) has been shown in pancreatic cancers (Kim et al., 2021), and could thus be an interesting topic to be further studied. Thirdly, cell metabolism is an important contributor to changes in cellular pH and acidity of tumors (Schornack and Gillies, 2003). We observes a decrease in intracellular pH in aggressive cancer cell lines KU19-19 and JMSU1. Interestingly, TFEB depletion leads to increase in cell pH correlating with lysosome clustering upon TFEB depletion. We thus take this as another indicator to the involvement of TFEB in regulating cellular pH that could possible underly lysosomal dispersion.

Lastly, in our bladder cancer model, we found an increase in the utilization of both glycolysis and oxidative phosphorylation in aggressive cancer cells (KU19-19 and JMSU1) that correlated lysosomal dispersion and TFEB hyperactivation. TFEB has been shown to regulate metabolic flexibility in skeletal muscles and is known to control expression of genes involved in glycolysis, mitochondrial respiration and mitochondrial biogenesis (Mansueto et al., 2017). Lysosome positioning has also been shown to regulate mitochondrial dynamics by marking the sited of mitochondrial fission via Rab7 GTPase (Wong et al., 2018). It is thus tempting to hypothesize that hyperactivation of

TFEB and lysosomal dispersion underly differences in energetic pathways of bladder cancer cells through transcriptional regulation of metabolic genes and the formation of differential membrane contact sites. These observations open several questions and prospects that can be explored in future to integrate altered lysosome positioning, TFEB hyperactivation and cancer metabolism in bladder cancers.

References

References

Adib, E., Klonowska, K., Giannikou, K., Do, K.T., Pruitt-Thompson, S., Bhushan, K., Milstein, M.I., Hedglin, J., Kargus, K.E., Sholl, L.M., et al. (2021). Phase II Clinical Trial of Everolimus in a Pan-Cancer Cohort of Patients with mTOR Pathway Alterations. Clin. Cancer Res. *27*, 3845–3853. https://doi.org/10.1158/1078-0432.CCR-20-4548.

Ahmad, I., Sansom, O.J., and Leung, H.Y. (2012). Exploring molecular genetics of bladder cancer: lessons learned from mouse models. Dis. Model. Mech. dmm.008888. https://doi.org/10.1242/dmm.008888.

Akkari, L., Gocheva, V., Kester, J.C., Hunter, K.E., Quick, M.L., Sevenich, L., Wang, H.-W., Peters, C., Tang, L.H., Klimstra, D.S., et al. (2014). Distinct functions of macrophage-derived and cancer cell-derived cathepsin Z combine to promote tumor malignancy via interactions with the extracellular matrix. Genes Dev. *28*, 2134–2150. https://doi.org/10.1101/gad.249599.114.

Allier, C., Morel, S., Vincent, R., Ghenim, L., Navarro, F., Menneteau, M., Bordy, T., Hervé, L., Cioni, O., Gidrol, X., et al. (2017). Imaging of dense cell cultures by multiwavelength lens-free video microscopy: Cell Cultures by Lens-Free Microscopy. Cytometry A *91*, 433–442. https://doi.org/10.1002/cyto.a.23079.

Antoni, S., Ferlay, J., Soerjomataram, I., Znaor, A., Jemal, A., and Bray, F. (2017). Bladder Cancer Incidence and Mortality: A Global Overview and Recent Trends. Eur. Urol. *71*, 96–108. https://doi.org/10.1016/j.eururo.2016.06.010.

Argani, P., Antonescu, C.R., Illei, P.B., Lui, M.Y., Timmons, C.F., Newbury, R., Reuter, V.E., Garvin, A.J., Perez-Atayde, A.R., Fletcher, J.A., et al. (2001). Primary Renal Neoplasms with the ASPL-TFE3 Gene Fusion of Alveolar Soft Part Sarcoma. Am. J. Pathol. *159*, 179–192. https://doi.org/10.1016/S0002-9440(10)61684-7.

Bagshaw, R.D., Callahan, J.W., and Mahuran, D.J. (2006). The Arf-family protein, Arl8b, is involved in the spatial distribution of lysosomes. Biochem. Biophys. Res. Commun. *344*, 1186–1191. https://doi.org/10.1016/j.bbrc.2006.03.221.

Bakker, J., Spits, M., Neefjes, J., and Berlin, I. (2017). The EGFR odyssey – from activation to destruction in space and time. J. Cell Sci. jcs.209197. https://doi.org/10.1242/jcs.209197.

Balla, T. (2013). Phosphoinositides: Tiny Lipids With Giant Impact on Cell Regulation. Physiol. Rev. *93*, 1019–1137. https://doi.org/10.1152/physrev.00028.2012.

Ballabio, A., and Bonifacino, J.S. (2020). Lysosomes as dynamic regulators of cell and organismal homeostasis. Nat. Rev. Mol. Cell Biol. *21*, 101–118. https://doi.org/10.1038/s41580-019-0185-4.

Baron, R., Neff, L., Brown, W., Courtoy, P.J., Louvard, D., and Farquhar, M.G. (1988). Polarized secretion of lysosomal enzymes: co-distribution of cation-independent mannose-6-phosphate receptors and lysosomal enzymes along the osteoclast exocytic pathway. J. Cell Biol. *106*, 1863–1872. https://doi.org/10.1083/jcb.106.6.1863.

Bar-Peled, L., Chantranupong, L., Cherniack, A.D., Chen, W.W., Ottina, K.A., Grabiner, B.C., Spear, E.D., Carter, S.L., Meyerson, M., and Sabatini, D.M. (2013). A Tumor Suppressor Complex with GAP Activity for the Rag GTPases That Signal Amino Acid Sufficiency to mTORC1. Science *340*, 1100–1106. https://doi.org/10.1126/science.1232044.

Bartolomeo, R., Cinque, L., De Leonibus, C., Forrester, A., Salzano, A.C., Monfregola, J., De Gennaro, E., Nusco, E., Azario, I., Lanzara, C., et al. (2017). mTORC1 hyperactivation arrests bone growth in lysosomal storage disorders by suppressing autophagy. J. Clin. Invest. *127*, 3717–3729. https://doi.org/10.1172/JCI94130.

Bassi, M.T., Manzoni, M., Monti, E., Pizzo, M.T., Ballabio, A., and Borsani, G. (2000). Cloning of the Gene Encoding a Novel Integral Membrane Protein, Mucolipidin—and Identification of the Two Major Founder Mutations Causing Mucolipidosis Type IV. Am. J. Hum. Genet. *67*, 1110–1120. https://doi.org/10.1016/S0002-9297(07)62941-3.

Bechtel, W., Helmstädter, M., Balica, J., Hartleben, B., Schell, C., and Huber, T.B. (2013). The class III phosphatidylinositol 3-kinase PIK3C3/VPS34 regulates endocytosis and autophagosome-autolysosome formation in podocytes. Autophagy *9*, 1097–1099. https://doi.org/10.4161/auto.24634.

Bellmunt, J., de Wit, R., Vaughn, D.J., Fradet, Y., Lee, J.-L., Fong, L., Vogelzang, N.J., Climent, M.A., Petrylak, D.P., Choueiri, T.K., et al. (2017). Pembrolizumab as Second-Line Therapy for Advanced Urothelial Carcinoma. N. Engl. J. Med. *376*, 1015–1026. https://doi.org/10.1056/NEJMoa1613683.

Ben-Sahra, I., Hoxhaj, G., Ricoult, S.J.H., Asara, J.M., and Manning, B.D. (2016). mTORC1 induces purine synthesis through control of the mitochondrial tetrahydrofolate cycle. Science *351*, 728–733. https://doi.org/10.1126/science.aad0489.

Berdik, C. (2017). Unlocking bladder cancer. Nature *551*, S34–S35. https://doi.org/10.1038/551S34a.

van Bergeijk, P., Adrian, M., Hoogenraad, C.C., and Kapitein, L.C. (2015). Optogenetic control of organelle transport and positioning. Nature *518*, 111–114. https://doi.org/10.1038/nature14128.

Böhm, M., Kirch, H., Otto, T., Rübben, H., and Wieland, I. (1997). Deletion analysis at the DEL-27, APC and MTS1 loci in bladder cancer: LOH at the DEL-27 locus on 5p13-12 is a prognostic marker of tumor progression. Int. J. Cancer *74*, 291–295. https://doi.org/10.1002/(sici)1097-0215(19970620)74:3<291::aid-ijc10>3.0.co;2-f.

Bonifacino, J.S., and Neefjes, J. (2017). Moving and positioning the endolysosomal system. Curr. Opin. Cell Biol. *47*, 1–8. https://doi.org/10.1016/j.ceb.2017.01.008.

Bretou, M., Sáez, P.J., Sanséau, D., Maurin, M., Lankar, D., Chabaud, M., Spampanato, C., Malbec, O., Barbier, L., Muallem, S., et al. (2017). Lysosome signaling controls the migration of dendritic cells. Sci. Immunol. *2*, eaak9573. https://doi.org/10.1126/sciimmunol.aak9573.

Bridges, D., Ma, J.-T., Park, S., Inoki, K., Weisman, L.S., and Saltiel, A.R. (2012). Phosphatidylinositol 3,5-bisphosphate plays a role in the activation and subcellular localization of mechanistic target of rapamycin 1. Mol. Biol. Cell *23*, 2955–2962. https://doi.org/10.1091/mbc.e11-12-1034.

Brown, C.L., Maier, K.C., Stauber, T., Ginkel, L.M., Wordeman, L., Vernos, I., and Schroer, T.A. (2005). Kinesin-2 is a Motor for Late Endosomes and Lysosomes: Kinesin-2 is a Late Endosome Motor. Traffic *6*, 1114–1124. https://doi.org/10.1111/j.1600-0854.2005.00347.x.

Burkhardt, J.K., Echeverri, C.J., Nilsson, T., and Vallee, R.B. (1997). Overexpression of the Dynamitin (p50) Subunit of the Dynactin Complex Disrupts Dynein-dependent Maintenance of Membrane Organelle Distribution. J. Cell Biol. *139*, 469–484. https://doi.org/10.1083/jcb.139.2.469.

Buscà, R., Berra, E., Gaggioli, C., Khaled, M., Bille, K., Marchetti, B., Thyss, R., Fitsialos, G., Larribère, L., Bertolotto, C., et al. (2005). Hypoxia-inducible factor 1α is a new target of microphthalmia-associated transcription factor (MITF) in melanoma cells. J. Cell Biol. *170*, 49–59. https://doi.org/10.1083/jcb.200501067.

Cabukusta, B., and Neefjes, J. (2018). Mechanisms of lysosomal positioning and movement. Traffic *19*, 761–769. https://doi.org/10.1111/tra.12587.

Cardoso, C.M.P., Groth-Pedersen, L., Høyer-Hansen, M., Kirkegaard, T., Corcelle, E., Andersen, J.S., Jäättelä, M., and Nylandsted, J. (2009). Depletion of Kinesin 5B Affects Lysosomal Distribution and Stability and Induces Peri-Nuclear Accumulation of Autophagosomes in Cancer Cells. PLoS ONE *4*, e4424. https://doi.org/10.1371/journal.pone.0004424.

Castellano, B.M., Thelen, A.M., Moldavski, O., Feltes, M., van der Welle, R.E.N., Mydock-McGrane, L., Jiang, X., van Eijkeren, R.J., Davis, O.B., Louie, S.M., et al. (2017). Lysosomal cholesterol activates mTORC1 via an SLC38A9–Niemann-Pick C1 signaling complex. Science *355*, 1306–1311. https://doi.org/10.1126/science.aag1417.

Chen, Y., and Yu, L. (2013). Autophagic lysosome reformation. Exp. Cell Res. *319*, 142–146. https://doi.org/10.1016/j.yexcr.2012.09.004.

Ching, C.B., and Hansel, D.E. (2010). Expanding therapeutic targets in bladder cancer: the PI3K/Akt/mTOR pathway. Lab. Invest. *90*, 1406–1414. https://doi.org/10.1038/labinvest.2010.133.

Choo, A.Y., and Blenis, J. (2009). Not all substrates are treated equally: Implications for mTOR, rapamycin-resistance, and cancer therapy. Cell Cycle *8*, 567–572. https://doi.org/10.4161/cc.8.4.7659.

Choo, A.Y., Yoon, S.-O., Kim, S.G., Roux, P.P., and Blenis, J. (2008). Rapamycin differentially inhibits S6Ks and 4E-BP1 to mediate cell-type-specific repression of mRNA translation. Proc. Natl. Acad. Sci. U. S. A. *105*, 17414–17419. https://doi.org/10.1073/pnas.0809136105.

Chow, A., Toomre, D., Garrett, W., and Mellman, I. (2002). Dendritic cell maturation triggers retrograde MHC class II transport from lysosomes to the plasma membrane. Nature *418*, 988–994. https://doi.org/10.1038/nature01006.

Clark, P.E., Agarwal, N., Biagioli, M.C., Eisenberger, M.A., Greenberg, R.E., Herr, H.W., Inman, B.A., Kuban, D.A., Kuzel, T.M., Lele, S.M., et al. (2013). Bladder Cancer. J. Natl. Compr. Canc. Netw. *11*, 446–475. https://doi.org/10.6004/jnccn.2013.0059.

Commisso, C., Davidson, S.M., Soydaner-Azeloglu, R.G., Parker, S.J., Kamphorst, J.J., Hackett, S., Grabocka, E., Nofal, M., Drebin, J.A., Thompson, C.B., et al. (2013). Macropinocytosis of protein is an amino acid supply route in Ras-transformed cells. Nature *497*, 633–637. https://doi.org/10.1038/nature12138.

Cordonnier, M.-N., Dauzonne, D., Louvard, D., and Coudrier, E. (2001). Actin Filaments and Myosin I Alpha Cooperate with Microtubules for the Movement of Lysosomes. Mol. Biol. Cell *12*, 4013–4029. https://doi.org/10.1091/mbc.12.12.4013.

Dahia, P.L. (2000). PTEN, a unique tumor suppressor gene. Endocr. Relat. Cancer 115–129. https://doi.org/10.1677/erc.0.0070115.

Damaghi, M., Tafreshi, N.K., Lloyd, M.C., Sprung, R., Estrella, V., Wojtkowiak, J.W., Morse, D.L., Koomen, J.M., Bui, M.M., Gatenby, R.A., et al. (2015). Chronic acidosis in the tumour microenvironment selects for overexpression of LAMP2 in the plasma membrane. Nat. Commun. *6*, 8752. https://doi.org/10.1038/ncomms9752.

Damrauer, J.S., Hoadley, K.A., Chism, D.D., Fan, C., Tiganelli, C.J., Wobker, S.E., Yeh, J.J., Milowsky, M.I., Iyer, G., Parker, J.S., et al. (2014). Intrinsic subtypes of high-grade bladder cancer reflect the hallmarks of breast cancer biology. Proc. Natl. Acad. Sci. *111*, 3110–3115. https://doi.org/10.1073/pnas.1318376111.

Davidson, S.M., Jonas, O., Keibler, M.A., Hou, H.W., Luengo, A., Mayers, J.R., Wyckoff, J., Del Rosario, A.M., Whitman, M., Chin, C.R., et al. (2017). Direct evidence for cancer-cell-autonomous extracellular protein catabolism in pancreatic tumors. Nat. Med. *23*, 235–241. https://doi.org/10.1038/nm.4256.

DeBoer, S.R., You, Y., Szodorai, A., Kaminska, A., Pigino, G., Nwabuisi, E., Wang, B., Estrada-Hernandez, T., Kins, S., Brady, S.T., et al. (2008). Conventional Kinesin Holoenzymes Are Composed of Heavy and Light Chain Homodimers. Biochemistry *47*, 4535–4543. https://doi.org/10.1021/bi702445j.

Dehmelt, L., and Halpain, S. (2004). The MAP2/Tau family of microtubule-associated proteins. Genome Biol. *6*, 204. https://doi.org/10.1186/gb-2004-6-1-204.

Demetriades, C., Doumpas, N., and Teleman, A.A. (2014). Regulation of TORC1 in Response to Amino Acid Starvation via Lysosomal Recruitment of TSC2. Cell *156*, 786–799. https://doi.org/10.1016/j.cell.2014.01.024.

Devereaux, K., Dall'Armi, C., Alcazar-Roman, A., Ogasawara, Y., Zhou, X., Wang, F., Yamamoto, A., De Camilli, P., and Di Paolo, G. (2013). Regulation of Mammalian Autophagy

by Class II and III PI 3-Kinases through PI3P Synthesis. PLoS ONE *8*, e76405. https://doi.org/10.1371/journal.pone.0076405.

Di Malta, C., Siciliano, D., Calcagni, A., Monfregola, J., Punzi, S., Pastore, N., Eastes, A.N., Davis, O., De Cegli, R., Zampelli, A., et al. (2017). Transcriptional activation of RagD GTPase controls mTORC1 and promotes cancer growth. Science *356*, 1188–1192. https://doi.org/10.1126/science.aag2553.

Di Paolo, G., and De Camilli, P. (2006). Phosphoinositides in cell regulation and membrane dynamics. Nature *443*, 651–657. https://doi.org/10.1038/nature05185.

Dong, J., Du, X., Wang, H., Wang, J., Lu, C., Chen, X., Zhu, Z., Luo, Z., Yu, L., Brown, A.J., et al. (2019). Allosteric enhancement of ORP1-mediated cholesterol transport by PI(4,5)P2/PI(3,4)P2. Nat. Commun. *10*, 829. https://doi.org/10.1038/s41467-019-08791-0.

Dong, X., Shen, D., Wang, X., Dawson, T., Li, X., Zhang, Q., Cheng, X., Zhang, Y., Weisman, L.S., Delling, M., et al. (2010). PI(3,5)P2 controls membrane trafficking by direct activation of mucolipin Ca2+ release channels in the endolysosome. Nat. Commun. *1*, 38. https://doi.org/10.1038/ncomms1037.

Dorrello, N.V., Peschiaroli, A., Guardavaccaro, D., Colburn, N.H., Sherman, N.E., and Pagano, M. (2006). S6K1- and ßTRCP-Mediated Degradation of PDCD4 Promotes Protein Translation and Cell Growth. Science *314*, 467–471. https://doi.org/10.1126/science.1130276.

Dozynkiewicz, M.A., Jamieson, N.B., MacPherson, I., Grindlay, J., van den Berghe, P.V.E., von Thun, A., Morton, J.P., Gourley, C., Timpson, P., Nixon, C., et al. (2012). Rab25 and CLIC3 Collaborate to Promote Integrin Recycling from Late Endosomes/Lysosomes and Drive Cancer Progression. Dev. Cell *22*, 131–145. https://doi.org/10.1016/j.devcel.2011.11.008.

Du, K., Zou, J., Liu, C., Khan, M., Xie, T., Huang, X., Zhang, K., Yuan, Y., and Wang, B. (2022). A Multi-Omics Pan-Cancer Analysis of 4EBP1 in Cancer Prognosis and Cancer-Associated Fibroblasts Infiltration. Front. Genet. *13*, 845751. https://doi.org/10.3389/fgene.2022.845751.

Dumont, F.J., and Su, Q. (1995). Mechanism of action of the immunosuppressant rapamycin. Life Sci. *58*, 373–395. https://doi.org/10.1016/0024-3205(95)02233-3.

Duong, T., Goud, B., and Schauer, K. (2012). Closed-form density-based framework for automatic detection of cellular morphology changes. Proc. Natl. Acad. Sci. U. S. A. *109*, 8382–8387. https://doi.org/10.1073/pnas.1117796109.

Durán, R.V., and Hall, M.N. (2012). Glutaminolysis feeds mTORC1. Cell Cycle *11*, 4107–4108. https://doi.org/10.4161/cc.22632.

de Duve, C., Pressman, B.C., Gianetto, R., Wattiaux, R., and Appelmans, F. (1955). Tissue fractionation studies. 6. Intracellular distribution patterns of enzymes in rat-liver tissue. Biochem. J. *60*, 604–617. https://doi.org/10.1042/bj0600604.

Düvel, K., Yecies, J.L., Menon, S., Raman, P., Lipovsky, A.I., Souza, A.L., Triantafellow, E., Ma, Q., Gorski, R., Cleaver, S., et al. (2010). Activation of a Metabolic Gene Regulatory Network Downstream of mTOR Complex 1. Mol. Cell *39*, 171–183. https://doi.org/10.1016/j.molcel.2010.06.022.

Ebner, M., Koch, P.A., and Haucke, V. (2019). Phosphoinositides in the control of lysosome function and homeostasis. Biochem. Soc. Trans. *47*, 1173–1185. https://doi.org/10.1042/BST20190158.

Encarnação, M., Espada, L., Escrevente, C., Mateus, D., Ramalho, J., Michelet, X., Santarino, I., Hsu, V.W., Brenner, M.B., Barral, D.C., et al. (2016). A Rab3a-dependent complex essential for lysosome positioning and plasma membrane repair. J. Cell Biol. *213*, 631–640. https://doi.org/10.1083/jcb.201511093.

Esrig, D., Elmajian, D., Groshen, S., Freeman, J.A., Stein, J.P., Chen, S.-C., Nichols, P.W., Skinner, D.G., Jones, P.A., and Cote, R.J. (1994). Accumulation of Nuclear p53 and Tumor Progression in Bladder Cancer. N. Engl. J. Med. *331*, 1259–1264. https://doi.org/10.1056/NEJM199411103311903.

Falcón-Pérez, J.M., Starcevic, M., Gautam, R., and Dell'Angelica, E.C. (2002). BLOC-1, a Novel Complex Containing the Pallidin and Muted Proteins Involved in the Biogenesis of Melanosomes and Platelet-dense Granules. J. Biol. Chem. *277*, 28191–28199. https://doi.org/10.1074/jbc.M204011200.

Fan, Y., Lu, H., Liang, W., Garcia-Barrio, M.T., Guo, Y., Zhang, J., Zhu, T., Hao, Y., Zhang, J., and Chen, Y.E. (2018). Endothelial TFEB (Transcription Factor EB) Positively Regulates Postischemic Angiogenesis. Circ. Res. *122*, 945–957. https://doi.org/10.1161/CIRCRESAHA.118.312672.

Ferron, M., Settembre, C., Shimazu, J., Lacombe, J., Kato, S., Rawlings, D.J., Ballabio, A., and Karsenty, G. (2013). A RANKL–PKCβ–TFEB signaling cascade is necessary for lysosomal biogenesis in osteoclasts. Genes Dev. *27*, 955–969. https://doi.org/10.1101/gad.213827.113.

Filipek, P.A., de Araujo, M.E.G., Vogel, G.F., De Smet, C.H., Eberharter, D., Rebsamen, M., Rudashevskaya, E.L., Kremser, L., Yordanov, T., Tschaikner, P., et al. (2017). LAMTOR/Ragulator is a negative regulator of Arl8b- and BORC-dependent late endosomal positioning. J. Cell Biol. *216*, 4199–4215. https://doi.org/10.1083/jcb.201703061.

Finck, B.N., and Kelly, D.P. (2006). PGC-1 coactivators: inducible regulators of energy metabolism in health and disease. J. Clin. Invest. *116*, 615–622. https://doi.org/10.1172/JCI27794.

Franco, I., Gulluni, F., Campa, C.C., Costa, C., Margaria, J.P., Ciraolo, E., Martini, M., Monteyne, D., De Luca, E., Germena, G., et al. (2014). PI3K Class II α Controls Spatially Restricted Endosomal PtdIns3P and Rab11 Activation to Promote Primary Cilium Function. Dev. Cell *28*, 647–658. https://doi.org/10.1016/j.devcel.2014.01.022.

Frasa, M.A.M., Maximiano, F.C., Smolarczyk, K., Francis, R.E., Betson, M.E., Lozano, E., Goldenring, J., Seabra, M.C., Rak, A., Ahmadian, M.R., et al. (2010). Armus Is a Rac1 Effector that Inactivates Rab7 and Regulates E-Cadherin Degradation. Curr. Biol. *20*, 198–208. https://doi.org/10.1016/j.cub.2009.12.053.

Gao, J., Huang, H.-Y., Pak, J., Cheng, J., Zhang, Z.-T., Shapiro, E., Pellicer, A., Sun, T.-T., and Wu, X.-R. (2004). p53 deficiency provokes urothelial proliferation and synergizes with activated Ha-ras in promoting urothelial tumorigenesis. Oncogene *23*, 687–696. https://doi.org/10.1038/sj.onc.1207169.

Garg, S., Sharma, M., Ung, C., Tuli, A., Barral, D.C., Hava, D.L., Veerapen, N., Besra, G.S., Hacohen, N., and Brenner, M.B. (2011). Lysosomal Trafficking, Antigen Presentation, and Microbial Killing Are Controlled by the Arf-like GTPase Arl8b. Immunity *35*, 182–193. https://doi.org/10.1016/j.immuni.2011.06.009.

Gingras, A.-C., Gygi, S.P., Raught, B., Polakiewicz, R.D., Abraham, R.T., Hoekstra, M.F., Aebersold, R., and Sonenberg, N. (1999). Regulation of 4E-BP1 phosphorylation: a novel two-step mechanism. Genes Dev. *13*, 1422–1437. https://doi.org/10.1101/gad.13.11.1422.

Gillooly, D. J., Morrow, I. C., Lindsay, M., Gould, R., Bryant, N. J., Gaullier, J. M., Parton, R. G., & Stenmark, H. (2000). Localization of phosphatidylinositol 3-phosphate in yeast and mammalian cells. The EMBO journal, 19(17), 4577–4588. https://doi.org/10.1093/emboj/19.17.4577

Glunde, K., Guggino, S.E., Solaiyappan, M., Pathak, A.P., Ichikawa, Y., and Bhujwalla, Z.M. (2003). Extracellular Acidification Alters Lysosomal Trafficking in Human Breast Cancer Cells. Neoplasia *5*, 533–545. https://doi.org/10.1016/S1476-5586(03)80037-4.

Gordis, L. (1966). Lysosomes and disease. J. Pediatr. *68*, 638–649. https://doi.org/10.1016/S0022-3476(66)80404-3.

Grabiner, B.C., Nardi, V., Birsoy, K., Possemato, R., Shen, K., Sinha, S., Jordan, A., Beck, A.H., and Sabatini, D.M. (2014). A Diverse Array of Cancer-Associated *MTOR* Mutations Are Hyperactivating and Can Predict Rapamycin Sensitivity. Cancer Discov. *4*, 554–563. https://doi.org/10.1158/2159-8290.CD-13-0929.

Gray, M.A., Choy, C.H., Dayam, R.M., Ospina-Escobar, E., Somerville, A., Xiao, X., Ferguson, S.M., and Botelho, R.J. (2016). Phagocytosis Enhances Lysosomal and Bactericidal Properties by Activating the Transcription Factor TFEB. Curr. Biol. *26*, 1955–1964. https://doi.org/10.1016/j.cub.2016.05.070.

Grossier, J.-P., Xouri, G., Goud, B., and Schauer, K. (2014). Cell adhesion defines the topology of endocytosis and signaling. EMBO J. *33*, 35–45. https://doi.org/10.1002/embj.201385284.

Guardia, C.M., Farías, G.G., Jia, R., Pu, J., and Bonifacino, J.S. (2016). BORC Functions Upstream of Kinesins 1 and 3 to Coordinate Regional Movement of Lysosomes along Different Microtubule Tracks. Cell Rep. *17*, 1950–1961. https://doi.org/10.1016/j.celrep.2016.10.062.

Guba, M., von Breitenbuch, P., Steinbauer, M., Koehl, G., Flegel, S., Hornung, M., Bruns, C.J., Zuelke, C., Farkas, S., Anthuber, M., et al. (2002). Rapamycin inhibits primary and metastatic tumor growth by antiangiogenesis: involvement of vascular endothelial growth factor. Nat. Med. *8*, 128–135. https://doi.org/10.1038/nm0202-128.

Gulati, P., and Thomas, G. (2007). Nutrient sensing in the mTOR/S6K1 signalling pathway. Biochem. Soc. Trans. *35*, 236–238. https://doi.org/10.1042/BST0350236.

Gupta, S., Hau, A.M., Beach, J.R., Harwalker, J., Mantuano, E., Gonias, S.L., Egelhoff, T.T., and Hansel, D.E. (2013). Mammalian Target of Rapamycin Complex 2 (mTORC2) Is a Critical Determinant of Bladder Cancer Invasion. PLoS ONE *8*, e81081. https://doi.org/10.1371/journal.pone.0081081.

Hao, F., Itoh, T., Morita, E., Shirahama-Noda, K., Yoshimori, T., and Noda, T. (2016). The PtdIns3-phosphatase MTMR3 interacts with mTORC1 and suppresses its activity. FEBS Lett. *590*, 161–173. https://doi.org/10.1002/1873-3468.12048.

Haq, R., and Fisher, D.E. (2011). Biology and Clinical Relevance of the Micropthalmia Family of Transcription Factors in Human Cancer. J. Clin. Oncol. *29*, 3474–3482. https://doi.org/10.1200/JCO.2010.32.6223.

Hara, K., Maruki, Y., Long, X., Yoshino, K., Oshiro, N., Hidayat, S., Tokunaga, C., Avruch, J., and Yonezawa, K. (2002). Raptor, a Binding Partner of Target of Rapamycin (TOR), Mediates TOR Action. Cell *110*, 177–189. https://doi.org/10.1016/S0092-8674(02)00833-4.

Harada, A., Takei, Y., Kanai, Y., Tanaka, Y., Nonaka, S., and Hirokawa, N. (1998). Golgi Vesiculation and Lysosome Dispersion in Cells Lacking Cytoplasmic Dynein. J. Cell Biol. *141*, 51–59. https://doi.org/10.1083/jcb.141.1.51.

He, R., Wang, M., Zhao, C., Shen, M., Yu, Y., He, L., Zhao, Y., Chen, H., Shi, X., Zhou, M., et al. (2019). TFEB-driven autophagy potentiates TGF-β induced migration in pancreatic cancer cells. J. Exp. Clin. Cancer Res. CR *38*, 340. https://doi.org/10.1186/s13046-019-1343-4.

He, X., Semenov, M., Tamai, K., and Zeng, X. (2004). LDL receptor-related proteins 5 and 6 in Wnt/β-catenin signaling:Arrows point the way. Development *131*, 1663–1677. https://doi.org/10.1242/dev.01117.

Hedegaard, J., Lamy, P., Nordentoft, I., Algaba, F., Høyer, S., Ulhøi, B.P., Vang, S., Reinert, T., Hermann, G.G., Mogensen, K., et al. (2016). Comprehensive Transcriptional Analysis of Early-Stage Urothelial Carcinoma. Cancer Cell *30*, 27–42. https://doi.org/10.1016/j.ccell.2016.05.004.

Hemesath, T.J., Steingrímsson, E., McGill, G., Hansen, M.J., Vaught, J., Hodgkinson, C.A., Arnheiter, H., Copeland, N.G., Jenkins, N.A., and Fisher, D.E. (1994). microphthalmia, a critical factor in melanocyte development, defines a discrete transcription factor family. Genes Dev. *8*, 2770–2780. https://doi.org/10.1101/gad.8.22.2770.

Hendrix, A., Maynard, D., Pauwels, P., Braems, G., Denys, H., Van den Broecke, R., Lambert, J., Van Belle, S., Cocquyt, V., Gespach, C., et al. (2010). Effect of the Secretory Small GTPase

Rab27B on Breast Cancer Growth, Invasion, and Metastasis. JNCI J. Natl. Cancer Inst. *102*, 866–880. https://doi.org/10.1093/jnci/djq153.

Hernández, S., López-Knowles, E., Lloreta, J., Kogevinas, M., Amorós, A., Tardón, A., Carrato, A., Serra, C., Malats, N., and Real, F.X. (2006). Prospective Study of *FGFR3* Mutations As a Prognostic Factor in Nonmuscle Invasive Urothelial Bladder Carcinomas. J. Clin. Oncol. *24*, 3664–3671. https://doi.org/10.1200/JCO.2005.05.1771.

Hesketh, G.G., Wartosch, L., Davis, L.J., Bright, N.A., and Luzio, J.P. (2018). The Lysosome and Intracellular Signalling. In Endocytosis and Signaling, C. Lamaze, and I. Prior, eds. (Cham: Springer International Publishing), pp. 151–180.

Heuser, J. (1989a). Changes in lysosome shape and distribution correlated with changes in cytoplasmic pH. J. Cell Biol. *108*, 855–864. https://doi.org/10.1083/jcb.108.3.855.

Heuser, J. (1989b). Changes in lysosome shape and distribution correlated with changes in cytoplasmic pH. J. Cell Biol. *108*, 855–864. https://doi.org/10.1083/jcb.108.3.855.

Hidas, G., Pode, D., Shapiro, A., Katz, R., Appelbaum, L., Pizov, G., Zorn, K.C., Landau, E.H., Duvdevani, M., and Gofrit, O.N. (2013). The natural history of secondary muscle-invasive bladder cancer. BMC Urol. *13*, 23. https://doi.org/10.1186/1471-2490-13-23.

Hirokawa, N., and Noda, Y. (2008). Intracellular Transport and Kinesin Superfamily Proteins, KIFs: Structure, Function, and Dynamics. Physiol. Rev. *88*, 1089–1118. https://doi.org/10.1152/physrev.00023.2007.

Hofmann, I., and Munro, S. (2006). An N-terminally acetylated Arf-like GTPase is localised to lysosomes and affects their motility. J. Cell Sci. *119*, 1494–1503. https://doi.org/10.1242/jcs.02958.

Hollenbeck, P.J., and Swanson, J.A. (1990). Radial extension of macrophage tubular lysosomes supported by kinesin. Nature *346*, 864–866. https://doi.org/10.1038/346864a0.

Holz, M.K., Ballif, B.A., Gygi, S.P., and Blenis, J. (2005). mTOR and S6K1 Mediate Assembly of the Translation Preinitiation Complex through Dynamic Protein Interchange and Ordered Phosphorylation Events. Cell *123*, 569–580. https://doi.org/10.1016/j.cell.2005.10.024.

Hong, Z., Pedersen, N.M., Wang, L., Torgersen, M.L., Stenmark, H., and Raiborg, C. (2017). PtdIns3P controls mTORC1 signaling through lysosomal positioning. J. Cell Biol. *216*, 4217–4233. https://doi.org/10.1083/jcb.201611073.

Hosokawa, N., Hara, T., Kaizuka, T., Kishi, C., Takamura, A., Miura, Y., Iemura, S., Natsume, T., Takehana, K., Yamada, N., et al. (2009). Nutrient-dependent mTORC1 Association with the ULK1–Atg13–FIP200 Complex Required for Autophagy. Mol. Biol. Cell *20*, 1981–1991. https://doi.org/10.1091/mbc.e08-12-1248.

Hsieh, A.C., Costa, M., Zollo, O., Davis, C., Feldman, M.E., Testa, J.R., Meyuhas, O., Shokat, K.M., and Ruggero, D. (2010). Genetic Dissection of the Oncogenic mTOR Pathway Reveals

Druggable Addiction to Translational Control via 4EBP-eIF4E. Cancer Cell *17*, 249–261. https://doi.org/10.1016/j.ccr.2010.01.021.

Huan, C., Kelly, M.L., Steele, R., Shapira, I., Gottesman, S.R.S., and Roman, C.A.J. (2006). Transcription factors TFE3 and TFEB are critical for CD40 ligand expression and thymus-dependent humoral immunity. Nat. Immunol. *7*, 1082–1091. https://doi.org/10.1038/ni1378.

Hudson, C.C., Liu, M., Chiang, G.G., Otterness, D.M., Loomis, D.C., Kaper, F., Giaccia, A.J., and Abraham, R.T. (2002). Regulation of Hypoxia-Inducible Factor 1α Expression and Function by the Mammalian Target of Rapamycin. Mol. Cell. Biol. *22*, 7004–7014. https://doi.org/10.1128/MCB.22.20.7004-7014.2002.

Ikegami, K., Heier, R.L., Taruishi, M., Takagi, H., Mukai, M., Shimma, S., Taira, S., Hatanaka, K., Morone, N., Yao, I., et al. (2007). Loss of α-tubulin polyglutamylation in ROSA22 mice is associated with abnormal targeting of KIF1A and modulated synaptic function. Proc. Natl. Acad. Sci. *104*, 3213–3218. https://doi.org/10.1073/pnas.0611547104.

Ishikawa, T. (2012). Structural biology of cytoplasmic and axonemal dyneins. J. Struct. Biol. *179*, 229–234. https://doi.org/10.1016/j.jsb.2012.05.016.

Itakura, E., Kishi, C., Inoue, K., and Mizushima, N. (2008). Beclin 1 Forms Two Distinct Phosphatidylinositol 3-Kinase Complexes with Mammalian Atg14 and UVRAG. Mol. Biol. Cell *19*, 5360–5372. https://doi.org/10.1091/mbc.e08-01-0080.

Iyer, G., Hanrahan, A.J., Milowsky, M.I., Al-Ahmadie, H., Scott, S.N., Janakiraman, M., Pirun, M., Sander, C., Socci, N.D., Ostrovnaya, I., et al. (2012). Genome Sequencing Identifies a Basis for Everolimus Sensitivity. Science *338*, 221–221. https://doi.org/10.1126/science.1226344.

Jevnikar, Z., Rojnik, M., Jamnik, P., Doljak, B., Fonović, U.P., and Kos, J. (2013). Cathepsin H Mediates the Processing of Talin and Regulates Migration of Prostate Cancer Cells. J. Biol. Chem. *288*, 2201–2209. https://doi.org/10.1074/jbc.M112.436394.

Johansson, M., Lehto, M., Tanhuanpää, K., Cover, T.L., and Olkkonen, V.M. (2005). The Oxysterol-binding Protein Homologue ORP1L Interacts with Rab7 and Alters Functional Properties of Late Endocytic Compartments. Mol. Biol. Cell *16*, 5480–5492. https://doi.org/10.1091/mbc.e05-03-0189.

Johansson, M., Rocha, N., Zwart, W., Jordens, I., Janssen, L., Kuijl, C., Olkkonen, V.M., and Neefjes, J. (2007). Activation of endosomal dynein motors by stepwise assembly of Rab7–RILP–p150Glued, ORP1L, and the receptor βIII spectrin. J. Cell Biol. *176*, 459–471. https://doi.org/10.1083/jcb.200606077.

Johnson, D.E., Ostrowski, P., Jaumouillé, V., and Grinstein, S. (2016). The position of lysosomes within the cell determines their luminal pH. J. Cell Biol. *212*, 677–692. https://doi.org/10.1083/jcb.201507112.

Justin, S., Rutz, J., Maxeiner, S., Chun, F.K.-H., Juengel, E., and Blaheta, R.A. (2020). Bladder Cancer Metastasis Induced by Chronic Everolimus Application Can Be Counteracted by Sulforaphane In Vitro. Int. J. Mol. Sci. *21*, 5582. https://doi.org/10.3390/ijms21155582.

Kamphorst, J.J., Nofal, M., Commisso, C., Hackett, S.R., Lu, W., Grabocka, E., Vander Heiden, M.G., Miller, G., Drebin, J.A., Bar-Sagi, D., et al. (2015). Human Pancreatic Cancer Tumors Are Nutrient Poor and Tumor Cells Actively Scavenge Extracellular Protein. Cancer Res. *75*, 544–553. https://doi.org/10.1158/0008-5472.CAN-14-2211.

Kapitein, L.C., van Bergeijk, P., Lipka, J., Keijzer, N., Wulf, P.S., Katrukha, E.A., Akhmanova, A., and Hoogenraad, C.C. (2013). Myosin-V Opposes Microtubule-Based Cargo Transport and Drives Directional Motility on Cortical Actin. Curr. Biol. *23*, 828–834. https://doi.org/10.1016/j.cub.2013.03.068.

Kashibuchi, K., Tomita, K., Schalken, J.A., Kume, H., Yamaguchi, T., Muto, S., Horie, S., and Kitamura, T. (2006). The Prognostic Value of E-Cadherin, α-, β-, and γ-Catenin in Urothelial Cancer of the Upper Urinary Tract. Eur. Urol. *49*, 839–845. https://doi.org/10.1016/j.eururo.2005.12.023.

Kauffman, E.C., Ricketts, C.J., Rais-Bahrami, S., Yang, Y., Merino, M.J., Bottaro, D.P., Srinivasan, R., and Linehan, W.M. (2014). Molecular genetics and cellular features of TFE3 and TFEB fusion kidney cancers. Nat. Rev. Urol. *11*, 465–475. https://doi.org/10.1038/nrurol.2014.162.

Kim, D., and Wirtz, D. (2013). Focal adhesion size uniquely predicts cell migration. FASEB J. *27*, 1351–1361. https://doi.org/10.1096/fj.12-220160.

Kim, E., Goraksha-Hicks, P., Li, L., Neufeld, T.P., and Guan, K.-L. (2008). Regulation of TORC1 by Rag GTPases in nutrient response. Nat. Cell Biol. *10*, 935–945. https://doi.org/10.1038/ncb1753.

Kim, J., Kundu, M., Viollet, B., and Guan, K.-L. (2011). AMPK and mTOR regulate autophagy through direct phosphorylation of Ulk1. Nat. Cell Biol. *13*, 132–141. https://doi.org/10.1038/ncb2152.

Kim, J.H., Lee, J., Cho, Y.-R., Lee, S.-Y., Sung, G.-J., Shin, D.-M., Choi, K.-C., and Son, J. (2021). TFEB Supports Pancreatic Cancer Growth through the Transcriptional Regulation of Glutaminase. Cancers *13*, 483. https://doi.org/10.3390/cancers13030483.

Kim, L.C., Cook, R.S., and Chen, J. (2017). mTORC1 and mTORC2 in cancer and the tumor microenvironment. Oncogene *36*, 2191–2201. https://doi.org/10.1038/onc.2016.363.

Kimmelman, A.C., and White, E. (2017). Autophagy and Tumor Metabolism. Cell Metab. *25*, 1037–1043. https://doi.org/10.1016/j.cmet.2017.04.004.

Kinzler, K.W., Nilbert, M.C., Su, L.-K., Vogelstein, B., Bryan, T.M., Levy, D.B., Smith, K.J., Preisinger, A.C., Hedge, P., McKechnie, D., et al. (1991). Identification of FAP Locus Genes from Chromosome 5q21. Science *253*, 661–665. https://doi.org/10.1126/science.1651562.

Kobos, R., Nagai, M., Tsuda, M., Merl, M.Y., Saito, T., Laé, M., Mo, Q., Olshen, A., Lianoglou, S., Leslie, C., et al. (2013). Combining integrated genomics and functional genomics to dissect the biology of a cancer-associated, aberrant transcription factor, the ASPSCR1-TFE3 fusion oncoprotein: Fusion oncoprotein target genes as potential therapeutic targets. J. Pathol. *229*, 743–754. https://doi.org/10.1002/path.4158.

Koponen, A., Arora, A., Takahashi, K., Kentala, H., Kivelä, A.M., Jääskeläinen, E., Peränen, J., Somerharju, P., Ikonen, E., Viitala, T., et al. (2019). ORP2 interacts with phosphoinositides and controls the subcellular distribution of cholesterol. Biochimie *158*, 90–101. https://doi.org/10.1016/j.biochi.2018.12.013.

Korolchuk, V.I., Saiki, S., Lichtenberg, M., Siddiqi, F.H., Roberts, E.A., Imarisio, S., Jahreiss, L., Sarkar, S., Futter, M., Menzies, F.M., et al. (2011). Lysosomal positioning coordinates cellular nutrient responses. Nat. Cell Biol. *13*, 453–460. https://doi.org/10.1038/ncb2204.

Ladanyi, M., Lui, M.Y., Antonescu, C.R., Krause-Boehm, A., Meindl, A., Argani, P., Healey, J.H., Ueda, T., Yoshikawa, H., Meloni-Ehrig, A., et al. (2001). The der(17)t(X;17)(p11;q25) of human alveolar soft part sarcoma fuses the TFE3 transcription factor gene to ASPL, a novel gene at 17q25. Oncogene *20*, 48–57. https://doi.org/10.1038/sj.onc.1204074.

Lamm, D.L., Blumenstein, B.A., Crissman, J.D., Montie, J.E., Gottesman, J.E., Lowe, B.A., Sarosdy, M.F., Bohl, R.D., Grossman, H.B., Beck, T.M., et al. (2000). Maintenance bacillus Calmette-Guerin immunotherapy for recurrent TA, T1 and carcinoma in situ transitional cell carcinoma of the bladder: a randomized Southwest Oncology Group Study. J. Urol. *163*, 1124–1129. .

LaPlante, J.M., Sun, M., Falardeau, J., Dai, D., Brown, E.M., Slaugenhaupt, S.A., and Vassilev, P.M. (2006). Lysosomal exocytosis is impaired in mucolipidosis type IV. Mol. Genet. Metab. *89*, 339–348. https://doi.org/10.1016/j.ymgme.2006.05.016.

Lawe, D.C., Patki, V., Heller-Harrison, R., Lambright, D., and Corvera, S. (2000). The FYVE Domain of Early Endosome Antigen 1 Is Required for Both Phosphatidylinositol 3-Phosphate and Rab5 Binding. J. Biol. Chem. *275*, 3699–3705. https://doi.org/10.1074/jbc.275.5.3699.

Leão, R., Lee, D., Figueiredo, A., Hermanns, T., Wild, P., Komosa, M., Lau, I., Mistry, M., Nunes, N.M., Price, A.J., et al. (2019). Combined genetic and epigenetic alterations of the *TERT* promoter affect clinical and biological behavior of bladder cancer. Int. J. Cancer *144*, 1676–1684. https://doi.org/10.1002/ijc.31935.

Lei, Q., Wang, D., Sun, K., Wang, L., and Zhang, Y. (2020). Resistance Mechanisms of Anti-PD1/PDL1 Therapy in Solid Tumors. Front. Cell Dev. Biol. *8*, 672. https://doi.org/10.3389/fcell.2020.00672.

Lemmon, M.A. (2008). Membrane recognition by phospholipid-binding domains. Nat. Rev. Mol. Cell Biol. *9*, 99–111. https://doi.org/10.1038/nrm2328.

Levine, A.J. (1997). p53, the Cellular Gatekeeper for Growth and Division. Cell *88*, 323–331. https://doi.org/10.1016/S0092-8674(00)81871-1.

Li, X., Rydzewski, N., Hider, A., Zhang, X., Yang, J., Wang, W., Gao, Q., Cheng, X., and Xu, H. (2016). A molecular mechanism to regulate lysosome motility for lysosome positioning and tubulation. Nat. Cell Biol. *18*, 404–417. https://doi.org/10.1038/ncb3324.

Lim, C.-Y., and Zoncu, R. (2016). The lysosome as a command-and-control center for cellular metabolism. J. Cell Biol. *214*, 653–664. https://doi.org/10.1083/jcb.201607005.

Lin, J.-F., and Hwang, T.I.S. (2017). Autophagy regulation in bladder cancer as the novel therapeutic strategy. Transl. Cancer Res. *6*, S708–S719. https://doi.org/10.21037/tcr.2017.06.26.

Lin, J., Handschin, C., and Spiegelman, B.M. (2005). Metabolic control through the PGC-1 family of transcription coactivators. Cell Metab. *1*, 361–370. https://doi.org/10.1016/j.cmet.2005.05.004.

Lin, Y.-C., Lin, J.-F., Wen, S.-I., Yang, S.-C., Tsai, T.-F., Chen, H.-E., Chou, K.-Y., and Hwang, T.I.-S. (2016). Inhibition of High Basal Level of Autophagy Induces Apoptosis in Human Bladder Cancer Cells. J. Urol. *195*, 1126–1135. https://doi.org/10.1016/j.juro.2015.10.128.

Liu, Q., Chang, J.W., Wang, J., Kang, S.A., Thoreen, C.C., Markhard, A., Hur, W., Zhang, J., Sim, T., Sabatini, D.M., et al. (2010). Discovery of 1-(4-(4-Propionylpiperazin-1-yl)-3-(trifluoromethyl)phenyl)-9-(quinolin-3-yl)benzo[h][1,6]naphthyridin-2(1 *H*)-one as a Highly Potent, Selective Mammalian Target of Rapamycin (mTOR) Inhibitor for the Treatment of Cancer. J. Med. Chem. *53*, 7146–7155. https://doi.org/10.1021/jm101144f.

Luo, J., Jiang, L., Yang, H., and Song, B.-L. (2017). Routes and mechanisms of post-endosomal cholesterol trafficking: A story that never ends: Luo ET AL . Traffic *18*, 209–217. https://doi.org/10.1111/tra.12471.

MacDonald, B.T., and He, X. (2012). Frizzled and LRP5/6 Receptors for Wnt/ -Catenin Signaling. Cold Spring Harb. Perspect. Biol. *4*, a007880–a007880. https://doi.org/10.1101/cshperspect.a007880.

Machado, E., White-Gilbertson, S., van de Vlekkert, D., Janke, L., Moshiach, S., Campos, Y., Finkelstein, D., Gomero, E., Mosca, R., Qiu, X., et al. (2015). Regulated lysosomal exocytosis mediates cancer progression. Sci. Adv. *1*, e1500603. https://doi.org/10.1126/sciadv.1500603.

Machado, E.R., Annunziata, I., van de Vlekkert, D., Grosveld, G.C., and d'Azzo, A. (2021). Lysosomes and Cancer Progression: A Malignant Liaison. Front. Cell Dev. Biol. *9*, 642494. https://doi.org/10.3389/fcell.2021.642494.

Mansueto, G., Armani, A., Viscomi, C., D'Orsi, L., De Cegli, R., Polishchuk, E.V., Lamperti, C., Di Meo, I., Romanello, V., Marchet, S., et al. (2017). Transcription Factor EB Controls Metabolic Flexibility during Exercise. Cell Metab. *25*, 182–196. https://doi.org/10.1016/j.cmet.2016.11.003.

Mansure, J.J., Nassim, R., Chevalier, S., Rocha, J., Scarlata, E., and Kassouf, W. (2009). Inhibition of mammalian target of rapamycin as a therapeutic strategy in the management of bladder cancer. Cancer Biol. Ther. *8*, 2339–2347. https://doi.org/10.4161/cbt.8.24.9987.

Marat, A.L., Wallroth, A., Lo, W.-T., Müller, R., Norata, G.D., Falasca, M., Schultz, C., and Haucke, V. (2017). mTORC1 activity repression by late endosomal phosphatidylinositol 3,4-bisphosphate. Science *356*, 968–972. https://doi.org/10.1126/science.aaf8310.

Marchand, B., Arsenault, D., Raymond-Fleury, A., Boisvert, F.-M., and Boucher, M.-J. (2015). Glycogen Synthase Kinase-3 (GSK3) Inhibition Induces Prosurvival Autophagic Signals in Human Pancreatic Cancer Cells. J. Biol. Chem. *290*, 5592–5605. https://doi.org/10.1074/jbc.M114.616714.

Marsit, C.J., Karagas, M.R., Andrew, A., Liu, M., Danaee, H., Schned, A.R., Nelson, H.H., and Kelsey, K.T. (2005). Epigenetic inactivation of SFRP genes and TP53 alteration act jointly as markers of invasive bladder cancer. Cancer Res. *65*, 7081–7085. https://doi.org/10.1158/0008-5472.CAN-05-0267.

Martina, J.A., and Puertollano, R. (2013). Rag GTPases mediate amino acid–dependent recruitment of TFEB and MITF to lysosomes. J. Cell Biol. *200*, 475–491. https://doi.org/10.1083/jcb.201209135.

Martina, J.A., Chen, Y., Gucek, M., and Puertollano, R. (2012). MTORC1 functions as a transcriptional regulator of autophagy by preventing nuclear transport of TFEB. Autophagy *8*, 903–914. https://doi.org/10.4161/auto.19653.

Martina, J.A., Diab, H.I., Lishu, L., Jeong-A, L., Patange, S., Raben, N., and Puertollano, R. (2014). The Nutrient-Responsive Transcription Factor TFE3 Promotes Autophagy, Lysosomal Biogenesis, and Clearance of Cellular Debris. Sci. Signal. *7*. https://doi.org/10.1126/scisignal.2004754.

Martinez, I., Chakrabarti, S., Hellevik, T., Morehead, J., Fowler, K., and Andrews, N.W. (2000). Synaptotagmin VII Regulates Ca2+-Dependent Exocytosis of Lysosomes in Fibroblasts. J. Cell Biol. *148*, 1141–1150. https://doi.org/10.1083/jcb.148.6.1141.

Marwaha, R., Arya, S.B., Jagga, D., Kaur, H., Tuli, A., and Sharma, M. (2017). The Rab7 effector PLEKHM1 binds Arl8b to promote cargo traffic to lysosomes. J. Cell Biol. *216*, 1051–1070. https://doi.org/10.1083/jcb.201607085.

Marx, A., Müller, J., Mandelkow, E.-M., Hoenger, A., and Mandelkow, E. (2006). Interaction of kinesin motors, microtubules, and MAPs. J. Muscle Res. Cell Motil. *27*, 125–137. https://doi.org/10.1007/s10974-005-9051-4.

Matsushita, M., Tanaka, S., Nakamura, N., Inoue, H., and Kanazawa, H. (2004). A Novel Kinesin-Like Protein, KIF1Bβ3 Is Involved in the Movement of Lysosomes to the Cell Periphery in Non-Neuronal Cells: Novel Kinesin Motor for Lysosomal Movement. Traffic *5*, 140–151. https://doi.org/10.1111/j.1600-0854.2003.00165.x.

Medina, D.L., Fraldi, A., Bouche, V., Annunziata, F., Mansueto, G., Spampanato, C., Puri, C., Pignata, A., Martina, J.A., Sardiello, M., et al. (2011). Transcriptional Activation of Lysosomal Exocytosis Promotes Cellular Clearance. Dev. Cell *21*, 421–430. https://doi.org/10.1016/j.devcel.2011.07.016.

Medina, D.L., Di Paola, S., Peluso, I., Armani, A., De Stefani, D., Venditti, R., Montefusco, S., Scotto-Rosato, A., Prezioso, C., Forrester, A., et al. (2015). Lysosomal calcium signalling regulates autophagy through calcineurin and TFEB. Nat. Cell Biol. *17*, 288–299. https://doi.org/10.1038/ncb3114.

Mesmin, B., Bigay, J., Moser von Filseck, J., Lacas-Gervais, S., Drin, G., and Antonny, B. (2013). A Four-Step Cycle Driven by PI(4)P Hydrolysis Directs Sterol/PI(4)P Exchange by the ER-Golgi Tether OSBP. Cell *155*, 830–843. https://doi.org/10.1016/j.cell.2013.09.056.

Mindell, J.A. (2012). Lysosomal acidification mechanisms. Annu. Rev. Physiol. *74*, 69–86. https://doi.org/10.1146/annurev-physiol-012110-142317.

Mitra, A.P., Datar, R.H., and Cote, R.J. (2006). Molecular Pathways in Invasive Bladder Cancer: New Insights Into Mechanisms, Progression, and Target Identification. J. Clin. Oncol. *24*, 5552–5564. https://doi.org/10.1200/JCO.2006.08.2073.

Miyamoto, H., Shuin, T., Ikeda, I., Hosaka, M., and Kubota, Y. (1996). Loss of heterozygosity at the p53, RB, DCC and APC tumor suppressor gene loci in human bladder cancer. J. Urol. *155*, 1444–1447. .

Mizushima, N. (2007). Autophagy: process and function. Genes Dev. *21*, 2861–2873. https://doi.org/10.1101/gad.1599207.

Mizushima, N., and Yoshimori, T. (2007). How to Interpret LC3 Immunoblotting. Autophagy *3*, 542–545. https://doi.org/10.4161/auto.4600.

Morgan, A.J., Platt, F.M., Lloyd-Evans, E., and Galione, A. (2011). Molecular mechanisms of endolysosomal Ca2+ signalling in health and disease. Biochem. J. *439*, 349–378. https://doi.org/10.1042/BJ20110949.

Moriyama, K., and Bonifacino, J.S. (2002). Pallidin is a Component of a Multi-Protein Complex Involved in the Biogenesis of Lysosome-related Organelles: Pallidin is a Component of a Multi-Protein Complex. Traffic *3*, 666–677. https://doi.org/10.1034/j.1600-0854.2002.30908.x.

Naegeli, K.M., Hastie, E., Garde, A., Wang, Z., Keeley, D.P., Gordon, K.L., Pani, A.M., Kelley, L.C., Morrissey, M.A., Chi, Q., et al. (2017). Cell Invasion In Vivo via Rapid Exocytosis of a Transient Lysosome-Derived Membrane Domain. Dev. Cell *43*, 403-417.e10. https://doi.org/10.1016/j.devcel.2017.10.024.

Nakamura, S., and Yoshimori, T. (2017). New insights into autophagosome–lysosome fusion. J. Cell Sci. jcs.196352. https://doi.org/10.1242/jcs.196352.

Nakata, T., and Hirokawa, N. (1995). Point mutation of adenosine triphosphate-binding motif generated rigor kinesin that selectively blocks anterograde lysosome membrane transport. J. Cell Biol. *131*, 1039–1053. https://doi.org/10.1083/jcb.131.4.1039.

Napolitano, G., Esposito, A., Choi, H., Matarese, M., Benedetti, V., Di Malta, C., Monfregola, J., Medina, D.L., Lippincott-Schwartz, J., and Ballabio, A. (2018). mTOR-dependent phosphorylation controls TFEB nuclear export. Nat. Commun. *9*, 3312. https://doi.org/10.1038/s41467-018-05862-6.

Napolitano, G., Di Malta, C., and Ballabio, A. (2022). Non-canonical mTORC1 signaling at the lysosome. Trends Cell Biol. S0962892422001179. https://doi.org/10.1016/j.tcb.2022.04.012.

Nawroth, R., Stellwagen, F., Schulz, W.A., Stoehr, R., Hartmann, A., Krause, B.J., Gschwend, J.E., and Retz, M. (2011). S6K1 and 4E-BP1 Are Independent Regulated and Control Cellular Growth in Bladder Cancer. PLoS ONE *6*, e27509. https://doi.org/10.1371/journal.pone.0027509.

Nazarian, R., Shi, H., Wang, Q., Kong, X., Koya, R.C., Lee, H., Chen, Z., Lee, M.-K., Attar, N., Sazegar, H., et al. (2010). Melanomas acquire resistance to B-RAF(V600E) inhibition by RTK or N-RAS upregulation. Nature *468*, 973–977. https://doi.org/10.1038/nature09626.

Nezich, C.L., Wang, C., Fogel, A.I., and Youle, R.J. (2015). MiT/TFE transcription factors are activated during mitophagy downstream of Parkin and Atg5. J. Cell Biol. *210*, 435–450. https://doi.org/10.1083/jcb.201501002.

Nicklin, P., Bergman, P., Zhang, B., Triantafellow, E., Wang, H., Nyfeler, B., Yang, H., Hild, M., Kung, C., Wilson, C., et al. (2009). Bidirectional transport of amino acids regulates mTOR and autophagy. Cell *136*, 521–534. https://doi.org/10.1016/j.cell.2008.11.044.

Nishimura, Y., Sameni, M., and Sloane, B.F. (1998). Malignant transformation alters intracellular trafficking of lysosomal cathepsin D in human breast epithelial cells. Pathol. Oncol. Res. *4*, 283–296. https://doi.org/10.1007/BF02905219.

Nishimura, Y., Itoh, K., Yoshioka, K., Tokuda, K., and Himeno, M. (2003). Overexpression of ROCK in human breast cancer cells: Evidence that ROCK activity mediates intracellular membrane traffic of lysosomes. Pathol. Oncol. Res. *9*, 83–95. https://doi.org/10.1007/BF03033750.

Nixon, R.A. (2013). The role of autophagy in neurodegenerative disease. Nat. Med. *19*, 983–997. https://doi.org/10.1038/nm.3232.

Nnah, I.C., Wang, B., Saqcena, C., Weber, G.F., Bonder, E.M., Bagley, D., De Cegli, R., Napolitano, G., Medina, D.L., Ballabio, A., et al. (2019). TFEB-driven endocytosis coordinates MTORC1 signaling and autophagy. Autophagy *15*, 151–164. https://doi.org/10.1080/15548627.2018.1511504.

Nobukuni, T., Joaquin, M., Roccio, M., Dann, S.G., Kim, S.Y., Gulati, P., Byfield, M.P., Backer, J.M., Natt, F., Bos, J.L., et al. (2005). Amino acids mediate mTOR/raptor signaling through

activation of class 3 phosphatidylinositol 3OH-kinase. Proc. Natl. Acad. Sci. *102*, 14238–14243. https://doi.org/10.1073/pnas.0506925102.

Nordmann, M., Cabrera, M., Perz, A., Bröcker, C., Ostrowicz, C., Engelbrecht-Vandré, S., and Ungermann, C. (2010). The Mon1-Ccz1 Complex Is the GEF of the Late Endosomal Rab7 Homolog Ypt7. Curr. Biol. *20*, 1654–1659. https://doi.org/10.1016/j.cub.2010.08.002.

Ohkuma, S., Moriyama, Y., and Takano, T. (1982). Identification and characterization of a proton pump on lysosomes by fluorescein-isothiocyanate-dextran fluorescence. Proc. Natl. Acad. Sci. *79*, 2758–2762. https://doi.org/10.1073/pnas.79.9.2758.

Ojha, R., Jha, V., and Singh, S.K. (2016). Gemcitabine and mitomycin induced autophagy regulates cancer stem cell pool in urothelial carcinoma cells. Biochim. Biophys. Acta BBA - Mol. Cell Res. *1863*, 347–359. https://doi.org/10.1016/j.bbamcr.2015.12.002.

Okosun, J., Wolfson, R.L., Wang, J., Araf, S., Wilkins, L., Castellano, B.M., Escudero-Ibarz, L., Al Seraihi, A.F., Richter, J., Bernhart, S.H., et al. (2016). Recurrent mTORC1-activating RRAGC mutations in follicular lymphoma. Nat. Genet. *48*, 183–188. https://doi.org/10.1038/ng.3473.

Olson, O.C., and Joyce, J.A. (2015). Cysteine cathepsin proteases: regulators of cancer progression and therapeutic response. Nat. Rev. Cancer *15*, 712–729. https://doi.org/10.1038/nrc4027.

Palm, W., and Thompson, C.B. (2017). Nutrient acquisition strategies of mammalian cells. Nature *546*, 234–242. https://doi.org/10.1038/nature22379.

Palmieri, M., Impey, S., Kang, H., di Ronza, A., Pelz, C., Sardiello, M., and Ballabio, A. (2011). Characterization of the CLEAR network reveals an integrated control of cellular clearance pathways. Hum. Mol. Genet. *20*, 3852–3866. https://doi.org/10.1093/hmg/ddr306.

Pankiv, S., Alemu, E.A., Brech, A., Bruun, J.-A., Lamark, T., Øvervatn, A., Bjørkøy, G., and Johansen, T. (2010). FYCO1 is a Rab7 effector that binds to LC3 and PI3P to mediate microtubule plus end–directed vesicle transport. J. Cell Biol. *188*, 253–269. https://doi.org/10.1083/jcb.200907015.

Pastore, N., Brady, O.A., Diab, H.I., Martina, J.A., Sun, L., Huynh, T., Lim, J.-A., Zare, H., Raben, N., Ballabio, A., et al. (2016). TFEB and TFE3 cooperate in the regulation of the innate immune response in activated macrophages. Autophagy *12*, 1240–1258. https://doi.org/10.1080/15548627.2016.1179405.

Pastore, N., Vainshtein, A., Klisch, T.J., Armani, A., Huynh, T., Herz, N.J., Polishchuk, E.V., Sandri, M., and Ballabio, A. (2017). TFE 3 regulates whole-body energy metabolism in cooperation with TFEB. EMBO Mol. Med. *9*, 605–621. https://doi.org/10.15252/emmm.201607204.

Patergnani, S., Marchi, S., Delprat, B., and Wieckowski, M.R. (2021). Editorial: Organelles Relationships and Interactions: A Cancer Perspective. Front. Cell Dev. Biol. *9*, 678307. https://doi.org/10.3389/fcell.2021.678307.

Pavlova, N.N., and Thompson, C.B. (2016). The Emerging Hallmarks of Cancer Metabolism. Cell Metab. *23*, 27–47. https://doi.org/10.1016/j.cmet.2015.12.006.

Pavlova, N.N., Zhu, J., and Thompson, C.B. (2022). The hallmarks of cancer metabolism: Still emerging. Cell Metab. *34*, 355–377. https://doi.org/10.1016/j.cmet.2022.01.007.

Pedersen, N.M., Wenzel, E.M., Wang, L., Antoine, S., Chavrier, P., Stenmark, H., and Raiborg, C. (2020). Protrudin-mediated ER–endosome contact sites promote MT1-MMP exocytosis and cell invasion. J. Cell Biol. *219*, e202003063. https://doi.org/10.1083/jcb.202003063.

Peña-Llopis, S., Vega-Rubin-de-Celis, S., Schwartz, J.C., Wolff, N.C., Tran, T.A.T., Zou, L., Xie, X.-J., Corey, D.R., and Brugarolas, J. (2011). Regulation of TFEB and V-ATPases by mTORC1: Regulation of TFEB and V-ATPases by mTORC1. EMBO J. *30*, 3242–3258. https://doi.org/10.1038/emboj.2011.257.

Peng, W., Wong, Y.C., and Krainc, D. (2020). Mitochondria-lysosome contacts regulate mitochondrial Ca $^{2+}$ dynamics via lysosomal TRPML1. Proc. Natl. Acad. Sci. *117*, 19266–19275. https://doi.org/10.1073/pnas.2003236117.

Perera, R.M., and Zoncu, R. (2016). The Lysosome as a Regulatory Hub. Annu. Rev. Cell Dev. Biol. *32*, 223–253. https://doi.org/10.1146/annurev-cellbio-111315-125125.

Perera, R.M., Stoykova, S., Nicolay, B.N., Ross, K.N., Fitamant, J., Boukhali, M., Lengrand, J., Deshpande, V., Selig, M.K., Ferrone, C.R., et al. (2015a). Transcriptional control of autophagy–lysosome function drives pancreatic cancer metabolism. Nature *524*, 361–365. https://doi.org/10.1038/nature14587.

Perera, R.M., Stoykova, S., Nicolay, B.N., Ross, K.N., Fitamant, J., Boukhali, M., Lengrand, J., Deshpande, V., Selig, M.K., Ferrone, C.R., et al. (2015b). Transcriptional control of autophagy–lysosome function drives pancreatic cancer metabolism. Nature *524*, 361–365. https://doi.org/10.1038/nature14587.

Perera, R.M., Di Malta, C., and Ballabio, A. (2019). MiT/TFE Family of Transcription Factors, Lysosomes, and Cancer. Annu. Rev. Cancer Biol. *3*, 203–222. https://doi.org/10.1146/annurev-cancerbio-030518-055835.

Peterson, T.R., Laplante, M., Thoreen, C.C., Sancak, Y., Kang, S.A., Kuehl, W.M., Gray, N.S., and Sabatini, D.M. (2009). DEPTOR Is an mTOR Inhibitor Frequently Overexpressed in Multiple Myeloma Cells and Required for Their Survival. Cell *137*, 873–886. https://doi.org/10.1016/j.cell.2009.03.046.

Peterson, T.R., Sengupta, S.S., Harris, T.E., Carmack, A.E., Kang, S.A., Balderas, E., Guertin, D.A., Madden, K.L., Carpenter, A.E., Finck, B.N., et al. (2011). mTOR Complex 1 Regulates Lipin 1 Localization to Control the SREBP Pathway. Cell *146*, 408–420. https://doi.org/10.1016/j.cell.2011.06.034.

Pfeffer, S.R. (2019). NPC intracellular cholesterol transporter 1 (NPC1)-mediated cholesterol export from lysosomes. J. Biol. Chem. *294*, 1706–1709. https://doi.org/10.1074/jbc.TM118.004165.

Pham, H.Q., Yoshioka, K., Mohri, H., Nakata, H., Aki, S., Ishimaru, K., Takuwa, N., and Takuwa, Y. (2018). MTMR4, a phosphoinositide-specific 3'-phosphatase, regulates TFEB activity and the endocytic and autophagic pathways. Genes Cells *23*, 670–687. https://doi.org/10.1111/gtc.12609.

Platt, F.M. (2018). Emptying the stores: lysosomal diseases and therapeutic strategies. Nat. Rev. Drug Discov. *17*, 133–150. https://doi.org/10.1038/nrd.2017.214.

Ploper, D., Taelman, V.F., Robert, L., Perez, B.S., Titz, B., Chen, H.-W., Graeber, T.G., von Euw, E., Ribas, A., and De Robertis, E.M. (2015). MITF drives endolysosomal biogenesis and potentiates Wnt signaling in melanoma cells. Proc. Natl. Acad. Sci. *112*. https://doi.org/10.1073/pnas.1424576112.

Porstmann, T., Santos, C.R., Griffiths, B., Cully, M., Wu, M., Leevers, S., Griffiths, J.R., Chung, Y.-L., and Schulze, A. (2008). SREBP Activity Is Regulated by mTORC1 and Contributes to Akt-Dependent Cell Growth. Cell Metab. *8*, 224–236. https://doi.org/10.1016/j.cmet.2008.07.007.

Posor, Y., Jang, W., and Haucke, V. (2022). Phosphoinositides as membrane organizers. Nat. Rev. Mol. Cell Biol. https://doi.org/10.1038/s41580-022-00490-x.

Prinz, W.A., Toulmay, A., and Balla, T. (2020). The functional universe of membrane contact sites. Nat. Rev. Mol. Cell Biol. *21*, 7–24. https://doi.org/10.1038/s41580-019-0180-9.

Pu, J., Schindler, C., Jia, R., Jarnik, M., Backlund, P., and Bonifacino, J.S. (2015). BORC, a Multisubunit Complex that Regulates Lysosome Positioning. Dev. Cell *33*, 176–188. https://doi.org/10.1016/j.devcel.2015.02.011.

Pu, J., Guardia, C.M., Keren-Kaplan, T., and Bonifacino, J.S. (2016). Mechanisms and functions of lysosome positioning. J. Cell Sci. *129*, 4329–4339. https://doi.org/10.1242/jcs.196287.

Pu, J., Keren-Kaplan, T., and Bonifacino, J.S. (2017). A Ragulator–BORC interaction controls lysosome positioning in response to amino acid availability. J. Cell Biol. *216*, 4183–4197. https://doi.org/10.1083/jcb.201703094.

Puertollano, R. (2014). mTOR and lysosome regulation. F1000Prime Rep. *6*. https://doi.org/10.12703/P6-52.

Puertollano, R., Ferguson, S.M., Brugarolas, J., and Ballabio, A. (2018). The complex relationship between TFEB transcription factor phosphorylation and subcellular localization. EMBO J. *37*. https://doi.org/10.15252/embj.201798804.

Puzio-Kuter, A.M., Castillo-Martin, M., Kinkade, C.W., Wang, X., Shen, T.H., Matos, T., Shen, M.M., Cordon-Cardo, C., and Abate-Shen, C. (2009). Inactivation of *p53* and *Pten* promotes invasive bladder cancer. Genes Dev. *23*, 675–680. https://doi.org/10.1101/gad.1772909.

Pyrpassopoulos, S., Shuman, H., and Ostap, E.M. (2017). Adhesion force and attachment lifetime of the KIF16B-PX domain interaction with lipid membranes. Mol. Biol. Cell *28*, 3315–3322. https://doi.org/10.1091/mbc.e17-05-0324.

Quintero-Fabián, S., Arreola, R., Becerril-Villanueva, E., Torres-Romero, J.C., Arana-Argáez, V., Lara-Riegos, J., Ramírez-Camacho, M.A., and Alvarez-Sánchez, M.E. (2019). Role of Matrix Metalloproteinases in Angiogenesis and Cancer. Front. Oncol. *9*, 1370. https://doi.org/10.3389/fonc.2019.01370.

Rabanal-Ruiz, Y., Byron, A., Wirth, A., Madsen, R., Sedlackova, L., Hewitt, G., Nelson, G., Stingele, J., Wills, J.C., Zhang, T., et al. (2021). mTORC1 activity is supported by spatial association with focal adhesions. J. Cell Biol. *220*, e202004010. https://doi.org/10.1083/jcb.202004010.

Raiborg, C. (2018). How Nutrients Orchestrate Lysosome Positioning: Contact https://doi.org/10.1177/2515256418756111.

Raiborg, C., Wenzel, E.M., Pedersen, N.M., Olsvik, H., Schink, K.O., Schultz, S.W., Vietri, M., Nisi, V., Bucci, C., Brech, A., et al. (2015). Repeated ER–endosome contacts promote endosome translocation and neurite outgrowth. Nature *520*, 234–238. https://doi.org/10.1038/nature14359.

Ramphal, R., Pappo, A., Zielenska, M., Grant, R., and Ngan, B.-Y. (2006). Pediatric Renal Cell Carcinoma: Clinical, Pathologic, and Molecular Abnormalities Associated With the Members of the MiT Transcription Factor Family. Am. J. Clin. Pathol. *126*, 349–364. https://doi.org/10.1309/98YE9E442AR7LX2X.

Rathmell, J.C., Fox, C.J., Plas, D.R., Hammerman, P.S., Cinalli, R.M., and Thompson, C.B. (2003). Akt-Directed Glucose Metabolism Can Prevent Bax Conformation Change and Promote Growth Factor-Independent Survival. Mol. Cell. Biol. *23*, 7315–7328. https://doi.org/10.1128/MCB.23.20.7315-7328.2003.

Reddy, A., Caler, E.V., and Andrews, N.W. (2001). Plasma Membrane Repair Is Mediated by Ca2+-Regulated Exocytosis of Lysosomes. Cell *106*, 157–169. https://doi.org/10.1016/S0092-8674(01)00421-4.

Reed, N.A., Cai, D., Blasius, T.L., Jih, G.T., Meyhofer, E., Gaertig, J., and Verhey, K.J. (2006). Microtubule Acetylation Promotes Kinesin-1 Binding and Transport. Curr. Biol. *16*, 2166–2172. https://doi.org/10.1016/j.cub.2006.09.014.

Robertson, A.G., Kim, J., Al-Ahmadie, H., Bellmunt, J., Guo, G., Cherniack, A.D., Hinoue, T., Laird, P.W., Hoadley, K.A., Akbani, R., et al. (2017). Comprehensive Molecular Characterization of Muscle-Invasive Bladder Cancer. Cell *171*, 540-556.e25. https://doi.org/10.1016/j.cell.2017.09.007.

Rocha, N., Kuijl, C., van der Kant, R., Janssen, L., Houben, D., Janssen, H., Zwart, W., and Neefjes, J. (2009). Cholesterol sensor ORP1L contacts the ER protein VAP to control Rab7–RILP–p150Glued and late endosome positioning. J. Cell Biol. *185*, 1209–1225. https://doi.org/10.1083/jcb.200811005.

Roczniak-Ferguson, A., Petit, C.S., Froehlich, F., Qian, S., Ky, J., Angarola, B., Walther, T.C., and Ferguson, S.M. (2012). The transcription factor TFEB links mTORC1 signaling to transcriptional control of lysosome homeostasis. Sci. Signal. *5*, ra42. https://doi.org/10.1126/scisignal.2002790.

Rodríguez, A., Webster, P., Ortego, J., and Andrews, N.W. (1997). Lysosomes Behave as Ca2+-regulated Exocytic Vesicles in Fibroblasts and Epithelial Cells. J. Cell Biol. *137*, 93–104. https://doi.org/10.1083/jcb.137.1.93.

Rodriguez-Navarro, J.A., Kaushik, S., Koga, H., Dall'Armi, C., Shui, G., Wenk, M.R., Di Paolo, G., and Cuervo, A.M. (2012). Inhibitory effect of dietary lipids on chaperone-mediated autophagy. Proc. Natl. Acad. Sci. U. S. A. *109*, E705-714. https://doi.org/10.1073/pnas.1113036109.

Rosa-Ferreira, C., and Munro, S. (2011). Arl8 and SKIP Act Together to Link Lysosomes to Kinesin-1. Dev. Cell *21*, 1171–1178. https://doi.org/10.1016/j.devcel.2011.10.007.

Rubinfeld, B., Souza, B., Albert, I., Müller, O., Chamberlain, S.H., Masiarz, F.R., Munemitsu, S., and Polakis, P. (1993). Association of the *APC* Gene Product with β-Catenin. Science *262*, 1731–1734. https://doi.org/10.1126/science.8259518.

Rutkovsky, A.C., Yeh, E.S., Guest, S.T., Findlay, V.J., Muise-Helmericks, R.C., Armeson, K., and Ethier, S.P. (2019). Eukaryotic initiation factor 4E-binding protein as an oncogene in breast cancer. BMC Cancer *19*, 491. https://doi.org/10.1186/s12885-019-5667-4.

Sameni, M., Elliott, E., Ziegler, G., Fortgens, P.H., Dennison, C., and Sloane, B.F. (1995). Cathepsin B and D are localized at the surface of human breast cancer cells. Pathol. Oncol. Res. *1*, 43–53. https://doi.org/10.1007/BF02893583.

Samie, M., and Cresswell, P. (2015). The transcription factor TFEB acts as a molecular switch that regulates exogenous antigen-presentation pathways. Nat. Immunol. *16*, 729–736. https://doi.org/10.1038/ni.3196.

Samie, M., Wang, X., Zhang, X., Goschka, A., Li, X., Cheng, X., Gregg, E., Azar, M., Zhuo, Y., Garrity, A.G., et al. (2013). A TRP Channel in the Lysosome Regulates Large Particle Phagocytosis via Focal Exocytosis. Dev. Cell *26*, 511–524. https://doi.org/10.1016/j.devcel.2013.08.003.

Sancak, Y., Thoreen, C.C., Peterson, T.R., Lindquist, R.A., Kang, S.A., Spooner, E., Carr, S.A., and Sabatini, D.M. (2007). PRAS40 Is an Insulin-Regulated Inhibitor of the mTORC1 Protein Kinase. Mol. Cell *25*, 903–915. https://doi.org/10.1016/j.molcel.2007.03.003.

Sancak, Y., Peterson, T.R., Shaul, Y.D., Lindquist, R.A., Thoreen, C.C., Bar-Peled, L., and Sabatini, D.M. (2008). The Rag GTPases Bind Raptor and Mediate Amino Acid Signaling to mTORC1. Science *320*, 1496–1501. https://doi.org/10.1126/science.1157535.

Sancak, Y., Bar-Peled, L., Zoncu, R., Markhard, A.L., Nada, S., and Sabatini, D.M. (2010). Ragulator-Rag Complex Targets mTORC1 to the Lysosomal Surface and Is Necessary for Its Activation by Amino Acids. Cell *141*, 290–303. https://doi.org/10.1016/j.cell.2010.02.024.

Sanders, A.A.W.M., and Kaverina, I. (2015). Nucleation and Dynamics of Golgi-derived Microtubules. Front. Neurosci. *9*. https://doi.org/10.3389/fnins.2015.00431.

Santama, N. (1998). KIF2beta , a new kinesin superfamily protein in non-neuronal cells, is associated with lysosomes and may be implicated in their centrifugal translocation. EMBO J. *17*, 5855–5867. https://doi.org/10.1093/emboj/17.20.5855.

Sardiello, M., Palmieri, M., di Ronza, A., Medina, D.L., Valenza, M., Gennarino, V.A., Di Malta, C., Donaudy, F., Embrione, V., Polishchuk, R.S., et al. (2009). A Gene Network Regulating Lysosomal Biogenesis and Function. Science *325*, 473–477. https://doi.org/10.1126/science.1174447.

Saxton, R.A., and Sabatini, D.M. (2017). mTOR Signaling in Growth, Metabolism, and Disease. Cell *168*, 960–976. https://doi.org/10.1016/j.cell.2017.02.004.

Sbano, L., Bonora, M., Marchi, S., Baldassari, F., Medina, D.L., Ballabio, A., Giorgi, C., and Pinton, P. (2017). TFEB-mediated increase in peripheral lysosomes regulates store-operated calcium entry. Sci. Rep. *7*, 40797. https://doi.org/10.1038/srep40797.

Schauer, K., Duong, T., Bleakley, K., Bardin, S., Bornens, M., and Goud, B. (2010a). Probabilistic density maps to study global endomembrane organization. Nat. Methods *7*, 560–566. https://doi.org/10.1038/nmeth.1462.

Schauer, K., Duong, T., Bleakley, K., Bardin, S., Bornens, M., and Goud, B. (2010b). Probabilistic density maps to study global endomembrane organization. Nat. Methods *7*, 560–566. https://doi.org/10.1038/nmeth.1462.

Schiefermeier, N., Scheffler, J.M., de Araujo, M.E.G., Stasyk, T., Yordanov, T., Ebner, H.L., Offterdinger, M., Munck, S., Hess, M.W., Wickström, S.A., et al. (2014). The late endosomal p14–MP1 (LAMTOR2/3) complex regulates focal adhesion dynamics during cell migration. J. Cell Biol. *205*, 525–540. https://doi.org/10.1083/jcb.201310043.

Schornack, P.A., and Gillies, R.J. (2003). Contributions of Cell Metabolism and H+ Diffusion to the Acidic pH of Tumors. Neoplasia *5*, 135–145. https://doi.org/10.1016/S1476-5586(03)80005-2.

Schröder, B.A., Wrocklage, C., Hasilik, A., and Saftig, P. (2010). The proteome of lysosomes. PROTEOMICS *10*, 4053–4076. https://doi.org/10.1002/pmic.201000196.

Seiler, R., Ashab, H.A.D., Erho, N., van Rhijn, B.W.G., Winters, B., Douglas, J., Van Kessel, K.E., Fransen van de Putte, E.E., Sommerlad, M., Wang, N.Q., et al. (2017). Impact of Molecular Subtypes in Muscle-invasive Bladder Cancer on Predicting Response and Survival after Neoadjuvant Chemotherapy. Eur. Urol. *72*, 544–554. https://doi.org/10.1016/j.eururo.2017.03.030.

Settembre, C., Di Malta, C., Polito, V.A., Arencibia, M.G., Vetrini, F., Erdin, S., Erdin, S.U., Huynh, T., Medina, D., Colella, P., et al. (2011). TFEB Links Autophagy to Lysosomal Biogenesis. Science *332*, 1429–1433. https://doi.org/10.1126/science.1204592.

Settembre, C., Zoncu, R., Medina, D.L., Vetrini, F., Erdin, S., Erdin, S., Huynh, T., Ferron, M., Karsenty, G., Vellard, M.C., et al. (2012). A lysosome-to-nucleus signalling mechanism senses and regulates the lysosome via mTOR and TFEB: Self-regulation of the lysosome via mTOR and TFEB. EMBO J. *31*, 1095–1108. https://doi.org/10.1038/emboj.2012.32.

Settembre, C., Fraldi, A., Medina, D.L., and Ballabio, A. (2013a). Signals from the lysosome: a control centre for cellular clearance and energy metabolism. Nat. Rev. Mol. Cell Biol. *14*, 283–296. https://doi.org/10.1038/nrm3565.

Settembre, C., De Cegli, R., Mansueto, G., Saha, P.K., Vetrini, F., Visvikis, O., Huynh, T., Carissimo, A., Palmer, D., Jürgen Klisch, T., et al. (2013b). TFEB controls cellular lipid metabolism through a starvation-induced autoregulatory loop. Nat. Cell Biol. *15*, 647–658. https://doi.org/10.1038/ncb2718.

Shimazui, T., Schalken, J.A., Giroldi, L.A., Jansen, C.F., Akaza, H., Koiso, K., Debruyne, F.M., and Bringuier, P.P. (1996). Prognostic value of cadherin-associated molecules (alpha-, beta-, and gamma-catenins and p120cas) in bladder tumors. Cancer Res. *56*, 4154–4158. .

Singh, R., and Cuervo, A.M. (2011). Autophagy in the cellular energetic balance. Cell Metab. *13*, 495–504. https://doi.org/10.1016/j.cmet.2011.04.004.

Singh, R., Kaushik, S., Wang, Y., Xiang, Y., Novak, I., Komatsu, M., Tanaka, K., Cuervo, A.M., and Czaja, M.J. (2009). Autophagy regulates lipid metabolism. Nature *458*, 1131–1135. https://doi.org/10.1038/nature07976.

Song, H.-I., and Yoon, M.-S. (2016). PLD1 regulates adipogenic differentiation through mTOR - IRS-1 phosphorylation at serine 636/639. Sci. Rep. *6*, 36968. https://doi.org/10.1038/srep36968.

Stahelin, R.V., Scott, J.L., and Frick, C.T. (2014). Cellular and molecular interactions of phosphoinositides and peripheral proteins. Chem. Phys. Lipids *182*, 3–18. https://doi.org/10.1016/j.chemphyslip.2014.02.002.

Starling, G.P., Yip, Y.Y., Sanger, A., Morton, P.E., Eden, E.R., and Dodding, M.P. (2016). Folliculin directs the formation of a Rab34– RILP complex to control the nutrient-dependent dynamic distribution of lysosomes. EMBO Rep. *17*, 823–841. https://doi.org/10.15252/embr.201541382.

Steffan, J.J., Dykes, S.S., Coleman, D.T., Adams, L.K., Rogers, D., Carroll, J.L., Williams, B.J., and Cardelli, J.A. (2014). Supporting a Role for the GTPase Rab7 in Prostate Cancer Progression. PLoS ONE *9*, e87882. https://doi.org/10.1371/journal.pone.0087882.

Steingrimsson, E., Tessarollo, L., Reid, S.W., Jenkins, N.A., and Copeland, N.G. (1998). The bHLH-Zip transcription factor Tfeb is essential for placental vascularization. Development *125*, 4607–4616. https://doi.org/10.1242/dev.125.23.4607.

Stoehr, R., Krieg, R.C., Knuechel, R., Hofstaedter, F., Pilarsky, C., Zaak, D., Schmitt, R., and Hartmann, A. (2002). No evidence for involvement of beta-catenin and APC in urothelial carcinomas. Int. J. Oncol. *20*, 905–911. .

Sullivan, W.J., Mullen, P.J., Schmid, E.W., Flores, A., Momcilovic, M., Sharpley, M.S., Jelinek, D., Whiteley, A.E., Maxwell, M.B., Wilde, B.R., et al. (2018). Extracellular Matrix Remodeling Regulates Glucose Metabolism through TXNIP Destabilization. Cell *175*, 117-132.e21. https://doi.org/10.1016/j.cell.2018.08.017.

Sung, H.-H., Telley, I.A., Papadaki, P., Ephrussi, A., Surrey, T., and Rørth, P. (2008). Drosophila Ensconsin Promotes Productive Recruitment of Kinesin-1 to Microtubules. Dev. Cell *15*, 866–876. https://doi.org/10.1016/j.devcel.2008.10.006.

Tam, C., Idone, V., Devlin, C., Fernandes, M.C., Flannery, A., He, X., Schuchman, E., Tabas, I., and Andrews, N.W. (2010). Exocytosis of acid sphingomyelinase by wounded cells promotes endocytosis and plasma membrane repair. J. Cell Biol. *189*, 1027–1038. https://doi.org/10.1083/jcb.201003053.

Teo, M.Y., Bambury, R.M., Zabor, E.C., Jordan, E., Al-Ahmadie, H., Boyd, M.E., Bouvier, N., Mullane, S.A., Cha, E.K., Roper, N., et al. (2017). DNA Damage Response and Repair Gene Alterations Are Associated with Improved Survival in Patients with Platinum-Treated Advanced Urothelial Carcinoma. Clin. Cancer Res. *23*, 3610–3618. https://doi.org/10.1158/1078-0432.CCR-16-2520.

The Cancer Genome Atlas Research Network (2014). Comprehensive molecular characterization of urothelial bladder carcinoma. Nature *507*, 315–322. https://doi.org/10.1038/nature12965.

Thomas, J., and Sonpavde, G. (2022). Molecularly Targeted Therapy towards Genetic Alterations in Advanced Bladder Cancer. Cancers *14*, 1795. https://doi.org/10.3390/cancers14071795.

Thompson, C.B. (2011). Rethinking the Regulation of Cellular Metabolism. Cold Spring Harb. Symp. Quant. Biol. *76*, 23–29. https://doi.org/10.1101/sqb.2012.76.010496.

Thoresen, S.B., Pedersen, N.M., Liestøl, K., and Stenmark, H. (2010). A phosphatidylinositol 3-kinase class III sub-complex containing VPS15, VPS34, Beclin 1, UVRAG and BIF-1 regulates cytokinesis and degradative endocytic traffic. Exp. Cell Res. *316*, 3368–3378. https://doi.org/10.1016/j.yexcr.2010.07.008.

Tian, T., Li, X., and Zhang, J. (2019). mTOR Signaling in Cancer and mTOR Inhibitors in Solid Tumor Targeting Therapy. Int. J. Mol. Sci. *20*, 755. https://doi.org/10.3390/ijms20030755.

Tran, L., Xiao, J.-F., Agarwal, N., Duex, J.E., and Theodorescu, D. (2021). Advances in bladder cancer biology and therapy. Nat. Rev. Cancer *21*, 104–121. https://doi.org/10.1038/s41568-020-00313-1.

Trivedi, P.C., Bartlett, J.J., and Pulinilkunnil, T. (2020). Lysosomal Biology and Function: Modern View of Cellular Debris Bin. Cells *9*, 1131. https://doi.org/10.3390/cells9051131.

Tsuruta, H., Kishimoto, H., Sasaki, T., Horie, Y., Natsui, M., Shibata, Y., Hamada, K., Yajima, N., Kawahara, K., Sasaki, M., et al. (2006). Hyperplasia and Carcinomas in Pten-Deficient

Mice and Reduced PTEN Protein in Human Bladder Cancer Patients. Cancer Res. *66*, 8389–8396. https://doi.org/10.1158/0008-5472.CAN-05-4627.

Urakami, S., Shiina, H., Enokida, H., Kawakami, T., Tokizane, T., Ogishima, T., Tanaka, Y., Li, L.-C., Ribeiro-Filho, L.A., Terashima, M., et al. (2006). Epigenetic inactivation of Wnt inhibitory factor-1 plays an important role in bladder cancer through aberrant canonical Wnt/beta-catenin signaling pathway. Clin. Cancer Res. Off. J. Am. Assoc. Cancer Res. *12*, 383–391. https://doi.org/10.1158/1078-0432.CCR-05-1344.

Uusi-Rauva, K., Kyttälä, A., van der Kant, R., Vesa, J., Tanhuanpää, K., Neefjes, J., Olkkonen, V.M., and Jalanko, A. (2012). Neuronal ceroid lipofuscinosis protein CLN3 interacts with motor proteins and modifies location of late endosomal compartments. Cell. Mol. Life Sci. *69*, 2075–2089. https://doi.org/10.1007/s00018-011-0913-1.

Vassilev, B., Sihto, H., Li, S., Hölttä-Vuori, M., Ilola, J., Lundin, J., Isola, J., Kellokumpu-Lehtinen, P.-L., Joensuu, H., and Ikonen, E. (2015). Elevated Levels of StAR-Related Lipid Transfer Protein 3 Alter Cholesterol Balance and Adhesiveness of Breast Cancer Cells. Am. J. Pathol. *185*, 987–1000. https://doi.org/10.1016/j.ajpath.2014.12.018.

Villar, V.H., Merhi, F., Djavaheri-Mergny, M., and Durán, R.V. (2015). Glutaminolysis and autophagy in cancer. Autophagy *11*, 1198–1208. https://doi.org/10.1080/15548627.2015.1053680.

Visvikis, O., Ihuegbu, N., Labed, S.A., Luhachack, L.G., Alves, A.-M.F., Wollenberg, A.C., Stuart, L.M., Stormo, G.D., and Irazoqui, J.E. (2014). Innate Host Defense Requires TFEB-Mediated Transcription of Cytoprotective and Antimicrobial Genes. Immunity *40*, 896–909. https://doi.org/10.1016/j.immuni.2014.05.002.

Vyas, J.M., Kim, Y.-M., Artavanis-Tsakonas, K., Love, J.C., Van der Veen, A.G., and Ploegh, H.L. (2007). Tubulation of Class II MHC Compartments Is Microtubule Dependent and Involves Multiple Endolysosomal Membrane Proteins in Primary Dendritic Cells. J. Immunol. *178*, 7199–7210. https://doi.org/10.4049/jimmunol.178.11.7199.

Wallerand, H., Bernhard, J.-C., Culine, S., Ballanger, P., Robert, G., Reiter, R.E., Ferrière, J.-M., and Ravaud, A. (2011). Targeted therapies in non-muscle-invasive bladder cancer according to the signaling pathways. Urol. Oncol. Semin. Orig. Investig. *29*, 4–11. https://doi.org/10.1016/j.urolonc.2009.07.025.

Wallroth, A., and Haucke, V. (2018). Phosphoinositide conversion in endocytosis and the endolysosomal system. J. Biol. Chem. *293*, 1526–1535. https://doi.org/10.1074/jbc.R117.000629.

Wang, T., and Hong, W. (2002). Interorganellar Regulation of Lysosome Positioning by the Golgi Apparatus through Rab34 Interaction with Rab-interacting Lysosomal Protein. Mol. Biol. Cell *13*, 4317–4332. https://doi.org/10.1091/mbc.e02-05-0280.

Wang, H., Ma, Q., Qi, Y., Dong, J., Du, X., Rae, J., Wang, J., Wu, W.-F., Brown, A.J., Parton, R.G., et al. (2019). ORP2 Delivers Cholesterol to the Plasma Membrane in Exchange for

Phosphatidylinositol 4, 5-Bisphosphate (PI(4,5)P2). Mol. Cell *73*, 458-473.e7. https://doi.org/10.1016/j.molcel.2018.11.014.

Wang, S., Chen, Y., Li, X., Zhang, W., Liu, Z., Wu, M., Pan, Q., and Liu, H. (2020). Emerging role of transcription factor EB in mitochondrial quality control. Biomed. Pharmacother. *128*, 110272. https://doi.org/10.1016/j.biopha.2020.110272.

Wang, W., Gao, Q., Yang, M., Zhang, X., Yu, L., Lawas, M., Li, X., Bryant-Genevier, M., Southall, N.T., Marugan, J., et al. (2015). Up-regulation of lysosomal TRPML1 channels is essential for lysosomal adaptation to nutrient starvation. Proc. Natl. Acad. Sci. *112*. https://doi.org/10.1073/pnas.1419669112.

Warburg, O. (1925). über den Stoffwechsel der Carcinomzelle. Klin. Wochenschr. *4*, 534–536. https://doi.org/10.1007/BF01726151.

Warburg, O. (1956). On the origin of cancer cells. Science *123*, 309–314. https://doi.org/10.1126/science.123.3191.309.

Whyard, T., Waltzer, W.C., Waltzer, D., and Romanov, V. (2016). Metabolic alterations in bladder cancer: applications for cancer imaging. Exp. Cell Res. *341*, 77–83. https://doi.org/10.1016/j.yexcr.2016.01.005.

Wieman, H.L., Wofford, J.A., and Rathmell, J.C. (2007). Cytokine Stimulation Promotes Glucose Uptake via Phosphatidylinositol-3 Kinase/Akt Regulation of Glut1 Activity and Trafficking. Mol. Biol. Cell *18*, 1437–1446. https://doi.org/10.1091/mbc.e06-07-0593.

Willett, R., Martina, J.A., Zewe, J.P., Wills, R., Hammond, G.R.V., and Puertollano, R. (2017). TFEB regulates lysosomal positioning by modulating TMEM55B expression and JIP4 recruitment to lysosomes. Nat. Commun. *8*, 1580. https://doi.org/10.1038/s41467-017-01871-z.

Wise, D.R., and Thompson, C.B. (2010). Glutamine addiction: a new therapeutic target in cancer. Trends Biochem. Sci. *35*, 427–433. https://doi.org/10.1016/j.tibs.2010.05.003.

Wong, Y.C., Ysselstein, D., and Krainc, D. (2018). Mitochondria-lysosome contacts regulate mitochondrial fission via RAB7 GTP hydrolysis. Nature *554*, 382–386. https://doi.org/10.1038/nature25486.

Wong, Y.C., Kim, S., Peng, W., and Krainc, D. (2019). Regulation and Function of Mitochondria–Lysosome Membrane Contact Sites in Cellular Homeostasis. Trends Cell Biol. *29*, 500–513. https://doi.org/10.1016/j.tcb.2019.02.004.

Wu, X.-R. (2005). Urothelial tumorigenesis: a tale of divergent pathways. Nat. Rev. Cancer *5*, 713–725. https://doi.org/10.1038/nrc1697.

Yang, L., Li, P., Fu, S., Calay, E.S., and Hotamisligil, G.S. (2010). Defective Hepatic Autophagy in Obesity Promotes ER Stress and Causes Insulin Resistance. Cell Metab. *11*, 467–478. https://doi.org/10.1016/j.cmet.2010.04.005.

Yang, S., Wang, X., Contino, G., Liesa, M., Sahin, E., Ying, H., Bause, A., Li, Y., Stommel, J.M., Dell'Antonio, G., et al. (2011). Pancreatic cancers require autophagy for tumor growth. Genes Dev. *25*, 717–729. https://doi.org/10.1101/gad.2016111.

Yoon, M.-S., Du, G., Backer, J.M., Frohman, M.A., and Chen, J. (2011). Class III PI-3-kinase activates phospholipase D in an amino acid–sensing mTORC1 pathway. J. Cell Biol. *195*, 435–447. https://doi.org/10.1083/jcb.201107033.

Yu, L., Wu, W.K.K., Gu, C., Zhong, D., Zhao, X., Kong, Y., Lin, Q., Chan, M.T.V., Zhou, Z., and Liu, S. (2016). Obatoclax impairs lysosomal function to block autophagy in cisplatin-sensitive and -resistant esophageal cancer cells. Oncotarget *7*, 14693–14707. https://doi.org/10.18632/oncotarget.7492.

Zhang, T., Guo, J., Li, H., and Wang, J. (2017). Meta-analysis of the prognostic value of p-4EBP1 in human malignancies. Oncotarget *9*, 2761–2769. https://doi.org/10.18632/oncotarget.23031.

Zhang, X., Chen, W., Gao, Q., Yang, J., Yan, X., Zhao, H., Su, L., Yang, M., Gao, C., Yao, Y., et al. (2019). Rapamycin directly activates lysosomal mucolipin TRP channels independent of mTOR. PLOS Biol. *17*, e3000252. https://doi.org/10.1371/journal.pbio.3000252.

Zhang, X.-M., Walsh, B., Mitchell, C.A., and Rowe, T. (2005). TBC domain family, member 15 is a novel mammalian Rab GTPase-activating protein with substrate preference for Rab7. Biochem. Biophys. Res. Commun. *335*, 154–161. https://doi.org/10.1016/j.bbrc.2005.07.070.

Zhang, Z.-T., Pak, J., Huang, H.-Y., Shapiro, E., Sun, T.-T., Pellicer, A., and Wu, X.-R. (2001). Role of Ha-ras activation in superficial papillary pathway of urothelial tumor formation. Oncogene *20*, 1973–1980. https://doi.org/10.1038/sj.onc.1204315.

Zhu, L., Somlo, G., Zhou, B., Shao, J., Bedell, V., Slovak, M.L., Liu, X., Luo, J., and Yen, Y. (2005). Fibroblast growth factor receptor 3 inhibition by short hairpin RNAs leads to apoptosis in multiple myeloma. Mol. Cancer Ther. *4*, 787–798. https://doi.org/10.1158/1535-7163.MCT-04-0330.

Zoncu, R., and Perera, R.M. (2022). Built to last: lysosome remodeling and repair in health and disease. Trends Cell Biol. *32*, 597–610. https://doi.org/10.1016/j.tcb.2021.12.009.

Zoncu, R., Bar-Peled, L., Efeyan, A., Wang, S., Sancak, Y., and Sabatini, D.M. (2011). mTORC1 Senses Lysosomal Amino Acids Through an Inside-Out Mechanism That Requires the Vacuolar H+-ATPase. Science *334*, 678–683. https://doi.org/10.1126/science.1207056.

Zuiverloon, T.C.M., de Jong, F.C., Costello, J.C., and Theodorescu, D. (2018). Systematic Review: Characteristics and Preclinical Uses of Bladder Cancer Cell Lines. Bladder Cancer Amst. Neth. *4*, 169–183. https://doi.org/10.3233/BLC-180167.

Appendix

Currently in revision for Communications Biology

Transcription Factor EB regulates phosphatidylinositol-3-phosphate levels on endomembranes and alters lysosome positioning in the bladder cancer model

Pallavi Mathur[1,2], Camilla De Barros Santos[1,2], Hugo Lachuer[1,2], Bruno Latgé[1,2], François Radvanyi[2,3], Bruno Goud[1,2], Kristine Schauer[1,2,4,*]

[1]Institut Curie, PSL Research University, Molecular Mechanisms of Intracellular Transport group, 75248 Paris, France
[2] Centre National de la Recherche Scientifique, UMR144, 75005 Paris, France
[3]Institut Curie, PSL Research University, Molecular Oncology group, 75248 Paris, France
[4]Institut Gustave Roussy, INSERM UMR1279, Université Paris-Saclay, 94805 Villejuif, France

[*]Corresponding author: Kristine Schauer; email: kristine.schauer@gustaveroussy.fr

Running title: Endosomal PIP level are under the control of TFEB

Keywords Lysosomes, cell organization, S6K, TFEB, phosphatidylinositol-3-phosphate

Abstract

Lysosomes orchestrate degradation and recycling of exogenous and endogenous material thus controlling cellular homeostasis. Little is known how this organelle changes during malignant transformation. We investigate the intracellular landscape of lysosomes in a cellular model of bladder cancer. Employing standardized cell culture on micropatterns we identify a phenotype of peripheral lysosome positioning prevailing in bladder cancer but not normal urothelium. We show that lysosome positioning is controlled by transcription factor EB (TFEB) with lysosomal dispersion resulting from TFEB activation downstream of lysosomal Ca^{2+} release. Mechanistically, TFEB regulates phosphatidylinositol-3-phosphate (PtdIns3P) levels on endomembranes which control recruitment of FYVE-domain containing proteins and dictate lysosomal positioning. This conceptually clarifies the dual role of TFEB as regulator of endosomal maturation and autophagy, two distinct processes controlled by PtdIns3P. Altogether, our findings uncover lysosome positioning as result of PtdIns3P activation downstream of TFEB as a potential biomarker for bladder cancer.

Statement of significance

Here we provide the first atlas for the landscape of the lysosomal compartment in bladder cancer and reveal the mechanistic role of TFEB in regulating endosomal PtdIns3P levels and subsequent lysosomal dispersion. We unveiled lysosomal positioning as a potential biomarker for malignant bladder cancer which might arise as an actionable target for cancer therapy.

Introduction

Accelerated cellular division and enhanced motility are pathological characteristics of malignant cells both leading to an increase in energetic demand. More than being the 'stomach' of eukaryotic cells for nutrient acquisition, late endosomes/lysosomes (referred to as lysosomes hereafter) have emerged as a cellular hub for metabolism and signaling (Ballabio and Bonifacino, 2020; Lawrence and Zoncu, 2019; Perera and Zoncu, 2016; Perera et al., 2019; Thelen and Zoncu, 2017) and play an important role during cancer development (Hämälistö and Jäättelä, 2016; Perera and Zoncu, 2016). Lysosomes are morphologically heterogeneous acidic compartments that are functionally similar to yeast and plant vacuoles. They are specialized in the degradation of extracellular molecules and pathogens internalized by endocytosis or phagocytosis, as well as the intracellular recycling of macromolecules and organelles sequestered by autophagy. In addition to the orchestration of cellular clearance, lysosomes play an important role in cellular nutrient availability controlled by the serine/threonine kinase complex of mammalian target of rapamycin complex 1 (mTORC1) (Saxton and Sabatini, 2017). Active mTORC1 assembles at the surface of lysosomes through the integration of chemically diverse nutrient and growth factor signaling to promote protein biosynthesis (Ballabio and Bonifacino, 2020; Saxton and Sabatini, 2017; Thelen and Zoncu, 2017) . Conversely, absence of nutrients triggers the dissociation and inactivation of mTORC1 and consequently to the activation of downstream catabolic pathways. Active mTORC1 targets MiT/TFE transcription factors, including transcription factor EB (TFEB) and MITF, that are both master regulators of lysosome biogenesis and autophagy (Settembre et al., 2011). MiT/TFE transcription factors have been implicated in the development of cancer, including renal cell carcinoma, pancreatic adenocarcinoma, sarcoma and melanoma, MITF being an

important oncogene in melanoma (Perera et al., 2019). Moreover, it has been shown that TFEB overexpression as well as a positive feedback mechanism between mTORC1 and TFEB was sufficient to promote cancer growth in mouse models (Calcagnì et al., 2016; Di Malta et al., 2017).

Although lysosomes are important for nutrient acquisition and the regulation of metabolism, both prerequisites for malignant growth, little is known how lysosomes change during cancer development. Here, we compare the intracellular landscape of the lysosomal compartment in a collection of bladder cancer cell lines to normal human urothelium (NHU). Bladder cancer represents one of the most frequently-diagnosed cancer types worldwide and is among the most common neoplasms in men in North America and Europe, thus representing an important health burden(Antoni et al., 2017). Bladder carcinomas are highly diverse and are classified into non-muscle-invasive bladder cancers (NMIBC) and muscle-invasive bladder cancers (MIBC) with luminal-like and basal-like subtypes (Choi et al., 2014; Rebouissou et al., 2014). NMIBC are often papillary (stage Ta) and low-grade but show a high recurrence rate (60%). Alternatively, NMIBC can be carcinoma in situ (CIS, stage Tis) showing flat lesions and frequent progression to invasive cancers (T1). MIBC are classified by stages T2-T4 and high-grade malignant transformation. Investigating the normal and pathologic landscape of lysosome positioning in cells representing different stages of bladder cancer, we here reveal organelle-level deregulation in malignant cells and identify TFEB as major regulator of phosphatidylinositol-3-phosphate (PtdIns3P) homeostasis in this context.

Results

High-grade bladder cancers are characterized by the peripheral positioning of lysosomes

Because of the importance of lysosomes in cellular homeostasis and their role in promoting cancer progression, we aimed at a systematic analysis of lysosome morphology in a panel of genetically diverse bladder cell lines in comparison to primary normal human urothelium (NHU) cells. We have analyzed the broadly studied bladder cancer cell lines RT4, MGHU3, RT112, KU19-19, T24, TCCSup and JMSU1 that represent the diversity of bladder carcinomas (Zuiverloon et al., 2018). RT4, MGHU3, RT112 represent low-grade, luminal cancers of the papillary subtype, whereas KU19-19 represents high-grade, basal cancers and T24, TCCSup and JMSU1 represent high-grade cancers of mixed subtypes (Warrick et al., 2016; Zuiverloon et al., 2018) . To compare these different cells at the morphological level, we cultured them on identical crossbow-shaped micropattern substrates. All tested cells were fully spread after 3 h of incubation, visualized by the average projection of the actin cytoskeleton (**Fig. S1A**), indicating that all cells adapted well to the micropatterns. We visualized the lysosomal compartment in all cells by immunofluorescence staining of the lysosomal-associated membrane protein 1 (LAMP1/CD107a) (**Fig. 1A**). Images were acquired in 3D and lysosomes were segmented to obtain quantitative information of their spatial organization, volume and numbers per cell. To visualize the average lysosome organization, we plotted 3D density maps (Duong et al., 2012; Schauer et al., 2010b) representing the smallest cellular volume that contains 50% of lysosomes (**Fig. 1B**). Notably, while in NHU cells lysosomes were positioned centrally, they were found to be spread out to the periphery in cancerous cells with the strongest phenotype exhibited in high-grade lines (**Fig. 1A, B**). Because the total cell area is standardized by the

micropattern and thus identical in all cells, we calculated the nearest neighbor distance (NND) of lysosomes in each cell. Concomitantly, whereas the average NND in low-grade RT4 and MGHU3 cells was not significantly different from NHU cells, those of all other analyzed cell lines was significantly increased (**Fig. 1C**), indicating that lysosomes are more scattered in these cells. No clear trend in the number of lysosomes per cell (**Fig. 1D**) or average volume (**Fig. 1E**) was found among the tested cell lines. However, lysosomal volume negatively correlated with lysosomal number (**Fig. S1B**), indicating that few large lysosomes are in balance with many small ones. Principal component analysis (PCA) of the transcriptome data of these cells indicated that replicates of the NHU clustered together and separately, and that RT4 and MGHU3 were the most different compared to the other cell lines (**Fig. S1C**). Comparison between selected low-grade MGHU3 (luminal-type and central lysosomes) and RT112 (luminal-type and scattered lysosomes), and high-grade KU19-19 (basal-type) and JMSU1 cells (mixed-type) in invasion assays into collagen matrix from spheroids revealed, as expected, that MHGU3 was the less invasive cell line (invasion at 5 d), followed by RT112 (invasion at 3 d), KU19-19 and finally JMSU1 that both invaded at 1 d with different efficiency (**Fig. S1D**). To verify that changes in lysosomal positioning were not induced by micropatterning, we additionally analyzed lysosomes in classical cell culture conditions in selected cell lines. We measured the averaged squared distance of lysosomes to the center of mass of the cell (statistical inertia) normalized to the cell size (**Fig. S1E,F**). In agreement with our density map and NND analysis, the lysosome dispersion significantly increased from MGHU3 to JMSU1 cells. Our analyses collectively indicate that the lysosomal compartment shows differences between NHU and bladder cancer cell lines. Whereas some low-grade bladder cancer cell lines reveal

central lysosomes similar to NHU cells, high-grade bladder cancer cells are characterized by a scattered, peripheral positioning of the lysosomal compartment.

Dispersed lysosomes reveal alterations in the mTORC1-TFEB signaling axis

Lysosomes are the cellular signaling platform for the mammalian target of rapamycin complex1 (mTORC1), a main regulator of metabolisms, proliferation and survival. Because mTORC1 is regulated by lysosomes positioning (Korolchuk et al., 2011; Perera and Zoncu, 2016), we tested whether altered lysosome landscape across different bladder cancer cell lines affected mTORC1 signaling. First, we analyzed mTORC1 localization by co-visualizing mTOR and LAMP1 by immunofluorescence and measuring the fraction of mTOR that localized on the LAMP1-positive compartment. We found that about 15-20 % of mTOR signal was found on lysosomes. Although RT112 showed slightly but significantly more mTOR on lysosomes, the levels of mTOR on lysosomes were comparable between the tested cell lines (**Fig. 2A, B**). Next, we tested mTORC1 activity monitoring the phosphorylation of the direct downstream substrate p70-S6 Kinase 1 (S6K1). Surprisingly, we found that less S6K1 was phosphorylated in high-grade as compared to low-grade cells although total S6K1 levels were similar in all cell lines (**Fig. 2C and S2A**). As expected, the mTORC1 inhibitor rapamycin (Dumont and Su, 1995; Liu et al., 2010) as well as starvation decreased S6K1 phosphorylation in all cell lines confirming mTORC1 specificity (**Fig. S2B**). Next, we tested another important mTORC1 substrate, the transcription factor EB (TFEB), which appears as a novel player in carcinogenesis (Calcagnì et al., 2016; Di Malta et al., 2017). We transfected cells with TFEB-EGFP and monitored its localization in cells 72 h post transfection. Whereas TFEB-EGFP showed cytosolic localization in MGHU3 and RT112 cells (40% of mean TFEB-EGFP intensity was

found in nucleus), more than 70% of the mean intensity of TFEB-EGFP was found in the nucleus of KU19-19 and JMSU1 cells (**Fig. 2D, E**). This nuclear localization indicated hyperactivation of TFEB in high-grade bladder cancer cells. Indeed, inspection of the gene expression of known TFEB-regulated genes such as *RAGD* and *TSC1* revealed an increase in the expression of these genes in high-grade as compared to low-grade cells (**Fig. S2C**). Inhibition of mTORC1 by rapamycin in low-grade RT112 led to a translocation of TFEB-EGFP to the nucleus (**Fig. 2F,G**) consistent with mTORC1-specific TFEB-EGFP phosphorylation. Contrary, activation of mTORC1 by U-18666 to stimulate phosphorylation of TFEB (Davis et al., 2021) in high-grade JMSU1 cells did not change TFEB-EGFP localization (**Fig. S2D, E**). It has been shown that the nuclear translocation of TFEB is additionally regulated through dephosphorylation by calcineurin (Medina et al., 2015). Calcineurin is activated by cytosolic calcium that is released from the lysosomes via mucolipin-1, also known as transient receptor potential cation channel, mucolipin subfamily, member 1 (TRPML1). Thus, we inhibited mucolipin-1 in high-grade bladder cancer cells using GW-405833 (ML-SI1) or incubated cells with the calcium chelator BAPTA for 2 h each. Both treatments led to the cytoplasmic translocation of TFEB-EGFP (**Fig. 2H, I**) indicating that increased dephosphorylation of TFEB by calcineurin in response to lysosomal calcium release strongly contributes to the nuclear accumulation of TFEB in high-grade bladder cancer cells. Together, our results indicate that peripheral lysosome positioning in high-grade KU19-19 and JMSU1 cells correlates with differences in the mTORC1-TFEB nutrient signaling pathway as compared to low-grade cell MGHU3 and RT112 although similar levels of mTORC1 recruitment on lysosomes was observed between the different grade cell lines. Moreover, our results depict an increased nuclear

localization of TFEB in high-grade KU19-19 and JMSU1 cells, thus, a possible transactivation of TFEB regulated genes.

Lysosome positioning changes are under the control of TFEB in bladder cancer cells

It has been previously reported that TFEB regulates lysosomal positioning (Willett et al., 2017), thus, we investigated whether increased nuclear translocation of TFEB in bladder cancer cell lines could lead to peripheral lysosome positioning. First, we tested whether stimulating nuclear translocation of TFEB in low-grade bladder cancer cells (RT112) triggered peripheral lysosome positioning. Cells were treated with rapamycin to induce TFEB nuclear translocation (**Fig. 2F,G and 3A**) and lysosomes were visualized by immunofluorescence against LAMP1. Inspection of classically cultured cells revealed recurrent accumulation of lysosomes at the cell periphery (**Fig. 3A**). To quantify this, we cultured cells on adhesive micropatterns and calculated the nearest neighbor distance (NND) of lysosomes in RT112 cells. Lysosomes were more dispersed after rapamycin treatment in micropatterned cells (**Fig. 3B**) and the average NND was significantly increased as compared to untreated controls (**Fig. 3C**). To specifically test the role of TFEB, we next targeted this member of the MiT/TFE family via RNA interference in high-grade (JMSU1) cells where TFEB is mostly nuclear. Silencing of TFEB by either a pool of four siRNAs or four individual siRNAs significantly reduced TFEB protein levels after 3 d and reversed the scattered lysosome phenotype in high-grade JMSU1 cells (**Fig. 3D and S3A-C**). Quantification on micropatterns revealed a significant decrease in the average NND of lysosomes (**Fig. 3E, F**) confirming TFEB-dependent regulation of lysosomes in these high-grade bladder cancer cells.

It has been shown that lysosomes translocate to the cell periphery upon overexpression of protrudin, and conversely, cluster perinuclearly upon protrudin depletion (Hong et al., 2017). Thus, we next tested whether recruitment of protrudin to lysosomes is TFEB-dependent. Again, we first induced nuclear translocation and thus activation of TFEB by rapamycin treatment of RT112 cells and visualized protrudin by immunofluorescence (**Fig. 3G**). Because protrudin is an ER- localized protein and only is found on lysosomes at ER-lysosome contact sites, we measured the fraction of protrudin that is found on LAMP1-positive lysosomes (**Fig. 3H**). We revealed that activation of TFEB significantly increased the fraction of protrudin found on lysosomes. Concomitantly, depletion of TFEB by siRNA in high-grade JMSU1 cells significantly reduced protrudin levels on LAMP1-positive lysosomes (**Fig. 3I, J**). Interestingly, protrudin gene expression was not up-regulated in high-grade cells (**Fig. S3D**), nor did the total protein level of protrudin change after rapamycin treatment in RT112 cells or when TFEB was targeted by siRNA in JMSU1 (**Fig. S3E, F**). This suggested that TFEB specifically regulated the recruitment of protrudin to lysosomes rather than its expression levels. Together our results indicate that lysosome positioning and protrudin recruitment on lysosomes in bladder cancer cells is under the control of TFEB.

TFEB regulates phosphatidylinositol-3-phosphate levels on endomembranes in bladder cancer cells

Recruitment of protrudin to lysosomes is regulated by the binding of its FYVE domain to phosphatidylinositol-3-phosphate (PtdIns3P) found on endomembranes (Hong et al., 2017). We thus tested whether TFEB could regulate lysosomal PtdIns3P levels. We expressed the PtdIns3P-binding FYVE domain from the human homologue of the hepatocyte growth factor-regulated tyrosine kinase substrate Hrs, duplicated in

tandem as an EGFP fusion construct (EGFP-FYVE) and monitored total level of this construct on LAMP1-positive lysosomes upon knock down of TFEB. PtdIns3P is found on early and late endosomes, thus as expected, EGFP-FYVE showed an endosomal staining but only partially colocalized with lysosomes (**Fig. 4A**). Silencing of TFEB by siRNA significantly decreased the fraction of EGFP-FYVE that was found on Lamp1-positve lysosomes in high-grade JMSU1 cells (**Fig. 4B**). Moreover, measuring the global cellular level of EGFP-FYVE showed a significant reduction on endomembranes after knock down of TFEB (**Fig. 4C, D**).

To further validate the TFEB regulated recruitment of PtdIns3P-binding proteins to endosomal membranes, we analyzed EEA1, a well-studied FYVE containing protein. Consistent with protrudin, we found a significant increase of EEA1 on endomembranes upon treatment of low-grade RT112 cells with rapamycin and activation of TFEB (**Fig. S4A, B**). Addition of the protein translation inhibitor cycloheximide along with rapamycin treatment abolished the increase of EEA1 on endomembranes. Surprisingly, total EEA1 protein levels did not change under tested conditions (**Fig. S4A-C**) although EEA1 expression has been previously described to be under the control of TFEB (Nnah et al., 2019). No increase of endosomal EEA1 was observed in the first 4 h after rapamycin treatment (**Fig. S4D-F**). Conversely, gene silencing of TFEB in high-grade JMSU1 cells significantly decreased EEA1 levels on endosomes without affecting the total amount of EEA protein level (**Fig. S4G-I**).

Finally, we tested the role of endosomal PtdIns3P levels on protein recruitment and lysosome positioning. As expected, inhibition of phosphatidylinositol-3-phosphate kinases by wortmannin in high-grade JMSU1 cells strongly depleted EEA1 from endosomes (**Fig. 4E, F**) mimicking the phenotype of TFEB knock down (**Fig. S4G-I**). Moreover, wortmannin treatment induced the central clustering of lysosomes in JMSU1

cells, leading to a significant reduction of the NND of lysosomes (**Fig. 3E, F**). This showed that dispersion of lysosomes towards cell periphery requires endosomal PtdIns3P. Altogether, our results indicate that endosomal PtdIns3P levels dictate lysosomal positioning and are regulated by TFEB in high-grade bladder cancer.

Discussion

Our study identifies and characterizes a novel cellular phenotype of aggressive malignancy in a cellular model of bladder cancer. We show that the lysosomal compartment is scattered to the cell periphery in all analyzed high-grade bladder cancer cells, a phenotype that we did not see in normal urothelial cells. This is different to the previously described expansion of the lysosomal compartment, characterized by an increase in volume or numbers of lysosomes in pancreatic ductal adenocarcinoma (PDA) and indicative of increased lysosome biogenesis (Perera et al., 2015). Moreover, lysosome positioning changes are correlated with changes in mTORC1 signaling that assembles on lysosomes. In high-grade cells, the classic mTORC1 substrate p70-S6K1 was less phosphorylated, and TFEB translocated to the nucleus, potentially due to either reduced phosphorylation by mTORC1 or increased dephosphorylation by the calcium-dependent phosphatase, calcineurin (Medina et al., 2015). Deregulation of mTORC1 signaling and TFEB hyper-activation parallels previous studies in other cancer types (Bar-Peled et al., 2013; Di Malta et al., 2017; Perera and Zoncu, 2016; Perera et al., 2019; Zoncu et al., 2011) and aligns with a genetic study of NMIBC that identified alterations in mTORC1 signaling in several bladder cancer subtypes (Hurst et al., 2017).

Peripheral dispersion of lysosomes has been previously reported in prostate cancer cells due to the acidification of the extracellular milieu (Steffan et al., 2009). Such a mechanism is unlikely in the case of bladder cancer cells, because all cells used

in this study were grown in the same pH-buffering medium. Reports that TFEB regulated lysosome positioning (Medina et al., 2011; Willett et al., 2017), and the fact that peripheral lysosomes correlated with a hyperactivated TFEB phenotype (nuclear localization of TFEB-GFP), let us to investigate if TFEB regulated lysosome positioning in bladder cancer cells. We found that induction of nuclear TFEB by rapamycin in low-grade RT112 cells induced lysosomal dispersion. Conversely, knockdown of TFEB in high-grade JMSU1 cells with nuclear TFEB-GFP induced perinuclear clustering of lysosomes. Thus, our results confirm that lysosome positioning is under the regulation of TFEB in the bladder cancer model.

TFEB is a key transcription factor that orchestrates the expression of many genes involved in metabolism (Sardiello et al., 2009; Settembre et al., 2013) but also in intracellular trafficking of organelles (Nnah et al., 2019). Investigating the molecular mechanisms by which TFEB controls lysosome positioning, we discovered that TFEB regulates endosomal PtdIns3P levels that leads to enhanced recruitment of FYVE-containing proteins such as protrudin. Protrudin is known to bind to PtdIns3P on endosomes at membrane contact sites with the endoplasmic reticulum (ER) and to recruit the kinesin-1 adaptors FYCO1 to promote the microtubule-dependent translocation of endosomes to the cell periphery (Pedersen et al., 2020; Raiborg et al., 2015). However, several alternative pathways for anterograde lysosome trafficking have been described that all require endosomal PtdIns3P and could additionally be harnessed by cancer cells. The alternative kinesin-1 adaptor SKIP (also known as PLEKHM2) also contains three lipid-binding pleckstrin homology (PH) that conceivably could bind to lysosomal PtdIns3P. Moreover, KIF16B, a highly processive kinesin-3 family member that participates in the trafficking of endosomes along microtubules contains a PX (Phox homology) motif binding PtdIns3P (Pyrpassopoulos et al., 2017). Importantly,

whereas we only observed a moderate change in the protein levels of the direct TFEB target EEA1 after knock down of TFEB, our data indicates that the upregulation of endosomal PtdIns3P levels is transcriptionally regulated. Indeed, increase of endosomal FYVE-protein recruitment was not obvious in the first 4 hours after nuclear TFEB induction and was abolished upon the protein translation inhibitor cycloheximide (**Fig. S4 A-F**). PtdIns3P formation depends on either the class II phosphatidylinositol 3-kinase (PI3K) PI3KC2A, or the class III PI3K Vps34 (or PIK3C3) (Burke, 2018). Although no experimental evidence currently shows that TFEB regulates the expression of class III PI3 kinase, it has been shown in skeletal muscles that TFEB overexpression induced the expression of several PI kinases subunits, for instance, PIK3CD, PIK3C2A (Mansueto et al., 2017). Moreover, TFEB is known to regulate genes involved in lipid catabolism in liver and skeletal muscle (Settembre et al., 2013), some via co-induction of peroxisome proliferator-activated receptor-γ coactivator1α (PGC1α) and peroxisome proliferator-activated receptors (PPAR). Because PIP metabolism is complex and dynamic, additional studies are required to reveal the specific mechanisms of PtdIns3P increase.

Interestingly, it has been shown that endosomal PtdIns3P levels regulate mTORC1 recruitment and signaling via amino acids and stimulation of class III PI3K/Vps34-mediated PtdIns3P synthesis (Gulati and Thomas, 2007). PtdIns3P also facilitates lysosomal recruitment of phospholipase D1 (PLD1) via its PX domain that produces phosphatidic acid, which triggers dissociation of the inhibitory DEPTOR subunit from mTORC1 (Song and Yoon, 2016). Additionally, the PtdIns3P3-phosphatase MTMR3 interacts with mTORC1, and overexpression of this enzyme inhibits mTORC1 activity (Hao et al., 2016). Finally, the formation of phosphatidylinositol 3,5-bisphosphate (PtdIns3,5P_2) from PtdIns3P regulates mTORC1

via raptor (Bridges et al., 2012). As increased endosomal PtdIns3P levels globally activate mTORC1 that deactivates TFEB, we speculate that PtdIns3P could be part of a feedback loop in the mTORC1/TFEB signaling axis. Indeed, TFEB has been shown to feedback on mTORC1 (Nnah et al., 2019). Our current understanding is that nutrient status, pH and growth factors assemble a sophisticated machinery on the surface of lysosomes to integrate the different inputs upstream of mTORC1 (Ballabio and Bonifacino, 2020; Lawrence and Zoncu, 2019; Shin and Zoncu, 2020). Because PtdIns3P and several motor proteins/adapters are part of this machinery, mTORC1 signaling is coupled with lysosome positioning (Korolchuk et al., 2011). Our data are consistent with the following model: In high-grade bladder cancer cells, TFEB localization is mostly nuclear. Nuclear presence of TFEB and its transcription activity leads to an increase in PtdIns3P levels on different endomembranes, including lysosomes. This increase leads to the recruitment of FYVE-domain containing proteins such as EEA1 and protrudin and supports anterograde movement of lysosomes. The anterograde movement gives rise to the typical signature of peripheral lysosomes that we find in all studied high-grade bladder cancer cells. Peripheral lysosomes have been shown to recruit more mTORC1 and increase phosphorylation of downstream substrates (Hong et al., 2017; Korolchuk et al., 2011; Perera and Zoncu, 2016). This would allow a feedback control of TFEB by mTORC1. However, this seems not to occur in high-grade bladder cancer cells, because mTOR levels on lysosomes do not increase, and another mTORC1 substrate (S6K) shows less phosphorylation. Instead, the efficient calcium-dependent dephosphorylation of TFEB hinders its cytoplasmic translocation and control by mTORC1 in bladder cancer cells. Together, our results provide a mechanistic explanation to the characteristic cellular phenotype of lysosome dispersion in high-grade bladder cancer cells. Yet, further studies will be required to reveal in detail the

deregulation of the mTORC1/TFEB axis in different bladder cancer cells. In addition to signaling, lysosome positioning has been implicated in the regulation of protease secretion/proteolysis (Pedersen et al., 2020), migration (Dozynkiewicz et al., 2012; Pu et al., 2015, 2016; Schiefermeier et al., 2014) and remodeling of the tumor environment through the release of exosomes (Hyenne et al., 2017). Thus, it is tempting to speculate that altered lysosome signaling could link dysfunctional cancer cell metabolism with cancer invasiveness.

In addition to revealing a novel cellular phenotype characteristic of cancer cells together with the underlying molecular mechanism, our results uncover a novel role of TFEB in regulating PtdIns3Ps levels on endosomes. Several studies have illustrated the crucial role of TFEB in regulating fundamental but distinct cellular processes such as endocytosis, lysosomal biogenesis and autophagy. Because these different compartments of the endolysosomal system retain their identities based on the lipid composition of their membranes and are regulated by PtdIns3P levels, our results conceptually clarify the role of TFEB as regulator of endosomal maturation.

Material and methods

Cell culture and treatments

Bladder cancer cells lines MGHU3, RT112, KU19-19, JMSU1, T24 and TCCSup were grown in RPMI-1640 medium (Life Technologies, Carlsbad, CA, USA), supplemented with 10% Fetal Bovine Serum (FBS; Eurobio, Courtaboeuf, France). Normal human urothelium (NHU) cells were from Jennifer Southgate (University of York, UK). NHU were grown in KSFMC medium according to (Southgate et al., 1994). For experiments with inhibitors, as per the experiment either the day after cell seeding or after transfection respective drugs were added for incubation time of 24 h or as indicated and cells were incubated, at 37ºC. The concentration of inhibitors used were as follows: rapamycin (10 μM), wortmannin (1 μM, 2 h), ML-SI1 (20 μM, 3 h), BAPTA AM (10μM, 3 h) and cycloheximide (20 μg/mL). For starvation experiments, the day after cell seeding, the medium was removed and cells were washed once with EBSS (Earle's Balanced Salt Solution) and incubated in EBSS for 4 or 24 h, as per the experiment, before lysate preparation or cell fixation with 4% PFA.

Cell transfection

For RNA interference studies, 200,000 cells were transfected in 12 well plate with 25 pmol siRNA (siTFEB : ON-TARGETplus Human TFEB, L-009798-00-0005, Dharmacon^{TM}) using Lipofectamine RNAiMAX Transfection Reagent (1:200; Life Technologies). Cells were incubated 72 h at 37°C prior to further manipulation or drug treatment. Efficiency of gene silencing was verified by western blot of cell lysate after three days of transfection.

For plasmid transfection, 200,000 cells were transfected in a 12 well plate. Transfection was performed using Lipofectamine LTX with Plus reagent (Invitrogen) using 1 μg of

plasmid. pEGFP-N1-TFEB plasmid was a gift from Shawn Ferguson (Addgene plasmid # 38119; http://n2t.net/addgene:38119; RRID:Addgene_38119n (Roczniak-Ferguson et al., 2012)) or EGFP-2X FYVE plasmid (kind gift from B. Payrastre, Toulouse). 48 h post transfection, cells were trypsinized and transferred to sterilized coverslips (12 mm) in 1 mL medium in 12 well plate. Cells were fixed with 4%PFA 72 h after transfection and used for immunofluorescence and imaging.

Micro-array analysis

Micro array data were analyzed with R (3.5.2). The annotation was performed using affy package (1.58.0) with a custom CDF (Chip Description File) from brain array (huex10st, genome version 23). Normalization was done with RMA algorithm using affy library (Gautier et al., 2004) and batch effect corrected with ComBat (Johnson et al., 2007). The PCA was computed from these normalized and corrected data.

Micropatterned coverslips preparation and cell seeding

Micropattern production was as previously described (Duong et al., 2012; Schauer et al., 2010a) using photo-lithography methods. Briefly, coverslips were coated with Poly-L-Lysine(20)-grafted[3.5]-Polyethyleneglycol(2) (PLL-g-PEG) from SuSoS (Dübendorf, Switzerland) at a final concentration of 0.1 mg/mL in 10 mM HEPES (pH 7,3) solution. Coverslips were exposed to deep UV during 5 min using a photomask containing arrays of crossbows (37 µm diameter, 7 µm thick). Prior to cell seeding, the patterned surface was incubated for 1 h with a mixture of 50 µg/mL fibronectin (Sigma-Aldrich, St. Louis, MO, USA), 5 µg/mL concanavalin A (Sigma-Aldrich, St. Louis, MO, USA) and 1 µg/mL fibrinogen–Cy5 (Invitrogen). Cells were seeded on micropatterns in RPMI medium supplemented with 20 mM HEPES (Life Technologies)

for 4 h prior the experiment.

Invasion assay

Cells were trypsinized and 10^4 cells/ml were re-suspended in RPMI medium containing 10% FBS and 1% Penicillin-Streptomycin (Life Technologies). Then 100 µl of cell suspension was plated in 48-well plates coated with 1% agarose (Life Technologies) and incubated for 3 days. In each well, a spheroid was formed from 10^3 cells. Next, the spheroids were plated on Lab-Tek chambers (Sigma), in a mixture of collagen I from rat tail (Corning) at a final concentration of 2 mg/ml, PBS, sodium hydroxide (NaOH) and serum-free medium. The spheroids were monitored for 5 consecutive days by using an inverted Leica microscope (Wetzlar, Alemanha) equipped with camera device using 4x objective.

Immunofluorescence

Cells were fixed with 4 % formaldehyde for 15 min at room temperature, washed three times with PBS and permeabilized in PBS containing 0.2% BSA and 0.05% saponin. Cells were then incubated with the primary antibodies (mouse monoclonal antibody against Lamp1/CD107a (555798, BP Pharmingen™), rabbit mAb against mTOR (7C10, #2983, Cell Signaling Technology), EEA1 (610456, BD Biosciences), protrudin / ZFYVE27 (12680-1-AP, Proteintech) and Alexa Fluor 488, or Alexa Fluor 647 or Cy3-coupled secondary antibodies (Jackson ImmunoResearch) for 1 h. Actin was visualized by FluoProbes 547H (557/572nm) coupled Phalloïdin (Interchim) and nuclei with 0.2 µg/mL 4',6-diamidino-2-phenylindole (DAPI; Sigma-Aldrich). Coverslips were mounted in Mowiol (Sigma-Aldrich).

Western Blot

250,000 cells were seeded in a 12 well plate one day prior to the experiment. Drug treatments or knock-down experiments were performed as mentioned before. Equal volumes of lysate from each cell line was loaded on a 10% or 12% polyacrylamide gel, resolved by SDS-PAGE and electrotransferred to nitrocellulose membranes. Membranes were incubated with primary antibodies at 4ºC overnight: Phospho P-70 (Thr389)-S6K (CST: 9205S, 1:1000 in 5% BSA in TBST), P-70 S6K (CST: 9202S, 1:1000 in 5% milk in TBST), GAPDH (Sigma: G9545, 1:10,000 in 5% milk in TBST), EEA1(610456, BD Biosciences, 1:500 in 5% milk in TBST), protrudin (ZFYVE27, Proteintech 12680-1-AP) and species specific HRP secondary antibodies (1:10,000) for 1 hour at room temperature, following ECL western blotting substrate.

Image acquisition

Images for immunolabelled cells on micropatterns were acquired with an inverted wide field Deltavision Core Microscope (Applied Precision) equipped with highly sensitive cooled interlined charge-coupled device (CCD) camera (CoolSnap Hq2, Photometrics). Z-dimension series were acquired every 0.5 µm.

Images for non-pattered immuolabelled cells were acquired with a spinning disk confocal microscope (Inverted Eclipse Ti-E (Nikon) + spinning disk CSU-X1 (Yokogawa) integrated with Metamorph software by Gataca Systems). Cells were imaged as Z-stacks with 0.2 µm distance and 12 µm total height.

Image processing and analysis

For cells on micropatterns, several tens of single cell images were aligned using the coordinates of the micropattern (determined on ImageJ (Bethesda, MD, USA) as

previously described (Grossier et al., 2014; Schauer et al., 2010b). To extract the 3D spatial coordinates of lysosomes, images were segmented with the multidimensional image analysis (MIA) interface on MetaMorph (Molecular Devices, Sunnyvale, CA, USA) based on wavelet decomposition. The coordinates of the segmented structures were processed for density estimation programmed in the ks library in R according to (Schauer et al., 2010b). For visualizing kernel density estimates, probability contours were visualized using the extension libraries mvtnorm, rgl, and miscd.

Levels of lysosome dispersion in non patterned MGHU3, RT112, KU19-19 and JMSU1 cells were measured using statistical inertia (=averaged squared distance to the center of mass). To control for variations in cell size differences, normalization to cell size has been applied. Lysosome coordinates have been divided by the coordinates of the center of the mass (setting the center mass at x=1, y=1). This quantifies the dispersing of the lysosome structures independently of homogeneous dilations due to cell size. To test statistical significance, a Kruskal-Wallis test with Dunn post-hoc test with Sidak correction for multiple comparisons has been applied.

Image analysis for the figures (2B, 3H, J, 4 B,D,F and S4B, E, H) was done using CellProfiler (version: 3.1.9) on one Z-plane of the images. The pipelines for different analysis were prepared as follows:

To detect the total and membrane bound intensities of protein of interest (labelled as total integrated intensity or spots/total, respectively, in the figures) or intensities of co-localized proteins the pipeline was created as follows:

Step 1: Module '*EnhanceorSuppressFeatures*' was applied to channels where the objects needs to be segmented, either to obtain their intensities or objects for the intensities of co-localized proteins, to get sharp and defined objects which makes segmentation easier (for eg. On channels with LAMP1 or EEA1 or GFP-FYVE).

Step 2: Nucleus was identified in the DAPI channel using the '*IndentifyPrimaryObject*' module

Step 3: Module '*IndentifyPrimaryObject*' was used again on the images obtained from Step 1 to segments objects whose measurements are required (such LAMP1, EEA1, EGFP-FYVE)

Step 4: Cells were segmented using the '*IdentifySecondaryObject*' module with nucleus as the 'primary object' (identified in step 2) and using phalloidin or another cytoplasmic protein channel to recognize the cell boundaries.

Step 5: Module '*RelateObjects'* was used to relate the objects obtained in step 3 to each cell obtained in Step 4. Output of this channel was saved as another object which gives the objects of protein of interest per cell.

Step 6: Objects from step 3 were masked on the channel whose co-location or membrane bound fraction had to be calculated using the '*MaskImage*' module. (for eg: to calculate EGFP-FYVE on lysosomes in Fig. 4B, Lysosomes were segmented in step 3 and the output objects were masked on EGFP-FYVE channel or to calculate membrane bound EGFP-FYVE, segmentation of EGFP-FYVE objects from step 3 was masked on EGFP-FYVE channel)). Output of this step was saved as a new image in the pipeline.

Step 7: '*MeasureObjectIntensity*' module was used to obtain total 'per cell intensity' and 'intensity on spots' of protein of interest. Intensities were picked from images from step 6 and raw images of channel of interest using cells from step 4 as the objects.

Step 8: Cell size was obtained using the module '*MeasureObjectSizeandShape*' on the cells segments in Step 4 as the objects

Step 9: Finally, all the measurements were exported to the excel sheet using the module '*ExporttoSpreadsheet*'

Step 10: The final values were exported to a csv file named 'cell'. This file had the values of cell size (in pixels), total intensity of protein of interest per cell, intensity of protein of interest on spots and intensity of co-localized protein on the object of interest (eg: GFP-FYVE on lysosomes). Integrated intensities were used for the analysis and to plot the graphs.

Statistical analysis

The statistical analysis of endolysosome volume, number and normalized NND was performed with R (3.6.0). For NND analysis, the centroids distance between structures was calculated from a constant number of lysosomes that was randomly sampled from each cell. Therefore, variation in NNDs cannot be imputed to variation in the number of lysosomes but to bona-fide variation of their spatial organization. The statistical analysis was a Kruskal-Wallis test with Dunn test for multiple comparisons correction.

For all experiment, a large number of cells were monitored from 3 to 6 independent experiments. Two-sided Mann-Whitney U test were performed for 2 conditions comparisons. For multiple comparisons, a Kruskal-Wallis has been used with Dunn's test for multiple comparisons. Additionally, to compare the global distribution of cell population, χ^2 tests were performed (R function "chi-square()") and Benjamini-Hochberg multiple comparison correction has been applied. For the statistical analysis on the data from CellProfiler, Prism was used. Mann-Whitney U test was applied for the two conditions comparison or Kruskall-Wallis test with Dunn test for multiple comparison.

Acknowledgements

We thank Jennifer Southgate (University of York, UK) for her gift of NHU cell extracts and Clémentine Krucker and Yann Neuzillet (Foch Hospital, France) for deriving these cells. We thank Elodie Chapeaublanc for help on the bioinformatics and Oliver Kepp for critical reading of the manuscript. The authors greatly acknowledge the Cell and Tissue Imaging Facility (PICT-IBiSA @Burg and @Pasteur) and the Nikon Imaging Center at Institut Curie (Paris) that are member of the French National Research Infrastructure France-BioImaging (ANR10-INBS-04). This project was supported by grants from the European Union's Horizon 2020 research and innovation program under the Marie Skłodowska-Curie grant agreement n° 666003 to PM; Capes/ Ciência sem Fronteiras/ Process (9121137) to CDBS; Grants from Fondation ARC pour la recherche sur le cancer to KS and HL, Institut Curie SIRIC grant to KS, Agence Nationale de la Recherche (#2010 BLAN 122902), the ITMO Nanotumor grant to KS, the Centre National de la Recherche Scientifique and Institut Curie. The Goud team is member of the Labex Cell(n)Scale (11-LBX-0038) and the Idex Paris Sciences et Lettres (ANR-10-IDEX-0001-02 PSL). The Molecular Oncology team (FR) is supported by La Ligue Contre le Cancer (Equipe labellisée program).

Conflict of Interest Statement

The authors declare no potential conflicts of interest.

References

Antoni, S., Ferlay, J., Soerjomataram, I., Znaor, A., Jemal, A., and Bray, F. (2017). Bladder Cancer Incidence and Mortality: A Global Overview and Recent Trends. Eur. Urol. *71*, 96–108.

Ballabio, A., and Bonifacino, J.S. (2020). Lysosomes as dynamic regulators of cell and organismal homeostasis. Nat. Rev. Mol. Cell Biol. *21*, 101–118.

Bar-Peled, L., Chantranupong, L., Cherniack, A.D., Chen, W.W., Ottina, K.A., Grabiner, B.C., Spear, E.D., Carter, S.L., Meyerson, M., and Sabatini, D.M. (2013). A Tumor Suppressor Complex with GAP Activity for the Rag GTPases That Signal Amino Acid Sufficiency to mTORC1. Science *340*, 1100–1106.

Bridges, D., Ma, J.-T., Park, S., Inoki, K., Weisman, L.S., and Saltiel, A.R. (2012). Phosphatidylinositol 3,5-bisphosphate plays a role in the activation and subcellular localization of mechanistic target of rapamycin 1. Mol. Biol. Cell *23*, 2955–2962.

Burke, J.E. (2018). Structural Basis for Regulation of Phosphoinositide Kinases and Their Involvement in Human Disease. Mol. Cell *71*, 653–673.

Calcagnì, A., Kors, L., Verschuren, E., De Cegli, R., Zampelli, N., Nusco, E., Confalonieri, S., Bertalot, G., Pece, S., Settembre, C., et al. (2016). Modelling TFE renal cell carcinoma in mice reveals a critical role of WNT signaling. ELife *5*.

Choi, W., Porten, S., Kim, S., Willis, D., Plimack, E.R., Hoffman-Censits, J., Roth, B., Cheng, T., Tran, M., Lee, I.-L., et al. (2014). Identification of Distinct Basal and Luminal Subtypes of Muscle-Invasive Bladder Cancer with Different Sensitivities to Frontline Chemotherapy. Cancer Cell *25*, 152–165.

Davis, O.B., Shin, H.R., Lim, C.-Y., Wu, E.Y., Kukurugya, M., Maher, C.F., Perera, R.M., Ordonez, M.P., and Zoncu, R. (2021). NPC1-mTORC1 Signaling Couples Cholesterol Sensing to Organelle Homeostasis and Is a Targetable Pathway in Niemann-Pick Type C. Dev. Cell *56*, 260-276.e7.

Di Malta, C., Siciliano, D., Calcagni, A., Monfregola, J., Punzi, S., Pastore, N., Eastes, A.N., Davis, O., De Cegli, R., Zampelli, A., et al. (2017). Transcriptional activation of RagD GTPase controls mTORC1 and promotes cancer growth. Science *356*, 1188–1192.

Dozynkiewicz, M.A., Jamieson, N.B., Macpherson, I., Grindlay, J., van den Berghe, P.V.E., von Thun, A., Morton, J.P., Gourley, C., Timpson, P., Nixon, C., et al. (2012). Rab25 and CLIC3 collaborate to promote integrin recycling from late endosomes/lysosomes and drive cancer progression. Dev. Cell *22*, 131–145.

Dumont, F.J., and Su, Q. (1995). Mechanism of action of the immunosuppressant rapamycin. Life Sci. *58*, 373–395.

Duong, T., Goud, B., and Schauer, K. (2012). Closed-form density-based framework for automatic detection of cellular morphology changes. Proc. Natl. Acad. Sci. U. S. A. *109*, 8382–8387.

Gautier, L., Cope, L., Bolstad, B.M., and Irizarry, R.A. (2004). affy--analysis of Affymetrix GeneChip data at the probe level. Bioinformatics *20*, 307–315.

Grossier, J.-P., Xouri, G., Goud, B., and Schauer, K. (2014). Cell adhesion defines the topology of endocytosis and signaling. EMBO J. *33*, 35–45.

Gulati, P., and Thomas, G. (2007). Nutrient sensing in the mTOR/S6K1 signalling pathway. Biochem. Soc. Trans. *35*, 236–238.

Hämälistö, S., and Jäättelä, M. (2016). Lysosomes in cancer-living on the edge (of the cell). Curr. Opin. Cell Biol. *39*, 69–76.

Hao, F., Itoh, T., Morita, E., Shirahama-Noda, K., Yoshimori, T., and Noda, T. (2016). The PtdIns3-phosphatase MTMR3 interacts with mTORC1 and suppresses its activity. FEBS Lett. *590*, 161–173.

Hong, Z., Pedersen, N.M., Wang, L., Torgersen, M.L., Stenmark, H., and Raiborg, C. (2017). PtdIns3P controls mTORC1 signaling through lysosomal positioning. J. Cell Biol. *216*, 4217–4233.

Hurst, C.D., Alder, O., Platt, F.M., Droop, A., Stead, L.F., Burns, J.E., Burghel, G.J., Jain, S., Klimczak, L.J., Lindsay, H., et al. (2017). Genomic Subtypes of Non-invasive Bladder Cancer with Distinct Metabolic Profile and Female Gender Bias in KDM6A Mutation Frequency. Cancer Cell *32*, 701-715.e7.

Hyenne, V., Lefebvre, O., and Goetz, J.G. (2017). Going live with tumor exosomes and microvesicles. Cell Adhes. Migr. *11*, 173–186.

Johnson, W.E., Li, C., and Rabinovic, A. (2007). Adjusting batch effects in microarray expression data using empirical Bayes methods. Biostatistics *8*, 118–127.

Korolchuk, V.I., Saiki, S., Lichtenberg, M., Siddiqi, F.H., Roberts, E.A., Imarisio, S., Jahreiss, L., Sarkar, S., Futter, M., Menzies, F.M., et al. (2011). Lysosomal positioning coordinates cellular nutrient responses. Nat. Cell Biol. *13*, 453–460.

Lawrence, R.E., and Zoncu, R. (2019). The lysosome as a cellular centre for signalling, metabolism and quality control. Nat. Cell Biol. *21*, 133–142.

Lin, C.-W., Lin, J.C., and Prout, G.R. (1985). Establishment and Characterization of Four Human Bladder Tumor Cell Lines and Sublines with Different Degrees of Malignancy. Cancer Res. *45*, 5070–5079.

Liu, Q., Chang, J.W., Wang, J., Kang, S.A., Thoreen, C.C., Markhard, A., Hur, W., Zhang, J., Sim, T., Sabatini, D.M., et al. (2010). Discovery of 1-(4-(4-Propionylpiperazin-1-yl)-3-(trifluoromethyl)phenyl)-9-(quinolin-3-yl)benzo[h][1,6]naphthyridin-2(1 *H*)-one as a Highly Potent, Selective Mammalian Target of Rapamycin (mTOR) Inhibitor for the Treatment of Cancer. J. Med. Chem. *53*, 7146–7155.

Mansueto, G., Armani, A., Viscomi, C., D'Orsi, L., De Cegli, R., Polishchuk, E.V., Lamperti, C., Di Meo, I., Romanello, V., Marchet, S., et al. (2017). Transcription Factor EB Controls Metabolic Flexibility during Exercise. Cell Metab. *25*, 182–196.

Marshall, C.J., Franks, L.M., and Carbonell, A.W. (1977). Markers of Neoplastic Transformation in Epithelial Cell Lines Derived From Human Carcinomas. JNCI J. Natl. Cancer Inst. *58*, 1743–1751.

Medina, D.L., Fraldi, A., Bouche, V., Annunziata, F., Mansueto, G., Spampanato, C., Puri, C., Pignata, A., Martina, J.A., Sardiello, M., et al. (2011). Transcriptional Activation of Lysosomal Exocytosis Promotes Cellular Clearance. Dev. Cell *21*, 421–430.

Medina, D.L., Di Paola, S., Peluso, I., Armani, A., De Stefani, D., Venditti, R., Montefusco, S., Scotto-Rosato, A., Prezioso, C., Forrester, A., et al. (2015). Lysosomal calcium signalling regulates autophagy through calcineurin and TFEB. Nat. Cell Biol. *17*, 288–299.

Morita, T., Shimohara, N., Honma, M., and Tokue, A. (1995). Establishment and characterization of a new cell line from human bladder cancer (JMSU1). Urol. Res. *23*, 143–149.

Nayak, S.K., O'Toole, C., and Price, Z.H. (1977). A cell line from an anaplastic transitional cell carcinoma of human urinary bladder. Br. J. Cancer *35*, 142–151.

Nnah, I.C., Wang, B., Saqcena, C., Weber, G.F., Bonder, E.M., Bagley, D., De Cegli, R., Napolitano, G., Medina, D.L., Ballabio, A., et al. (2019). TFEB-driven endocytosis coordinates MTORC1 signaling and autophagy. Autophagy *15*, 151–164.

Pedersen, N.M., Wenzel, E.M., Wang, L., Antoine, S., Chavrier, P., Stenmark, H., and Raiborg, C. (2020). Protrudin-mediated ER–endosome contact sites promote MT1-MMP exocytosis and cell invasion. J. Cell Biol. *219*, e202003063.

Perera, R.M., and Zoncu, R. (2016). The Lysosome as a Regulatory Hub. Annu. Rev. Cell Dev. Biol. *32*, 223–253.

Perera, R.M., Stoykova, S., Nicolay, B.N., Ross, K.N., Fitamant, J., Boukhali, M., Lengrand, J., Deshpande, V., Selig, M.K., Ferrone, C.R., et al. (2015). Transcriptional control of autophagy–lysosome function drives pancreatic cancer metabolism. Nature *524*, 361–365.

Perera, R.M., Di Malta, C., and Ballabio, A. (2019). MiT/TFE Family of Transcription Factors, Lysosomes, and Cancer. Annu. Rev. Cancer Biol. *3*, 203–222.

Pu, J., Schindler, C., Jia, R., Jarnik, M., Backlund, P., and Bonifacino, J.S. (2015). BORC, a multisubunit complex that regulates lysosome positioning. Dev. Cell *33*, 176–188.

Pu, J., Guardia, C.M., Keren-Kaplan, T., and Bonifacino, J.S. (2016). Mechanisms and functions of lysosome positioning. J. Cell Sci. *129*, 4329–4339.

Pyrpassopoulos, S., Shuman, H., and Ostap, E.M. (2017). Adhesion force and attachment lifetime of the KIF16B-PX domain interaction with lipid membranes. Mol. Biol. Cell *28*, 3315–3322.

Raiborg, C., Wenzel, E.M., Pedersen, N.M., Olsvik, H., Schink, K.O., Schultz, S.W., Vietri, M., Nisi, V., Bucci, C., Brech, A., et al. (2015). Repeated ER–endosome contacts promote endosome translocation and neurite outgrowth. Nature *520*, 234–238.

Rebouissou, S., Bernard-Pierrot, I., de Reynies, A., Lepage, M.-L., Krucker, C., Chapeaublanc, E., Herault, A., Kamoun, A., Caillault, A., Letouze, E., et al. (2014). EGFR as a potential therapeutic target for a subset of muscle-invasive bladder cancers presenting a basal-like phenotype. Sci. Transl. Med. *6*, 244ra91-244ra91.

Roczniak-Ferguson, A., Petit, C.S., Froehlich, F., Qian, S., Ky, J., Angarola, B., Walther, T.C., and Ferguson, S.M. (2012). The transcription factor TFEB links mTORC1 signaling to transcriptional control of lysosome homeostasis. Sci. Signal. *5*, ra42.

Sardiello, M., Palmieri, M., di Ronza, A., Medina, D.L., Valenza, M., Gennarino, V.A., Di Malta, C., Donaudy, F., Embrione, V., Polishchuk, R.S., et al. (2009). A Gene Network Regulating Lysosomal Biogenesis and Function. Science *325*, 473–477.

Saxton, R.A., and Sabatini, D.M. (2017). mTOR Signaling in Growth, Metabolism, and Disease. Cell *168*, 960–976.

Schauer, K., Duong, T., Bleakley, K., Bardin, S., Bornens, M., and Goud, B. (2010a). Probabilistic density maps to study global endomembrane organization. Nat. Methods *7*, 560–566.

Schauer, K., Duong, T., Bleakley, K., Bardin, S., Bornens, M., and Goud, B. (2010b). Probabilistic density maps to study global endomembrane organization. Nat. Methods *7*, 560–566.

Schiefermeier, N., Scheffler, J.M., de Araujo, M.E.G., Stasyk, T., Yordanov, T., Ebner, H.L., Offterdinger, M., Munck, S., Hess, M.W., Wickström, S.A., et al. (2014). The late endosomal p14-MP1 (LAMTOR2/3) complex regulates focal adhesion dynamics during cell migration. J. Cell Biol. *205*, 525–540.

Settembre, C., Di Malta, C., Polito, V.A., Arencibia, M.G., Vetrini, F., Erdin, S., Erdin, S.U., Huynh, T., Medina, D., Colella, P., et al. (2011). TFEB Links Autophagy to Lysosomal Biogenesis. Science *332*, 1429–1433.

Settembre, C., Fraldi, A., Medina, D.L., and Ballabio, A. (2013). Signals from the lysosome: a control centre for cellular clearance and energy metabolism. Nat. Rev. Mol. Cell Biol. *14*, 283–296.

Shin, H.R., and Zoncu, R. (2020). The Lysosome at the Intersection of Cellular Growth and Destruction. Dev. Cell *54*, 226–238.

Song, H.-I., and Yoon, M.-S. (2016). PLD1 regulates adipogenic differentiation through mTOR - IRS-1 phosphorylation at serine 636/639. Sci. Rep. *6*, 36968.

Southgate, J., Hutton, K.A., Thomas, D.F., and Trejdosiewicz, L.K. (1994). Normal human urothelial cells in vitro: proliferation and induction of stratification. Lab. Investig. J. Tech. Methods Pathol. *71*, 583–594.

Steffan, J.J., Snider, J.L., Skalli, O., Welbourne, T., and Cardelli, J.A. (2009). Na^+/H^+ Exchangers and RhoA Regulate Acidic Extracellular pH-Induced Lysosome Trafficking in Prostate Cancer Cells. Traffic *10*, 737–753.

Tachibana, M., Miyakawa, A., Tazaki, H., Nakamura, K., Kubo, A., Hata, J., Nishi, T., and Amano, Y. (1995). Autocrine growth of transitional cell carcinoma of the bladder induced by granulocyte-colony stimulating factor. Cancer Res. *55*, 3438–3443.

Thelen, A.M., and Zoncu, R. (2017). Emerging Roles for the Lysosome in Lipid Metabolism. Trends Cell Biol. *27*, 833–850.

Warrick, J.I., Walter, V., Yamashita, H., Chung, E., Shuman, L., Amponsa, V.O., Zheng, Z., Chan, W., Whitcomb, T.L., Yue, F., et al. (2016). FOXA1, GATA3 and PPAR□ Cooperate to Drive Luminal Subtype in Bladder Cancer: A Molecular Analysis of Established Human Cell Lines. Sci. Rep. *6*, 38531.

Willett, R., Martina, J.A., Zewe, J.P., Wills, R., Hammond, G.R.V., and Puertollano, R. (2017). TFEB regulates lysosomal positioning by modulating TMEM55B expression and JIP4 recruitment to lysosomes. Nat. Commun. *8*, 1580.

Zoncu, R., Bar-Peled, L., Efeyan, A., Wang, S., Sancak, Y., and Sabatini, D.M. (2011). mTORC1 Senses Lysosomal Amino Acids Through an Inside-Out Mechanism That Requires the Vacuolar H+-ATPase. Science *334*, 678–683.

Zuiverloon, T.C.M., van Kessel, K.E.M., Bivalacqua, T.J., Boormans, J.L., Ecke, T.H., Grivas, P.D., Kiltie, A.E., Liedberg, F., Necchi, A., van Rhijn, B.W., et al. (2018). Recommendations for follow-up of muscle-invasive bladder cancer patients: A consensus by the international bladder cancer network. Urol. Oncol. Semin. Orig. Investig. *36*, 423–431.

Figure legends

Figure 1. High-grade cancer cell lines are specifically characterized by scattered, peripheral positioning of lysosomes

A. Representative images of lysosomes visualized by immunofluorescence staining against the lysosomal-associated membrane protein 1 (LAMP1/CD107a) in normal human urothelium (NHU) and bladder cancer cell lines RT4 (ATCC® HTB-2™), MGHU3 (Lin et al., 1985), RT112 (Marshall et al., 1977), KU19-19 (Tachibana et al., 1995), T24, TCCSup (Nayak et al., 1977), JMSU1 (Morita et al., 1995) cells cultured on crossbow-shaped adhesive micropatterns for better comparison. Scale bar is 10 µm. **B**. 3D probabilistic density maps of lysosomes of n cells of NHU, MGHU3, RT112, KU19-19 and JMSU1. The 50% contour visualizes the smallest cellular volume containing 50% of lysosomes. **C**. Nearest neighbor distance (NND) between lysosomes in NHU (n=76), RT4 (n=73), MGHU3 (n=65), RT112 (n=64), KU19-19 (n=64), T24 (n=72), TCCSup (n=48) and JMSU1 (n=60). Adjusted p-values of testing against NHU condition are RT4: >0.9999, MGHU3: 0.1943; RT112: <0.0001; KU19-19: <0.0001; T24: <0.0001; TCCsup: <0.0001; JMSU1: <0.0001 in a Kruskal-Wallis test with Dunn's test for multiple comparisons; ns p >0.1 and **** p < 0.0001, error bars are SEM. **D**. Average numbers of lysosomes per cell in NHU (n=76), RT4 (n=73), MGHU3 (n=65), RT112 (n=64), KU19-19 (n=64), T24 (n=72), TCCSup (n=48) and JMSU1 (n=60). Adjusted p-values of testing against NHU condition are RT4: <0.0001; MGHU3: <0.0001; RT112: >0.9999; KU19-19: 0.8807; T24: >0.9999; TCCsup: 0.2068; JMSU1: <0.0001 in a Kruskal-Wallis test with Dunn's test for correction for multiple comparisons; ns p > 0.1 and **** p < 0.0001, error bars are SEM. **E**. Average volume of lysosomes in NHU (n=76), RT4 (n=73), MGHU3 (n=65), RT112 (n=64), KU19-19 (n=64), T24 (n=72), TCCSup (n=48) and JMSU1 (n=60). Adjusted p-values of testing against NHU condition are RT4: 0.1414; MGHU3: <0.0001; RT112: 0.0048; KU19-19: 0.0110; T24:

>0.9999; TCCsup: 0.0003; JMSU1: <0.0001 in a Kruskal-Wallis test with Dunn's test for multiple comparisons; ns p > 0.1, * p < 0.1, *** p < 0.001 and **** p < 0.0001, error bars are SEM.

Figure 2. Dispersed lysosomes reveal alterations in the mTORC1-TFEB signaling axis

A. Immunofluorescence staining of the lysosomal-associated membrane protein 1 (LAMP1, CD107a) and mTOR in MGHU3, RT112, KU19-19 and JMSU1. The zoom shows the merged image for both proteins in the white box. Scale bars equal 15 µm **B**. Quantification of mTOR intensity on lysosomes normalized to total cellular mTOR (approximately 50 cells for each cell line; **** p <0.0001; Kruskal-Wallis test with Dunn's test for multiple comparison, error bars are SEM. **C**. Western blot analysis of phosphorylated p70-S6 Kinase 1 (P-p70-S6K1 Thr389) and total p70-S6K1 as well as GAPDH loading control in MGHU3, RT112, KU19-19 and JMSU1 cells and quantification of P-p70-S6K1 levels from n=7 experiments, error bars are SEM. **D**. Representative images of MGHU3, RT112, KU19-19 and JMSU1 cells transfected with TFEB-EGFP for 72 h. Scale bars equal 10 µm. **E**. Quantification of the nuclear fraction of the total mean TFEB-EGFP fluorescent intensity in MGHU3 (n=23), RT112 (n=31), KU19-19 (n-39) and JMSU1 cells (n=57). **** p <0.0001; Kruskal-Wallis test with Dunn's test for multiple comparison. Data are depicted as mean ± SD. **F**. Representative images of RT112 cells transfected with TFEB-EGFP for 72 h and treated with 10 µM rapamycin for 2 h. Scale bars equal 10 µm. **G**. Quantification of the nuclear fraction of the total mean TFEB-EGFP fluorescent intensity in control and rapamycin conditions (for n>20 cells in each condition). **** p <0.0001; Mann-Whitney test. Data are depicted as mean ± SD. **H**. Representative images of JMSU1 cells transfected with TFEB-EGFP for 72 h and treated with ML-SI1 or BAPTA AM for 3 h. Scale bars equal 10 µm. **I**. Quantification of the nuclear fraction of the total mean TFEB-EGFP fluorescent intensity in control, ML-SI1 and

BAPTA AM treatment conditions (for >15 cells in each condition). *** p<0.001 and **** p <0.0001; Mann-Whitney test. Data are depicted as mean ± SD.

Figure 3. Lysosome positioning changes are under the control of TFEB in bladder cancer cells

A. Immunofluorescence staining of the lysosomal-associated membrane protein 1 (LAMP1, CD107a) in control (DMSO) and rapamycin (10 µM) treated RT112 cells. White arrow shows the peripheral clustering of lysosomes. Scale bars equal 10 µm. **B**. Representative images of lysosomes visualized by immunofluorescence staining against LAMP1 in micropatterned RT112 cells in control and rapamycin treatment. **C**. Nearest neighbor distance (NND in µm) between lysosomes in micropatterned control (n=25) and rapamycin treated (n=27) RT112 cells; * p <0.05 in a Mann-Whitney U test, error bars are SEM. **D**. Immunofluorescence staining of LAMP1 in JMSU1 cells treated with siLUC and siTFEB for 72 h. White arrow shows the perinuclear clustering of lysosomes. Scale bars equal 10 µm. **E**. Representative images of lysosomes visualized by immunofluorescence staining against LAMP1 in micropatterned JMSU1 cells in control and siTFEB treatment conditions. **F**. Nearest neighbor distance (NND in µm) between lysosomes in micropatterned control (n= 23) and siTFEB (n= 34) treated JMSU1 cells; ** p < 0.005 in a Mann-Whitney U test, error bars are SEM. **G**. Immunofluorescence staining of LAMP1 (red) and protrudin (green) in control (DMSO) and rapamycin (10 µM) treated RT112 cells. Zoom shows the merged image of both proteins in the white box. White arrow shows the colocalization between LAMP1 and protrudin. Scale bars are 15 µm. **H**. Quantification of protrudin integrated intensity on lysosomes normalized to total cellular protrudin, in 290 control and 227 rapamycin treated RT112 cells; ****p<0.0001 in a Mann-Whitney U test, error bars are SEM. **I**. Immunofluorescence staining of LAMP1 (red) in and protrudin (green) in JMSU1 cells in control (siLUC) and

siTFEB (72 h) treatment conditions. Zoom shows the merged image of the two proteins in the white box. White arrow shows the colocalization between LAMP1 and protrudin. Scale bars are 15 µm. **J**. Quantification of protrudin integrated intensity on lysosomes normalized to total cellular protrudin, in 131 control (siLUC) and 167 siTFEB JMSU1 cells; **** $p<0.0001$ in a Mann-Whitney U test, error bars are SEM.

Figure 4. TFEB regulates phosphatidylinositol-3-phosphate levels on endomembranes in bladder cancer cells

A. Immunofluorescence staining of the lysosomal-associated membrane protein 1 (LAMP1/CD107a) (red) in control (siLUC) and siTFEB (72 h) treated JMSU1 cells transfected with EGFP-FYVE (green). Zoom shows the merged images of LAMP1 and EGFP-FYVE in white box. White arrow shows the colocalization between LAMP1 and EGFP-FYVE. Scale bars equal 10 µm. **B**. Quantification of EGFP-FYVE integrated intensity on lysosomes normalized to total cellular EGFP-FYVE, in 147 siLUC and 167 siTFEB treated JMSU1 cells; **** $p<0.0001$ in a Mann-Whitney U test, error bars are SEM. **C**. Representative images of control (siLUC) and siTFEB (72 h) treated JMSU1 cells expressing EGFP-FYVE. Zoom shows EGFP-FYVE in white box. Scale bars equal 15 µm. **D**. Quantification of EGFP-FYVE integrated intensity on segmented spots normalized to total cellular EGFP-FYVE, in 241 siLUC and 307 siTFEB JMSU1 cells; $p<0.0001$ in a Mann-Whitney U test, error bars are SEM. **E**. Immunofluorescence staining of early endosome antigen 1 (EEA1) in control (DMSO) and wortmannin (1 µM) treated JMSU1 cells. Zoom shows one single cell in white box. Scale bars equal 15 µm. **F**. Quantification of EEA1 integrated intensity on segmented spots normalized to total cellular EEA1, in 228 control and 56 wortmannin treated JMSU1 cells; **** $p<0.0001$ in a Mann-Whitney U test, error bars are SEM. **G**. Immunofluorescence staining of LAMP1 in control (DMSO) and wortmannin (1

µM) treated JMSU1 cells. White arrows show the perinuclear clustering of lysosomes. **H**. Representative images of lysosomes visualized by immunofluorescence staining against LAMP1 in micropatterned control and wortmannin (1 µM) treated JMSU1 cells. **I**. Nearest neighbor distance (NND in µm) between lysosomes in micropatterned in control (n=19) and wortmannin (n=25) JMSU1 cells; *** $p < 0.0005$ p-value in a Mann-Whitney U test, error bars are SEM.

Supplemental figure legends

Figure S1. High-grade cancer cell lines are specifically characterized by scattered, peripheral positioning of lysosomes

A. Average intensity projections of the actin cytoskeleton visualized by phalloidin of n cells of normal human urothelium (NHU) and bladder cancer cell lines RT4 (ATCC® HTB-2™), MGHU3 (Lin et al., 1985), RT112 (Marshall et al., 1977), KU19-19 (Tachibana et al., 1995), T24, TCCSup (Nayak et al., 1977), JMSU1 (Morita et al., 1995). Scale bar equals 10 µm. **B**. Correlation analysis between average endolysosomal volume and average numbers per cell shows a weak (R^2=0.19) but significant association; p-value < 0.001 in a t-test for correlation. **C**. Principal component analysis of transcriptome data of normal human urothelium (NHU) cells and the bladder cancer cell lines RT4, MGHU3, RT112, KU19-19, T24, TCCSup and JMSU1. **D**. Average day of invasion from spheroids into collagen matrix of MGHU3 (n=13), RT112 (n=9), KU19-19 (n=5), and JMSU1 (n=8), and representative images of 3D spheroids from KU19-19 (upper panel) and JMSU1 (lower panel) at 1 day after matrix embedding. White arrow indicates invasion of collagen matrix by escaping cells. Scale bar equals 500 µm. **E**. Schematic representation of the analysis of endolysosome distribution in classical cell culture conditions (see **F**). **F**. Normalized lysosome dispersion in non patterned MGHU3,

RT112, KU19-19 and JMSU1 cells based on statistical inertia measurement (=averaged squared distance to the center of mass normalized to cell size) for n>60 cells per cell line analyzed, **** $p < 0.0001$ in a Kruskal-Wallis test with Dunn‘s test for multiple comparison .

Figure S2. Altered lysosomes correlate with changes in the mTORC1-TFEB nutrient signaling pathway

A. Quantification of total p70-S6 Kinase 1 levels from n=3 Western Blot experiments in MGHU3, RT112, KU19-19 and JMSU1 (see also Figure 2C). Error bars show SEM. **B**. Western Blot analysis of phosphorylated p70-S6 Kinase 1 (P-p70-S6K1 Thr389) and GAPDH loading control in MGHU3, RT112, KU19-19 and JMSU1 cells in control conditions (full media) and after treatment with rapamycin at 10 µM for 2 h or grown under starvation in EBSS (Earle's Balanced Saline Solution) for 4 h. **C**. Normalized Log2 RNA expression levels of housekeeping gene (GAPDH) and TFEB regulated genes (RRAGD and TSC1) in NHU, MGHU3, RT112, KU19-19 and JMSU1. **D**. Representative images of JMSU1 cells transfected with TFEB-EGFP for 72 h and treated with NPC1 inhibitor U18666A (10 µM, 2 h, 37°C). Scale bars are 10 µm. **E**. Quantification of the nuclear fraction of the total mean TFEB-EGFP fluorescent intensity in in control and U18666A treated JMSU1 cells (for n>15 cells in each condition). ns is $p > 0.1$; Mann-Whitney test. Data are depicted as mean ± SD.

Figure S3. Lysosome positioning changes are under the control of TFEB in bladder cancer cells

A. Western blot analysis of siTFEB (72 h, with siRNA pool) in JMSU1 cells and quantification of TFEB levels normalized to GAPDH. Error bars are SEM of 7 independent experiments. **B**. Western blot of TFEB knockdown with individual siTFEB RNAs (72 h). **C**. Immunofluorescence staining against the lysosomal-associated membrane protein 1 (LAMP1, CD107a) in JMSU1 cells after TFEB knockdown with individual siTFEB RNAs (72 h).

White arrows show the perinuclear clustering of lysosomes. Scale bar is 15 µm. **D**. Normalized Log2 RNA expression levels of protrudin (ZFYVE27). **E**. Western blot analysis of protrudin in RT112 cells in control (DMSO) and rapamycin (10 µM, 24 h) treatment conditions. **F**. Western blot analysis of protrudin in JMSU1 cells in control (siLUC) and siTFEB (72 h) conditions.

Figure S4. TFEB regulates phosphatidylinositol-3-phosphate levels on endomembranes in bladder cancer cells

A. Representative images of EEA1 staining in RT112 cells in control (DMSO), rapamycin (10 µM, 24 h) and cycloheximide (20 µg/mL, 24 h) conditions. Zoom shows one single cell in white box. Scale bars are 15 µm. **B**. Quantification of EEA1 integrated intensity on segmented spots normalized to total cellular EEA1, in control, rapamycin and cycloheximide treatment conditions in 234 control, 245 rapamycin and 201 cycloheximide treated RT112 cells; ****p<0.0001, ***p<0.001 in a Kruskal-Wallis test with Dunn's test for multiple comparison, error bars are SEM. **C**. Western blot analysis of EEA1 in RT112 cells in control, rapamycin and cycloheximide treatment conditions. **D**. Representative images of EEA1 staining in RT112 cells in control (DMSO) and rapamycin (10 µM, 4 h) conditions. Zoom shows one single cell in white box. Scale bars are 15 µm. **E**. Quantification of EEA1 integrated intensity on segmented spots normalized to total cellular EEA1, in control and rapamycin conditions in 332 control and 330 rapamycin treated RT112 cells; ns p>0.1 in a Mann-Whitney test, error bars are SEM. **F**. Western blot analysis of EEA1 in RT112 cells in control and rapamycin (4 h) conditions, error bars are SEM from 3 independent experiments. **G**. Representative images of EEA1 staining in JMSU1 cells in control (siLUC) and siTFEB (72 h) conditions. Zoom shows one single cell in white box. Scale bars are 15 µm. **H**. Quantification of EEA1 integrated intensity on segmented spots normalized to total cellular

EEA1, in control and siTFEB conditions in 94 siLUC and 212 siTFEB JMSU1 cells; ** $p<0.01$ in Mann-Whitney test, error bars are SEM). **I**. Western blot analysis of EEA1 in JMSU1 cells in control and siTFEB (72 h) conditions, error bars are SEM from 9 independent experiments.

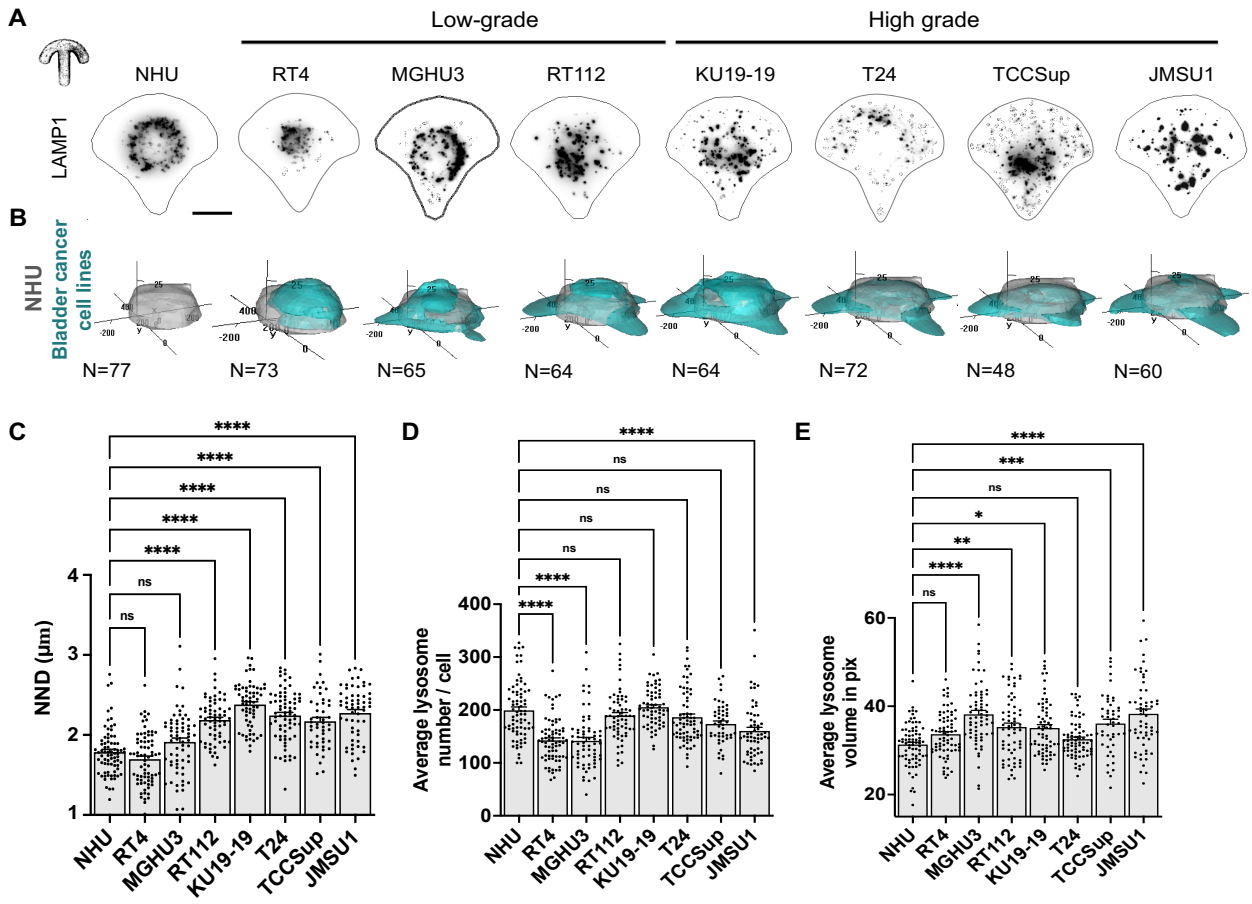
A
Low-grade
High grade
NHU
RT4
MGHU3
RT112
KU19-19
T24
TCCSup
JMSU1
LAMP1
B
NHU
Bladder cancer cell lines
N=77
N=73
N=65
N=64
N=64
N=72
N=48
N=60
C
NND (µm)
D
Average lysosome number / cell
E
Average lysosome volume in pix

Figure 1

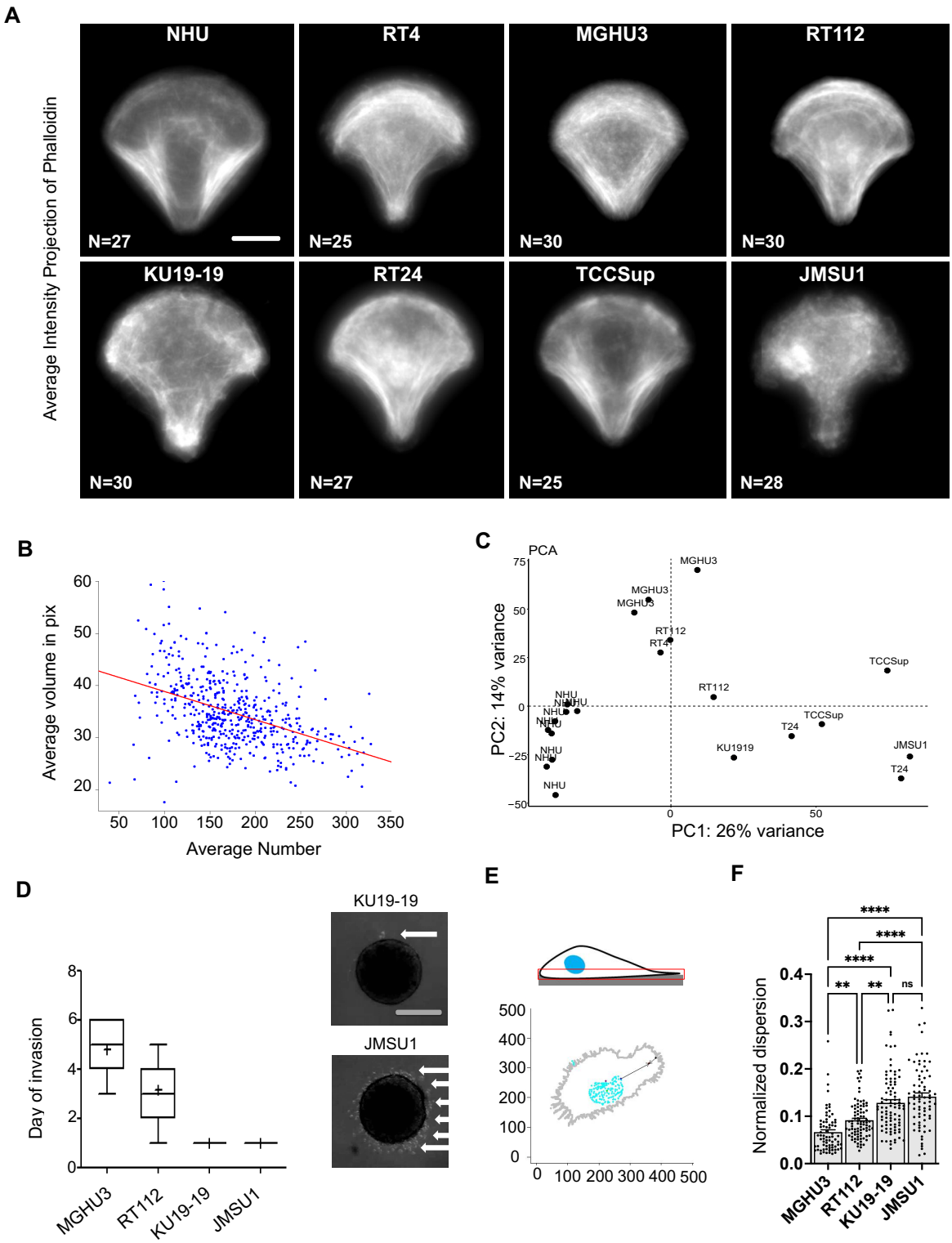

Supplementary Figure 1

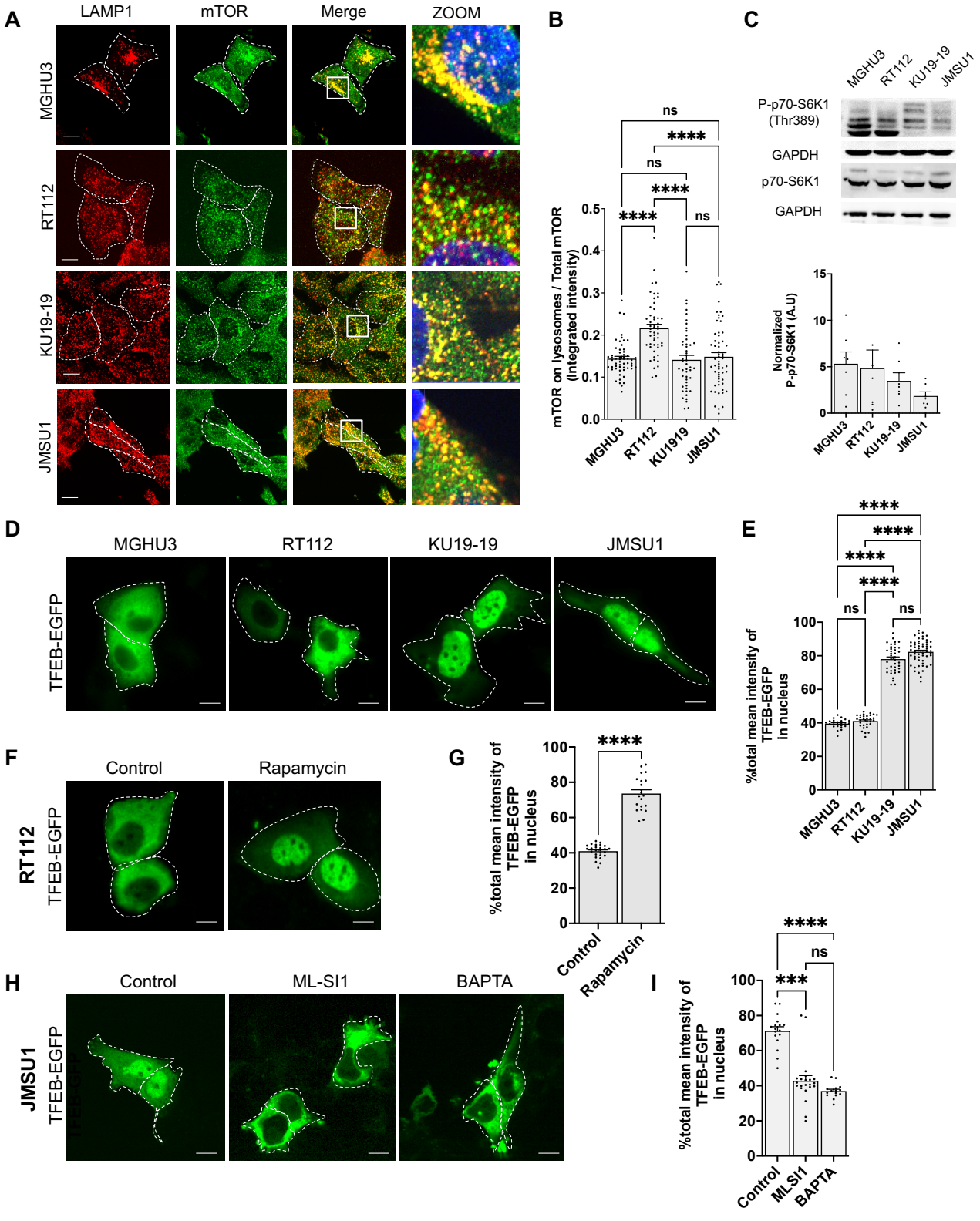
A
LAMP1
mTOR
Merge
ZOOM
MGHU3
RT112
KU19-19
JMSU1
B
mTOR on lysosomes / Total mTOR (Integrated intensity)
ns
****
****
ns
****
ns
MGHU3
RT112
KU1919
JMSU1
C
MGHU3
RT112
KU19-19
JMSU1
P-p70-S6K1 (Thr389)
GAPDH
p70-S6K1
GAPDH
Normalized P-p70-S6K1 (A.U)
D
MGHU3
RT112
KU19-19
JMSU1
TFEB-EGFP
E
%total mean intensity of TFEB-EGFP in nucleus
****
****
****
****
ns
ns
F
Control
Rapamycin
RT112
TFEB-EGFP
G
%total mean intensity of TFEB-EGFP in nucleus
****
Control
Rapamycin
H
Control
ML-SI1
BAPTA
JMSU1
TFEB-EGFP
I
%total mean intensity of TFEB-EGFP in nucleus
****
***
ns
Control
MLSI1
BAPTA

Figure 2

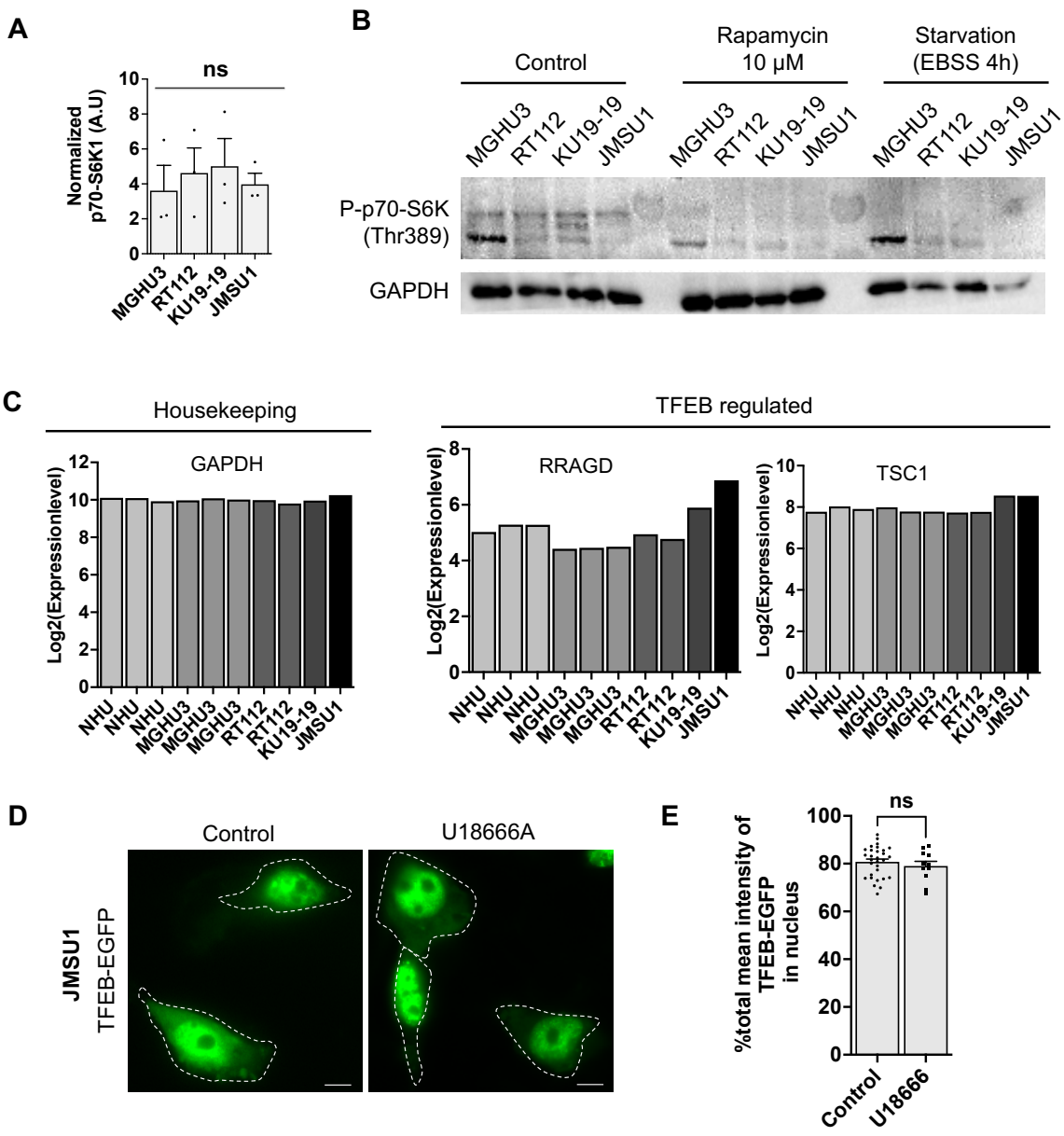

Supplementary Figure 2

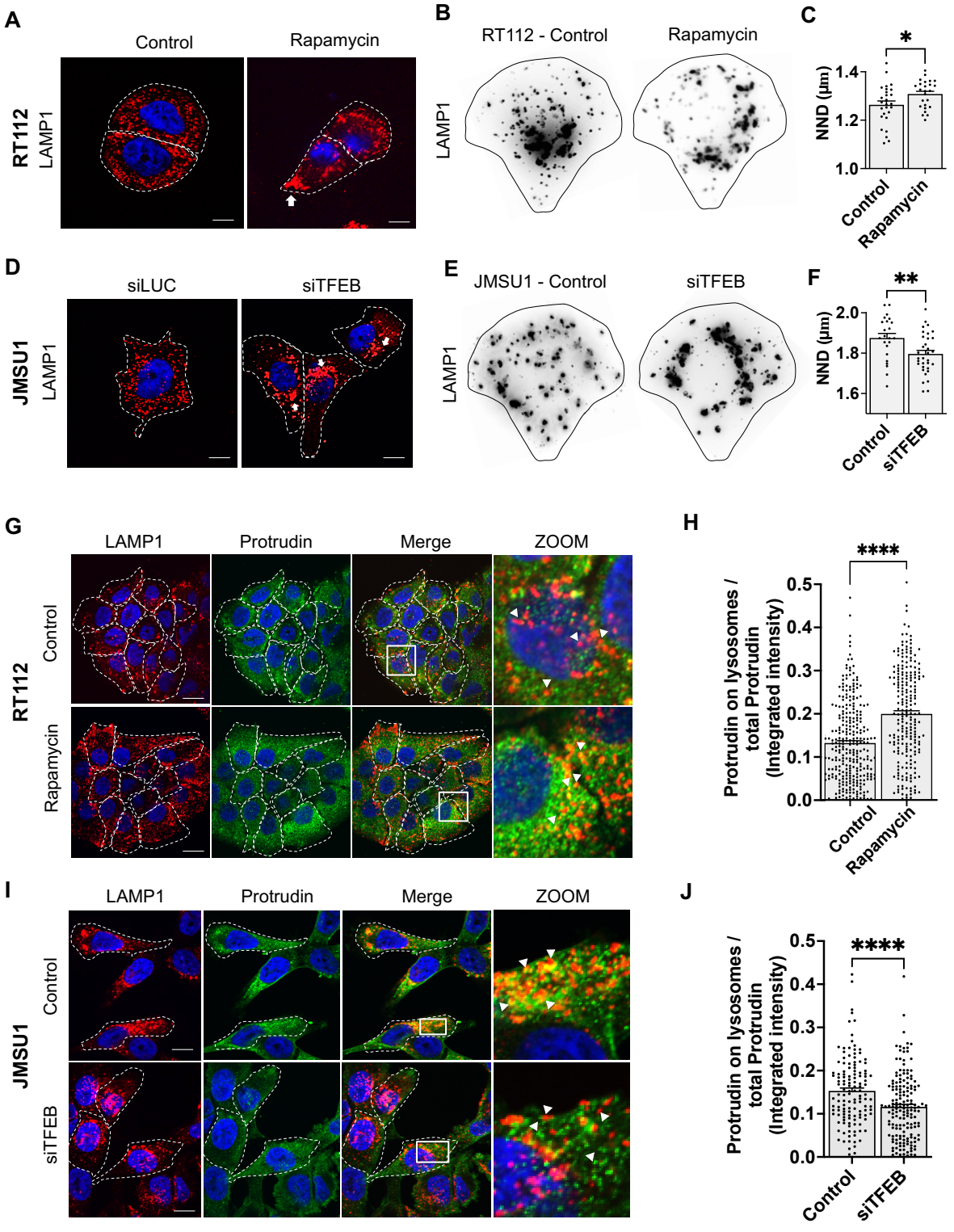
A
Control
Rapamycin
RT112
LAMP1
B
RT112 - Control
Rapamycin
LAMP1
C
NND (µm)
1.4
1.2
1.0
*
Control
Rapamycin
D
siLUC
siTFEB
JMSU1
LAMP1
E
JMSU1 - Control
siTFEB
LAMP1
F
NND (µm)
2.0
1.8
1.6
**
Control
siTFEB
G
LAMP1
Protrudin
Merge
ZOOM
RT112
Control
Rapamycin
H
Protrudin on lysosomes / total Protrudin (Integrated intensity)
0.5
0.4
0.3
0.2
0.1
0.0
****
Control
Rapamycin
I
LAMP1
Protrudin
Merge
ZOOM
JMSU1
Control
siTFEB
J
Protrudin on lysosomes / total Protrudin (Integrated intensity)
0.5
0.4
0.3
0.2
0.1
0.0
****
Control
siTFEB

Figure 3

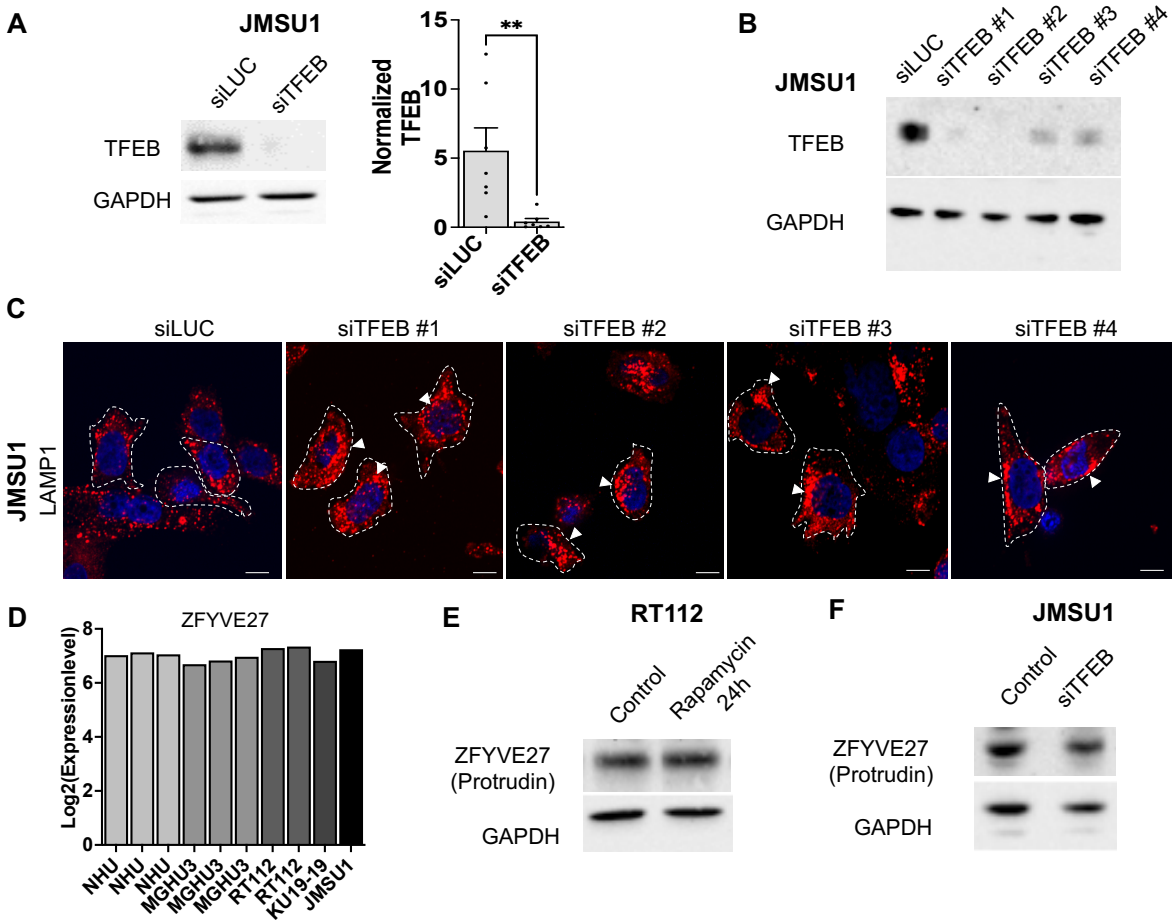

Supplementary Figure 3

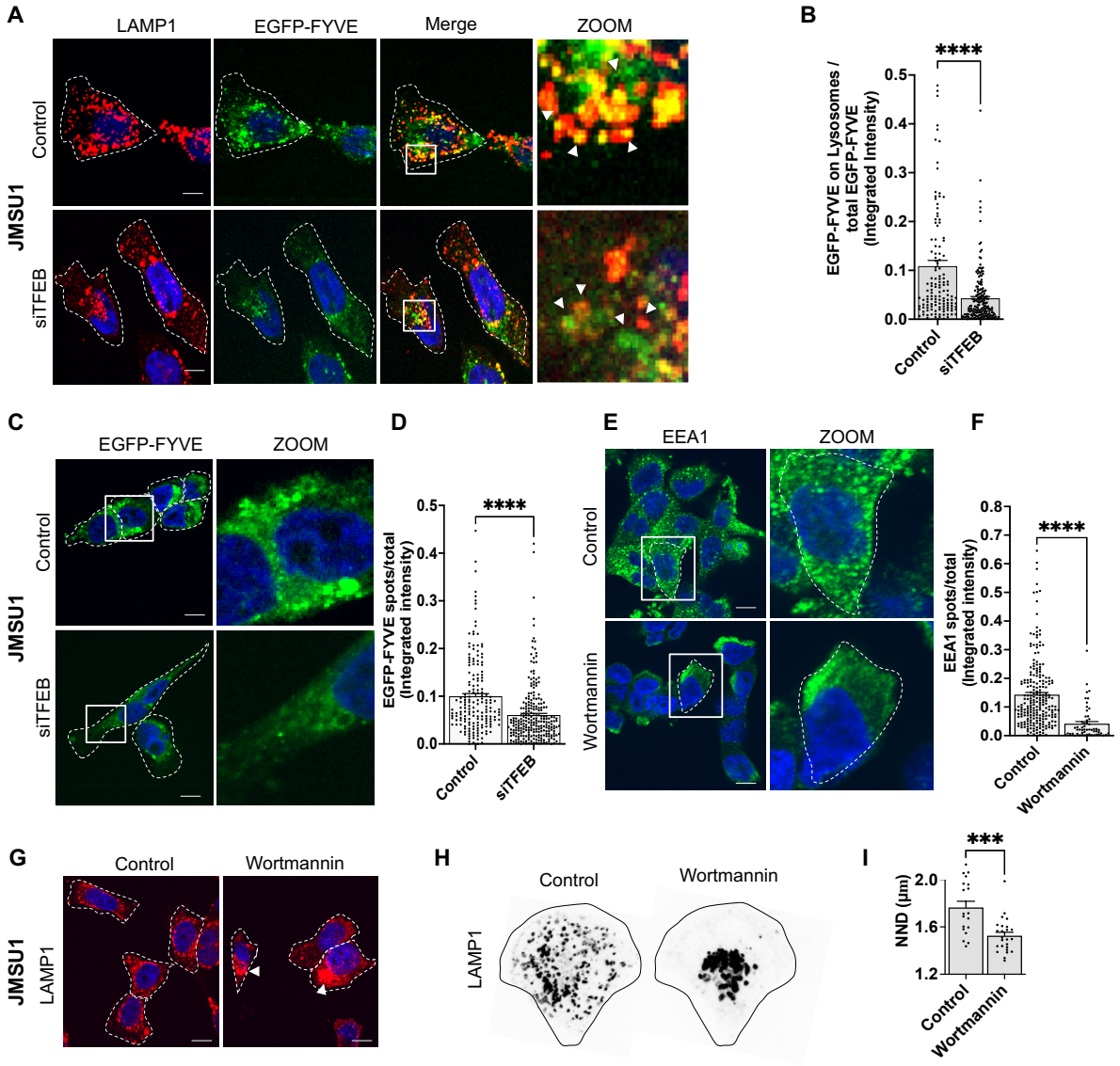
A
LAMP1
EGFP-FYVE
Merge
ZOOM
Control
siTFEB
JMSU1
B
EGFP-FYVE on Lysosomes / total EGFP-FYVE (Integrated Intensity)
****
Control
siTFEB
C
EGFP-FYVE
ZOOM
D
EGFP-FYVE spots/total (Integrated intensity)
E
EEA1
ZOOM
Wortmannin
F
EEA1 spots/total (Integrated intensity)
G
Control
Wortmannin
LAMP1
H
I
NND (µm)
***

Figure 4

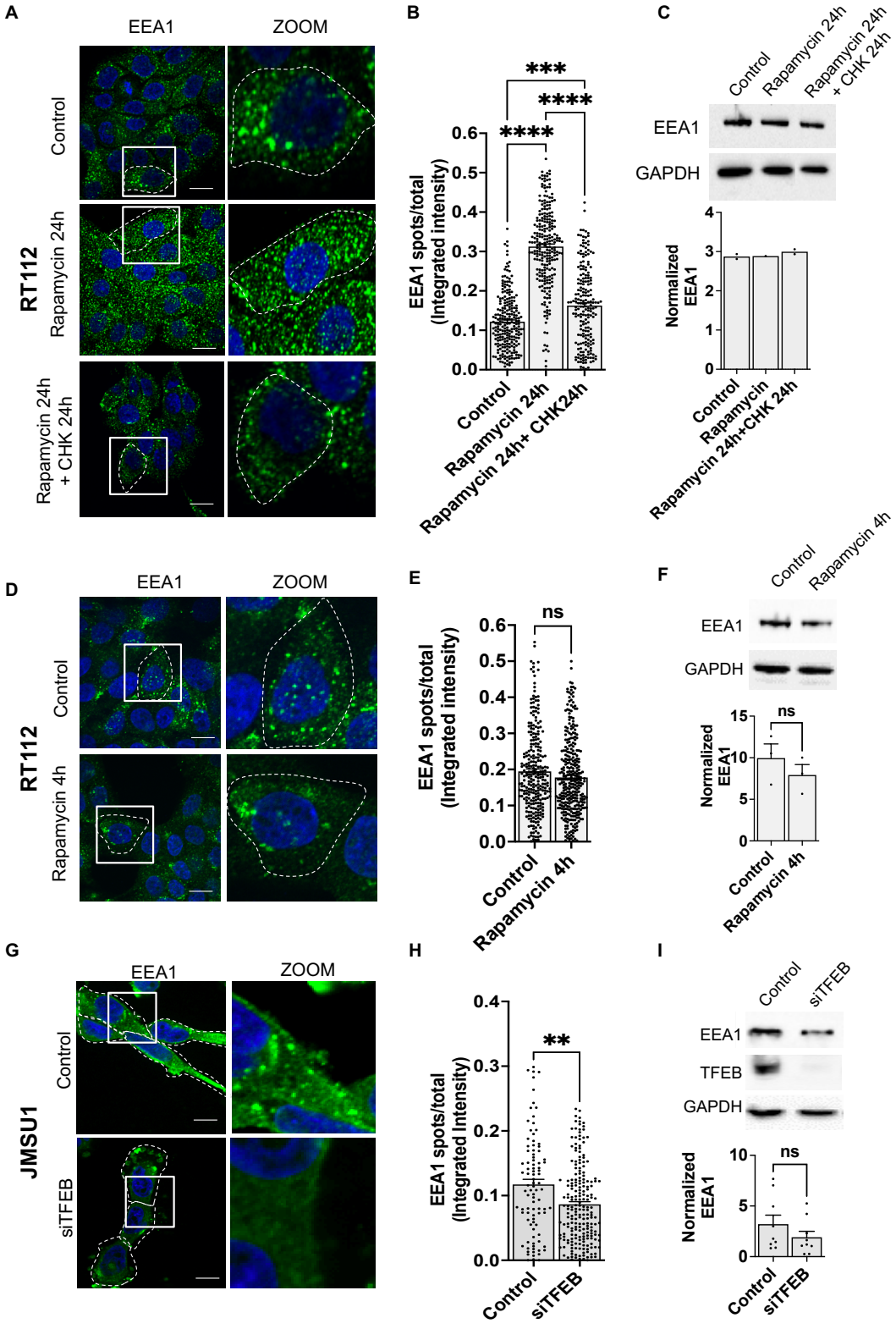

Supplementary Figure 4

RÉSUMÉ

Les lysosomes sont un centre de régulation intracellulaire pour le métabolisme et la signalisation. De nombreuses fonctions des lysosomes sont impliquées dans le cancer et ils restent donc une cible intéressante pour les thérapies anticancéreuses. Nous avons précédemment étudié le paysage intracellulaire de cet organite dans une collection de lignées cellulaires de cancer de la vessie et de cellules urothéliales humaines normales et nous avons constaté que les lysosomes sont plus dispersés vers la périphérie des cellules dans les cellules agressives de cancer de la vessie. Nous constatons ici une régulation différentielle de la kinase mTORC1 (cible mammalienne du complexe 1 de rapamycine), qui émet des signaux à partir des lysosomes, entre des lignées cellulaires de cancer de la vessie non agressives et agressives, et nous constatons une translocation nucléaire constitutive du facteur de transcription EB (TFEB) dans les cellules de cancer de la vessie agressives. Le silençage de TFEB dans les cellules cancéreuses agressives inverse le phénotype de dispersion des lysosomes, ce qui suggère un rôle de TFEB dans la régulation de la dispersion lysosomale dans ces cellules. De manière cohérente, nous constatons que l'induction de la translocation nucléaire de TFEB après l'inhibition de mTORC1 induit un mouvement périphérique des lysosomes dans les cellules non agressives. Les phosphoinositols étant des régulateurs importants de la fonction et du mouvement des lysosomes, en particulier le phosphatidylinositol-3-phosphate (PI3P) qui est impliqué dans le positionnement des lysosomes, nous avons testé si TFEB régule les niveaux de PI3P dans les cellules cancéreuses agressives de la vessie et donc la dispersion des lysosomes. Nous constatons que la GFP-FYVE qui se lie à PI3P est fortement diminuée après un traitement avec un siTFEB dans les cellules agressives.

L'ensemble de nos résultats indique que le positionnement des lysosomes est sous le contrôle de TFEB et que l'hyperactivation de TFEB conduit au phénotype cellulaire caractéristique de dispersion des lysosomes dans les cellules cancéreuses de la vessie agressives. De plus, nos résultats montrent que l'activation de TFEB entraîne une augmentation globale de PI3P au niveau des lysosomes et un fort recrutement des protéines contenant le domaine FYVE. Ainsi, nos résultats révèlent un nouveau rôle de TFEB dans la régulation des niveaux de PI3P. Cela clarifie conceptuellement le double rôle de TFEB en tant que régulateur de la maturation endosomale et de l'autophagie, deux processus cellulaires fondamentaux mais distincts qui dépendent et sont régulés par les niveaux de PI3P. Nous proposons que les changements de positionnement des lysosomes soient un biomarqueur crucial des altérations de la voie PI3P dans le modèle de cancer de la vessie.

MOTS CLÉS

Lysosome positionnement, mTORC1, TFEB, PI3P

ABSTRACT

Lysosomes are an intracellular regulatory hub for metabolism and signaling. Many functions of lysosomes are implicated in cancer and thus they remain an interesting target for cancer therapies. We had previously investigate the intracellular landscape of this organelle in a collection of bladder cancer cell lines and normal human urothelium cells and found that lysosomes become increasingly scattered towards the cell periphery in aggressive bladder cancer cells. Here we find differential regulation of mTORC1 (mammalian target of rapamycin complex 1) kinase, which signals from lysosomes, between non- aggressive and aggressive bladder cancer cell lines and we find constitutive nuclear translocation of the transcription factor EB (TFEB) in aggressive bladder cancer cells . Silencing of TFEB in aggressive cancer cells reverses the scattered lysosome phenotype, suggesting a role of TFEB in regulation of lysosomal dispersion in these cells. Consistently, we find that inducing nuclear translocation of TFEB after inhibition of mTORC1 induces peripheral movement of lysosomes in non-aggressive cells. Since phosphoinositols are important regulators of lysosomal function and movement, especially phosphatidylinositol-3-phosphate (PI3P) which is involved in lysosomal positioning, we tested whether TFEB regulates levels of PI3P in aggressive bladder cancer cells and thus lysosomal dispersion. We find that GFP-FYVE that binds to PI3P is strongly decreased after siTFEB in aggressive cells.

Together our results indicate that lysosome positioning is under the control of TFEB and that hyperactivation of TFEB leads to the characteristic cellular phenotype of lysosome dispersion in aggressive bladder cancer cells. Moreover, our results show that activation of TFEB leads to a global increase of PI3P at lysosomes and strong recruitment of FYVE-domain-containing proteins. Thus, our findings uncover a novel role of TFEB in regulating PI3Ps levels. This conceptually clarifies the double role of TFEB as regulator of endosomal maturation and autophagy, two fundamental but distinct cellular processes that rely and are regulated by PI3P levels. We propose that lysosome positioning changes are a crucial biomarker of alterations in the PI3P pathway in the bladder cancer model.

KEYWORDS

Lysosome positioning, mTORC1, TFEB, PI3P